Faculty of Science and Engineering
Department of Civil Engineering

Geoenvironmental Study on Solid Waste Landfill Liner

Mochamad Arief Budihardjo

This thesis is presented for the Degree of
Doctor of Philosophy
of
Curtin University

September 2015

Declaration

To the best of my knowledge and belief this thesis contains no material previously published by any other person except where due acknowledgment has been made.

This thesis contains no material which has been accepted for the award of any other degree or diploma in any university.

Signature: 

Date : 07 September 2015

Abstract

This research investigates the performance of geosynthetic clay liner (GCL) as a solid waste landfill liner and the improvement of stability through the use of bentonite and sand as liner subgrade, along with the modelling of heavy metal migration from landfill and simulation of ground deformation. A series of experimental and microanalytical tests were conducted to investigate the hydraulic performance, physical deformation and response of GCL to different types of permeants (organic salt and leachate). The laboratory tests selected for examining the performance of GCL included the Atterberg limits, swell tests, permeability tests, leachate quality tests and physical response tests. Micronanalytical analyses were also performed using optical microscopy, scanning electron microscopy (SEM), energy dispersive X-ray spectroscopy (EDS), Fourier transform infrared spectroscopy (FTIR) and X-ray diffraction (XRD). The main laboratory tests used to study the improvement in stability due to bentonite and sand included the direct shear test and cyclic triaxial test. Preliminary tests such as particle size distribution and the standard compaction test were also performed to support the main laboratory testing. The simulation of contaminant transport through the liner system was conducted using Pollute v.7, while the ground deformation modelling was performed using PLAXIS 2D 2012 finite element method (FEM) software. Two types of GCL containing different types of bentonite (powdered and granular) were used in this study, while locally sourced bentonite and sand were used for stability improvement experiments. According to the GCL performance test, the GCL containing powdered bentonite produced a higher swelling index and lower permeability than the GCL containing granular bentonite. It was also found that increasing the confining pressure reduces the hydraulic conductivity of the GCL. The static load resulting from all material above the GCL, such as gravel and waste pile, seemed to alter the surface of the GCL. However, placing a geomembrane in between the GCL and gravel layer reduces the degree of GCL surface deformation. When the water pressure underneath the GCL was higher than the water pressure coming from the top, bentonite boiling occurred on the GCL surface. Bentonite boiling did not occur when the GCL was only subjected to water pressure from beneath, with no water retained above it. Instead, the backward pressure caused the GCL layer to curve and created a dome shape with a thinner area in the middle of the dome. At the microscopic scale, exposure to inorganic salt and leachate resulted in morphological surface alteration of the bentonite inside the GCL. It was also found that the leachate

concentration declined after passing through the GCL layer. In the subgrade stability improvement experiment, it was found that the addition of sludge improved the shear stability of the bentonite subgrade. Meanwhile, the presence of carbon reduced the shear strength of sand subgrade. The shear strength of sand increased after slag and wood sticks were added. The addition of slag to sand also increased the resistance of the sand layer to liquefaction. In the heavy metal transport simulation, the concentration of both Pb and Cr declined by more than 70% after permeating the semi-permeable layer. Meanwhile the Ni and Cd migration patterns over the 1–15 year period showed that their concentrations increased as the contaminants accumulated each year. The simulation of ground deformation showed that groundwater extraction in the sand aquifer containing low permeability material resulted in a wavy ground surface. In the case of the overlying load applied in the middle of the aquifer, the increasing groundwater extraction led to surface deformation. The presence of a dynamic load and/or seismic excitation also affected the shape, degree and direction of the surface deformation.

Publications

The following publications have resulted from this research.

Refereed published journal papers:

1. Budihardjo, M.A., A. Chegenizadeh, and H. Nikraz. 2012. "Experimental Setup for Investigation of Internal Erosion in Geosynthetic Clay Liners." *International Journal of Biological, Ecological and Environmental Sciences (IJBEES)*, 1(3): 113–116.
2. Budihardjo, M.A., A. Chegenizadeh, and H. Nikraz. 2012. "A Review of Key Factors on Geosynthetic Clay Liners' Performance as Liner System." *International Journal of Biological, Ecological and Environmental Sciences (IJBEES)*, 1(3): 117–119.
3. Budihardjo, M.A., A. Chegenizadeh, and H. Nikraz. 2014. "Land Subsidence: The Presence of Well and Clay Layer in Aquifer." *Australian Journal of Basic & Applied Sciences*, 8(6): 217–224.
4. Budihardjo, M.A., A. Chegenizadeh, and H. Nikraz, 2014. "Prediction of Heavy Metal Contamination from Landfill: Lead and Chromium." *Australian Journal of Basic & Applied Sciences*, 8(7): 207–214.
5. Amiralian, S., M.A. Budihardjo, A. Chegenizadeh, and H. Nikraz. 2015. "Study of Scale Effect on Strength Characteristic of Stabilised Composite with Sewage Sludge – Part A: Preliminary Study." *Construction and Building Materials*, 80: 339–345.
6. Amiralian, S., M.A. Budihardjo, A. Chegenizadeh, and H. Nikraz. 2015. "Study of Scale Effect on Strength Characteristic of Stabilised Composite with Sewage Sludge – Part B: Critical Investigation." *Construction and Building Materials*, 80: 346–350.
7. Yang, S., A. Chegenizadeh, M.A. Budihardjo, and H. Nikraz. 2015. "Investigation of Seismic Footing Settlement Due to Subsidence for the Sand Aquifer with Pumping Wells Using PLAXIS." *Journal of Applied Sciences*, 15: 232–239.
8. Budihardjo, M.A., S. Yang, A. Chegenizadeh, and H. Nikraz. 2015. "Footing Under Static Loading: Land Subsidence." *American Journal of Applied Sciences*, 12(1): 58–63.
9. Hasan, U., A. Chegenizadeh, M.A. Budihardjo, and H. Nikraz. 2015. "A Review of the Stabilisation Techniques on Expansive Soils." *Australian Journal of Basic & Applied Sciences*, 9(7): 541–548.

Refereed published conference papers:

1. Budihardjo, M.A., A. Chegenizadeh, and H. Nikraz. 2012. "Preliminary Investigation of the GCL's Boiling toward An Upward Water Flow." International Conference on Civil and Architectural Applications (ICCAA'2012), December 18–19 2012, Phuket, Thailand.
2. Budihardjo, M.A., A. Chegenizadeh, and H. Nikraz. 2012. "Geosynthetic Clay Liner as Landfill's Leachate Barrier." International Conference on Civil and Architectural Applications (ICCAA'2012), December 18–19 2012, Phuket, Thailand.
3. Budihardjo, M.A., A. Chegenizadeh, and H. Nikraz. 2012. "Study on the GCL's Response to Hydraulic Uplift." International Conference on Civil and Architectural Applications (ICCAA'2012), December 18–19 2012, Phuket, Thailand.
4. Budihardjo, M.A., A. Chegenizadeh, and H. Nikraz. 2015. "Application of Wood to Sand-slag and its Effect on Soil Strength." *Procedia Engineering*, 102: 640–646. The 7th World Congress on Particle Technology (WCPT7), May 19-22, 2014, Beijing, China.
5. Budihardjo, M.A., A. Chegenizadeh, and H. Nikraz. 2015. "Investigation of the Strength of Carbon-sand Mixture." *Procedia Engineering*, 102: 634–639. The 7th World Congress on Particle Technology (WCPT7), May 19-22, 2014, Beijing, China.

Paper submitted to peer review journal:

1. Budihardjo, M.A. and U. Hasan. "Prediction of the Migration of High Concentration of Cadmium (Cd) and Nickel (Ni) as an Effect of Climate Change from Landfill with Single and Double Liners System." (Manuscript submitted).
2. Ghadhimi, B., M.A. Budihardjo, and U. Hasan. "Temperature Effects on the Numerical Modelling of Flexible Pavement due to Climate Change." (Manuscript submitted).
3. Hasan, U., A. Chegenizadeh, M.A. Budihardjo, and H. Nikraz. "Experimental Evaluation of Construction Waste and Ground Granulated Blast Furnace Slag as Alternative Soil Stabilisers." (Manuscript submitted).
4. Hasan, U., A. Chegenizadeh, M.A. Budihardjo, and H. Nikraz. "Shear Strength Evaluation of Expansive Soil Stabilised with Recycled Materials." (Manuscript submitted).

Acknowledgements

I would like to extend my sincere gratitude and profound respect to my supervisor, Professor Hamid Nikraz, for his patience, advice, support and encouragement during my study. I am greatly indebted to him for his timely advice, hearty concern for my research and the intensive, regular meetings to guide me throughout my time as his student.

I would also like to express my gratitude to Dr. Amin Chegenizadeh, my co-supervisor, for his invaluable suggestions, motivation, stimulating discussions and perpetual direction throughout my study time in our regular meetings. His guidance and support have been invaluable on both personal and academic levels.

I would like to convey my gratitude to Dr. Ranjan Sarukaligee for being the chairperson of my thesis committee. I sincerely thank the Department of Civil Engineering at Curtin University for providing a pleasant research environment, with specific thanks to Dr. Andrew White, Suci Leong, Franky Sia, and also many thanks to Mrs. Diane Garth for her assistance. I extend my gratitude to Mark Whittaker, Darren Isaac, Mirzet Sehic and Elaine Miller for their continued assistance during my laboratory work.

A special thanks to Associate Professor Anna Heitz, Dr. Bal Krishna and Korakod Nusit for their professional support and provision of their time to assist me with my research. I would also like to thank Camilla Brokking for performing the long task of reading through my manuscript and making this dissertation more readable in a very short time. I would also like to extend my thanks to my colleagues, Saeid Amiralian, Su Yang, Umair Hasan, Hassan Malekzehtab, Yogie Rinaldy Ginting, Berli P. Kamiel, Agus Ika Putra and Gunawan Wibisono for their kind assistance in many technical and non-technical matters. I also express my gratitude to Peter Ng for his life experience and kindness.

Finally, I would like to express my deepest love to my parents for their sincere prayers which have kept me on the path to success. Sincere thanks and great appreciation to my beloved wife and my boys for their support and love in good and bad times.

Table of Contents

List of Figures

List of Tables

List of Acronyms, Abbreviations and Notations

The following is a list of acronyms, abbreviations and notations used in this thesis.

ΔL	:	Change in length
ASTM	:	American standards for testing of materials
BOD	:	Biochemical Oxygen Demand
CBR	:	California bearing ratio
CCL	:	Compacted clay liner
Cd	:	Cadmium
CEC	:	Cation exchange capacity
CFA	:	Class-C fly ash
CH	:	Clay with high plasticity
COD	:	Chemical Oxygen Demand
Cr	:	Cromium
DDL	:	Diffuse double layer
DST	:	Direct shear test
EDS	:	Energy dispersive X-ray spectroscopy
Eref	:	Reference elastic modulus
FEM	:	Finite element method
FEM	:	Finite element method
FTIR	:	Fourier transform infrared spectroscopy
GAC	:	Granular activated carbon
GBFS	:	Granulated blast furnace slag
GCL	:	Geosynthetic clay liner
GGBS	:	Ground granulated blast furnace slag
LDPE	:	Low-density polyethylene
MDD	:	Maximum dry density
MDD	:	Maximum dry density
MSW	:	Municipal solid waste
Ni	:	Nickel

OIT	:	Oxidative induction time
OMC	:	Optimum moisture content
OMC	:	Optimum moisture content
Pb	:	Lead
PC	:	Portland cement
PI	:	Plasticity index
PSD	:	Particle size distribution
SEM	:	Scanning electron microscopy
TOC	:	Total Organic Carbon
TSS	:	Total Suspended Solid
u_a	:	Pore air-pressure
UCS	:	Unconfined compressive strength
uw	:	Pore water pressure
$\bar{x}$	:	Mean
XRD	:	X-ray diffraction
γsat	:	Saturated unit weight
$\gamma unsat$	:	Unsaturated unit weight
γw	:	Unit weight of water
C	:	Modulus of elasticity
c	:	Cohesion
c_{ref}	:	Reference cohesion
ε	:	Strain
θ	:	Angle of incident or angle of diffraction
λ	:	Wavelength of light
σ	:	Normal stress
σ'	:	Effective stress
τ	:	Shear stress
υ	:	Poisson's ratio
ϕ	:	Internal angle of friction

Chapter 1
Introduction

1.1 Background of the Study

Industrialisation, economic and urban development and the population boom have resulted in the generation of unprecedentedly high quantities of domestic waste (Jha et al. 2011; Hoornweg and Bhada-Tata 2012). In 2012, approximate per person solid waste generation exceeded 1.2 kg, resulting in an annual global solid waste generation of 1.3 billion tonnes. It has been predicted that by 2025, the municipal solid waste (MSW) generated by every urban resident will rise to 1.42 kg/person each day as the global urban population is estimated to increase to 4.3 billion in 2025 (Hoornweg and Bhada-Tata 2012).

Rising amount of collected solid waste in municipalities has instigated researchers and waste management authorities to introduce alternative waste management strategies (Zhang, Tan and Gersberg 2010; Jha et al. 2011). The concepts of solid waste reduction, reuse and recycling have been implemented to reduce the amount of MSW for final disposal or even incineration. However, landfilling still remains the most preferred method for solid waste disposal in most countries (Tonjes and Greene 2012).

In general, MSW can be categorised into three categories based on the degradability: degradable, partially degradable and non-degradable (Tchobanoglous and Kreith 2002). Degradable materials include food, straw, paper, textiles and yard waste. Partially degradable waste consists of materials like soft wood, sludge, disposable napkins and sanitary residues. Other materials such as plastics, leathers, metals, rubbers, hard woods, glass and electronic waste can be classified as non-degradable materials (Tchobanoglous, Theisen and Vigil 1993; Burnley 2007; Jha et al. 2011).

Solid wastes start decomposing after being dumped into landfills and generate leachate. This decomposition process starts from the beginning of the landfill operation and continues until landfill closure (Tchobanoglous and Kreith 2002; Lee,

Nikraz and Hung 2010). The leachate contains various organic and inorganic materials, pathogens and heavy metals in various concentrations, depending on parameters such as the nature of the generated waste, environmental conditions, soil characteristics and landfill properties. The leachate constituents are potentially harmful to the surrounding environment including groundwater and long term exposure to them may be risky for human health (Giusti 2009).

In order to inhibit the environmental impact of landfill leachate, landfills are equipped with leachate barrier to prevent leachate contaminating the surrounding soil and groundwater. The leachate barrier commonly referred to as landfill liner is an impermeable liner that functions to stop the leachate escaping from the landfill system (Tchobanoglous and Kreith 2002). According to Ludwig, Hellweg, and Stucki (2002), a common practice of landfill operators is to place an impermeable soil layer such as compacted clay liner (CCL) at the bottom of a landfill site to prohibit leachate infiltration.

However, over the decades geosynthetic clay liner (GCL) has replaced CCL due to its greater benefits, such as availability, transport, handling, installation and cost (Bouazza 2002). The thin layers of bentonite in GCL result in a more watertight liner than compacted clay liners (Lake and Kerry Rowe 2000), and this has been used for landfills liners in some developed countries (Shan and Chen 2003).

GCL contains bentonite which swells and becomes impermeable when hydrated. It also has the ability to heal itself from small punctures (Bouazza and Bowders 2010). These baseline behaviours have made GCL a more favourable choice as a landfill liner. GCL might be installed as a single or a composite liner material together with other materials such as geomembrane, geonet and geosynthetic as a liner system (Bouazza 2002).

Rowe and Orsini (2003) have proposed that, although GCL permeability can be influenced by its bentonite type, increased permeability and internal erosion may be triggered by the hydraulic gradient. In addition, GCL may be pierced or deflated and significantly lose its performance due to the “pushing aside” of bentonite in contact areas due to waste generating diverse pressures. However, Lake and Kerry Rowe (2000) believe that GCL has good characteristics like self-healing, especially of

punctures. Li, Shu, and Wu (2009) also claim that the characteristics and thickness of bentonite are the main factors influencing the self-healing of GCL.

Research conducted in previous years has generally focused on GCL behaviour under the influence of water pressure only from above (Rowe and Orsini 2003; Shan and Chen 2003; Li, Shu and Wu 2009; Dickinson and Brachman 2010), i.e. there is no investigation of the effect of water pressure from beneath the GCL. The effects of pressure from over and underlying water masses such as soil subgrade groundwater, and the influence of well-pumping from aquifers in the vicinity of the landfill have not been explored in detail.

Some other major factors also influence GCL performance, such as subgrade stability and the bearing capacity of the landfill area. Furthermore, the subgrade of a landfill contributes to the overall stability, durability and performance of landfill. Therefore, it is necessary to study the response of landfill subgrade layers to overlying stresses, either from accumulated solid waste or dynamic loading from waste compaction and disposal activities, as well as from seismic action. In addition, the effect of additive stabilisation of subgrade soil in terms of load bearing capacity should be properly researched.

Therefore, this research will examine the performance of some GCLs supplied by local manufacturers to investigate GCL behaviour under various conditions which may occur during its use as landfill liner. Since the performance of a liner also relies on the stability of the subgrade, this research will also investigate the effect of improving subgrade stability to support the liner system.

1.2 Research Objectives

According to the background described previously, the objectives of this research are to:

1. Examine the performance of GCLs under various conditions such as applied confining pressure, direction of water pressure, static loading and different permeant liquids;

2. Determine the optimum proportion of additional materials such as slag, wood and carbon to improve landfill's subgrade stability;
3. Performing simulation of contaminant transport in landfill;
4. Performing simulation of ground surface deformation under various condition.

1.3 Significance

The results of this study will be significant for a number of reasons:

1. By investigating the performance of GCL, the research provides technical evidence of the performance of GCL as a landfill lining at different sites with varying features and conditions. This information will provide important technical considerations for the design of landfills in which GCL will be used as a leachate barrier.
2. This research will develop some alternative approaches to improve the methods of landfill subgrade stabilisation.
3. This research will also provide modelling results depicting the migration of contaminants from a municipal solid waste landfill and also landfill stability.

1.4 Thesis Outline

Several experimental and numerical techniques were employed in this study and a detailed literature review was conducted to establish the research objectives. The research results and findings are compiled in this thesis, which is organised into eight chapters, as follows.

Chapter 1 aims to familiarise the reader with the research undertaken in this study. It introduces the background of the study including global solid waste generation, the use of landfills and leachates; the research objectives, such as the examination of GCL performance, landfill subgrade stability analysis and the prediction of pollutant transportation; and the outline of the thesis.

Chapter 2 presents background and a literature review on solid waste landfill, leachate generation, landfill liner systems, geosynthetic clay liner as an impermeable layer, and the stability of landfill liner and subgrade improvement. The problems associated with

solid waste including leachate generation and groundwater contamination are presented, and the configuration of landfills and the constituents of a landfill liner system are discussed. Moreover, the concept of GCL as a leachate barrier is discussed in terms of its swelling and permeability behaviour. The sources, characteristics and contaminants contained within the generated leachate as a result of solid waste decomposition are outlined. In the end, GCL laboratory analyses are reviewed including permeability, confining pressures, hydraulic gradient, microanalytical and elemental analysis, landfill stability tests and analysis, and landfill failure mechanisms.

Chapter 3 presents the purpose of the experimental study, the types of material used in the experiment, sample preparation methods, details of the experimental program and a description of the numerical analysis. Properties of the GCL samples, locally sourced sand and geomembrane are presented, as well as those of other materials such as leachate, sludge, slag, wood and carbon. The methodology for the adapted laboratory tests is also discussed.

Chapter 4 discusses the performance of geosynthetic clay liner as a leachate barrier. Two types of GCLs with different forms of bentonite are studied with regard to their hydraulic performance, as well as their performance under confining pressures and groundwater backward pressure. The physical deformation of the GCLs after being subjected to actual field loading conditions is also investigated. The final stage examines the response of bentonite to permeating liquids in terms of morphological and elemental variations.

Chapter 5 presents and discusses the experimental results for the stabilisation of landfill subgrade. Landfill stability is highly reliant upon the stability of the subgrade material. Two subgrade materials, bentonite and sand, were studied. The shear strength characteristics of bentonite stabilised with sludge and sand stabilised with slag, carbon and wood are discussed.

Chapter 6 discusses contaminant migration forecasting using numerical analysis. Leachate permeation through landfills is an unavoidable occurrence and this chapter is intended to provide prediction models for the migratory patterns of heavy metal contaminants through a landfill. For this purpose, two cases were established. The first

case deals with lead and chromium as heavy metal contaminants migrating through geomembrane, while the second case focused on cadmium and nickel migration through single and double liners.

Chapter 7 presents the results obtained from a simulation of soil deformation using PLAXIS finite element modelling techniques. Land subsidence and soil deformation hazards in terms of landfill are briefly described and the occurrence of land subsidence from groundwater extraction activities such as well-pumping is studied using three cases with different scenarios.

Finally, Chapter 8 summarises and concludes the research findings and provides some recommendations for further studies.

Chapter 2
Background and Literature Review

2.1 Introduction

Landfilling still remains the most preferred solid waste disposal method globally. Once in the landfill, solid waste starts to decompose and generates leachate. In order to inhibit the environmental impact of landfill leachate, landfills are equipped with an impermeable bottom liner to prevent leachate contaminating the surrounding soil and groundwater (Christensen 2012).

Generally, low permeable materials such as compacted clay liner (CCL) and geosynthetic clay liner (GCL) can function as landfill liner. However, GCL has become more promising compared to compacted clay liner due to several advantages such as cost, handling, availability, transport and installation. GCL contains bentonite (in powder or granular form) that swells and becomes impermeable upon complete hydration. These advantages have made GCL a more favourable choice as landfill liner (Bouazza 2002).

The performance of the impermeable layer also depends on the stability of the soil subgrade supporting the liner (Rowe and Orsini 2003). Subgrade failure will have an impact on the performance of the impermeable liner. Contaminant migration simulation can be conducted to provide a clear understanding of the performance of a liner system (Rowe and Booker 2005). Furthermore, the stability of the area around landfill can also be modelled to examine the potential deformation that may occur in the landfill area (Budhu 2010b).

Based on this background, the objective of this chapter is to review municipal solid waste landfills, the landfill configuration and liners, the characteristics of GCL as a landfill liner, laboratory analyses used to examine GCL, the stability of landfill and subgrade stabilisation improvement, simulation of contaminant transport from landfill, and simulation of ground stability. The outline of this chapter is depicted in Figure 2.1.

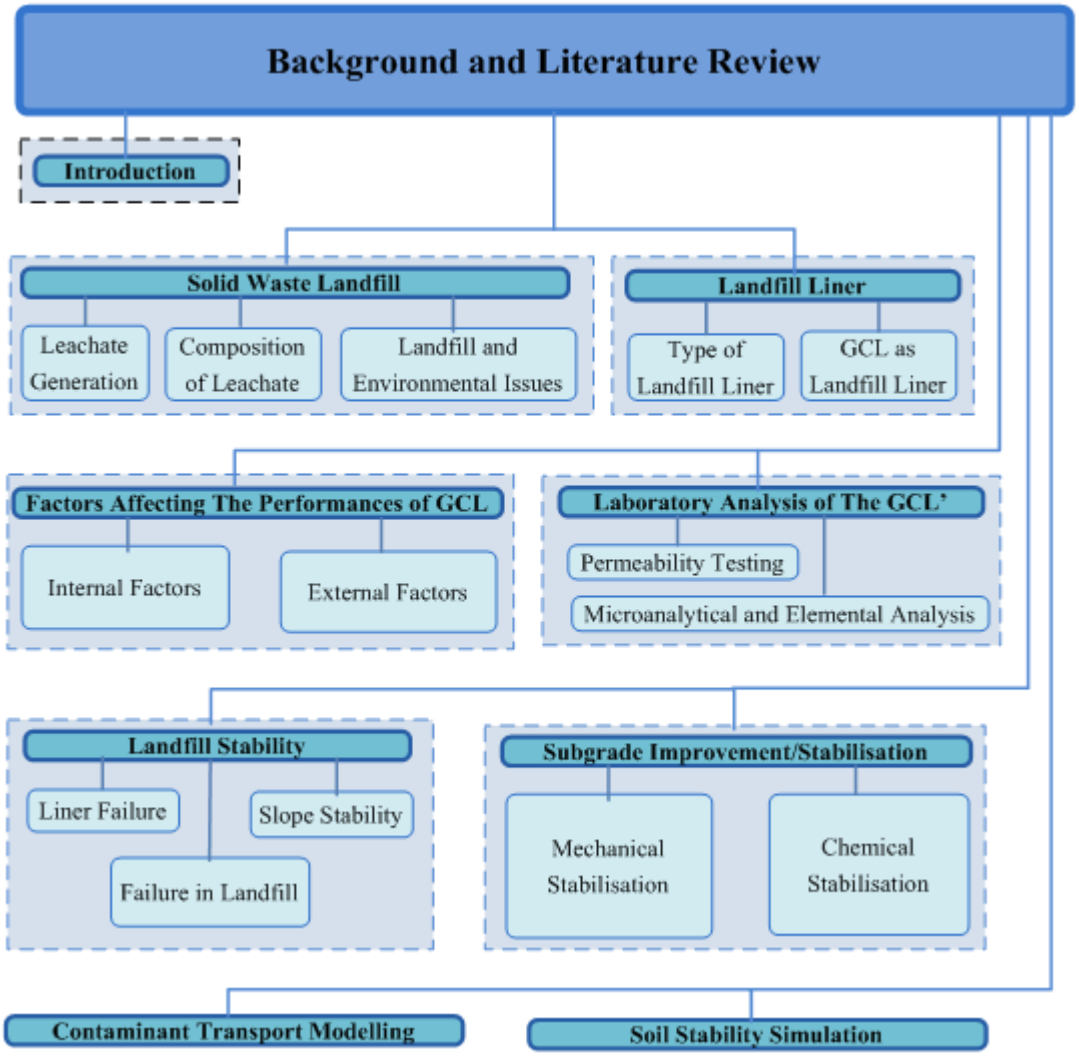

Figure 2.1 Structure of background and literature review

2.2 Solid Waste Landfill

Industrialisation, economic and urban development and the population boom have resulted in the generation of unprecedentedly high quantities of domestic waste globally. In 2012 alone, 3 billion urban residents generated around 1.3 billion tonnes of MSW, which corresponds to 1.2 kg/person/day. It has been predicted that by 2025, everyday MSW generation by urban residents will rise to 1.42 kg or 2.2 billion tonnes/year, as the urban population is estimated to increase to 4.3 billion in 2025. (Hoornweg and Bhada-Tata 2012).

Proper management of MSW has become a global concern due to changing lifestyles and rapid urbanisation (Contreras et al. 2008; Bovea et al. 2010). In common practice,

there are three ways to handle and dispose of MSW, including burial, reusing or recycling and incineration (Qian, Koerner and Gray 2001). In the United States, in spite of improved measures for recycling, reusing and reducing waste, nearly 54% of MSW is landfilled, while about 12% of it is combusted and landfilled (U.S. EPA 2013). Considering that, landfills are still considered to be the most cost-effective waste management technique. It is expected that the need for landfilling will continue in almost all countries in the long run (Tchobanoglous and Kreith 2002).

Generally, landfill can be considered a dumpsite for solid waste disposal, as depicted in Figure 2.2. It is the cheapest and simplest method and requires adequate land for the landfill site (Tchobanoglous, Theisen and Vigil 1993). Most of the waste will decompose naturally in landfill, and leachate and gas will be generated throughout the decomposition process (Scott et al. 2005). Hence, the operation of landfills may produce several environmental problems including the generation of leachate (Christensen 2012).

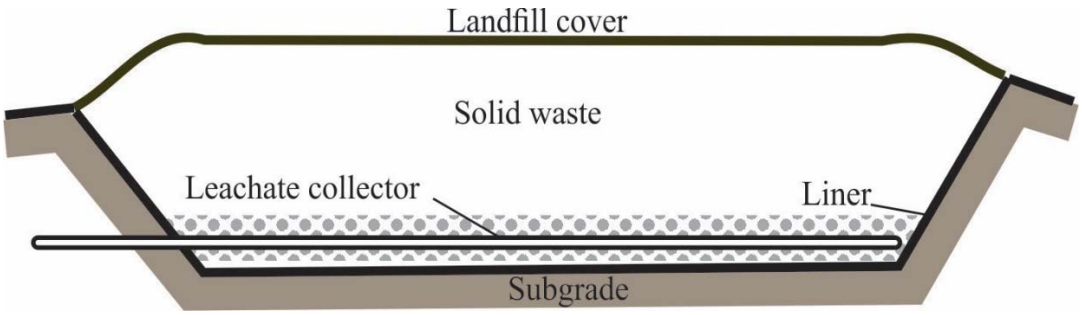

Figure 2.2 Illustration of MSW landfill (Qian, Koerner and Gray 2001)

Consequently, landfills are compartmented and equipped with leachate and gas collection systems to prevent any contamination which might potentially endanger humans and the environment (Tchobanoglous, Theisen and Vigil 1993). Landfill stability is a significant factor, i.e., the whole landfill system must be supported and no protection system failure must occur during and after the operational period (post-closure) of the MSW landfill (Blight 2008).

2.2.1 Leachate Generation

The liquid percolation occurring in landfill waste is called leachate, and this draining procedure varies widely according to the age and type of waste (Kjeldsen et al. 2002; Kulikowska and Klimiuk 2008). Landfill leachate consists of percolated water that has infiltrated the landfill or liquids that may have been expelled by the deposited wastes and solutes from the solid waste (Tchobanoglous, Theisen and Vigil 1993; Yesiller and Shackelford 2010). Traditionally, there are three major categories of leachate as listed in Table 2.1, consisting of organic fractions, inorganics and xenobiotic organics.

Table 2.1 Major categories of MSW leachate (Kjeldsen et al. 2002)

Category	Constituent
Organic fraction	Acids, aldehydes, BOD, COD, Volatile fatty acids
Inorganic	Chloride, sulphate, ammonium
Xenobiotic	Hydrocarbon, phenols

Aside from these, leachate also contains barium, arsenate, cobalt, borate, mercury, lithium, sulphide and selenate, although in smaller quantities and at less significant levels. Leachates also usually contain zinc, nickel, lead, mercury, chromium, copper, cadmium and similar heavy metals (Pohland and Harper 1985; Lema, Mendez and Blazquez 1988; Al-Yaqout and Hamoda 2003; Smith 2009). These metals are normally generated by physical processes such as corrosion and complexation or from soluble components in waste (Ehrig 1983; Flyhammar 1997; Kylefors 2002).

2.2.2 Composition of Leachate

Typically, factors like the age and type of wastes and the landfill approach affect the composition of the landfill-generated leachate (Lee, Nikraz and Hung 2010). Several studies have reported that the concentration of organic and inorganic matter in leachates is greater than in groundwater, as the leachates percolate through decomposing waste strata (Ehrig 1983; Andreottola et al. 1992; Barlaz and Ham 1993; Chu, Cheung and Wong 1994; Reinhart and Al-Yousfi 1996).

The composition of a typical leachate is demonstrated in Table 2.2, which illustrates several components mainly found in the leachate.

Table 2.2. Typical composition of leachate (Tchobanoglous, Theisen and Vigil 1993)

Parameter	Concentration (mg/l)	
	Mature Landfill (<10 years)	Young Landfill (>10 years)
BOD_5 (Biochemical Oxygen Demand)	20-1000	2000-30000
COD (Chemical Oxygen Demand)	5000-20000	3000-60000
pH	7.5-9	4.6-6.5
TOC (Total Organic Carbon)	80-160	1500-20000
TSS (Total Suspended Solid)	100-400	200-2000
Nitrate	5-10	5-40
Magnesium	50-200	50-1500
Sodium	100-200	200-2500
Chloride	100-400	200-3000
Heavy metals	More than 2	Less than 2

Leachate quality varies according to the stabilisation of organic matter as the landfill ages. Studies have indicated that pollutant concentration usually reaches peak levels in the early lifespan of the landfill (within 2–3 years), after which there is a steady degeneration of most constituents in later years in terms of BOD, COD, TOC and microorganisms, all of which are organic indicators (Kulikowska and Klimiuk 2008; Lee, Nikraz and Hung 2010).

2.2.3 Landfill and Environmental Issues

Generally, environmental issues associated with improper MSW landfilling take the form of groundwater and soil pollution. Once the waste has been covered up in the landfill, the ever-existing water brings about physical, chemical and biochemical reactions. The generation of leachate occurs when externally originated water saturates a considerable portion of the landfill wastes. The major environmental issue related to leachate generation is pollution in surface and groundwater. The severity of the environmental hazard becomes significant if the landfill is not equipped with the proper engineering solutions such as liners and leachate collection systems (El-Fadel, Findikakis and Leckie 1997; Abu-Rukah and Al-Kofahi 2001).

Leachate is subjected to a downward percolation when the waste decomposes in the landfill. In the meantime, the waste also absorbs the more naturally present chemical compounds and microbes in leachate. The bacteria and chemicals in leachate can

become harmful because of the gradually degrading subsurface water and may have adverse effects on life and the environs (Renou et al. 2008). Even under the controlled conditions in a carefully planned and well-run landfill, there are still chances for leachate to penetrate through the natural ground and cause groundwater contamination (Christensen 2012).

The environmental impact is particularly substantial for landfills that lack engineering control systems like liners and proper leachate collection systems (Lema, Mendez and Blazquez 1988; Scott et al. 2005; Mor et al. 2006). These environmental influences have major potential effects including oxygen depletion in natural water and toxicity in aquatic fauna and flora (Chofqi et al. 2004; Singh et al. 2008).

2.3 Landfill Liner

Severe environmental and health hazards are possible if the leachate escapes from a landfill and contaminates the surroundings, such as the groundwater. Thus, the most critical function of landfill design and construction is to contain liquid and gas pollutants (Christensen 2012) in order to reduce the environmental and public health impacts of a landfill. Another important target for landfills is to properly collect and transfer the leachate to a facility for further treatment. Landfills must be able to function as a hydraulic barrier to prevent leaks, or as a proper collection and treatment system for the leachate (Yesiller and Shackelford 2010).

Alternating layers of low permeability materials can be employed in MSW landfills to perform barrier functions (Tchobanoglous and Kreith 2002). In a landfill, liner is utilised to minimise landfill contamination through the effective control and isolation of the leachate produced inside a landfill (see Figure 2.2). There are a variety of liners that can be used in landfill sites, and the proper choice of landfill liner should consider factors like absorptivity and shear and strength factors (Allen 2001; Katsumi et al. 2001).

2.3.1 Types of MSW Landfill Liners

Landfill liners is primarily intended to act as an impervious barrier made of different compounds having high elastic moduli, puncture and yield strengths, and weathering

and chemical resistances (Brachman and Gudina 2008). Normally, the applicable resources for hydraulic barrier liner are compacted clay, geosynthetic clay and geomembranes (Du et al. 2009). In areas where clay is available nearby, the lower permeability, chemical compatibility and retardation, ductility, internal and interface shear strength and good constructability of compacted clay makes it one of the most cost-effective liner materials (Christensen 2012). However, clay liner can be impacted by different aspects such as soil composition, construction requirements and post construction modifications (Daniel 1993). Thus, altered clay such as bentonite is used as a replacement for clay (Czurda 2006).

Generally, there are two types of barrier components: single and composite liner. The single liner used in landfills is typically made from GCL or geomembrane, CCL or clay liner, and is utilised for construction waste due to its cost-effectiveness in building and maintenance (Dixon and Jones 2005). Composite liners, composed of a combination of clay liners and geomembranes, are usually employed by municipal solid waste landfills because of their ability to limit leachate migration. Double liners can contain either a couple of single liners, a composite or coupled composite liners. The upper liner being used for leachate collection and the lower liner acting as a backup to prevent from any leakage and usually employed in municipal hazardous waste landfills (Azad et al. 2012).

Two basic types of liner systems are single (Figure 2.3 A) and double liner systems (Figure 2.3 B). A permeable leachate-collection layer overlays the hydraulic barrier layer in single liner systems. Double liner systems consist of two hydraulic barrier layers separated by the drainage layer known as a leak detection system. These two barrier layers are also overlaid by a leachate collection system.

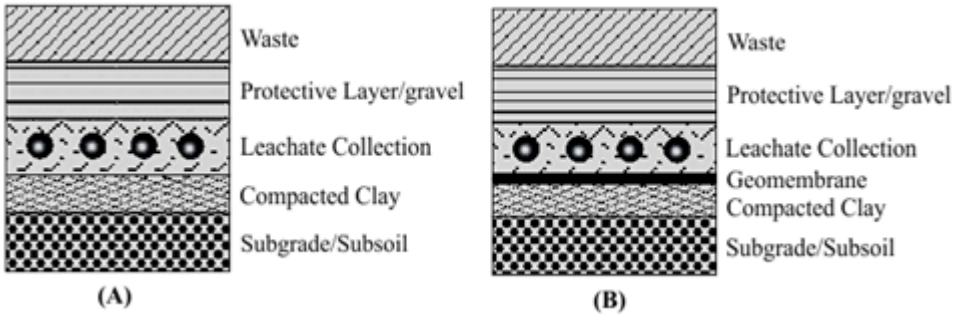

Figure 2.3 Single liner (A) and double liner (B) (Tchobanoglous and Kreith 2002)

2.3.2 GCL as Landfill Liner

Geosynthetic clay liner (GCL) is among the latest liner technologies applied in municipal solid waste landfills because of its low penetrability, convenience for installation, and its swelling behaviour (Bouazza 2002). Characteristically, GCL consists mainly of bentonite, either fused with the geomembrane or placed in between two geotextile layers (Figure 2.4). A geotextile with woven or nonwoven material is more permeable and has a comparatively higher resistance to penetration damage than a geomembrane with polymeric sheet material. The advantages of GCL include its faster and easier installation, lower penetrability, availability around the landfill area, better swell characteristics and economic effectiveness compared to conventional landfill liners like CCL (Daniel, Shan and Anderson 1993).

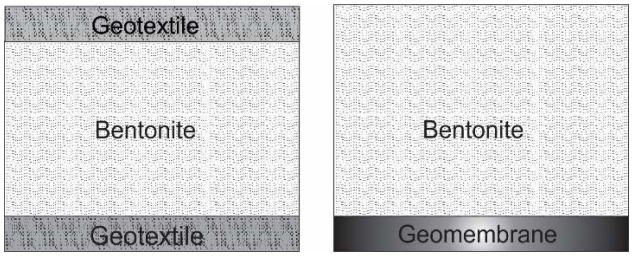

Figure 2.4 Typical configuration of GCL (Bouazza 2002)

Furthermore, gravel and sand comprise the collection systems for leachates, draining the leachate and transferring it into collection ponds for further treatment. A protective sheet containing soil, sand and gravel or soft waste (for example organic wastes, papers, rubbers etc.) is also added as a cushioning liner to prevent damage (Seeger and Müller 1996; Reddy and Saichek 1998).

Generally, GCLs are applied in the form of a single hydraulic barrier along with composite barriers which normally also contain geomembranes. The characteristics of GCLs include very low permeability to pure water. However, in the real application, GCLs are usually subjected to a variety of liquids other than pure water. The performance of GCLs can be examined by using a compatibility test, a method that is widely utilised to assess hydraulic conductivity to the actual field where the GCLs are deployed (Koerner and Koerner 2005). In this test, the actual field liquid can be used as well as any other artificial liquid that simulates the actual field liquid.

The hydraulic performance of GCLs, i.e. their permeability or hydraulic conductivity, is a dominant factor, along with a few other important factors related to the hydraulic conductivity. Factors influencing the permeability of GCLs include: 1) bentonite qualities (content, size and type of clay minerals); 2) liquid properties (concentration, valence and dielectric constant); 3) pre-hydration conditions; and 4) effective stress (Bouazza 2002).

2.4 Factors Affecting the Performance of GCL

In general, there are two factors contributing to the performance of GCLs. Those can be categorised as internal and external factors. The details of each factor are as follows.

2.4.1 Internal Factors

Internal factors affecting the performance of GCLs are mainly related to the bentonite, i.e. the bentonite quality, the mass and type of bentonite, and the bulk void ratio and initial moisture content of the bentonite.

2.4.1.1 Quality of Bentonite

There are two grades of bentonite available; high quality bentonite and low quality bentonite. By definition, high quality bentonite has a higher plasticity index, montmorillonite content and cation exchange capacity (CEC) compared to low quality bentonite. It has been also suggested that, when permeated with water, GCL consisting of low quality bentonite demonstrates a higher hydraulic conductivity than GCL made of high quality bentonite (Lee et al. 2005). The higher amount of montmorillonite in the high quality bentonite is believed to be the reason for this difference due to the water absorption ability of montmorillonite leading to greater swelling.

As specified by Ashmawy et al. (2002), an increase in montmorillonite content (from 49% to 91%) can lead to decreased GCL permeability (from 10^{-9} to 10^{-10} m/s) upon water permeation. Moreover, since the montmorillonite swelling and the relevant hydraulic conductivity in GCLs are influenced by the permeant liquids, the higher montmorillonite content leads to greater vulnerability under the influence of non-standard permeant liquids (Lee and Shackelford 2005).

Stern and Shackelford (1998) and Ashmawy et al. (2002) have noted that, of the different montmorillonite types, calcium montmorillonite always demonstrates a lower swelling tendency than sodium montmorillonite (Dananaj, Frankovská and Janotka 2005). The swelling rate and characteristics of the initial hydration are affected by the machined aggregate-size distribution (Shackelford et al. 2000). Since the particles that are deeper in the interior of the aggregate require more time for the permeant liquid to reach them, it takes longer for the interiors of the larger bentonite aggregates to be hydrated.

2.4.1.2 Mass and Thickness of the Bentonite

Generally, GCL is subject to greater shrinkage when the mass per unit area of the bentonite is under a certain threshold value. For a very low value of dry mass per unit area of the bentonite (3700–4000 g/m^2), the shrinkage was severe at approximately 12.5%. Specimens with mass per unit areas of the bentonite in the range of 4000–5000 g/m^2 exhibited a significantly low shrinkage of about 7.3% (Bowders Jr and Daniel 1987; Shang, Lo and Quigley 1994; Stern and Shackelford 1998). Little variance in shrinkage is seen between specimens with mass per unit areas in the range of 4000–5000 g/m^2, except when the bentonite distributions are irregular.

Non-uniform bentonite distributions lead to greater shrinkage compared with the specimens having uniform bentonite distribution, despite the value of the specimen mass. A high degree of shrinkage is found for all specimens with low or high mass/area specimens with an irregular distribution of bentonite. There is a trend towards increasing susceptibility to shrinkage with decreasing uniformity. Shrinkage was found to be more likely in locations with fewer bentonite particles. In thin areas, a similar susceptibility to shrinkage is found between unrestrained specimens and restrained specimens (Bostwick et al. 2010).

2.4.1.3 Type and Granularity of the Bentonite

A number of experiments were conducted by Rowe, Bostwick and Take (2011) to test the influence of granularity and bentonite type on the physical deformation of GCL (the change in properties from their original status). In the tests, GCL specimens had three different granularities and three varied sodium bentonite compositions. The granularity of the tested specimen fell into three ranges: fine granular (D_{50}

approximately 0.003 mm), powdered (D_{50} approximately 0.03 mm) and coarse granular (D_{50} approximately 0.08 mm).

During the initial five wet-dry cycles, bentonite granularity and type barely had any influence on the stability of the GCL. Following the fifth cycle, the degree of shrinkage started to decline with each cycle in the granular bentonite specimens, but the powdered bentonite specimens continued shrinking at a high rate. After about 30 cycles, a relatively steady shrinkage rate was achieved for GCLs with granular bentonite, however GCL specimens with powdered bentonite failed to reach a constant value of shrinkage even after 75 cycles. Due to the similarity between the shrinkage rate for the initial several cycles and the phenomenon stated above, powdered bentonite showed a greater final shrinkage than the granular bentonite (Rowe, Bostwick and Take 2011).

2.4.1.4 Bulk Void Ratio

Void ratio (e) can be describe as the ratio of total volume of the pore space to the volume of the solid for a porous medium. The permeability of bentonite and GCLs have been found to be significantly influenced by the void ratio (Shackelford et al. 2000). In general, although the materials with larger particle sizes tend to bring out larger individual voids or spaces, the total volume of void is not necessarily greater, or is usually smaller, compared to the fine-grained materials. The void ratio of bentonite is higher as sandy soil has greater permeability in comparison with bentonite. This is due to the smaller sizes of the individual voids in the bentonite, which makes it more difficult for water to permeate. Figure 2.5 demonstrates the velocity distribution for liquids flowing through the voids. Larger void spaces lead to easier liquid permeation, in other words, higher hydraulic conductivity (Katsumi 2010).

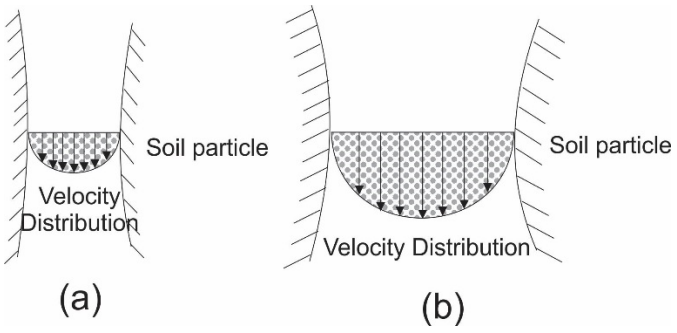

Figure 2.5 Water passing through small (a) and large void (b) (Katsumi 2010)

Mesri and Olson (1971) have suggested that the log values of permeability ($\log k$) and void ratio ($\log e$) are directly related when various aqueous solutions are passing through homo-ionic bentonites. Petrov and Rowe (1997) presented similar results showing $\log k$ values to be linearly related with original void ratio values.

2.4.1.5 Initial Moisture Content

There is no significant correlation found between the observed shrinkage and the final and initial GCL moisture contents. A higher initial moisture content has been found to lead to more shrinkage for GCL specimens in the first wet-dry cycle than those with a lower initial moisture content. Meanwhile, during the initial cycles, greater shrinkage resulted in higher strain accumulation.

The influence of initial moisture percentage became minimal with further cycles, and there was no significant influence on the ultimate value of maximum shrinkage at equilibrium (Rowe, Bostwick and Take 2011). Rowe, Bostwick and Take (2011) tested the initial moisture content effect on the response of GCL by adding sufficient water to achieve an artificial increase in moisture content from 5% (gravimetric moisture content) to 19%, 64% and 72%, which represents the extreme ranges of real initial conditions.

2.4.2 External Factors

2.4.2.1 Hydration

The degree of hydration has a greater influence on shrinkage at lower degrees of hydration than at higher degrees (Rowe, Bostwick and Take 2011). The amount of shrinkage for specimens hydrated with less water is lower than for specimens with the baseline amount of water. When hydrated to nearly 40% gravimetric moisture content, the amount of overall shrinkage seen in specimens is about 25% less than for specimens with around 65% of gravimetric moisture content. It remains unclear whether an eventual equilibrium, which represents the same amount of shrinkage as the base line, will be reached (Thiel et al. 2006).

Thiel et al. (2006) suggested that there would be much less shrinkage with the addition of a smaller amount of water compared to the baseline results. Contrarily, Rowe, Bostwick, and Take (2011) pointed out that no significant change is caused by adding

more water than for the baseline results. Both results have certain grounds as the experiments for these two studies were conducted on different GCL types. Alternatively, the phenomenon can be explained as the baseline hydration representing a moisture content higher than the plastic limit, while the reduced hydration has a lower moisture content than the plastic limit (Vangpaisal and Bouazza 2004).

2.4.2.2 Effective Stress

Due to the correlation between void ratios and effective stress, the permeability of GCL is largely influenced by effective stress (Lu and Likos 2006). Basically, a higher effective stress tends to result in a lower permeability during the permeation procedure, and vice versa. Several experimental investigators indicated a reduction in void ratio and thus a decreasing hydraulic conductivity for GCL caused by increments in effective stresses (Shan and Daniel 1991; Petrov, Rowe and Quigley 1997). Hydraulic conductivity is significantly influenced by the ionic strength when the effective stress is relatively low.

By contrast, k is relatively unchanged with a changing ionic strength at relatively large effective stresses. Due to the resulting compression from increased effective stress for GCL specimens, the application of greater effective stress tends to blur the influence made by the permeant liquid (decreased flow paths) (Lee et al. 2005). Bouazza (2002) demonstrated changes in permeability at various effective stresses when permeated with water (Figure 2.6). After comparing the results obtained for permeability, it was found that variation in hydraulic conductivity is more significant at low levels of effective stress.

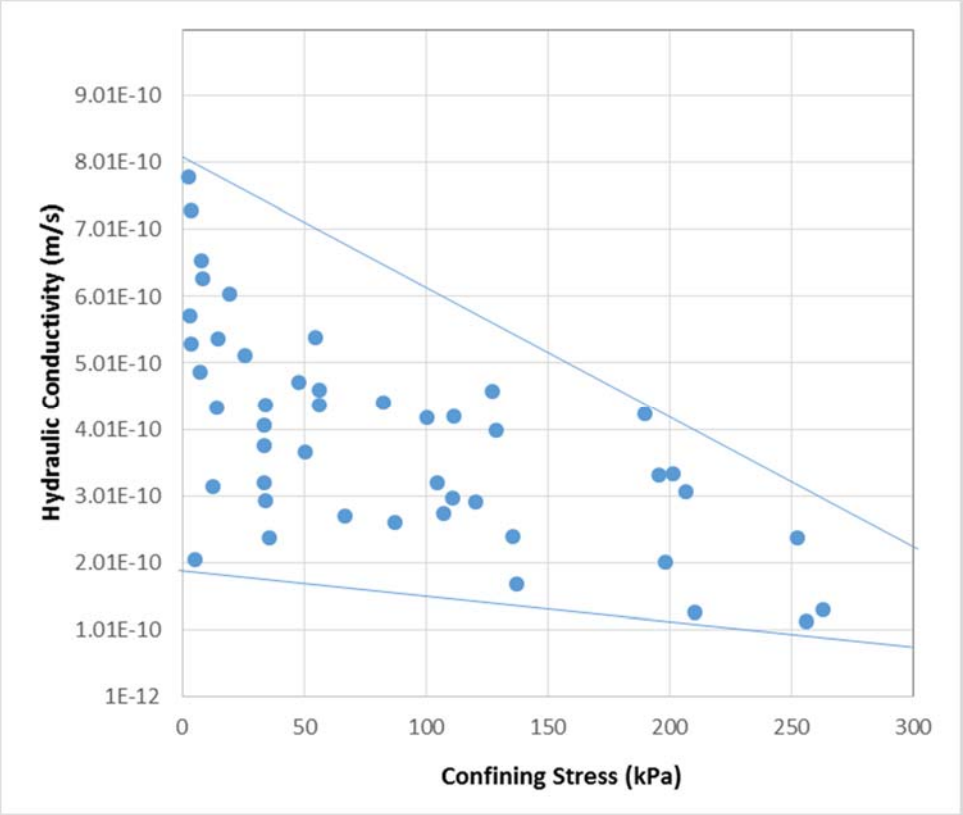

Figure 2.6 Confining stress vs hydraulic conductivity (Bouazza 2002)

2.4.2.3 Electrolyte Concentration

Based on the findings of Sivapullaiah and Savitha (1999), bentonite particles in water can experience inter-particle separation, which leads to a higher swelling index. However, this phenomenon is inhibited by electrolyte solutions, which bring about a reduced swelling index and may also cause a reduction in the thickness of the diffuse double layer (DDL). Zhu et al. (2013) derived a permeability value of 4.14×10^{-10} m/s when there is 0% salt concentration in the permeating liquid, however, when an increased salt concentration of 5% is present, the permeability of bentonite is increased to 1.31×10^{-9}.

Based on the double layer theory, an increased electrolyte concentration results in reduction in the height (thickness) of the adsorbed layer, and therefore, a raise in permeability value. Studies have also demonstrated a correlation between bentonite swelling and leachate composition, and thus the hydraulic conductivity (Egloffstein 2001; Ashmawy et al. 2002; Katsumi et al. 2002; Shackelford, Sevick and Eykholt 2010).

Utilising ASTM D5890 (ASTM D5890-11 2011), Kolstad et al. (2004) did free swelling tests with various concentrations of chemical solutions. The results (Figure 2.7) demonstrate that the swelling amount of bentonite declines with an increase in ionic strength (concentration). Katsumi et al. (2008) also investigated the relationship between permeability and free swelling (Figure 2.8). Mostly, greater swelling corresponds to lower hydraulic conductivity.

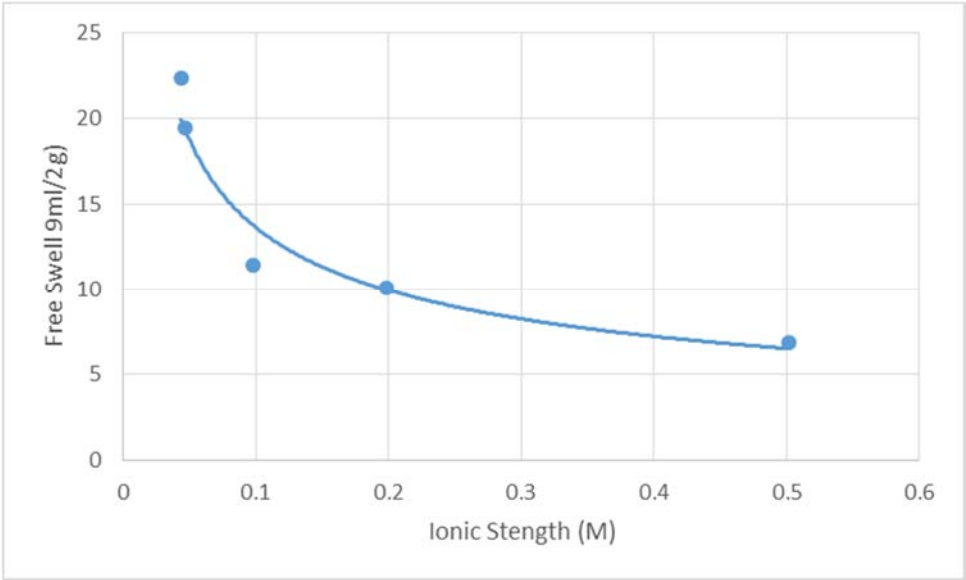

Figure 2.7 The correlation of free swell and ionic strength (Kolstad et al. 2004)

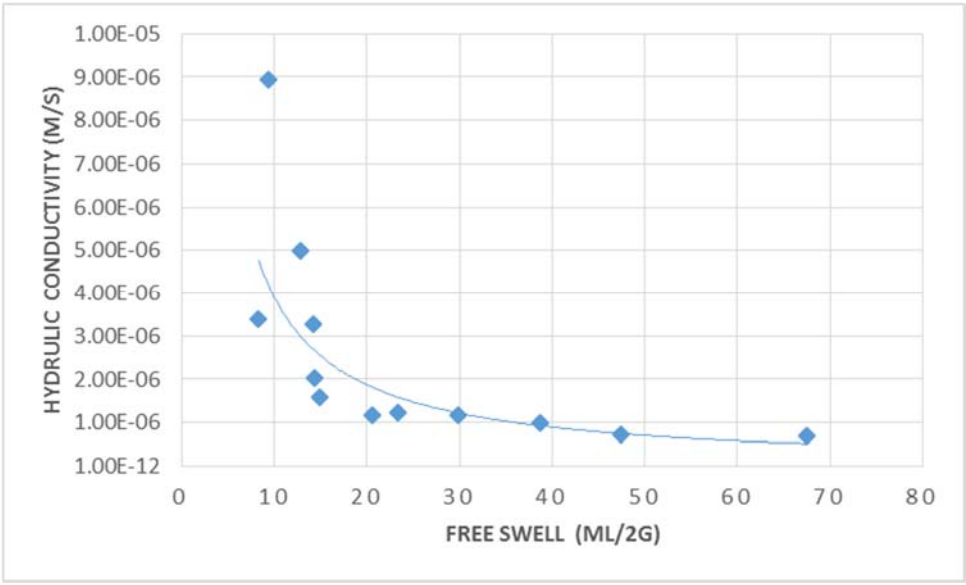

Figure 2.8 Correlation of swelling and permeability (Katsumi et al. 2008)

2.4.2.4 *Influence of Cation Valence*

Generally, cation valence influences DDL thickness. Shackelford et al. (2000) conducted free swelling tests on bentonite specimens obtained from GCL, and the results proved the effect of cation valence on the hydraulic properties of GCL. This experiment used deionised water and three different types of 0.025 M chloride solution to permeate the specimen. The results, in Figure 2.9, describe the relationship between cation valence and the change in swelling. For instance, Al^{3+}, the highest valence, resulted in the greatest reduction in terms of bentonite swelling; thus conforming with the theory of double layers. The level of swelling found in LiCl solutions is only slightly lower than for deionised water, since Li^{+} is monovalent. Jo et al. (2001) conducted research on types of salt and the influence of cation valence. They found that the type of salt does have an influence on the degree of swelling, but the extent of influence is lower than for the valence.

A more significant swell reduction is caused by multivalent cations than by monovalent cations (Figure 2.10). Test outcomes have shown that Ca^{2+} from dilute solutions is able to gradually replace naturally occurring Na^{+} in the exchange complex. The replacement induces consequential compression as well as a gradual hydraulic conductivity increase for the adsorbed layer (Shackelford et al. 2000). Consistent findings were suggested by James, Fullerton, and Drake (1997) and Melchior (1997) according to in-field investigations.

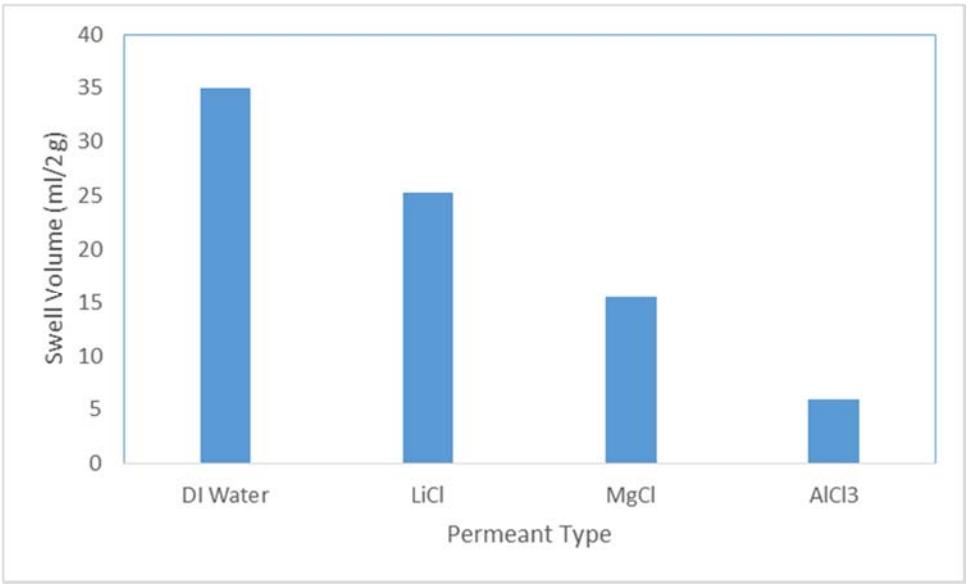

Figure 2.9 Bentonite's free swell comparison (Shackelford et al. 2000)

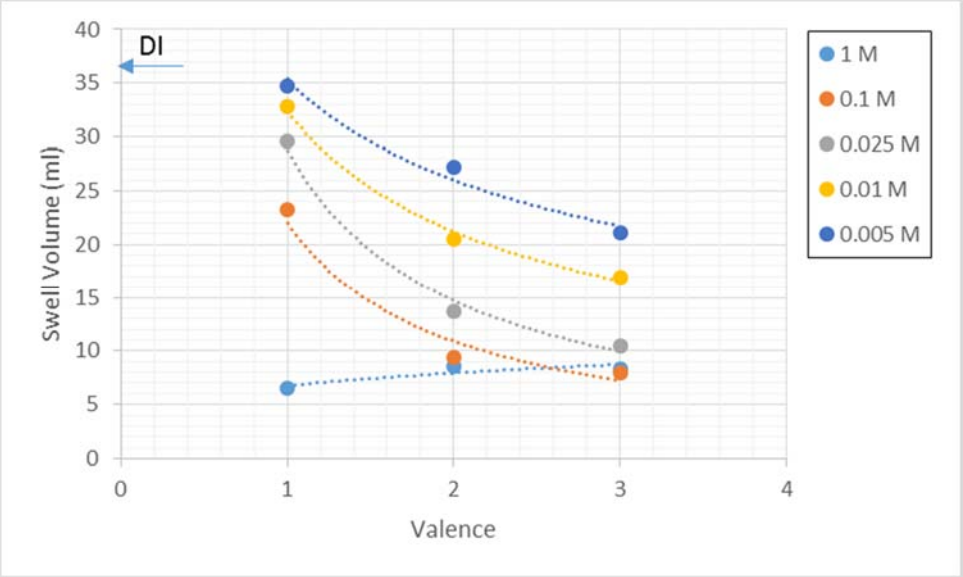

Figure 2.10 Swelling vs cation valence (Jo et al. 2001)

2.4.2.5 Influence of Dielectric Constant

A reduced dielectric constant (e) for the permeant liquid can collapse the DDL and it can be inferred that this will lead to a higher hydraulic conductivity. It is widely known that, compared to water permeation, the permeation of organic or inorganic solutions through DDL will result in higher hydraulic conductivity (Bowders Jr and Daniel 1987; Yılmaz, Yetimoglu and Arasan 2008). This is partly due to the dielectric constant value (e=80) of water being higher than for the organic or inorganic solutions (ethanol=24.3, density ~0.8 g/cm^3). With the permeant's dielectric constant reduced from 80 to 20, results obtained by Fernandez and Quigley (1985) showed an increased hydraulic conductivity from about 1 x 10^{-10} m/s to about 1 x 10^{-8} m/s (Figure 2.11).

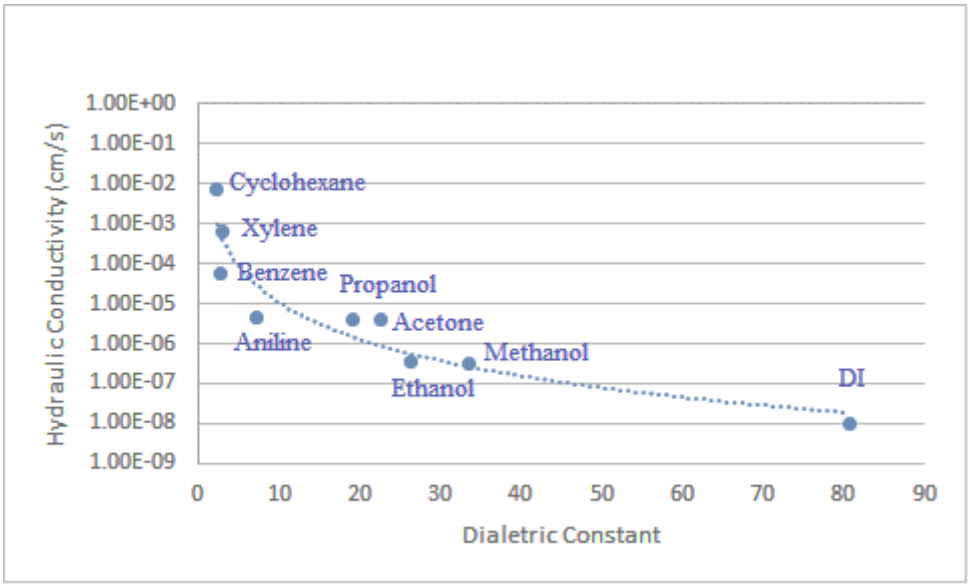

Figure 2.11 Hydraulic conductivity and dielectric constant (Fernandez and Quigley 1985)

2.5 Laboratory Analysis of the GCL

2.5.1 Permeability Testing

The permeability of GCL is affected by several properties: the mineralogical makeup of the bentonite, liquid absorption capacity, thickness and the cation exchange capacity of the bentonite. These properties are normally related to each other and interdependent, but change with the specific makeup of the soil. In addition, these properties vary with changes in the makeup of the permeating liquid, the confining pressure applied by the test and the hydraulic gradient.

2.5.1.1 Permeant Type and First Wetting Liquid

In the method set out in ASTM D5084-10 (2010), it is recommended that laboratory permeability experiments be conducted with a hydration period of 48 hours, after which the chemical liquid of interest is permeated. When GCL is hydrated with water, its thickness mounts dramatically, although the degree to which the thickness increases varies with the soil mineralogy. An artificially low permeability value can be expected when the thickness of the double layer increases. As suggested by Ruhl (1994), a virgin hydration with water indicates a hydraulic conductivity of $2x10^{-11}$ m/s for materials that constitute GCL, which is followed by the permeation of landfill leachate

or relevant simulating liquid. An increased hydraulic conductivity of $2x10^{-7}$ m/s is obtained when the GCLs are hydrated and permeated by the leachate.

As a chemically neutral substance, water has no adverse effect on the permeability of soil. By contrast, liquids carrying a certain amount of organic and/or inorganic compounds may negatively affect a soil's hydraulic conductivities. For example, montmorillonite permeability might increase by an order of magnitude when permeated with certain organic-bearing liquids like aromatic hydrocarbons. Brown and Brindley (1980) recorded a permeability of $3.6x10^{-10}$ m/s for bentonite permeated with water. However, a bentonite permeated with xylene yielded a value of $1.76x10^{-6}$ m/s, a fourfold increase.

A significant increase in bentonite permeability can be seen when the permeating liquid contains certain inorganic chemical compounds like sodium chloride, calcium chloride and magnesium chloride. Lin and Benson (2000) reported that when a bentonite material was permeated with pure water followed by calcium solution (0.0125 mol/L of calcium), the hydraulic conductivity increased from $5x10^{-11}$ m/s to $8x10^{-8}$ m/s.

2.5.1.2 Confining Pressure

According to soil mechanics, a consolidation effect will become obvious when a high confining pressure is imposed on a soil, leading to lower permeability. As a result, high confining pressure is not recommended for permeability testing. Daniel and Scranton (1997) performed a permeability test on GCL materials, where a confining pressure of 5 kPa and 10 kPa led to a permeability of 10^{-11} m/s. A 300 kPa confining pressure led to a dramatic decline in permeability by one order of magnitude. ASTM D5887-09 (2009) sets an upper limit of 35 kPa confining pressure for carrying out permeability tests, whereas there is no lower limit. The confining pressure should vary based on the intended use, and should be representative of normal field conditions.

2.5.1.3 Hydraulic Gradient

With regarding to permeability tests on soils with finer particle sizes, it is usual to apply a relatively high hydraulic gradient to the tests, since the low permeability of these soils will make the whole test highly time consuming. Alternatively, Jo et al. (2001) recommend using a representative real condition of hydraulic gradient, since a

hydraulic gradient that is higher than reality would lead to low permeability due to consolidation. Despite the recommendations by ASTM D5887-09 (2009) for an upper limit hydraulic gradient of 30, professionals and researchers still tend to adopt higher hydraulic gradients to run permeability tests on soils with low hydraulic conductivities.

By definition, the hydraulic gradient, which is known as the Darcy slope, is a parameter controlling the discharge quantity of the leachate permeating a porous medium. The formula for calculating the hydraulic gradient (i) is as follows:

$$i = \frac{dh}{dl} = \frac{h_2 - h_1}{Length} \tag{2.1}$$

Where i is the Darcy slope (dimensionless hydraulic gradient), dh represents the variance between the two hydraulic heads (metre), and dl denotes the length of the flow path (meter). ASTM D5084-10 (2010) recommends a hydraulic gradient no greater than 30 for low permeability media ($k < 10^{-9}$ m/s). However in practice, the typical hydraulic gradients for measuring the permeability of GCLs fall into the range of 50 to 600, for the sake of shortening the test duration to a minimum level in order to attain effluent-influent chemical equilibrium (Lin and Benson 2000; Lee et al. 2005).

Shackelford et al. (2000) proposed that the headwater and tail water ends are locations where maximum and minimum effective stresses (σ′) occur during permeation, and this is demonstrated in:

$$\sigma'_{max,min} = \sigma_c - u_b \pm \Delta\sigma' = \sigma'_b \pm \frac{i\gamma_w L}{2} \tag{2.2}$$

$$\sigma'_{max,min} = \sigma_c - u_b \pm \Delta\sigma' = \sigma'_b \pm \frac{i\gamma_w L}{2} \tag{2.3}$$

Here backpressure, effective stress and cell pressure are represented by u_b, σ' and σ_c respectively. $\Delta\sigma'$ denotes the effective stress changes caused by the hydraulic gradient applications, γ_w represents the unit weight of water, while L stands for the specimen length or thickness. The seepage force of the specimen per unit volume is represented

by the product $i\gamma_w$. As stated above, the permeability can be lowered by an increased hydraulic gradient, which results in consolidation.

2.5.2 Microanalytical and Elemental Analysis

Alterations in the mineralogy, composition and morphology of bentonite after being permeated with different liquids are studied through microanalytical methods. Microanalytical and elemental analysis consists of optical microscopy, scanning electron microscopy (SEM) and energy dispersive X-ray spectroscopy (EDS), Fourier transform infrared spectroscopy (FTIR) and X-ray diffraction (XRD).

2.5.2.1 Optical Microscopy

There are two types of digital microscope: the two-dimensional microscope/biological microscope (light microscope) and the three-dimensional (3D) stereo microscope (Murphy and Davidson 2012). Based on light source, microscopes can be classified into light microscopes and electron microscopes. The light microscope, also known as the "compound light microscope", utilises a dedicated light source rather than natural sunlight during the observation. Light microscopy requires three lenses to support observations, and these are the objective lens, ocular lens and condenser lens (Slayter 1992).

Generally, a microscope has two main parts, namely the optical and non-optical parts. The optical part consists of a condenser, objective lens and an eyepiece, while the non-optical part includes the leg and arm of the microscope, a diaphragm, an object table or counter preparations, smooth and rough rotator, a glass clamp and the light source (Slayter 1992). Objects under the optical microscope can also be captured by a light-sensitive digital camera. Commonly, the digital camera is connected to a computer which is equipped with specific software to display the digital image directly on a monitor (Carlsson 2007). This latest development in optical microscopy offers the ease of observing the object directly from the computer screen (Figure 2.12) without the need for eyepieces (Murphy and Davidson 2012).

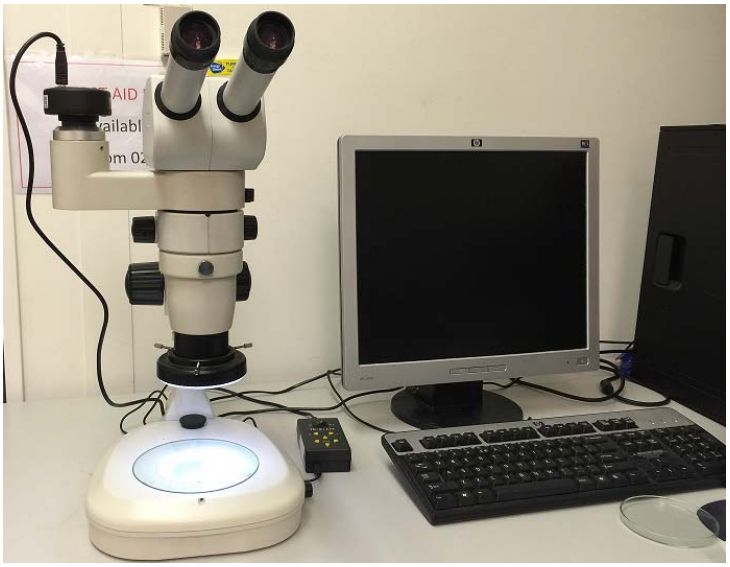

Figure 2.12 Optical microscopy

2.5.2.2 SEM and EDS

An electron microscope which utilise an electron beam to produce a picture of the material being analysed is referred as a scanning electron microscope (SEM) (Figure 2.13). The working principle of the SEM is to scan the material with an electron beam generated by the machine. The surface material is exposed to the electron beam, which is reflected (secondary electron beam) in all directions (Tarrant 2011).

The SEM has a higher resolution compared to the optical microscope. Its depth of field is quite large, which can focus on more sample points at the same time and produce an image with shadow on the monitor. The SEM also produces high resolution images that can be enlarged with high magnification (up to six orders of magnitude) (Garratt-Reed and Bell 2003). SEM can show some of the characteristics of the material being tested such as morphology and shape. It can also be connected to an energy dispersive X-ray spectroscopy (EDS) machine and provide the material's chemical composition (Tarrant 2011).

EDS can determine the elements inside or on the surface of the material tested. EDS can also be used to examine the elemental and chemical composition of the material. The EDS may be equipped with an ultra-thin window and software, and its X-ray detector is able to display the X-ray spectra, element maps and both qualitative and quantitative numeric data (Goodge 2011).

Figure 2.13 Scanning electron microscope

2.5.2.3 FTIR

The Fourier transform infrared spectroscopy (FTIR) technique is employed to determine the presence of functional groups, particularly organic compounds. The plot of absorbance percentage or transmittance percentage versus frequency will produce an infrared spectrum (Gaffney, Marley and Jones 2012). Qualitative analysis of organic compounds using a FTIR spectrophotometer is done by looking at the shape of the spectrum and comparing it with the results of the analysis to indicate the type of functional group possessed by the compound. Quantitative analysis can be performed using spectra made of standard compounds at various concentrations (Meyer-Jacob 2010).

The PerkinElmer Spectrum 100 FTIR Spectrometer was used to conduct the FTIR spectroscopy in this research. The recorded spectrum range is 4000–650 cm^{-1} (4 cm^{-1} resolution) through the ATR (attenuated total reflectance) technique. FTIR can analyse the level of interaction between soil and other particles (Figure 2.14).

Figure 2.14 FTIR device

2.5.2.4 XRD

X-ray powder diffraction (XRD) is employed to define the soil samples' mineralogical constitution, both qualitatively and quantitatively (Figure 2.15). According to Whittig and Allardice (1986), X-rays are in essence electromagnetic radiation produced by the oscillation of electromagnetic and electrostatic fields, when the wavelength is equal to the crystal's interatomic distance. At 40 kV and 40 mA, the radiation can be produced with a Cu-Ka X-ray beam (λ= 0.15404 *nm*). Under a 0.02°/s scanning rate, 2θ data ranging from 0° to 60° can be collected by the XRD measurement (Brown and Brindley 1980; Whittig and Allardice 1986; Kunze and Dixon 2003).

As dictated by this study's scope, the XRD process can be carried out with qualitative or quantitative analysis. Due to its simplicity, the qualitative analysis requires less experience than the quantitative analysis. If the analysis is not properly conducted, it can lead to the wrong conclusions (Moore and Reynolds 1989). Either an internal or external standard method can be used to carry out the quantitative analysis.

Figure 2.15 XRD device

2.6 Landfill Stability

As commonly utilised MSW management facilities, landfills should meet compliance rules for location, monitoring, operation, design and finance. Technically, some geotechnical aspects should be considered in the design of the landfill. For the operational and post-closure periods, the major geotechnical consideration is stability. The ground settlement and the slope stability of the landfills need thorough consideration since they have a potentially negative influence on the landfill liner.

2.6.1 Liner Failure

Generally, liners are subject to two kinds of failure: leakage and liner destruction. Liner leakage occurs due to a loss of material permeability or damage in the form of holes, which may lead to leachate release. By contrast, liner destruction manifests as extensive liner movement or extensive reduction in the mechanical properties; these are produced by puncture and creep (Mitchell and Mitchell 1993).

Creep is defined as material deformation over an extended time period with constant acting pressure (Mitchell, Seed and Seed 1990; Seed, Mitchell and Seed 1990). The

factors influencing creep may include load, temperature and time, while creep deformation takes the form of compression, tension, torsion and flexure (Filz, Esterhuizen and Duncan 2001). Creep has three phases; firstly, strain increase with a decreasing rate of increase; secondly, strain increase with a constant rate of strain; and thirdly, material rupture caused by a rapid surge in both strain and rate of strain. A typical landfill liner creep curve is illustrated in Figure 2.16.

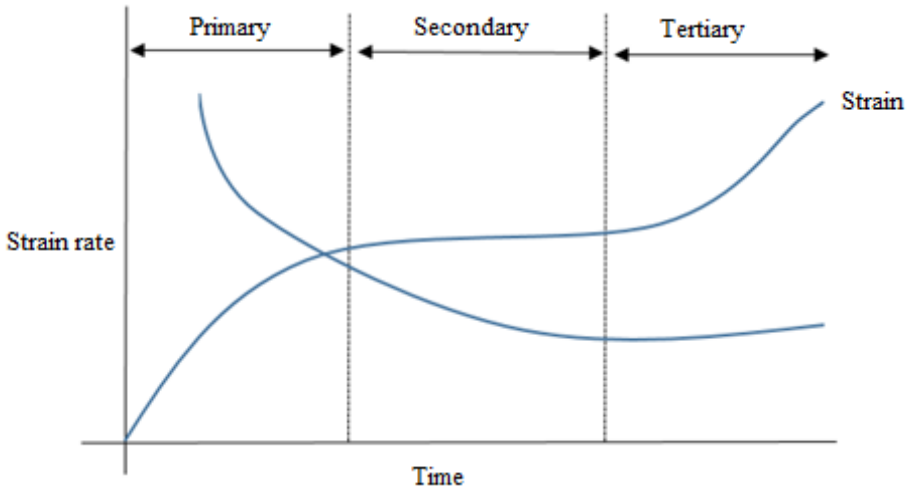

Figure 2.16 Common creep (Mitchell, Seed and Seed 1990)

Puncture is among the most serious damage incurred by landfill liner. While assessment of the puncture phenomenon is normally difficult, puncture can be induced by either short-term or long-term puncture forces. Short-term forces include those that are generated during installation, such as the setting up of a leachate collection layer, whereas long-term forces include permanent loads, for example, of waste (Hullings and Koerner 1991).

Alternatively, puncture triggers can be static or dynamic in origin. For example, height falling during the installation process induces dynamic forces, which are usually short-term, while contact with static normal stresses, like traffic load or the weight of waste, may lead to static puncture. Figure 2.17 illustrates the puncture resistance of liners with different components (Artieres and Delmas 1995).

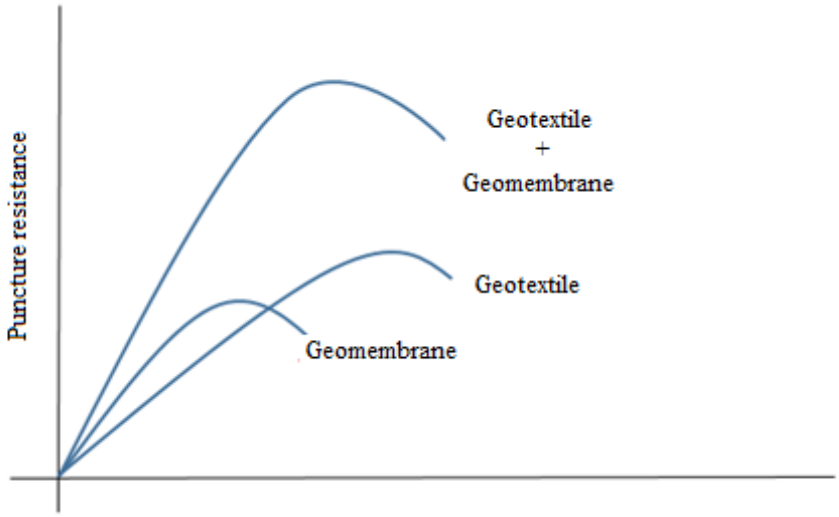

Figure 2.17 Puncture resistance of liners (Artieres and Delmas 1995)

2.6.2 Slope Stability

Eid et al. (2000) and Qian, Koerner, and Gray (2001) have listed the factors affecting the stability of landfill, such as material shear strength, pore water pressure, geometry, settlement, loading conditions and operations.

2.6.2.1 Shear Strength

Shear strength is a major engineering parameter that defines the soil's ability to resist failure. For landfills, stability is controlled by MSW shear strength, soil, and liner soils plus the interface between different geosynthetic materials (Mitchell and Mitchell 1993). Importantly, the presence and amount of water can have a critical influence on the shear strength of various materials.

2.6.2.2 Pore Water Pressure

In soil mechanics, an increase in pore pressure leads to a reduced effective stress and thus the force with which a material can resist failure or excessive deformation. The stability of a landfill will be negatively affected by the presence of increased pore water pressure (Mitchell and Mitchell 1993; Reddy and Basha 2014). By contrast, the vertical effective stress will improve with declining pore pressure (e.g. suction pressure or any other negative pore pressure), which then enhances the slope stability. For most wastes, there is a higher liquid content due to any surface permeation or

leachate circulation. Consequently, reasonable control is required in these cases to counter the destabilising responses (Abramson 2002).

2.6.2.3 Settlement

Landfill settlements can cause both positive and negative effects. Mitchell and Mitchell (1993) suggested that uniform settlement will increase the unit weight of the MSW because of the densification and consequently will lead to improved stability. By contrast, localised uneven settlement results in surface water infiltrating through the mass, which is likely to cause both piezometric head and pore water pressure to increase.

2.6.2.4 Loading Conditions

With regard to stability considerations for landfills, typical static loadings include the wastes and the external load weights, for instance, soils amassing waste fill. In addition, normal loads on existing waste, liner and base material can be increased by vertical expansion and the placement of stockpiles. Vehicular movements and compaction activities can also induce dynamic loadings that may influence the stability of landfills (Reddy and Basha 2014).

2.6.2.5 Operations

Operations on landfill also have an influence on landfill stability. As a result, the following parameters are subject to regular examination: the degree of waste saturation, gas extraction systems, air-injection systems, and liquid injection systems and piezometer heads (Reddy and Basha 2014).

2.6.3 Failure in Landfill

Typical landfill failure mechanisms are illustrated schematically in Figure 2.18 and Figure 2.19. For waste mass failures, Qian, Koerner, and Gray (2001) have proposed that block failure surfaces and circular arc (slip) are two important factors. As shown in Figure 2.21, slip failure occurs within the waste mass and completely outside of the influence of the liner system. Normally, rotational failure is triggered by steep waste slopes, high water/liquid content and lack of placement controls. When there is a weak failure plane inside the waste mass, block sliding surfaces will potentially form (Figure 2.22). Block failure analysis should be conducted in order to estimate the safety factor

against sliding if the landfill material has a greater shear strength than the foundation soils.

Another form of failure is rotational failure, which generally occurs in soft soils and develops upwards through the whole waste mass. When exposed to a significant load, subgrades with low shear strength may be subject to bearing capacity failure (Qian, Koerner, and Gray 2001). The presence of a liner system adds a stabilising factor but it is negligible in is influence on the stability analysis and design, as illustrated in Figure 2.21. For a potential failure plane, it is reasonable to assume a circular arc failure surface.

Figure 2.18 Landfill's slip surface failure (Qian, Koerner and Gray 2001)

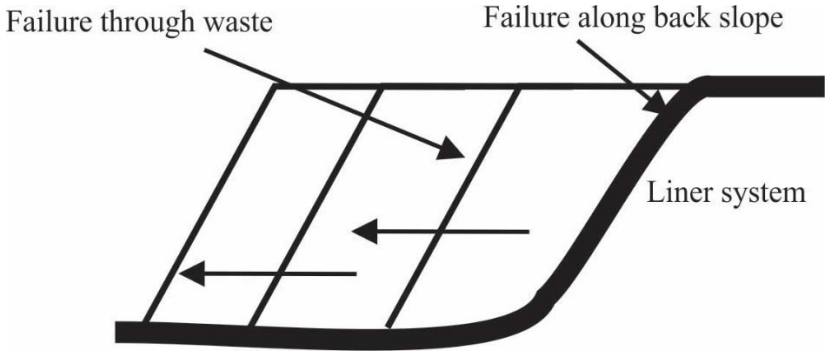

Figure 2.19 Landfill's block failure (Qian, Koerner and Gray 2001)

2.7 Subgrade Improvement/Stabilisation

There are unfavourable soil properties in many sites, including insufficient bearing capacity, excessive potential for shrinking and swelling, and undue susceptibility to moisture etc. (Sharma, Swain and Sahoo 2012; Harichane, Ghrici and Missoum 2011). For example, in the case of road construction, using a soft soil with a subgrade layer

of pavement can be regarded as inappropriate use of an inadequate soil in building and construction. The consequence can be a rapidly damaged pavement that causes premature pavement failure and attracts attention (Sharma, Swain and Sahoo 2012). By contrast, in landfill structures the consequences of landfill collapse because of unstable soil/subgrade are not visible and unattractive. However, it may lead to a damaged landfill liner and the release of leachate into the soil and groundwater. This can pose a very significant risk to humans and the surrounding environment. Moreover, the remediation of contaminated soil and water and landfill liner reconstruction entail an enormous effort (Christensen 2012).

To cope with the issues mentioned above, soil stabilisation has been in wide use for a number of years due to its environmental friendliness, cost-effectiveness and efficiency. While each project may have specific engineering requirements, the method of soil stabilisation can be amended to account for them (Kolias, Kasselouri-Rigopoulou and Karahalios 2005; Castro-Fresno et al. 2011; Harichane et al. 2011; Ramadas, Kumar and Yesuratnam 2011).

The benefit of soil stabilisation is to optimise the cost of the earthworks while providing soil treatment that sustains, adjusts or improves the engineering performance of the soil (Patel and Patel 2012). There are two types of soil stabilisation method: mechanical (i.e., through grading modification) and chemical (i.e., through changing the chemical composition of the soil).

2.7.1 Mechanical Stabilisation

This type of soil stabilisation is conducted by mixing various types of natural soils together to attain a mixture of a more suitable quality and particle size than each individual component. In order to meet various specifications and obtain the desired mixture, the percentage of finer and coarser particles in blended soil can be modified through adjustment of the proportion of each soil component. Also, the blend of materials can be reasonably located and compacted. The newly obtained soil combination should have improved strength properties through altered friction angle and cohesion. The soil's bearing capacity should also be enhanced by the improved stability of the composite (Ramadas, Kumar and Yesuratnam 2011).

2.7.2 Chemical Stabilisation

Chemical stabilisers can improve the engineering properties of soils, especially the weak/soft soils used in construction as subgrade material. Soil strength properties can be further developed by increasing cohesion. This can be helpful for the construction of reinforced structures such as embankments. Such treatments will eventually decrease construction expenditure (Patel and Patel 2012). Available additives for the chemical stabilisation of soft soils include silica, fly ash, lime, cement, rice husk, slag and silica fume (Petry and Little 2002).

Soil stabilisation can also be achieved using local natural and industrial resources including slag, which is able to bring about a significant improvement in the engineering properties of soils (Degirmenci, Okucu and Turabi 2007; Kavak and Akyarl 2007; Kim and Prezzi 2008; Tu 2009; Harichane et al. 2011; Kavak, Bilgen and Capar 2011; Seco et al. 2011; McCarthy et al. 2012). Several factors dictate the selection of appropriate stabilisers, including the condition of the construction site and the financial situation (Castro-Fresno et al. 2011).

2.8 Modelling of Contaminant Transport from Landfill

Nature, flora and fauna, and especially the humans in any region are susceptible to toxic contaminants in the environment. Public environment and health management officials can help to understand and quantify such pollutants and the relationship with their sources, aiding in the mitigation of the associated risks. This is conventionally achieved through the modelling of the lifecycle, transformation and transportation of the pollutant. The conservation of mass and Darcy's law are widely accepted as governing the groundwater flow process. Theoretical foundations of the solute-transport equation have been widely discussed (Bear, Sorek and Borisov 1997; Domenico and Schwartz 1998; Zheng and Bennett 2002). A theoretical outline for the analysis and modelling of the groundwater solute-transport process has been proposed by Reilly et al. (1987).

Dynamic groundwater systems are subjected to chemical concentration variations primarily caused by four distinct processes as follows: (1) advective transport, i.e., contaminant movement through groundwater flow; (2) diffusive transport, i.e.,

contaminant movement by concentration gradient; (3) dispersion, i.e., contaminant mixing at a relatively higher flow because of localised changes in the groundwater flow-velocity or their mixing and spreading in the form of dissolved molecules and ions through porous media resulting from the non-homogeneity of aquifer; (4) contaminant absorption, reaction or decay (Rowe and Booker 2005). Thus, the contaminant mass transported by advection per unit area per unit time, when dealing with contaminants in groundwater, is expressed as:

$$f = nvc = vac \tag{2.4}$$

where the soil effective porosity is expressed by 'n', groundwater velocity by 'v' (seepage velocity), Darcy velocity by 'va' and the contaminant concentration at a certain time and point by 'c'. The contaminants move from higher chemical potentials (concentrations) points to lower potential points during diffusion. When contaminant migration is associated with relatively high flows (as in many aquifers), there is a third transport mechanism to be considered, i.e. mechanical dispersion. Mechanical dispersion involves mixing that occurs because of localised changes in groundwater flow velocity. The dispersion of contaminants also involves mixing and spreading of the contaminants due to non-homogeneity in the aquifer. Although this mechanism is totally different from the diffusion process, it can be modelled similarly for majority of real-world applications.

Therefore, the two processes are often taken as a combined factor 'Dh', called the coefficient of hydrodynamic dispersion expressed as:

$$Dh=De+D_{md} \tag{2.5}$$

where 'De' is effective molecular diffusion coefficient dependent upon the type of the contaminant, and the mechanical dispersion coefficient is represented by 'D_{md}'. Dh is usually controlled by diffusion with only negligible dispersion if the transportation occurs in clayey soils that are intact, while the process is reversed for aquifers where dispersion is the dominant parameter.

Environmental protection purposes are satisfied if the landfill barrier system has a negligible influence on the quality of groundwater during the whole contamination

lifespan of the landfill. However, particular attention should be paid if there is an early landfill liner failure, since this may lead to significant increases in the peak impact of groundwater contamination. When heavy metals (Pb, Cr, Ni, Cd, etc.) are present in the landfill leachate, it must be examined for the influence of insulation on prolonging the service-life of the main leachate barrier and, subsequently, the contaminant transportation through a liner system (Rowe et al. 2004).

Rowe et al. (2004) developed contaminant transport software based on the governing theory which takes diffusion through the landfill liner into consideration. Diffusion through the liner system was simulated by setting the GCL porosity value at 1 as well as providing a coefficient of hydrodynamic dispersion value equal to the coefficient of permeation (P).

2.9 Soil Stability Analysis using the FEM

The finite element method (FEM) is extensively employed for analysing soil stability. A geotechnical software that has been developed based on FEM is PLAXIS. PLAXIS is a well-known geotechnical numerical modelling software capable of both two- and three-dimensional analyses for cases like slope deformation and stability. Moreover, inhomogeneous soil as well as time-dependent scenarios can also be simulated in PLAXIS (Brinkgreve 2002; Hammouri, Malkawi and Yamin 2008; Brinkgreve, Engin and Swolfs 2013). In certain views, PLAXIS can give qualitative representative data for the engineering behaviour of soils through the numerical models it produces. However, it is also stated clearly that the result might contain some predictable modelling and numerical errors. Thus, to obtain reliable outputs from the numerical modelling software, the users of PLAXIS need to select the correct soil parameters, understand the ‘staged construction’ process and the relevant limitations (Brinkgreve, Engin and Swolfs 2013).

PLAXIS 2D 2012 has been used for performing the numerical simulations in this study. The consolidation process is determined in the PLAXIS finite element modelling software on the basis of Biot’s consolidation theory. The characteristics and deformations of different soils can be analysed using this software and realistic results can be obtained (Chow and Chai 2007). The program incorporates a user-friendly graphical interface, enabling the user to simulate different aquifer scenarios. Stability

and deformation analyses of geotechnical structures are performed through finite element calculation methods. Furthermore, better analyses of the soil profile can be performed as per the input data, as the geometry model and mesh element can be constructed based upon the stated cross-section. In this study, the numeric workload can be reduced using axial symmetry or plane strain and hydrostatic pressure is considered due to the presence of groundwater. PLAXIS contains four subprograms – input, calculation, output and curves – and is equipped with the choice of six points/nodes or 15 nodes. Researchers have long used PLAXIS for the estimation of land subsidence due to groundwater extraction activities and the simulation results are widely considered reliable. Nonetheless, it is inevitable that some divergences of simulation results from actual situations will occur in all computer modelling programs, as the programming is developed from certain governing assumptions.

This study has utilised the Mohr-Coulomb model as a soil material model due to the representation of the linearly elastoplastic material model. The Mohr-Coulomb model is also appropriate for the 2D plane strain model run in this study. The formula of the material model is as follows:

$$\frac{1}{2}(\sigma_1 - \sigma_2) + \frac{1}{2}(\sigma_1 + \sigma_2)\sin\phi - c \times \cos\phi \leq 0 \tag{2.6}$$

The parameters incorporated in this equation are the principal stresses in the corresponding plane strain ($\sigma_1$and σ_2), material internal angle of friction (ϕ) and the material cohesion (c) (PLAXIS, 2014). The value of c was ignored as this model had incorporated sand as a base material which is classified as cohesionless material. PLAXIS has also used the following classical equation for performing the dynamic calculations:

$$F = M_a + K_u + C_v \tag{2.7}$$

In this equation; F represents the load vector whereas the letters M, K and C respectively correspond to stiffness, mass and damping matrices. Moreover, the subscript letters a, u and v symbolise the acceleration, displacement and velocity (Brinkgreve 2002).

The boundary effect is another critical factor that must be considered during the execution of seismic modelling as seismic energy may be amplified due to the bouncing waves triggered by the use of a boundary, thereby producing unrealistic results. Viscous boundary conditions were therefore applied to avoid the effect of bouncing. Lysmer and Kuhlemeyer (1969) have introduced the following equations for the viscous boundary:

$$\sigma_n = -C_1 \rho V_p v_x \tag{2.8}$$

$$\tau = -C_2 \rho V_s v_y \tag{2.9}$$

In the above equations, the pressure and shear wave velocity are symbolised by V_P and V_s, while the normal and shear stresses are represented by σ_n and τ. The C_1 and C_2 stand for relaxation coefficients while v_x and v_y represent the velocities in relevant directions (Brinkgreve, Engin and Swolfs 2013).

Chapter 3
Materials and Methods

3.1 Introduction

This chapter presents the details of the materials used in this research as well as the experimental and simulation work conducted in this study. The background of the selected materials, their chemical and physical characteristics, specimen preparation, and testing procedures/program are described. The modelling software employed to perform the numerical analysis is also described in this chapter. This chapter is organised as depicted in Figure 3.1.

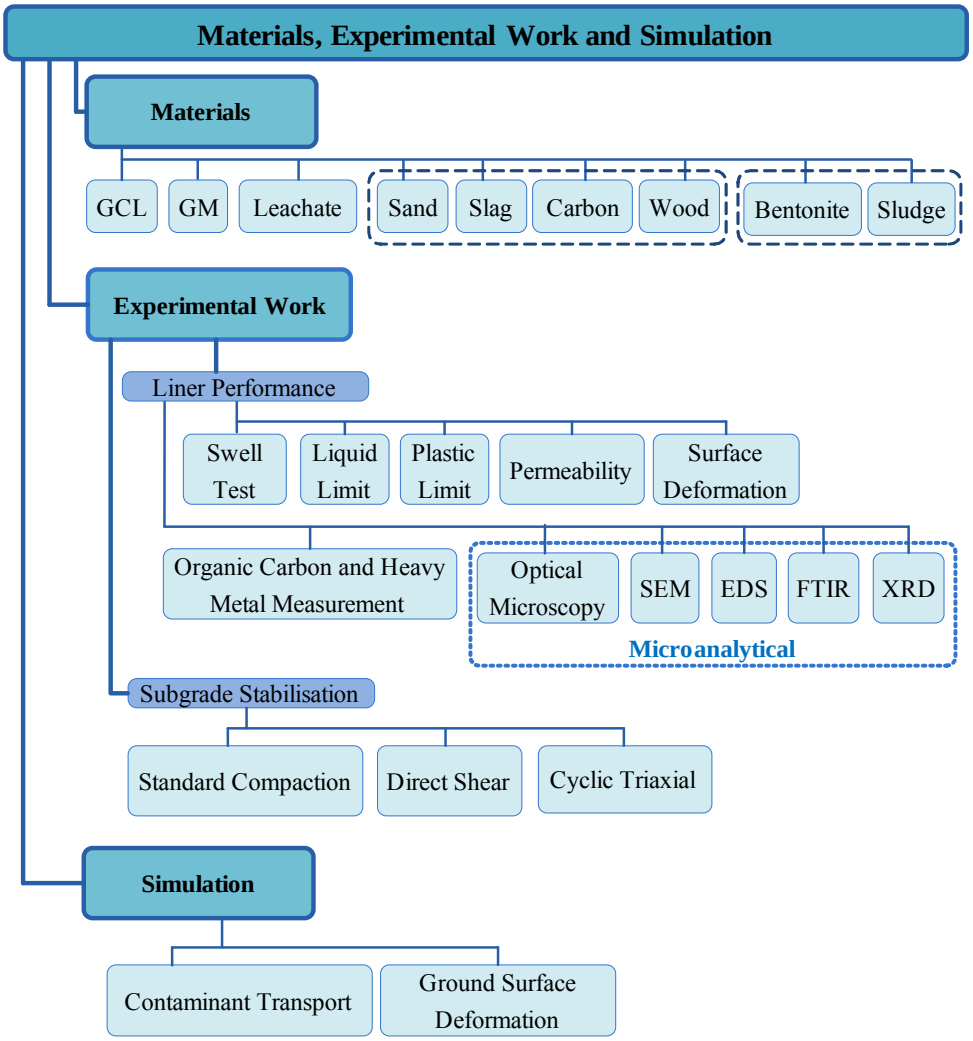

Figure 3.1 Structure of materials, experiments and simulation work

3.2 Materials

This research was designed to examine the performance of geosynthetic clay liner (GCL) as a landfill liner and its sand subgrade under various conditions when used in municipal solid landfill applications. Locally sourced materials were selected according to their wide application and availability in Perth, Western Australia.

3.2.1 Geosynthetic Clay Liner

This study utilised two types of GCL obtained from two different manufacturers. Each manufacturer supplied a different form of bentonite. One supplied GCLs containing bentonite in a powdered form and the other provided GCLs with granular bentonite. All of the GCLs were reinforced by needle punching. The samples were coded A and B. The specifications of the GCLs are listed in Table 3.1 and include mass/unit area, preliminary moisture content, carrier and cover of the geotextile and the type of bonding.

Table 3.1 Properties of GCLs

GCL Code	A	B
Bentonite form	Powder	Granular
GCL (mass/unit area) (gr/sqm)	4380	4905
Bentonite (mass/unit area) (gr/sqm)	~4000	~4600
Initial moisture content (%)	+ 9%	+ 7%
Bentonite type	Sodium	Sodium
Bentonite colour	White	Brown
Carrier geotextile	Woven	Woven
Cover geotextile	Nonwoven	Nonwoven
Bonding	Needle-punched	Needle-punched

All of the GCL samples came in the form of rolls about 4–8 m in length and 2–4 m in width. Because most of the experiments only required GCL samples with dimensions of about 200 mm x 200 mm, some of the samples were cut into 500 mm x 500 mm pieces to simplify storage. All of the GCL samples were kept inside plastic sealed bags during the research to prevent any change in moisture caused by climatic changes.

3.2.2 Geomembrane

Geomembrane is also employed in some landfills as a leachate barrier due to its impermeability. In this study, however, the main role of the geomembrane was to protect the GCL from the vertical load caused by the gravel material, dumped solid waste and heavy vehicles operating during the landfill's operation. The geomembrane functioned as a protective layer for the GCL and prevented the GCL from being punctured or experiencing extreme deformation under any load. The geomembrane used in this experiment was a low-density polyethylene (LDPE) supplied by a local supplier in Perth, Western Australia. It can be classified as smooth geomembrane of 0.75 mm thickness. Table 3.2 presents the characteristics of the geomembrane utilised for this research work.

Table 3.2 Properties of geomembrane (Global Synthetics 2010)

Properties	Unit	Test method	Value
Thickness average (-5%)	mm	ASTM D 5199	0.75
Thickness minimum (-15%)	mm	ASTM D 5199	0.68
Density (max)	g/cm^3	ASTM D 792	0.939
Tensile properties:			
Break strength	kN/m	ASTM D 6693 (Type IV)	20
Break elongation	%	ASTM D 6693 (Type IV)	550
Tear resistance	N	ASTM D 1004	70
Puncture resistance	N	ASTM D 4833	210
Carbon black content	%	ASTM D 1603	2.0–3.0
Carbon black dispersion	Cat	ASTM D 5596	1–2
Oxidative induction time (OIT)	Min	ASTM D 3895	100

3.2.3 Leachate

The leachate used in this research were obtained from two different locations. The first leachate specimen (L1) was collected from Redhill Landfill in Toodyay Road, Red Hill, Western Australia, which is under the management of the Eastern Metropolitan Regional Council and is classified as a Class IV Waste Management Facility. Under licence from the Department of Environment, the Redhill Waste Management Facility is allowed to receive Class I-IV waste. This includes residential and domestic waste including contaminated waste (contaminated soils and waste coming from industrial processes) and asbestos material. The leachate was collected from the leachate collection system outlet point before it entered the leachate treatment system.

The second leachate specimen (L2) was obtained from Tamala Park Landfill, which is under the management of the Mindarie Regional Council, Western Australia. The landfill is located at 1700 Marmion Avenue, Tamala Park, Clarkson, Western Australia and is licenced as a Class 2 waste disposal facility, accepting mostly biodegradable waste. As well as the biodegradable waste, Tamala Park also accepts a wide range of waste such as general and hazardous household waste, car bodies, recyclables, paint, gas bottles and e-waste, including batteries, computers and mobile phones. The Tamala Park landfill also makes use of a leachate circulation system which means that the landfill leachate returns in order to speed up the biodegradation of biodegradable materials. The leachate sample from the Tamala Park landfill was obtained by pumping it out and collecting it from the leachate recirculating pipe system before it re-entered the landfill.

Generally, leachate contains organic and inorganic contaminants in high concentrations that vary from one landfill to another. Leachate often contains heavy metals and xenobiotic organic compounds (Christensen 2012). All of the leachate samples were stored in a refrigerator at a temperature of about 4°C in order to reduce the possibility of significant changes in the concentration of the contaminants due to the action of organic matter in the leachate. The leachate samples were then analysed in the Chemical Laboratory at Curtin University to obtain the concentration of the dominant parameter that would be used to examine the phenomenon of contaminant transport through the GCLs. The contaminant content of the leachate is presented in Table 3.3.

Table 3.3 Selected leachate parameter

Parameter	Unit	Concentration	
		L1	L2
pH	-	8.1	8.3
TOC	mg/l	220	430
Mn	mg/l	0.047	0.012
Fe	mg/l	6.981	4.209
Pb	mg/l	0.93	0.18
Cr	mg/l	0.93	0.21
Cd	mg/l	4.5	1.03
Ni	mg/l	6.99	2.35

3.2.4 Sand

In order to simulate solid waste landfill liner construction, sand was chosen as the subgrade upon which to rest the GCL layer. The sand used in this experiment was locally sourced from the Baldivis area, about 50 km south of Perth, Western Australia. Baldivis sand is also well-known as yellow sand and has been widely used in geotechnical construction projects in Western Australia. It is also popular for making concrete and mortar, footings and also for carrying out mixing. The particle size distribution of Baldivis sand is presented in Figure 3.2.

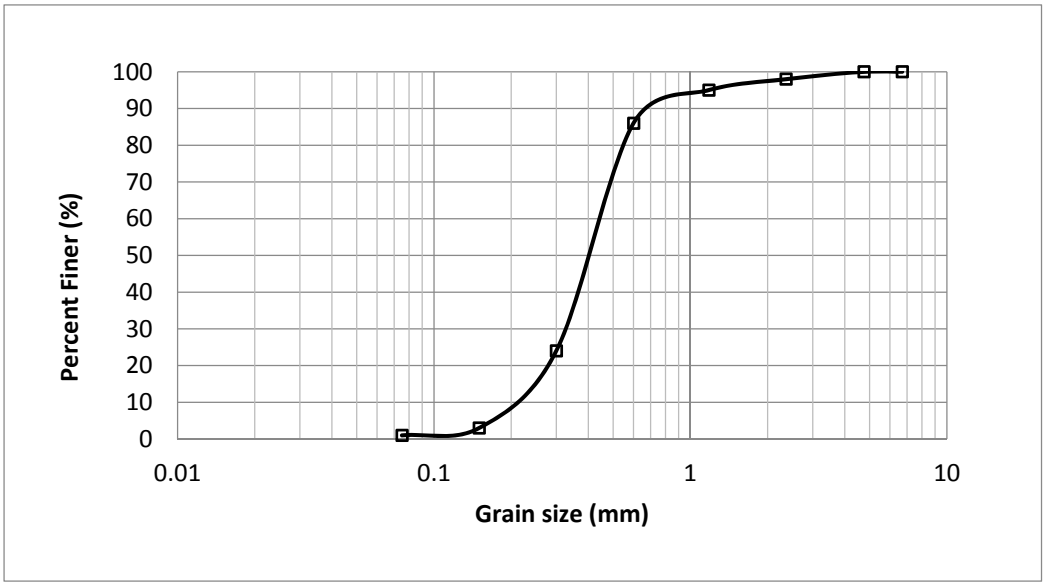

Figure 3.2 Grain size distribution curve

3.2.5 Slag

Slag was used as an additive for the sand subgrade. The slag used was classified as ground granulated blast furnace slag (GGBS). The slag used in this experiment was obtained from a local supplier, BGC Cement, Western Australia. GGBS is a by-product of steel industry manufacturing and has a similar chemical composition to Portland cement (PC), containing silica (SiO_2), calcium oxide or quick lime (CaO), magnesium oxide (MgO), and aluminium oxide (Al_2O_3). The chemical compounds and the physical properties of the slag are listed in Table 3.4 and Table 3.5 respectively.

Table 3.4 Chemical composition of GGSB (Ecocem Ireland Ltd 2012)

SiO_2	CaO	MgO	Al_2O_3
35%	40%	8%	10%

Table 3.5 Physical properties of GGBS (Ecocem Ireland Ltd 2012)

Colour	Relative density	Bulk density: vibrated (tonnes/m^3)	Bulk density: loose (tonnes/m^3)	Surface area (m^2/kg)
Off-white powder	2.85–2.95	1.2–1.3	1.0–1.1	400–600

3.2.6 Wood

Aspen timber was chosen as an additional material to be introduced to the sand subgrade, in order to examine any consequent changes in the sand shear strength using the direct shear test method. Only a small amount of wood (wood sticks in dimension of 3×3×20mm) was needed to run the direct shear test. The specific gravity of the wood was 0.36 and 12% of the initial moisture content (Kretschmann 2010). The aspen timber properties are presented in Table 3.6.

Table 3.6 Properties of aspen timber (Kretschmann 2010)

Specific gravity	Moisture content (%)	Modulus of elasticity (c) (MPa)	Modulus of rupture (kPa)	Shear parallel to grain (kPa)
0.36	12	7,700	37,000	5,000

3.2.7 Carbon

Sand composite containing carbon was prepared in order to examine sand subgrade stability. The carbon used in this research was granular activated carbon (GAC) obtained from a local supplier in Perth, Western Australia. The GAC was widely used in the water purification process and any other liquid filtration to remove contamination. This type of carbon has a very large adsorption surface area of about 650–1000 m^2/gram. It was made from one or more carbon sources such as coal, lignite, wood or nutshells by a combustion process in the absence of air. The properties of carbon are presented in Table 3.7.

Table 3.7 Properties of GAC (Laine and Calafat 1989)

Specific gravity	Moisture content (%)	Modulus of elasticity (*c*) (MPa)	Modulus of rupture (kPa)	Shear parallel to grain (kPa)
0.36	12	7,700	37,000	5,000

3.2.8 Bentonite

The bentonite clay collected from Sibelco Australia Limited Factory in Western Australia was used as a cohesive soil. The specific gravity of bentonite clay is 2.75 and its chemical composition is shown in Table 3.8.

Table 3.8. Chemical composition of bentonite clay

Chemical composition	Proportion (%)
Smectite	>74%
Quartz	<18%
Kaolinite	<8%

As described in Figure 3.3, the main component of bentonite is silicon (Si), followed by oxygen (O), aluminium (Al), magnesium (Mg), sodium (Na), titanium (Ti), iron (Fe) and calcium (Ca). The high proportion of silicon in bentonite is indicated by both the high peak in the line spectrum graph and the most dominant colour in the elemental mapping. Basically, the presence of the smectite group, quartz and kaolinite materials are illustrated by all components.

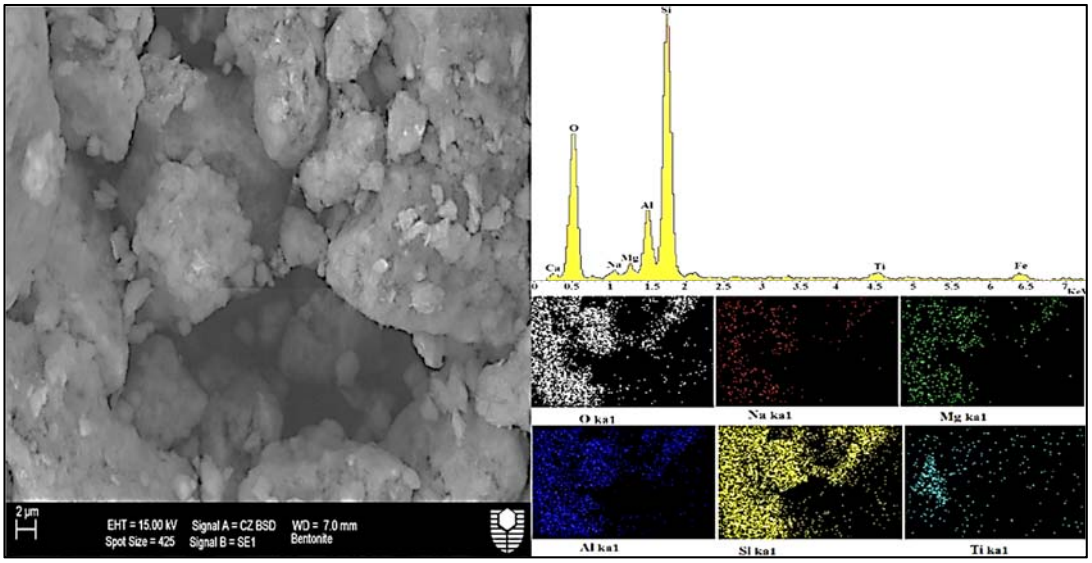

Figure 3.3 SEM micrograph and EDS of bentonite

3.2.9 Sludge

The sewage sludge was gathered from the Beenyup Wastewater Treatment Plants (WWTP) in Perth, Western Australia. Figure 3.4 shows the key components of sewage sludge by SEM/EDS analysis. The line spectrum behaviour of sludge and bentonite seem roughly similar at first glance, but sludge shows additional peaks for calcium, iron and potassium (K). Based on the EDS data, Si, Al and Fe are the main components of sewage sludge, while the existence of oxygen atoms implies that SiO_2, Al_2O_3 and Fe_2O_3 are the basic oxides for a pozzolanic reaction.

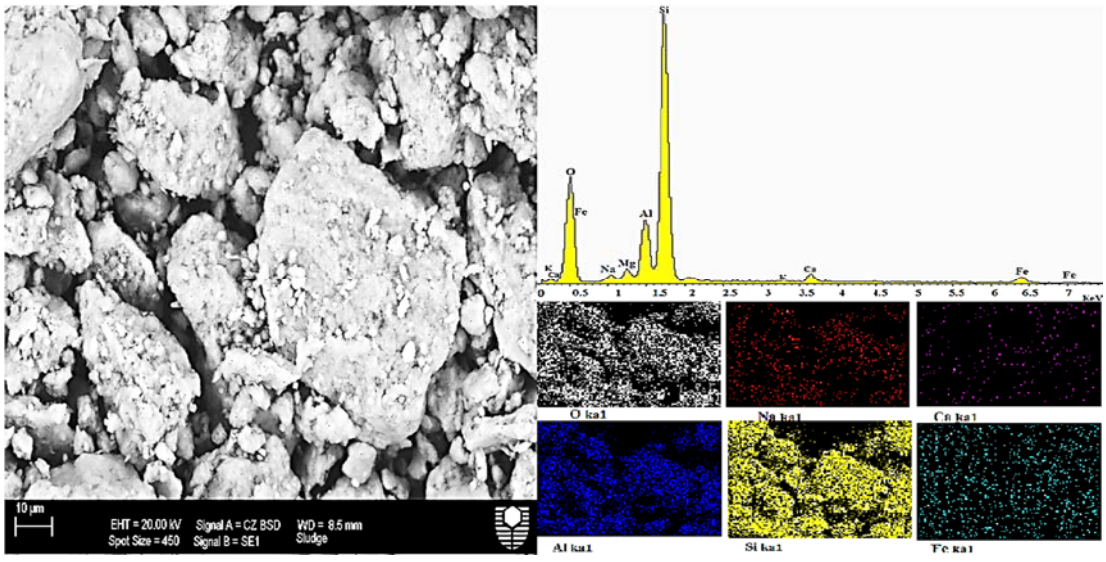

Figure 3.4 SEM micrograph and EDS of sludge

3.3 Experimental Program

The experimental program of this research mainly focused on investigating the performance of three main materials including geosynthetic clay liner (GCL), bentonite and sand. A series of laboratory tests was used to examine GCL as landfill liners while another laboratory experiment was conducted to study the stabilisation of bentonite and sand as liner subgrade in a landfill.

The basic laboratory tests selected to examine GCL performance included the swell test, liquid and plastic limit tests and the permeability test. The extended experimental tests investigating the performance of GCL as landfill liner included the physical deformation test, the effect of uplifting water pressure and leachate infiltration. Microanalysis was also done to examine any microscopic and elemental changes to bentonite particles inside the GCL after permeation with different liquids. The microanalysis observation consisted of optical microscopy, scanning electron microscopy (SEM), energy-dispersive X-ray spectroscopy (EDS), Fourier transform infrared spectroscopy (FTIR) and X-ray diffraction (XRD).

Another series of experiments examined the effect of additives on the stability performance of bentonite and sand as landfill subgrade. The main laboratory test used to investigate the stability of bentonite and sand was the direct shear test, however the cyclic triaxial test was also used to examine liquefaction of sand.

3.3.1 Test for Liner Performance

3.3.1.1 Swell Test

The swell tests were conducted based on two methods. The first method was to measure the free swelling properties of bentonite particles using distilled water and kerosene following the Indian Standards (1977). The second method involved a one-dimensional consolidation technique to measure the swelling of the GCL.

For the first swell method, 2 g bentonite was collected from each of the GCL samples. Two graduated cylinders were prepared to run the experiment. Two grams of bentonite were poured into each cylinder. The first cylinder then was filled with 100 ml distilled water and the other with the same volume of kerosene. All samples were then left for

24 hours to fully swell. The final volume of each cylinder was then recorded and calculated to obtain swell index.

The second swell test to measure the GCL swelling was conducted using a swelling test kit (Figure 3.5). To measure the swelling behaviour of each GCL, the GCL sample was cut to fit into the cylindrical ring. Prior to the test, the sample was positioned inside the cylindrical ring on top of the porous stone and compacted. Water was added to the container to soak the sample and any change in the sample due to swelling was recorded.

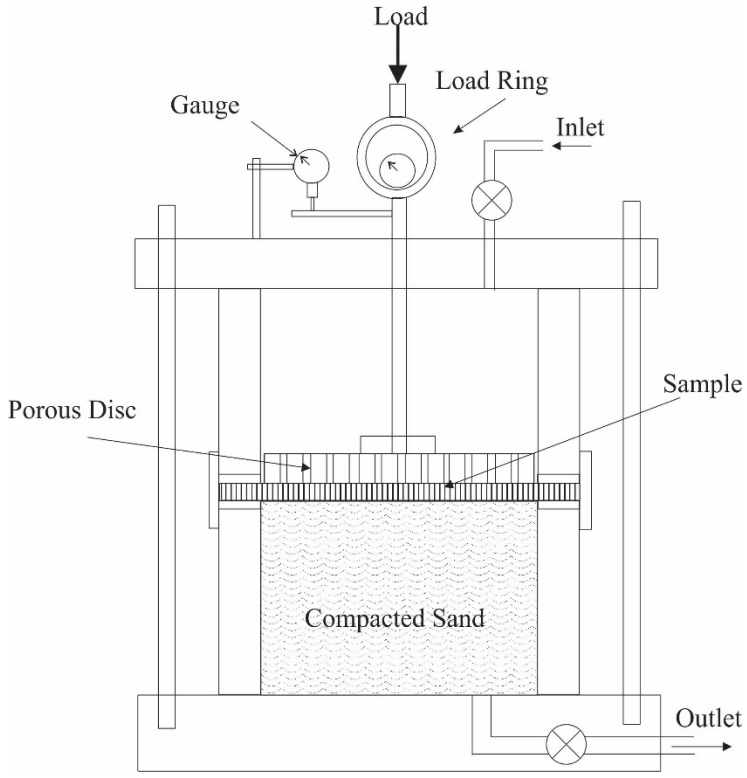

Figure 3.5 Sketch of GCL swelling test kit

3.3.1.2 *Liquid Limit*

The liquid limit test was performed using the cone liquid limit method according to Standards Australia (2002). The test required a cone penetrometer and a bentonite sample mixed with distilled water. About 250 g of the sample was required to run the test. After mixing with water, the mixture was kept for at least 24 hours for curing. The curing process was performed by putting the mixture in a closed container to minimise evaporation.

Once the curing stage was complete, the sample was remixed thoroughly and used to fill the cup, after which the top of the sample was trimmed to level the surface. The cup was placed into the penetrometer under the cone. The cone tip was positioned to contact the sample surface and the reading gauge was reset to zero. The shaft was released for 20 seconds and allowed the cone to penetrate into the sample and the displacement of the cone was measured using the gauge. Water was added and mixed with the sample to run the next test.

The same procedure was repeated until the range of the displacement of the cone was achieved. The expected displacement ranged from 15 to 25 mm. At least four points were needed in that range to plot the liquid limit and the displacement. In practice, two values in the 15–20 mm range and two values in the 20–25 mm range were expected to be obtained. Referring to the graph, the value of the liquid limit at 20 0m displacement was determined to be the liquid limit.

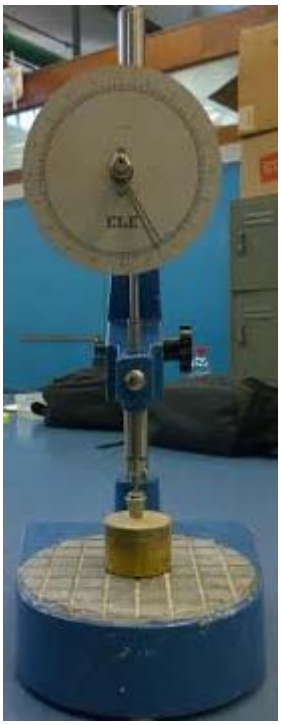

Figure 3.6 Liquid limit test kit

3.3.1.3 Plastic Limit

The plastic limit was measured in accordance with Standards Australia (2009a), which requires the mixing of a small amount of water with the soil material and the rolling of the mixed material into a thread-like shape having a diameter of about 3 mm. The

procedure is repeated by adding water until the mixed soil material begins to crumble at the 3 mm diameter. The rolled material is weighed and placed in a drying oven to obtain the water content of the sample, which represents the plastic limit (PL).

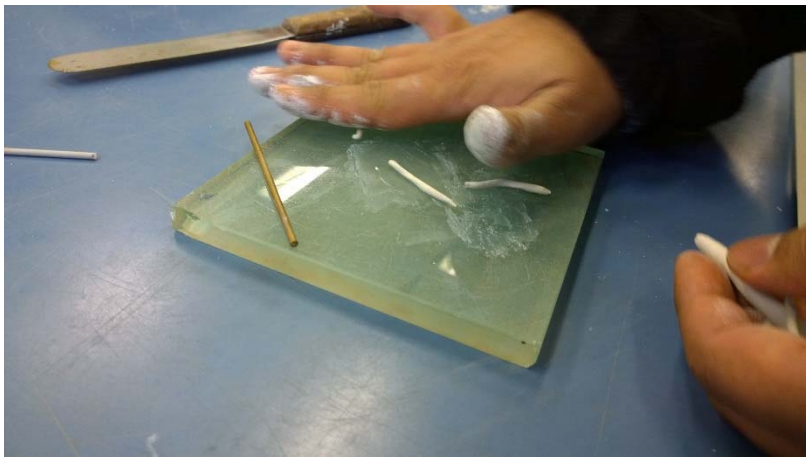

Figure 3.7 Plastic limit measurement

3.3.1.4 Plasticity Index

The plasticity index can be determined according to Standards Australia (2009b) once the liquid limit and the plastic limit have been obtained. The plasticity index (PI) is calculated as follows:

$$PI = LL - PL \tag{3.1}$$

Where the plasticity index is expressed by 'PI', liquid limit by 'LL' and plastic limit by 'PL'. In general, the degree of plasticity of soil can be classified as presented in Table 3.9.

Table 3.9 Plasticity index and soil description (Burmister 1949)

Plasticity index (PI)	Soil description
0	Non-plastic
1–5	Slightly plastic
5–10	Low plastic
10–20	Medium plastic
20–40	High plastic
> 40	Very high plastic

It is expected that all of the materials used in this experiment will fall into the 'very high plastic' category, however, the value of the PI will be useful for the hydraulic performance discussion.

3.3.1.5 Permeability Test

The permeability test, which is also known as the hydraulic conductivity test, was performed according to methods provided by Standards Australia (2001a) with some alterations based on the flexible wall method set out in ASTM D5084-10 (2010) and conditions which may affect the GCL in landfill applications such as hydraulic head. The hydraulic head was calculated with reference to the average leachate level which developed during landfill operation.

A transparent cylinder with a diameter of 200 mm was used to perform the hydraulic conductivity test. The use of the transparent cylinder allowed visual monitoring throughout the test. Circular PVC plates were used as the bottom and the cap and were equipped with two fittings per plate. The fittings were connected to the hose to allow the water to flow in.

Prior to the hydraulic conductivity test, the GCL samples were prepared by cutting them into a circular shape so they could be fitted into the permeameter cylinder. They were cut carefully using a very sharp knife in order to prevent any bentonite loss along the edge. The cutting GCL sample was positioned inside the mould. A thin layer of silicone glue was applied along the GCL edge and cylinder wall to prevent any side wall seepage during the test. The sample was allowed to stand for 24 hours to let the silicon glue dry. Once the glue was dry, water was admitted into the cylinder to saturate the sample. The permeability test started with the connection of the mould to the pressure-volume controller. The water pressure in the device was adjusted based on the average hydraulic gradient of the leachate in the landfill.

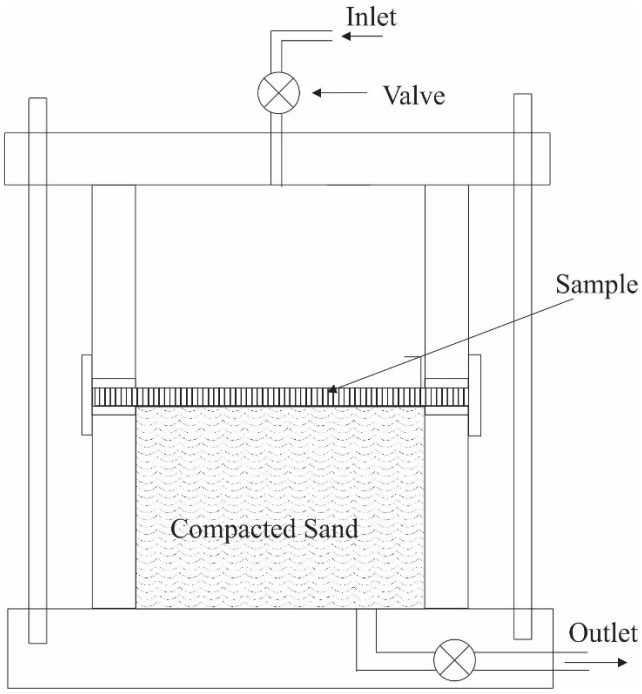

Figure 3.8 Sketch of the permeability apparatus

3.3.1.6 Surface Deformation

The examination of GCL surface deformation was conducted using the same apparatus used to measure the hydraulic conductivity, with some modifications. The top cap of the apparatus was modified to accommodate a rod to transfer the vertical load which would be applied to the GCL. During the experiment, the GCL was rested on a layer of compacted sand under a circular layer of gravel to simulate real conditions in the landfill. A perforated steel plate which connected to the loading rod was used to apply the load to the gravel.

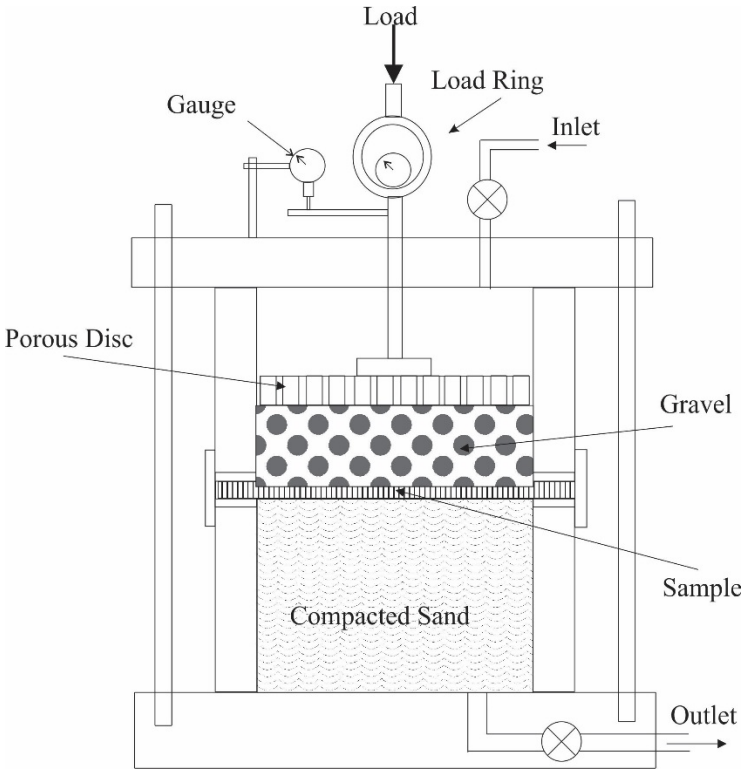

Figure 3.9 Sketch of the modified apparatus

After completion of the hydration stage, load was then gradually applied to the rod to exert pressure on the GCL sample through a layer of gravel. After reaching the intended pressure, the pressure was kept constant for hydration purpose. This pressure was selected based on a prediction of the load that might be received by the GCL during landfill operation, coming from the protection layer (gravel) and the weight of the solid waste itself. After for period of time under loading, the profile of the GCL surface was captured and the thickness in some areas was recorded. The same procedure was performed for an investigation of the effect of geomembrane on the deformation response of the GLC, except in the sample preparation, the geomembrane was laid on the GCL under the gravel layer.

3.3.1.7 Measuring Total Organic Carbon and Heavy Metal in the Leachate

In this experimental work, the leachate quality was tested before and after passing through the GCL. The GCL was placed in the middle of a transparent cylinder cell. Leachate flowed into the upper part of the cell above the GCL. Pressure was applied to induce the leachate to pass through the GCL. The concept of the leachate quality

test is quite similar to the permeability test. The only difference between those two tests was the liquid used in the test.

Figure 3.10 TOC analyser

After some time, the leachate infiltrated through the GCL and was collected in a sample bottle. The test was run in a controlled temperature room and any contact of the leachate with the open air was minimised by covering the bottle sample with a sealed plastic bag. Once there was sufficient leachate obtained, the sample bottles were collected and stored in the refrigerator. TOC testing was conducted using a laboratory Total Organic Carbon (TOC) analyser namely Sievers 5310 C (Figure 3.10), while heavy metal content analysis was performed using a spectrometer (Figure 3.11).

Figure 3.11 Spectrometer

3.3.2 Microanalytical Analysis

The microanalytical analysis was performed to examine any changes to the GCLs (geosynthetic and bentonite) on the microscopic scale. The microanalytical experiments involved devices or techniques such as optical microscopy, SEM, EDS, XRD and FTIR.

3.3.2.1 Optical Microscopy

The microscopic analysis was conducted using a Nikon SMZ800 stereo microscope equipped with Image Pro Plus software. The Nikon SMZ800 has a spot insight colour camera that can produce low noise and remarkable images. The software has the ability to deliver a live image on the computer screen, as well as to control the panning, focusing and exposure setting. The microscopic image captured can be saved directly to the PC's storage as a high quality image and can be transferred for editing, printing and documentation purposes.

Figure 3.12 Optical microscopy (Nikon SMZ800)

3.3.2.2 Scanning Electron Microscopy (SEM)

A scanning electron microscope (SEM) was used for the investigation of microstructure and morphology. The model of SEM used was the 40XVP Evo Zeiss with 15 kV and 20kV of accelerating voltage (Figure 3.13). The information obtained from the SEM included the morphology, topography and composition of the sample.

Figure 3.13 Evo Zeiss SEM

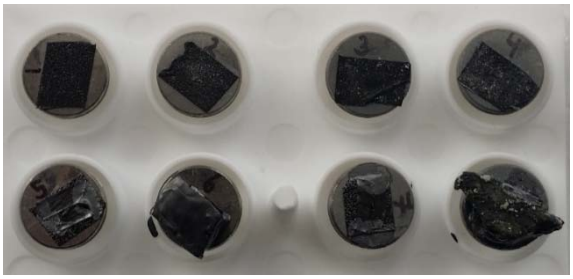

Figure 3.14 Sample for SEM

3.3.2.3 Energy-dispersive X-ray Spectroscopy (EDS)

Energy dispersive spectroscopy (EDS) was employed to detect atom types on a surface area containing multiple atoms. EDS is integrated into the SEM and most SEM devices are equipped with this feature. EDS generates the information obtained from the characteristics of the X-rays emitted when electrons of the outer shell of an atom move to the deeper layers of the atom's skin. The energy of the electron beam in the form of X-rays is detected and measured by the energy-dispersive spectrometer (EDS), providing output in the form of graphs with peaks representing the elements. EDS can also perform element mapping by assigning different colours to each of the elements found on the surface of the material. EDS was also used to quantify the percentage of

each element (Goodge 2011). Oxford Inca software was employed to provide the illustrations. The X-ray spectra, the qualitative and quantitative data and also the element maps were illustrated using the Oxford Inca software and the SiLi X-ray detector（Figure 3.15）.

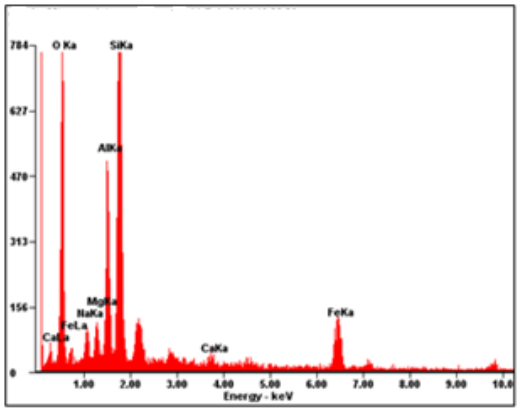

Element	Wt%	At%
OK	39.17	55.50
NaK	03.16	03.12
MgK	02.38	02.22
AlK	12.50	10.50
SiK	27.67	22.33
CaK	01.19	00.67
FeK	13.93	05.65
Matrix	Correction	ZAF

Figure 3.15 Sample of EDS result

3.3.2.4 X-ray Powder Diffraction (XRD)

Soil sample mineral compositions were identified using X-ray diffraction (Bruker D8 Advance) in conjunction with the LynxEye detector. The XRD was used to evaluate the changes in the mineral samples (in this case bentonite) when the leachate infiltrates the GCL samples. The X-ray diffraction technique (XRD) is a method of material characterisation usually used to identify the crystalline phases of the material by determining the structure of lattice parameters. The X-ray radiation has a high energy of about 200 eV to 1 MeV as a result of the interaction between the electrons from the external electron beam inside the atomic shell (Kunze and Dixon 2003).

The XRD analysis can be performed qualitatively, quantitatively or a combination of the two. In this study, the qualitative analysis was chosen because the purpose was to determine whether any mineral changes occurred after the permeation of leachate through GCL.

Figure 3.16 X-Ray diffraction (Bruker D8 Advance)

3.3.2.5 Fourier Transform Infrared Spectroscopy (FTIR)

Chemical analyses are performed using Fourier transform infrared (FTIR) spectroscopy. The absorption of different light wavelengths by a sample is correlated against an established standard in order to identify the chemical composition of the specimen. In contrast to dispersive spectrometers that can only measure narrower wavelength ranges, simultaneous spectral data collection over wider ranges can be performed using FTIR spectrometers. FTIR spectroscopy has opened up novel applications for infrared spectroscopic methods, thereby rendering dispersive infrared spectroscopy almost obsolete apart from some near-infrared applications. A PerkinElmer Spectrum 100 FTIR Spectrometer (Figure 3.17) was used to perform the Fourier transform infrared spectroscopy (FTIR).

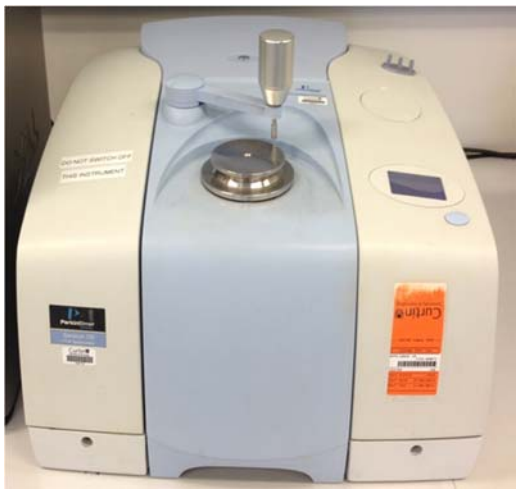

Figure 3.17 FTIR device

3.3.3 Test for Subgrade Stabilisation

3.3.3.1 Standard Compaction Test

The compaction test was conducted to obtain the soil sample optimum moisture content (OMC) and maximum dry density (MDD) according to Standards Australia (2003a). A compaction mould and a hammer (rammer) were the main equipment needed to perform the test. The sample was prepared by removing the initial sample moisture content by oven drying at a temperature of 100±1ºC for 24 hours. The soil sample was then sieved using a sieve with an aperture of 4.76 mm. Sample mixing was done after adding a certain volume of water. The sample was kept in a sealed container for 24 hours for curing.

The sample was placed into a mould at a certain even height in each layer and compacted using a standard compaction hammer. The same number of blows at a specific height was applied in every layer. Once the compaction was finished, the weight of the mould containing the sample was calculated. Moisture content was measured in three parts of the sample, at the bottom, middle and top. The same procedure was performed for other amounts of water added. The dry density and moisture content were plotted onto a graph to produce a compaction curve. The compaction curve peak point corresponded to the MDD and OMC of the sample.

Figure 3.18 Compaction mould and standard compaction hammer

3.3.3.2 Direct Shear Test (DST)

In order to examine the shear performance of the landfill subgrade (bentonite mixture and sand composite), a series of DST tests were conducted for both materials according to Standards Australia (2001c). The direct shear test was conducted using an automated direct shear machine (Figure 3.19). Various normal stresses – 50, 150 and 250 kPa – were applied for each test.

Figure 3.19 Direct shear device

The additional mixture for the bentonite was sludge while the additives used for the sand were slag, wood and carbon. The percentage of each additive is detailed in Chapter 5. The sample was prepared based on its optimum moisture content and maximum dry density which were determined by standard Proctor compaction test. A porous stone was installed into the shear box and the sample was poured up to a certain height and compacted using a small tamper. Once the compaction was finished, a porous plate was positioned on top of the sample followed by the cap load positioning. The shear box was then filled with distilled water and the first normal load was applied and the consolidation phase started. After being consolidated for 24 hours, the horizontal load was applied. The same procedure was carried out for the second and the third of the normal loads.

3.3.3.3 Cyclic Triaxial Test

The cyclic triaxial test was performed to examine the performance of sand and sand mixture with slag with regard to liquefaction. The test was run according to ASTM D5311/D5311M-13 (2013). An automated triaxial machine was used to perform this experiment (Figure 3.20).

Figure 3.20 Automated triaxial equipment

Prior to the cyclic triaxial test, some of the following procedures were followed. The sample was prepared at height of 137 mm and a diameter of 63 mm using a specific mould. The top of the specimen base was placed under a soaked porous stone and filter paper. The sample was then placed and compacted using a small tamper. Another

porous stone and soaked filter paper were laid on top of the sample followed by the specimen cap. A thin membrane covered the sample from the specimen base to the specimen cap. Two pairs of under-tension O-rings were used at the specimen base and cap to seal the membrane.

The cyclic triaxial test has a number of phases, the first of which is the saturation phase. Before the saturation phase, a certain back pressure was applied to the sample after which water was allowed to flow into the sample. The degree of saturation (B parameter/Skempton's pore pressure) should not be less than 0.95, which indicates that adequate saturation of the sample has been achieved. After saturation, the sample was consolidated isotropically for at least 24 hours under an effective confining pressure which corresponds to field conditions. Following the completion of the consolidation phase, a uniform frequency and cyclic loading were applied to the sample at various cyclic stress ratios (CSR).

3.4 Simulation Analysis

Simulation analyses were performed to observe the phenomenon of contaminant transport from leachate to the surrounding landfill area and to investigate the stability of the landfill area against groundwater level change and dynamic loading. Two types of modelling software with different features were used to perform the simulation analysis.

3.4.1 Simulation of Contaminant Transport

The contaminant transport analysis was performed using Pollute v.7 software. The Pollute v.7 software was provided by Curtin University, Western Australia (Figure 3.21). Pollute v.7 software mainly focuses on contaminant transport and is very useful for forecasting the concentration of contaminants at various soil depths and times.

Figure 3.21 Pollute v.7 interface

Table 3.10 shows the stages for running the simulation. The first stage was to choose the model that would function as the basic scenario. In this case, a blank model was chosen since this provides the user with the freedom to develop custom scenarios for the simulation. The initial data was then inputted to the model followed by the layer data input and boundary set up. Some default input values were also available to assist the user when some parameters could not be obtained. Once these stages were complete, the model could be run by choosing the output.

Table 3.10 Procedures to run Pollute v.7

Stage	Option/Input/Output
Model selection	Blank model
Initial data input	Total of layers, thickness of each layer, total depth and the Darcy velocity
Input the layer data	Number of sublayers, thickness, layer parameters i.e. dry density, porosity, permeability, coefficient of hydrodynamic, dispersion and distribution coefficient
Determine the boundary conditions	Top and bottom boundary
Run the parameters	Concentration vs time, Concentration vs depth, depth vs time

In order to obtain a precise simulation result, a calibration should be performed with reference to field data. The model should reflect field conditions by performing a validation stage using one of three methods, being the chi squared, root square of errors and sum squared for errors methods.

Another stage was the sensitivity analysis. This was conducted to confirm that the result was highly flexible to different situations and changing conditions (Malczewski 1999). The sensitivity analysis was performed by systematic trial and error with relation to some of the default values (i.e. permeability, dry density and porosity).

3.4.2 Simulation of Ground Deformation

In this study, the stability of the landfill liner covered a subsidence as a result of two different things, which were changes in the groundwater level and various loads. Numerical analysis was also carried out to explore the stability of the landfill. The subsidence of landfill area could trigger liner failure and cause leachate to be released into the surrounding soil and contaminate the groundwater.

PLAXIS 2D 2012 software was used to perform the stability analysis. The software used was under the licence of Curtin University, Western Australia. PLAXIS was chosen due to its ability to perform consolidation analysis based on the consolidation theory of Biot. This software has the advantage of being able to analyse the deformation of various soil layer types close to real conditions (PLAXIS 1998). Table 3.11 presents the main stages involved in the PLAXIS simulation. The calculations in this software were based on the finite element method which is commonly used in the geotechnical field for such things as soil stability and deformation.

Table 3.11 Stages of PLAXIS 2D 2012

Stage	Option/input/output
Initial option	Plane strain/axis_ symmetry 6/15 nodes Geometry dimension
Create the model	Draw the geometry Input the properties Mesh generation Set the fixities
Calculation	Method of calculation

The Mohr coulomb model was used for all PLAXIS model since it represented a 'first-order' estimation of soil behaviour. Besides the common Mohr-Coulomb criterion, various advanced characteristics were also used, such as those listed in Table 3.12.

Table 3.12 Model properties in PLAXIS

Property	Symbol	Unit
Saturated unit weight	γ_{sat}	kN/m3
Unsaturated unit weight	γ_{unsat}	kN/m3
Poisson's ratio	υ	N/A
Reference elastic modulus	E_{ref}	N/m^2
Reference cohesion	c_{ref}	kN/m^2

Various stages can be simulated throughout the whole construction using the 'staged construction' function, which contains options like the activation or deactivation of certain loads, geogrids, interfaces and soil layers through different stages of the analysis. One of the benefits of this feature is that the time effect can be taken into account (Brinkgreve, Engin and Swolfs 2013).

Phi-c reduction is an applicable approach to determine the factor of safety. In this approach, two strength parameters 'θ' and 'c' are reduced to reach the critical state of failure occurrence for slopes (Hammouri, Malkawi and Yamin 2008).

Chapter 4
Performance of the Geosynthetic Clay Liner

4.1 Introduction

This chapter presents the investigation into the performance of geosynthetic clay liners (GCLs) under various conditions. In this experiment, the GCLs were presumed to function as leachate barriers in municipal solid waste landfills. The investigation emphasised the GCLs' hydraulic performance, physical or surface deformations after being subjected to confining loads, and microscopic observations of the GCLs when exposed to different liquids.

In the first stage, the hydraulic performance of the GCLs was investigated in conjunction with their swelling behaviour. Prior to examining the swelling behaviour of the GCLs, Atterberg limits tests were performed to obtain the plasticity index (PI) of the bentonite contained in the GCL. The PI can be calculated by obtaining the plastic limit and liquid limit of the bentonite. The free swell test was also performed to determine the free swell index of the bentonite. The results of the Atterberg limits tests and free swell index test are discussed in relation to the swelling behaviour and hydraulic performance of the GCLs. The experiment involved two types of GCL containing different forms of bentonite (powder and granular), supplied by two different manufacturers.

The following investigation was performed to examine the responses of the GCLs to loading conditions. The loading conditions were based upon actual loads that the GCL could be subjected to when serving as landfill liner. In this experiment, the GCLs were rested on top of a subgrade layer which was sand and under a layer of gravel (spherical) which functioned as part of the leachate collection system. Any physical deformations in the GCLs were discussed. Geomembrane was also utilised in this section as a secondary material forming part of the additional liner material.

The subsequent experiment was conducted to examine the response of the GCLs to backward pressure from groundwater. This experiment only utilised one type of GCL (GCL 'A'), which consisted of bentonite in powder form. In this stage, the uplift pressure effect to the GCL is also discussed.

The next stage was to investigate the response of bentonite when exposed to two different types of liquid, leachate and salt solution. The investigation focused on microscopic observation, using scanning electron microscopy (SEM), X-ray diffraction (XRD) and Fourier transform infrared spectroscopy (FTIR) to examine any changes in the mineralogy of bentonite.

4.2 Experimental Details

In this section, the details of each stage of the experiment are presented, along with sample preparation and test methods.

4.2.1 Materials Tested

This experiment used the GCLs as the primary material, yellow sand as the subgrade material and gravel as the underlying layer. Two types of GCLs produced by two different manufacturers were employed in this research. For the investigation of the hydraulic performance and physical response, the samples were labelled 'A' and 'B'. GCL sample 'A' contained powdered bentonite and GCL sample 'B' granular bentonite. In the physical response experiment, the geomembrane was also involved during the conduction of the test. The geomembrane was labelled 'M'. The properties of both GCL samples employed in this study are presented in Table 4.1.

Table 4.1 Properties of the GCL

Properties	GCL A	GCL B
Lower geotextile	Woven	Woven
Upper geotextile	Non-woven	Non-woven
Bentonite form	Powder	Granular
Bentonite mass/area (g/m^2)	4340	3600
Structure	Needle-punched	Needle-punched
Initial thickness (mm)	8.9	7.7
Initial moisture content (%)	8.0	5.0

The same materials and notations were also used in investigating the effect of two different types of liquids, leachate and NaCl solution. At this stage, the extended codes for bentonite taken from the GCL samples were also introduced. The dry bentonite samples were labelled 'D', the bentonite exposed to water was marked 'A', the sample subjected to leachate was labelled 'L', and 'S' was used for the bentonite exposed to the salt solution. Table 4.2 lists the sample labels adopted in this study.

Table 4.2 Sample labelling

Sample code	Hydraulic perform.	Physical resp.	Microanalytical				Bentonite form	
			Dry	Water	Leachate	NaCl	Powder	Granular
A	√	√					√	
B	√	√						√
A–M		√					√	
B–M		√						√
A–D			√				√	
A–A				√			√	
A–L					√		√	
A–S						√	√	
B–D			√					√
B–A				√				√
B–L					√			√
B–S						√		√

Previous research (Rowe and Orsini 2003) has shown that sand subgrade performs well as support for GCL samples during experiments, and it was therefore employed as the subgrade material for this study. The gravel was positioned on a perforated disc at the bottom of the test apparatus; this could be used to retain any sand that might be eroded away by water.

4.2.2 Sample Preparation

To perform the plastic limit, liquid limit and swell index tests, the bentonite was taken from every GCL sample by removing the carrier and cover geotextile using a sharp knife. Once the bentonite samples were obtained from each source, the bentonite was pulverised and sieved using sieve number 40 (425 μm size).

For the experiment on GCL performance, each GCL sample was cut and trimmed into circular shapes for the experiments on hydraulic performance, physical deformation and liquid exposure response. The preparation method adopted for each GCL sample

was based on the approaches suggested by Jo et al. (2001). The sample was sandwiched between two O-rings, which acted as sample holders to keep any side wall seepage to a minimum. The GCL was then placed inside the sample holder and secured with nuts and bolts. Trimming with a sharp cutter was needed to carve out the desired shape. Silicone paste was rubbed around the interfering circumference; this was then followed by one day of drying.

4.2.3 Test Methods

Prior to conducting the hydraulic performance investigation, plastic limit, liquid limit and swell index tests were performed. The plastic limit was conducted according to AS 1289.3.2.1-2009 (Standards Australia 2009a) while the liquid limit tests referred to AS 1289.3.9.1-2002 (Standards Australia 2002) specifications and the swell index test followed the AS 1289.7.1.1 (Standards Australia 2003b) criterion.

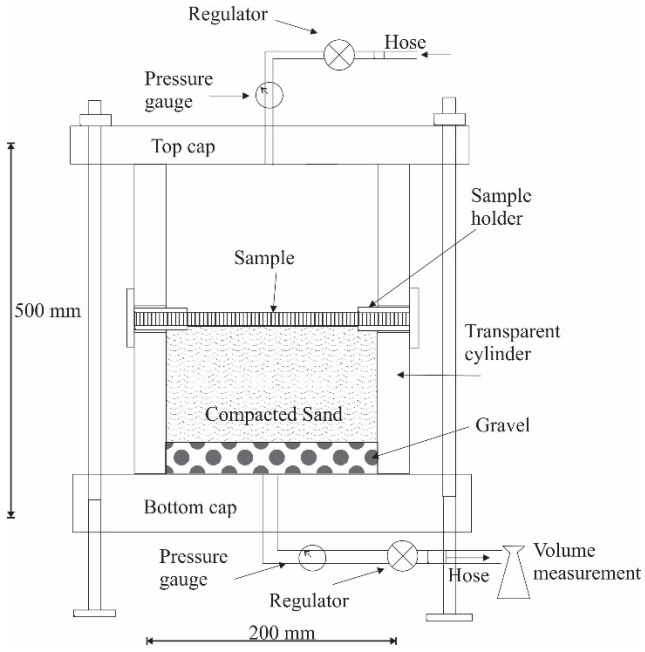

Figure 4.1 Detail of the test kit

To perform the experiment, an apparatus was assembled based on the test kit developed by Rowe and Orsini (2003) to examine the internal erosion of GCL subjected to two directions of water flow. The apparatus was also capable of investigating the hydraulic performances of certain GCLs. However, as side wall seepage was found during the test execution in the previous study, a modification was

made in the apparatus assembly by using double O-rings as sample holders and applying silicone sealant along the sample edges to avoid` any leakage.

In general, this experimental kit consisted of six main components including a transparent cylindrical cell, two caps, a sample holder, hose, water pressure gauge and water pressure regulator (

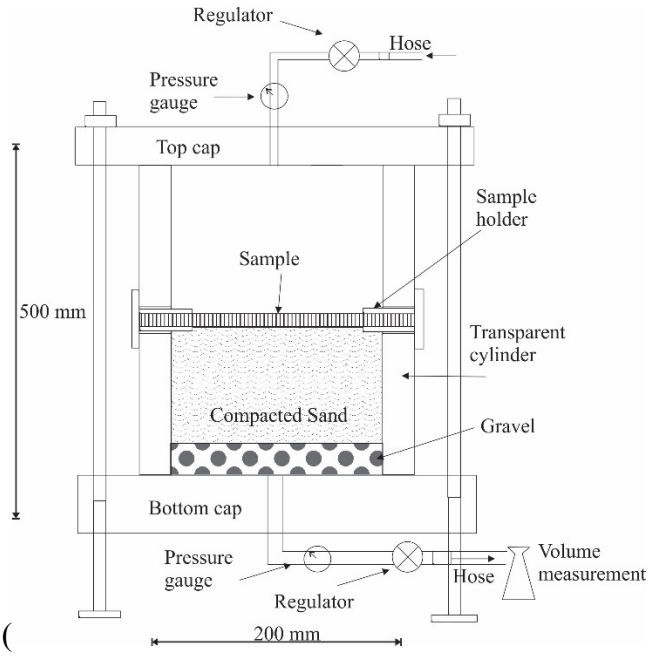

Figure 4.1). A hose was connected to each cap to accommodate water flow in both directions during the test execution. A flow rate calculation was made by measuring the effluent collected in a volumetric glass bottle and recording the time.

A 40 mm thick gravel layer was placed at the bottom of the apparatus in order to provide adequate support for the sand subgrade and restrain the sand from escaping during the test. The yellow sand was compacted to achieve 95% compaction within the apparatus. The main subgrade consisted of a 160 mm thick sand layer. Following the placement of these two subgrade layers, approximately half of the cell volume was occupied by the subgrade.

Overlaying the subgrade layer, the GCL sample was neatly placed inside the apparatus. The sample holder was secured and any sidewall leakage was prevented by applying silicon sealant around the perimeter (Figure 4.2). Also to prevent any leakage, a treated rod was used to secure and tighten the cap. The main parts of the experiment started a day after the application of the sealant in order to achieve a completely dried silicone paste.

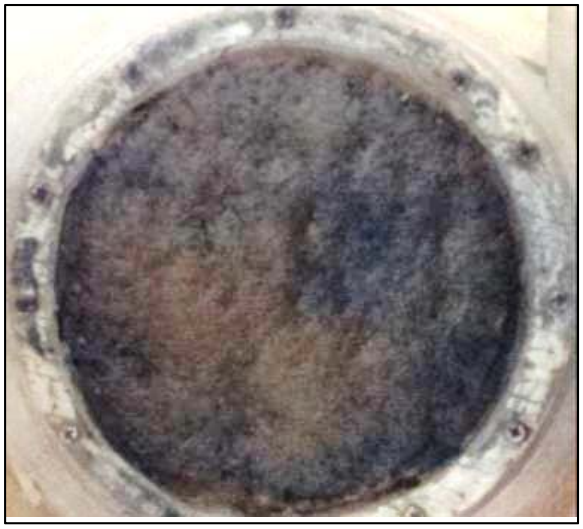

Figure 4.2 Sample placement

Hydration of the sample was the first stage of the experimental procedure. Distilled water was employed as the permeant liquid and was injected into the cylindrical cell through a hose. It was then followed by sample hydration for a couple of days. During hydration, the specimens were monitored for any changes in thickness and physical conditions. The specific procedures relating to the details of the experiments will be further explained in each experiment section.

4.3 Hydraulic Performance and Physical Response

This section covers the result of the hydraulic performance test and the surface profile alteration of the two types of GCL samples obtained from local manufactures; GCL A containing bentonite in powder from while GCL B contained bentonite in granular form; both subjected to vertical loads. Prior to the hydraulic performance test, Atterberg's limits and free swell test were performed to examine the behaviour of the GCL bentonite. It was then followed by an experiment to test the GCL swelling behaviour under unconfined and confined conditions. After the GCL samples had fully swollen, the hydraulic conductivity of both GCL samples were tested. In the surface alteration test, a significant static load was applied to the GCL sample through the gravel layer to imitate the real application of the GCL as a solid waste liner. In this experiment a low-density polyethylene (LDPE) geomembrane was also used in some scenarios which functioned as a protection layer to the GCL.

4.3.1 Atterberg's Limits and Swell Test

The Atterberg's limits test (plastic limit and liquid limit) and swelling test were performed before conducting the hydraulic performance test. The plastic limit test was done by rolling the soil sample using bare hand to form which break apart when reaching diameter of about 3.2 mm. The plastic limit of bentonite from GCL A was 55% while bentonite from GCL B was 50% (Table 4.3).

The liquid limit of bentonite was determined by cone penetration testing. In this method, a steel cone having a slope angle of 30° and weight of 80 g was dropped freely. The dropping started at the point where the cone touched the sample and allowed to penetrate the soil for 5 seconds and the dial gauge was read. The liquid limit of the sample was defined according to water content of the sample at 20 mm penetration of the cone. It was found that the liquid limit of bentonite from GCL A was 530% while bentonite from GCL B was 433% (Table 4.3).

Table 4.3 The result of the plastic limit and liquid limit tests on the GCL

Sample code	Bentonite type	Plastic limit	Liquid limit	Swell index
A	Powder (off-white)	55	530	44
B	Granular	50	433	31

Two types of swelling tests were conducted in this research, which were bentonite swelling followed by the GCL swelling test. Initially, bentonite swelling characteristics were determined by free swell test to obtain the free swell index. Bentonite sample was dried in the oven, pulverised and sieved with 425µm sieving. Two graduated glass cylinders of 100ml each were prepared for each type of bentonite and 10g of bentonite was poured into each glass cylinder. One glass cylinder was then filled with distilled water while kerosene was used for the other. These suspensions were stirred with a rod to remove any trapped air and then left for 24hours. The final volume was recorded and the free swell index was calculated using the following equation:

$$\text{Free swell index} = \frac{V_d - V_k}{V_k} \times 100\% \quad (4.1)$$

Where; V_d is the sample volume with distilled water and V_k is the sample volume with kerosene.

Table 4.3 lists the results of the free swell test. The results show that the bentonite taken from bentonite A (powdered form) has a higher swelling index compared with the bentonite taken from GCL B (granular form). A higher free swell index is an indicator for better quality of bentonite even though the correlation with hydraulic performance has not been yet established.

Figure 4.3 Free swell test

The GCL hydraulic performance test was started after the hydration process using the test kit. The hydraulic conductivity of GCL A and GCL B were 1.24 x 10^{-11} m/sec and 6.91 x 10^{-11} m/sec respectively.

4.3.2 GCL Swelling and Hydraulic Performance Test

The swelling test that was performed in the second stage was to calculate the swelling of the GCL. The GCL which consisted of two geosynthetic layers, cover and carrier, on the top and bottom bentonite were tested under various loads. In this part, the GCL

responses towards vertical stress and its swelling characteristics were investigated under hydration phase and various confining pressures. The role of the cover and carrier layers of the GCL to condense the bentonite swelling were to be studied by performing this test. Once the GCL had been fully swollen, the hydraulic conductivity test would be performed for each applied confining pressure.

Unconfined swelling tests were performed without the application of any vertical load, however, a small load of about 4 kPa was still present due to the weights of the perforated disk and axial rod. In the confining test, two different loads of 50 kPa and 150 kPa were applied to both types of GCLs. The hydration stage was commenced by soaking the GCL with distilled water. Any height changes were recorded until the height reached a constant. Once the sample had fully swollen, the hydraulic conductivity test was carried out.

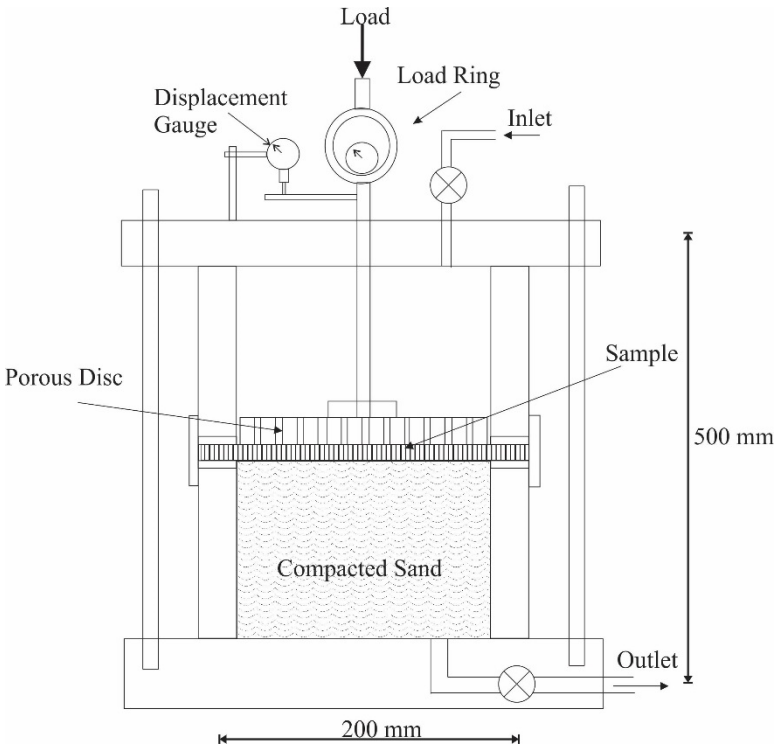

Figure 4.4 Swelling test kit

On average, the initial thickness of GCL A was 6.4mm and it reached the fully swollen stage in about 25 days. Figure 4.5 shows the swelling characteristic of GCL A during the test. The final thickness of GCL A was 15.6mm without the application of any load. Meanwhile, GCL A swelled up to 12.7mm and 9.2mm respectively under 50 kPa and 150 kPa of applied load. Under 50 kPa of load, the GCL sample was compressed

up to 18.14% while under vertical load of 150 kPa, the GCL was compressed up to 41% (refer to the unconfined height of the GCL). The hydraulic conductivity of GCL A sample without any confining pressure was recorded at 1.24 x 10^{-11} m/sec. Meanwhile, with 50 kPa of confining pressure, the hydraulic conductivity decreased to 1.06 x 10^{-11} m/sec. The lowest hydraulic conductivity was recorded for the GCL under an applied load of 150 kPa, which was 7.79 x 10^{-12} m/sec (Table 4.4)

Table 4.4 GCL performance under various load

GCL Type	Load Applied (kPa)	Initial Thickness (mm)	Final Thickness (mm)	Compression Index (%)*	Hydraulic Conductivity (m/sec)
A	4	6.4	15.6	0 (Ref.)	1.24 x 10^{-11}
A	50	6.4	12.7	18.14	1.06 x 10^{-11}
A	150	6.4	9.2	41	7.79 x10^{-12}
B	4	4.9	11.04	0 (Ref.)	6.91 x 10^{-11}
B	50	4.9	9.6	13.3	6.15 x10^{-11}
B	150	4.9	7.5	31.9	4.49 x10^{-11}

*Compression index is calculated based on the final thickness of GCL under 4 kPa load as the references

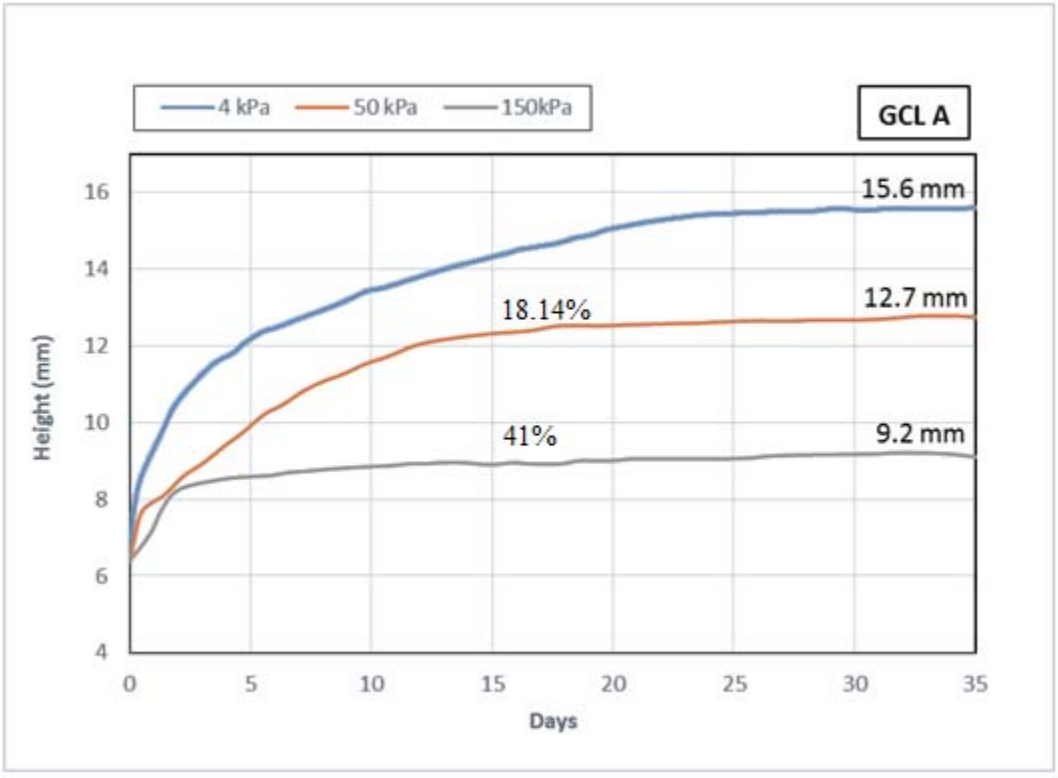

Figure 4.5 Swelling of GCL A

The swelling characteristics of GCL B are shown in Figure 4.6. The initial thickness of GCL B on average was 4.9mm. When hydrated without any confining pressure, GCL B reached a maximum height of 11.4mm in about 30 days. Meanwhile under 50 kPa and 150 kPa, the final thicknesses of GCL B were 9.6mm and 7.5mm, respectively (Figure 4.6). This shows that under 50 kPa of confining pressure, GCL B compressed to 13.3% while under the confining pressure of 150 kPa GCL B compression was at 31.9%. The applied confining pressure also altered the hydraulic conductivity of GCL. In a load-free condition, the hydraulic conductivity of GCL B was 6.91x 10^{-11} m/sec, however, under 50 kPa the hydraulic conductivity of GCL B slightly dropped to 6.15x 10^{-11} m/sec. The lowest hydraulic conductivity shown by GCL B was under 150 kPa, which was 4.49x10^{-11} m/sec.

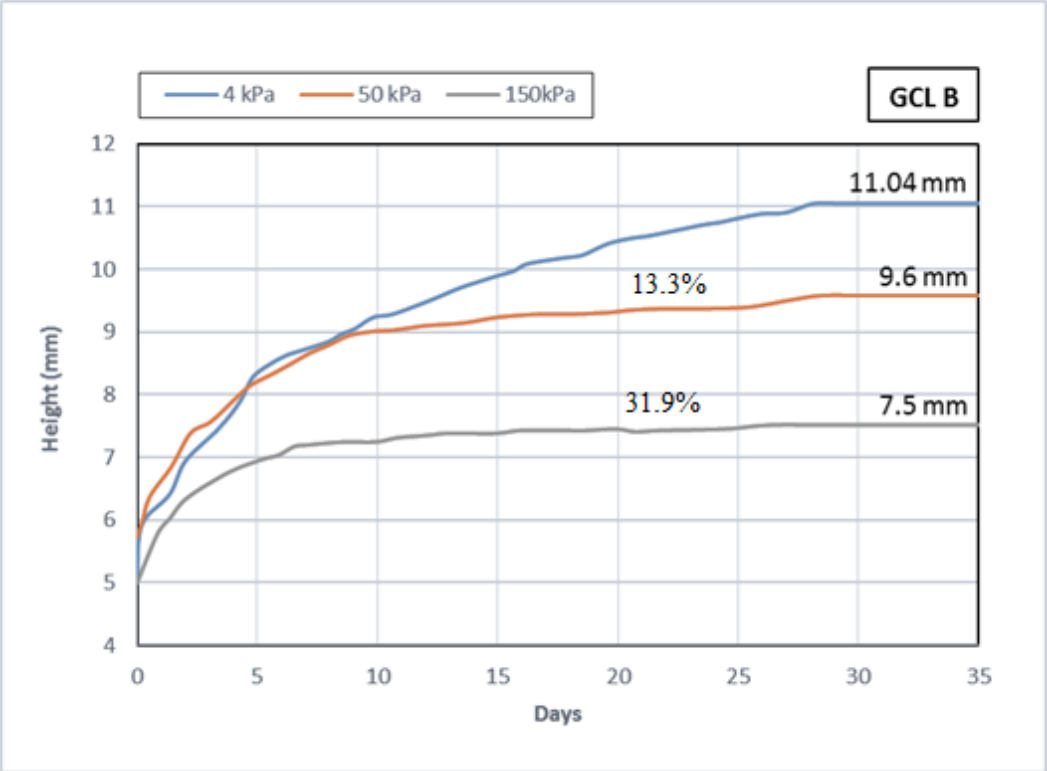

Figure 4.6 Swelling of GCL B

4.3.3 Surface Deformation

This experiment was conducted to examine any surface profile alternations of the GCL when subjected to load from all of the overlying materials during its function as a landfill liner. Two types of GCLs and LDPE geomembrane were used in this

experiment. To simulate the solid waste landfill configuration, the sample was laid on the compacted sand layer under a layer of gravel.

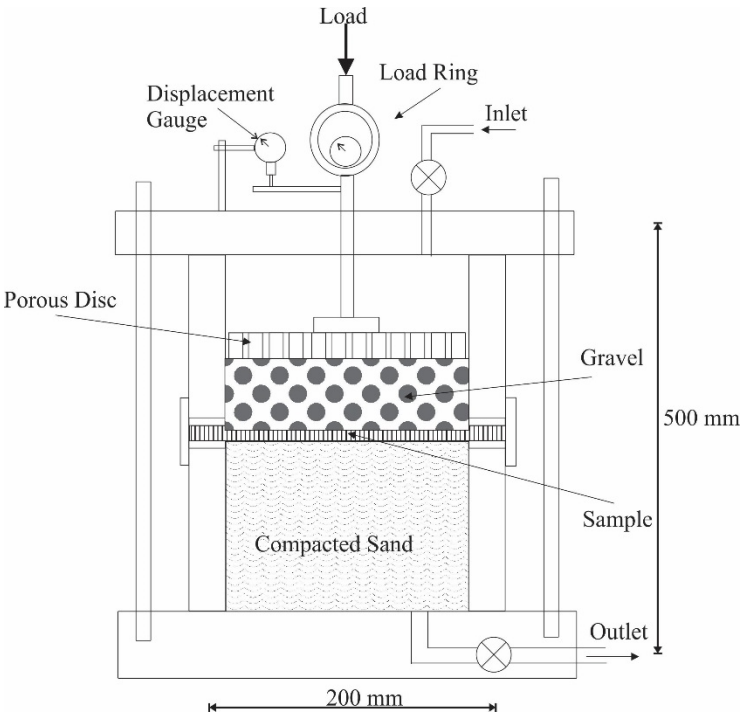

Figure 4.7 Surface deformation test kit

An uneven deformation which roughly followed the shape of the gravel layer was observed in the surface profile of GCL A. This observation was noted after GCL A layer had been subjected to a 450 kPa of static load and exposed to a hydration period exceeding 25 days. Due to the presence of voids between the particles of the gravel layer, it created somewhat wavy contours on the surface of the GCL. Furthermore, the maximum height observed for the surface of GCL A was +15.6mm, whereas the minimum height was measured at +9.0mm (Figure 4.8), this corresponds to a height difference of 6.6mm between the maximum and minimum points. In addition, due to the wavy appearance of the surface, the variation in the height was not uniform and the minimum and maximum points were not uniformly distributed as can be seen from Figure 4.8 where a height of +15.5mm was observed after the trough height of +9.0mm.

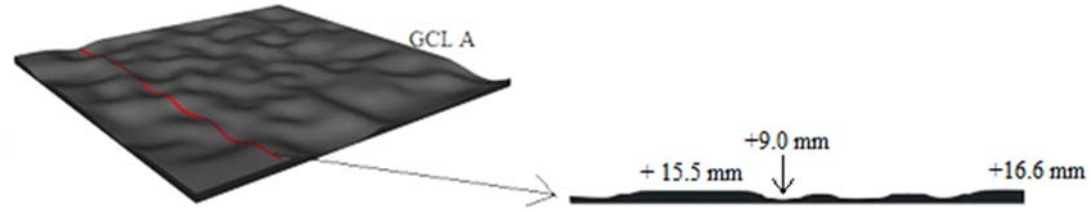

Figure 4.8 GCL A surface profile

Similar appearance of surface profile deformation was observed for the surface of GCL B. After being pushed with static load, the surface profile of GCL B also became somewhat undulant, as was observed in case of GCL A surface profile deformation. The maximum height of the surface profile was observed at +11.04mm while the minimum height was +7.4mm (Figure 4.9). This shows that a height variation of 3.64mm was noted between the maximum and minimum points of the crests and troughs of the GCL B surface profile deformation. Moreover, the heights of the crests and troughs varied throughout the surface profile and the depressions in the layer generally followed the shape of the gravels whereas the humps occurred where voids were observed between the particles, similar to GCL A deformation pattern.

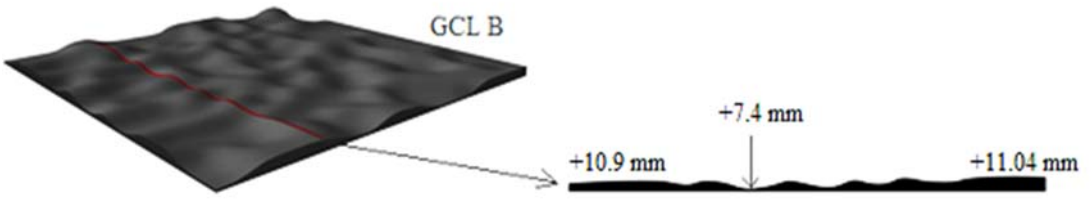

Figure 4.9 GCL B surface profile

The placement of the LDPE geomembrane in between the GCL and gravel layer appeared to have reduced the displacement of the GCL surface. After being subjected to the same vertical static load, the surface GCL A containing the geomembrane, showed the maximum height of +11.4mm, which was 4.2mm lower than that observed for GCL A without the presence of any LDPE geomembrane. Furthermore, the minimum height of +10.1mm was observed for GCL A after the provision of an LDPE geomembrane (Figure 4.10). This corresponded to a height variation of 1.1mm between the minimum heights of GCLA with and without LDPE geomembrane,

overall showing smaller variations between the minimum and maximum of surface deformation contours after the provision of LDPE geomembrane.

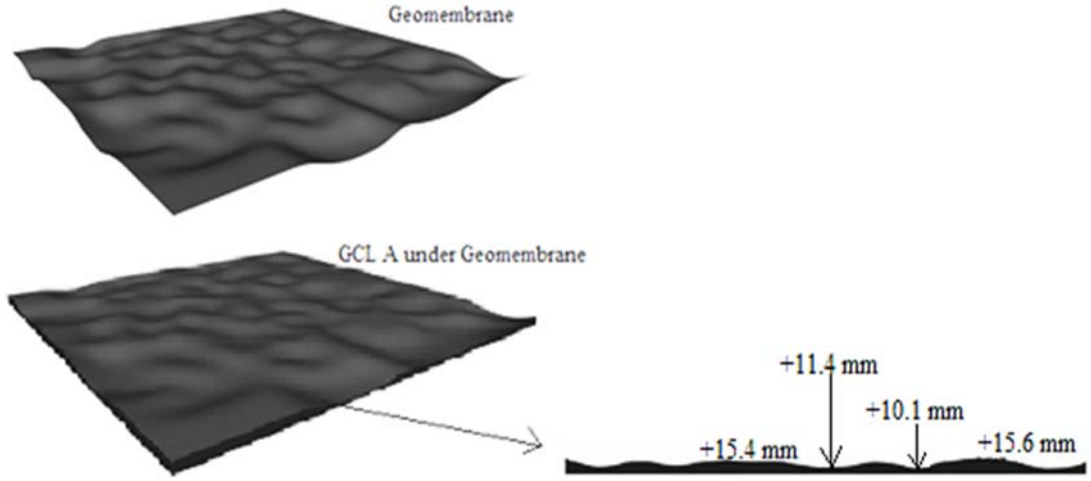

Figure 4.10 Surface profile GCL A under geomembrane

A similar condition of reduction in the degree of variation between the heights of the crests and troughs of the surface profile deformation contours also occurred in the case of GCL B when a layer of LDPE geomembrane was installed on top of it. Although the magnitude of the applied static vertical load was constant and it still generated a wavy contour, the minimum height of the profile was higher than for the GCL without the installation of LDPE geomembrane. The maximum height profile of GCL B was recorded at +11.04mm while the minimum height was observed at +8.1mm (Figure 4.11). This exhibited a much smaller difference between the two points, at 2.94mm compared to an earlier observation of 3.64mm for the same type of GCL under similar loading conditions.

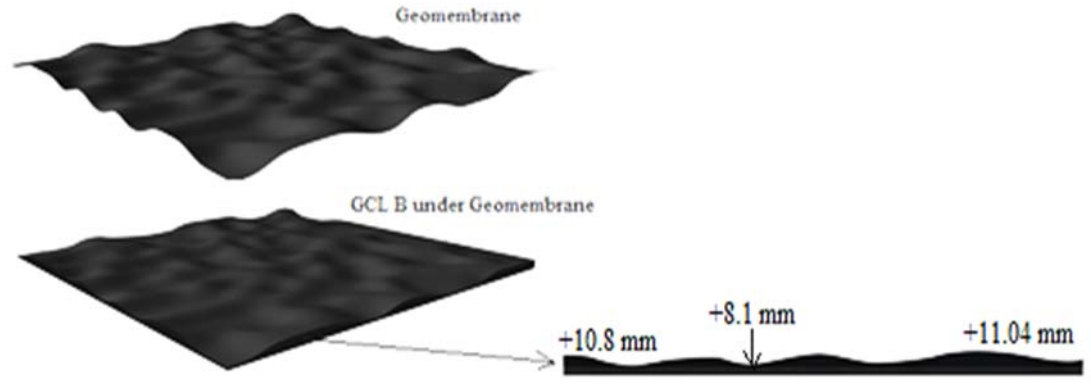

Figure 4.11 Surface profile of GCL B under geomembrane

4.3.4 The Effect of Uplift Pressure

Uplift hydraulic pressure is a condition where the hydraulic pressure beneath the GCL layer is higher than the hydraulic pressure coming from above the GCL. In solid waste landfill, this condition is mostly likely to occur as a result of an increasing groundwater level surrounding the landfill area, particularly when a solid waste landfill is located in an area with a high groundwater level. It is reasonable to presume that there will be areas of lifting and deformation when GCL is subjected to hydraulic uplift pressure. Consequently, the deformation of GCL caused by hydraulic uplift pressure has the potential to alter the hydraulic performance of GCL.

The present study concentrated on the response of the GCL to hydraulic pressure uplift after the application of downward water pressure. The water pressure was measured by two pressure gauges that were installed in the system. The test monitored the physical changes along with the changes in the GCL's hydraulic performance. A specific water pressure was applied to the GCL sample to simulate the hydraulic pressure imposed on GCL acting as landfill liner.

In this experiment, the GCL was laid on compacted sand (as subgrade layer). Silicone sealant was used to enhance the seal and prevent sidewall leakage around the perimeter of the sample holder (Figure 4.12). The cylindrical apparatus was further restrained by placing a cap above the apparatus, which was secured and tightened. The sample was left for one day so that the silicone paste would be completely dry before commencement of the experiment.

The first stage of this experiment was the hydration phase. Water was introduced through the hose into the cylindrical cell as the permeant liquid. The hydration was performed for a week to achieve a completely hydrated GCL. Modification of the water column in the falling head permeameter was performed to fit the experimental apparatus and connected to the pressure controller, and was used to start the hydraulic test. Due to the importance of capturing bentonite migration as well as pressure changes, visual monitoring was used to observe the phenomena. A digital camera was also utilised to monitor any variations in liquid turbidity and the form of GCL and sand subgrade.

Figure 4.12 Sample in the apparatus

Prior to the test, a 20 kPa downward hydraulic water pressure was applied from the top of the sample. This was to simulate the hydraulic pressure generated during leachate development. Upwards water pressure was then applied by introducing water from the base of the apparatus. The pressure applied from the bottom was 40 kPa higher than the downward pressure, which was equivalent to about 4 m in water head differences. During this upward flow phase, the water pressure imposed an uplifting force on the sample, pushing the sample up at the centre to form a curved conical shape (Figure 4.13). This condition occurred due to the hydraulic uplift pressure being greater than the downward pressure. The following equational solutions further explain the mechanisms of the variations between the upward and downward pressures.

Submerged unit weights (γ') (4.2)

$$Unit\ weight\ of\ saturated\ bentonite = \gamma_{sat} = 12.68 \quad kN/m^3$$

$$Unit\ weight\ of\ water = \gamma_w = 9.81 \quad kN/m^3$$

$$Submerged\ unit\ weight = \gamma' = \gamma_{sat} - \gamma_w$$

$$\gamma' = 12.68 - 9.81 = 2.87 \ kN/m^3$$

Total stress at the bottom of the sample (σ) (4.3)

$$\sigma = h_1\gamma_w + h_2\gamma_{sat}$$

$$\sigma = 0.3(9.81) + 0.01\ (12.68) = 3.07\ \ kN/m^3$$

Gradient hydraulic (i)

$$i = \frac{h_1}{h_2}$$

$$i = \frac{4\ m}{0.1\ m} = 40$$

Effective stress below the sample (σ′)

$$\sigma' = z\,\gamma' - iz\gamma_w$$

$$\sigma' = 0.01\ (2.87) - 40\ (0.01)(9.81) = -1.933\ kN/m^2$$

Water pressure below the sample (u)

$$u = \sigma - \sigma'$$

$$\mathrm{u} = 3.07 - (-1.93) = 1.14\ kN/m^2$$

Figure 4.13 GCL starting to be lifted

The bottom of the sample was subjected to an effective stress of –1.933 kN/m^2, while the water pressure in this area was 1.14 kN/m^2. Force summation showed that the sample would be lifted if the uplifting force became greater than the downward force. The dome-like shape of the GCL caused stretching and void development on the GCL surface.

After being exposed to a 40 kPa of uplift water pressure for approximately three days, the sample surface displayed significant changes during the test as the bentonite started to boil on the surface of the cover layer. At its largest, the bentonite boiling had a diameter of approximately 30 mm and a height of about 15 mm (Figure 4.14).

Figure 4.14 Bentonite boiling

The bentonite boiling phenomenon observed was similar to soil boiling, which can happen when the soil encounters an upward water flow causing loss of shear strength among the soil particles. This condition may also occur in cohesive soils subjected to excess pore water pressures (Terzaghi 1996). In this case, there was a stretch out and void development on the surface of the GCL, so that the water might seep through the void. The uplift water pressure, which generated large stresses in the GCL sample, was believed to trigger the boiling bentonite phenomenon. However, when the upward water pressure was released and the downward water pressure was kept constant, the surface of the GCL returned to its initial appearance (flat) and the GCL was able to hold the applied pressure.

The next experiment was conducted to examine GCL behaviour when upward hydraulic pressure was applied without any water pressure coming from the top. To perform this experiment, the remaining water above the GCL sample was drained and 40 kPa of upward water pressure was applied to the GCL at a very slow incremental rate. Once the hydraulic pressure started to build up, the GCL began to deform into a dome shape similar to the previous test. However, in this experiment, there was no

boiling phenomenon present. The water pressure from underneath the GCL pushed the bentonite particle. Without any water pressure from the top, the bentonite particle flow with the water from underneath thus no boiling phenomenon occurred.

Figure 4.15 Tested sample

Hydraulic failure started after the GCL had undergone about three days of upward water pressure. Two small holes in the thinnest area of the sample enabled the water to flow easily (Figure 4.16). The water pressure dropped to 20 kPa while the GCL sample lost its capability to retain a certain water pressure in less than 12 hours.

Since it was not possible to capture the water flow through the GCL with a camera, blue textile dye was injected to the water reservoir to colour the water. This allowed the occurrence of water discharge to be easily captured. The water flow passing through the GCL is shown in Figure 4.16.

Figure 4.16 GCL failure

The sample then was removed from the apparatus for thickness measurement. It was observed that the top (dome apex) of the GCL was about 24.7 mm high (Figure 4.15). Meanwhile, the thickest part of the GCL was 15.8 mm, while the thinner part was 3.2 mm (Figure 4.17). It was also observed that the bentonite moved aside from the centre of the GCL sample into the lower pressure areas.

Figure 4.17 The final GCL form

4.4 Effect of Inorganic Salt and Leachate

4.4.1 NaCl Hydration

This section covers the two types of prepared GCL samples obtained from two different suppliers. Sodium bentonite was present in all samples: the letter ‘A’ label represented powder bentonite while ‘B’ was used for granular bentonite. Hydration salt solutions with a concentration of 100 mM were then prepared using distilled water and salt. The second letter of the sample label indicated the sample condition. Original GCL samples (dry) were marked ‘D’ while label ‘A’ represented GCL samples after being hydrated with distilled water and label ‘S’ indicated hydration with sodium chloride solution (Table 4.5).

Table 4.5 GCL sample code

Sample code for microscopic images	Bentonite type	Hydration condition
A-D	Powder	Dry
B-D	Granular	Dry
A-A	Powder	DI water
B-A	Granular	DI water
A-S	Powder	NaCl
B-S	Granular	NaCl
A-L	Powder	Leachate
B-L	Granular	Leachate

As stated earlier, microscopic imaging was used to investigate the GCL samples, while a scanning electron microscope (SEM) was employed to examine the bentonite particles. Microscopic images of the GCL were produced utilising a Nikon ME600 light microscope and analysed with Top View, an image processing software for light microscopes. A Zeiss Evo 40XVP was used to obtain the SEM images, and it could determine the elemental composition of samples by connecting to an Oxford Instruments energy dispersive X-ray detector (EDS). Equipped with INCA peak matching software, the EDS was able to identify elements faster.

Optical Microscopy

Following the two weeks' hydration, the moisture content of the GCL samples was removed by placing them in the oven. Next, optical microscopy was used to observe any physical changes both before and after hydration (Figure 4.18).

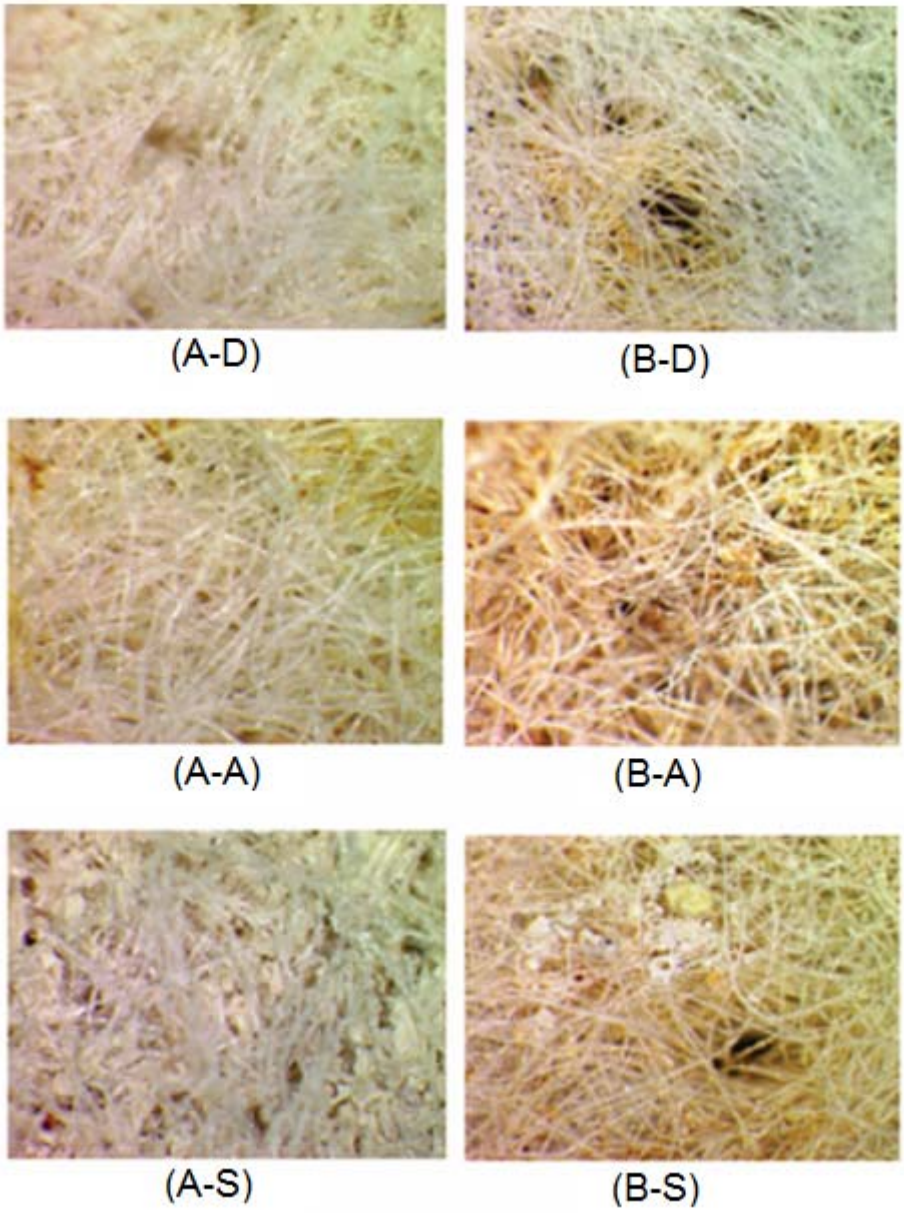

Figure 4.18 Microscopic view of the physical appearances of GCL samples; A-D and B-D: initial condition of GCL; A-A and B-A: GCLs after hydration using distilled water; A-S and B-S: GCLs after hydration of NaCl solution

There were no differences in the physical appearance of samples A-D, A-A and B-D, B-A. This demonstrates that distilled water hydration and drying afterwards had no influence on the form of the GCL sample as it remained unchanged under microscopic observation. However, some crystal deposits were found on the A-S and B-S samples on the top of the bentonite layer and attached to the geosynthetic cover, the crystal deposits were of NaCl in its dry form.

SEM and EDS

The GCL was then examined utilising the scanning electron microscope (SEM) for the morphological and mineralogical characterisation of the specimens. SEM could show the binding characteristics of the liner membrane and was used to observe the physical changes in the interparticle interaction due to hydration with different solutions. The morphology of the investigated GCL samples is shown in Figure 4.19, which illustrates the images of GCL particles both before and after hydration using distilled water and NaCl solution.

Referring to Figure 4.19, the images of samples A-D and B-D represent the raw form of bentonite before being hydrated with any type of solution. Sample A-D was the powder form of bentonite and sample B-D was the granular form. Comparing the images for A-D and B-D showed that the surface morphology of the bentonite particles varied between the powdered and granular forms. The analysis of SEM images of powdered bentonite exhibited larger and denser clods of particles compared with the granular form of bentonite particles.

Comparing A-A and B-A revealed that distilled water hydration had led to the flocculation of the particle clods resulting in the formation of a more solid bentonite surface appearance as well as a tighter attachment between particles. Therefore, it can be stated that: 1. the hydration of bentonite with distilled water has a significant influence on the bentonite particles rather than the structure and crystallography of the particles; and 2. bentonite hydration with distilled water tends to dwindle the interparticle spaces or voids.

The structure of bentonite particles after being hydrated with NaCl solution is shown in images A-S and B-S (Figure 4.19). The morphological patterns, particle arrangements and interactions exhibited in these two images are different from those observed in the previous SEM images. Compared to distilled water hydration as shown in A-A and B-A (Figure 4.19), bentonite particles in A-S and B-S (Figure 4.19) experienced less swelling. As a result, it can be assumed that NaCl solution is able to change the response of bentonite particles.

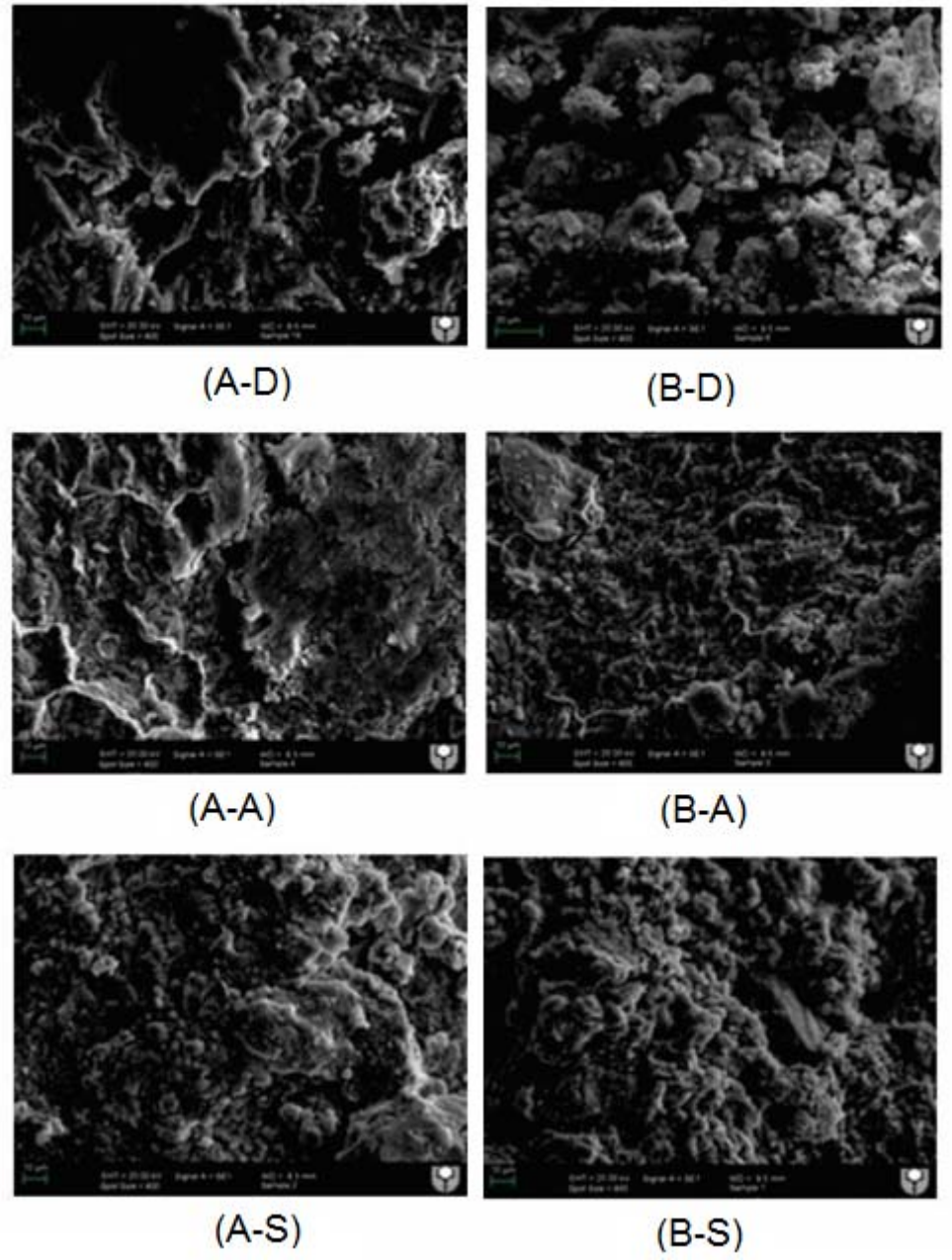

Figure 4.19 The SEM views of bentonite particles in GCL samples under the following conditions: A-D and B-D: initial status before hydration; A-A and B-A: after hydration with distilled water; A-S and B-S: after hydration with NaCl solution

In order to further examination the effect of hydration with other solutions on both types of bentonite particles, another investigation of the bentonite particles was conducted using an energy dispersive X-ray detector (EDS). The element distribution within each sample was then produced.

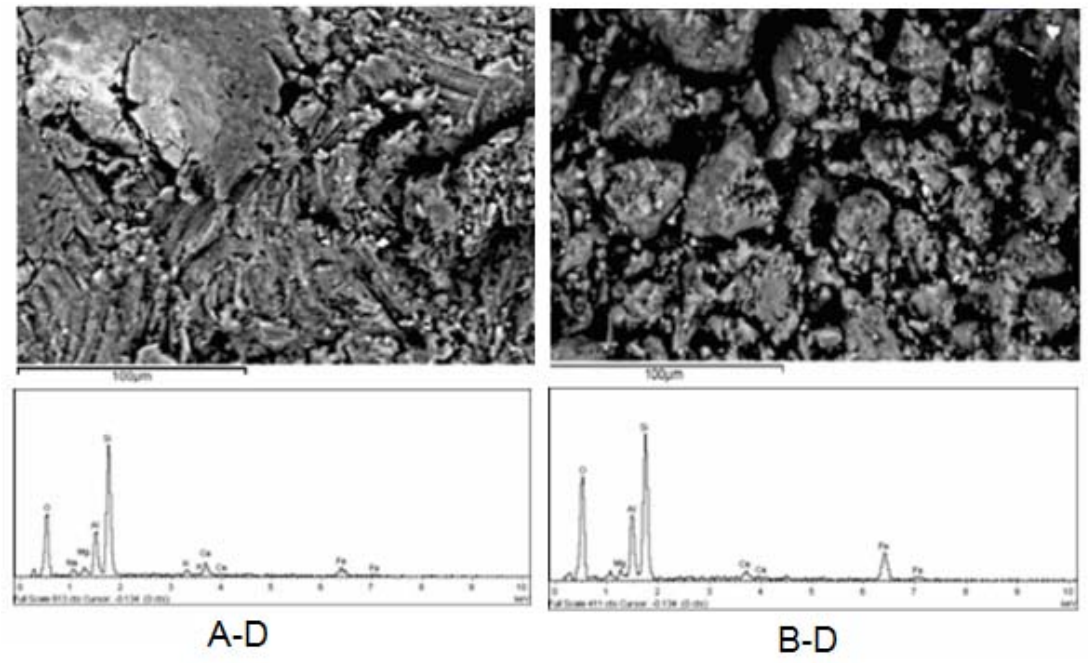

Figure 4.20 Samples A-D and B-D elemental distribution images before hydration

Figure 4.20 shows the original elemental composition of bentonite in the two different GCL samples of powdered and granular bentonite. Generally, bentonite particles contain elements such as iron (Fe), aluminium (Al) and silicone (Si), which may be carried along in the form of iron (III) oxide (Fe_2O_3), aluminium oxide (Al_2O_3) and silicates (SiO_2). Other minor elements of the alkali groups including magnesium (Mg), potassium (K) and sodium (Na) may also be found as constitutional elements of bentonite (Buckley, Gates and Gibbs 2012). As Figure 4.21 indicates, almost no diversion was observed in the elemental distribution of the particles when bentonite was hydrated with distilled water, since in this case H_2O was the only additive in the mixture. At this stage, it should be noted that no moisture content was found in all of the samples after oven-drying.

Silicon, in the form of silicate, forms the main component of bentonite among all other elements, followed by aluminium and oxygen. Despite the morphologic alteration of the bentonite particles, no change could be observed in the quantities of the dominant elements.

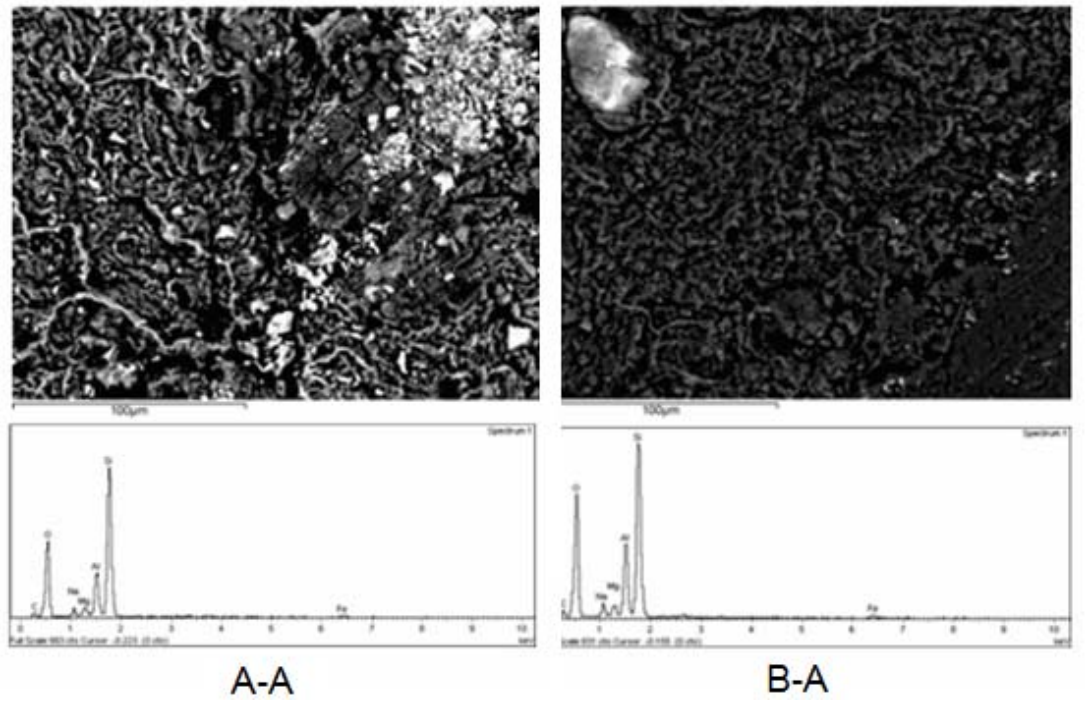

Figure 4.21 SEM-EDS of bentonite particles hydrated with distilled water

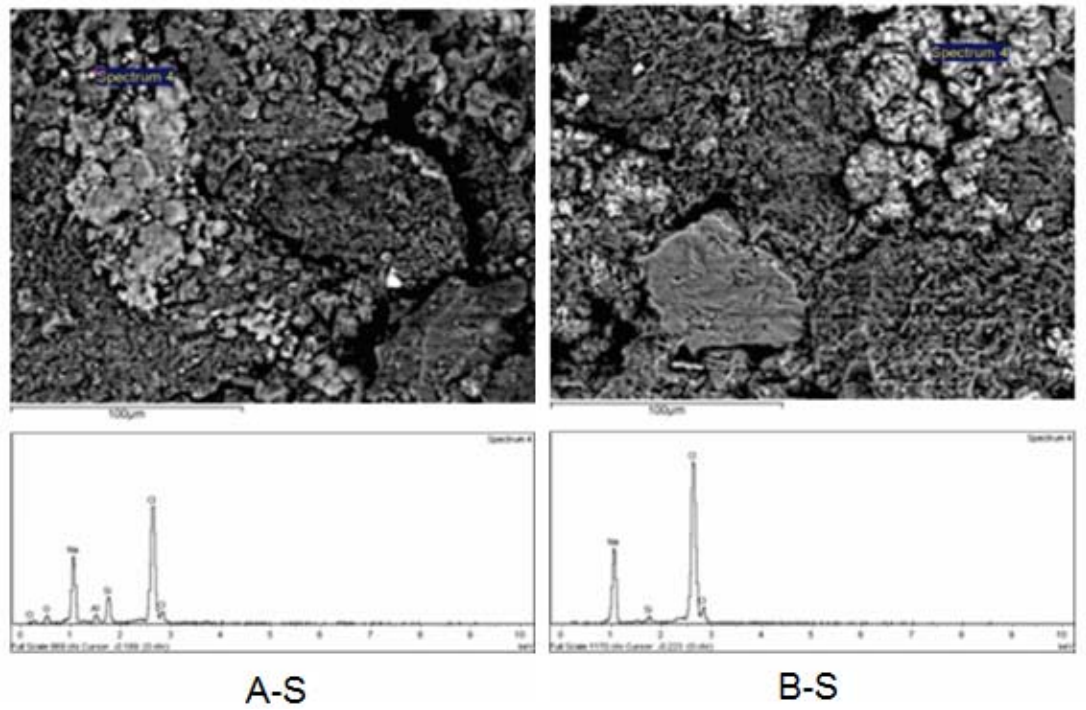

Figure 4.22 SEM-EDS of bentonite particles hydrated with NaCl

The elemental distribution of bentonite particles after hydration with 100 mM concentration of a sodium chloride (NaCl) solution was shown in Figure 4.22. Sodium

chloride had been absorbed by the bentonite as indicated by chlorine elements found during EDS analysis. However, chlorine only appeared in a small area in the surface of the bentonite, which is highlighted as the brighter area in the graph (i.e. spectrum 4). Consequently, it was concluded that the bonding structure of the bentonite particles encountered only minor changes. Both granular and powder bentonite forms showed this phenomenon.

Effect of NaCl on Hydraulic Performance

The permeability of the bentonite layer sandwiched between the geotextile changes with variations in the water quantity imposed on the bentonite surface (Jo et al. 2005). As leachate barrier in landfill liner, incompatibility in the permeability of GCLs is a major issue influencing the performance of the GCL during the design life of the landfill (National Research Council 2007). Therefore, the hydraulic performance of GCL when subjected to hydration by both types of permeant solutions – distilled water and sodium chloride – was also assessed in this study. The results are illustrated in Figure 4.23.

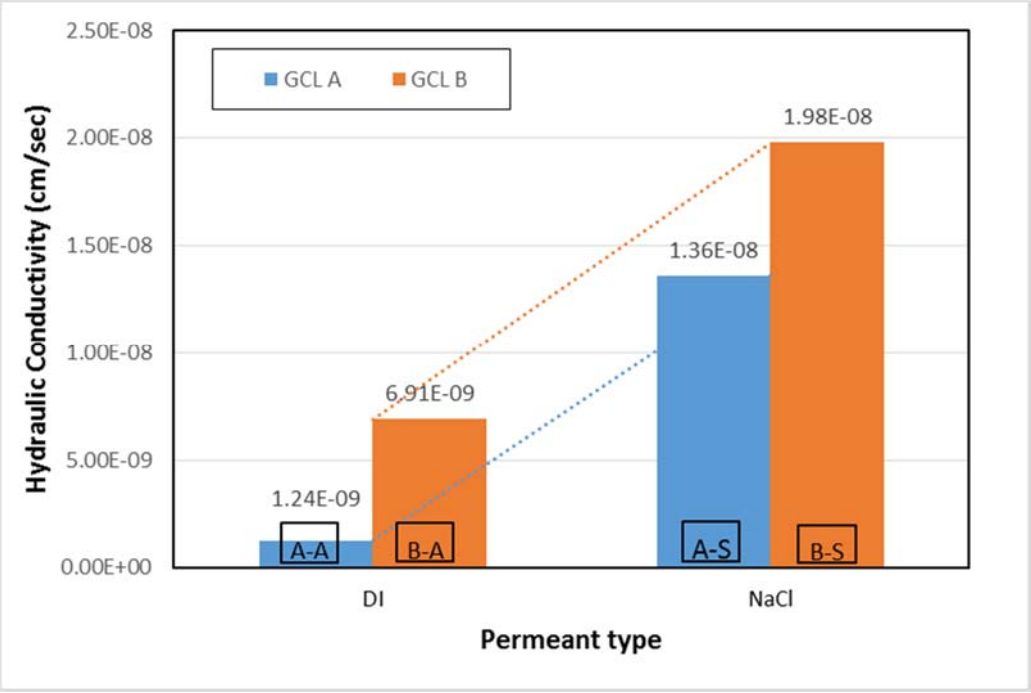

Figure 4.23 Hydraulic conductivity of GCL after hydration with both distilled water (A-A, B-A) and NaCl (A-S, B-S)

As stated earlier, the study also investigated the feasibility of GCL as an effective hydraulic barrier in the presence of NaCl in the permeating solution so that the

influence of the types of permeant solutions on the hydrated GCL could be established. It was found that the respective hydraulic conductivities of both samples were 1.24 x 10^{-11} m/sec and 6.91 x 10^{-11} m/sec. Furthermore, hydration with NaCl was observed to have slightly altered the permeability of the GCL and a rise in the hydraulic conductivities was noted for both samples. As displayed in Figure 4.23, the hydraulic conductivity of sample A-S jumped to 1.36 x 10^{-10} m/sec while the hydraulic conductivity of B-S increased to 1.98 x 10^{-10} m/sec.

4.4.2 Leachate Hydration

In this section, both GCL samples were permeated with leachate. The effect of leachate on the bentonite layer was investigated using micro analytical methods. The list of dominant parameters found in the leachate sample is shown in Table 4.6.

Table 4.6 Leachate content

Parameter	Unit	Concentration	
		L1	L2
pH	-	8.1	8.3
TOC	mg/l	220	430
Mn	mg/l	0.047	0.012
Fe	mg/l	6.981	4.209
Pb	mg/l	0.93	0.18
Cr	mg/l	0.93	0.21
Cd	mg/l	4.5	1.03
Ni	mg/l	6.99	2.35

SEM and EDS

SEM analysis was conducted to observe any alteration in morphology and mineralogy of bentonite after permeating with leachate. Figure 4.24 shows the morphology of the powder bentonite (GCL A) after being permeated with distilled water (a) and after being exposed to leachate (b). The analysis of the SEM images shows that after being permeated with distilled water, powdered bentonite formed layers and exhibited denser clods of particles compared to the bentonite sample hydrated with leachate. It seems that leachate hydration produces a more porous surface of bentonite particles.

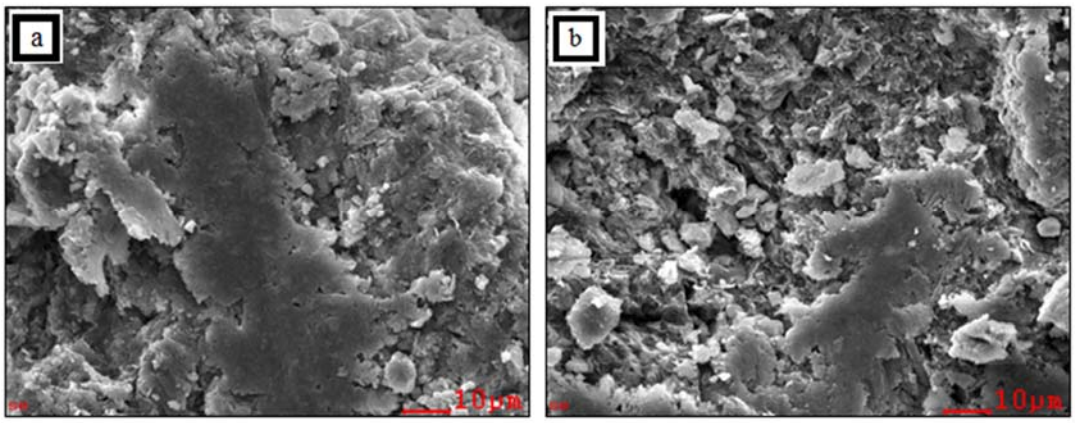

Figure 4.24 SEM micrograph of (a) A-A and (b) A-L specimen

The SEM image of granular bentonite after being hydrated with distilled water and leachate shows minor changes that are noticeable in surface profile (Figure 4.25). Leachate exposure seems to slightly alter the morphological surface of granular bentonite. The surface of the bentonite in Figure 4.25 (a) is more compact and condensed after being permeated with distilled water. However, as shown by Figure 4.25 (b), the leachate hydration seems to result in a spongy bentonite surface.

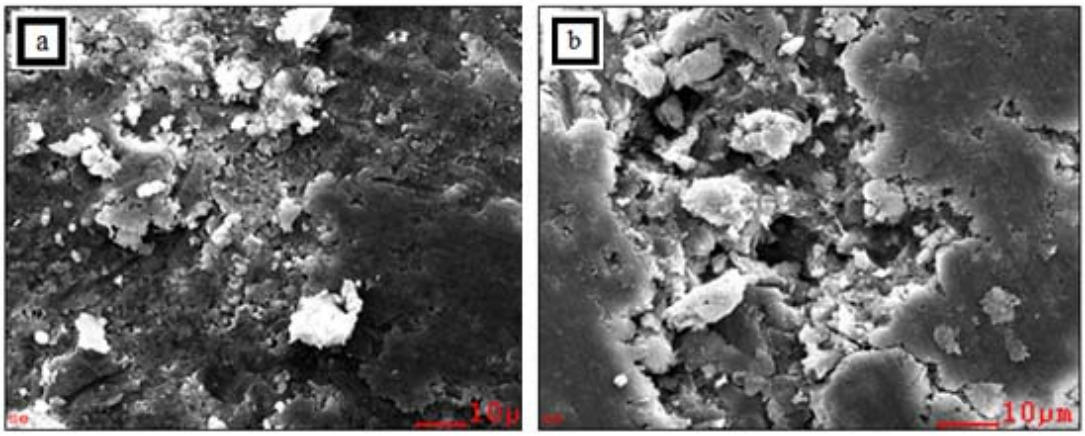

Figure 4.25 SEM micrograph of (a) B-A and (b) B-L specimen

Another investigation using the energy dispersive X-ray detector (EDS) was performed to examine the effect of leachate hydration on both types of bentonite particles. Original elemental composition is demonstrated for bentonite in the two different GCL samples of powdered (Figure 4.26) and granular bentonite (Figure 4.27). Generally, bentonite particles contain elements such as iron (Fe), aluminium

(Al) and silicone (Si), which may be carried along in the form of iron (III) oxide (Fe_2O_3), aluminium oxide (Al_2O_3) and silicates (SiO_2). Furthermore, some minor elements of the alkali groups including magnesium (Mg), potassium (K) and sodium (Na) may also be found as constitutional elements of bentonite (Buckley, Gates and Gibbs 2012).

As illustrated in Figure 4.26 and Figure 4.27, it is obvious from the analysis of the peaks that the high peak in the line spectrum graph is associated with the high proportion of silicon in bentonite. In general, all components confirmed the availability of the smectite group, quartz and kaolinite materials. Despite the morphologic alteration of the bentonite particles, no change could be observed in the quantities of the dominant elements.

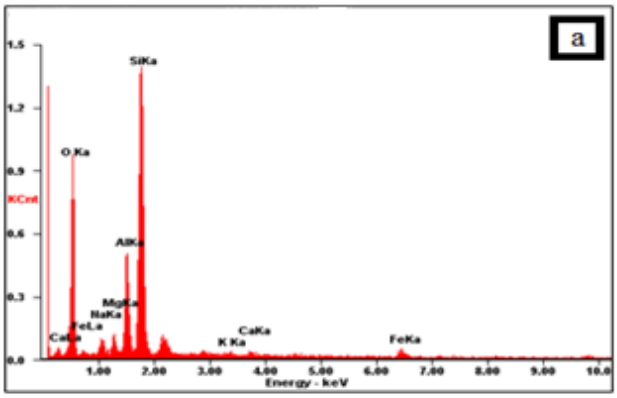

Element	Wt%	At%
OK	45.24	59.41
NaK	02.86	02.61
MgK	02.34	02.02
AlK	11.29	08.79
SiK	33.96	25.40
KK	00.43	00.23
CaK	00.49	00.26
FeK	03.40	01.28
Matrix	Correction	ZAF

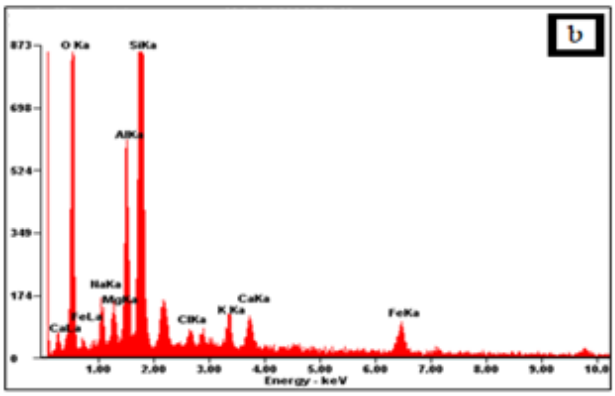

Element	Wt%	At%
OK	42.25	57.70
NaK	03.39	03.22
MgK	02.43	02.18
AlK	10.34	08.37
SiK	28.90	22.49
ClK	01.12	00.69
KK	02.62	01.46
CaK	02.48	01.35
FeK	06.47	02.53
Matrix	Correction	ZAF

Figure 4.26 EDX spectra and quantitative data of (a) A-A and (b) A-L

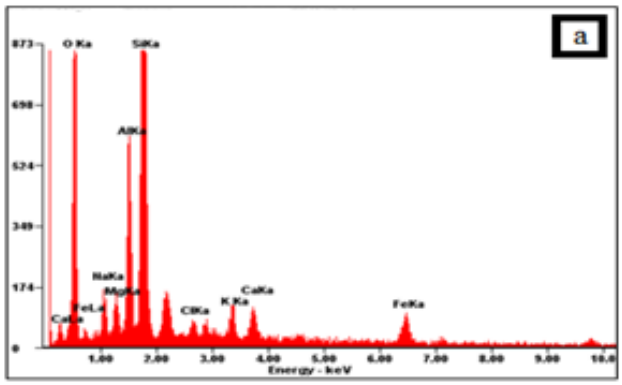

Element	Wt%	At%
OK	42.13	57.71
NaK	03.10	02.95
MgK	02.78	02.50
AlK	12.24	09.94
SiK	27.40	21.38
KK	01.68	00.94
CaK	01.80	00.98
TiK	01.45	00.66
FeK	07.43	02.92
Matrix	Correction	ZAF

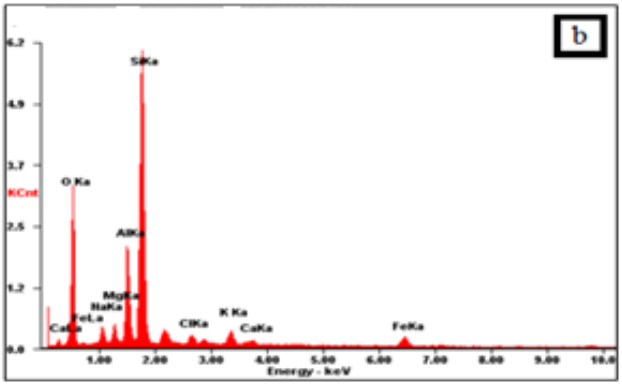

Element	Wt%	At%
OK	41.66	56.55
NaK	02.75	02.59
MgK	02.17	01.94
AlK	11.00	08.85
SiK	33.13	25.62
ClK	01.35	00.83
KK	02.54	01.41
CaK	00.77	00.42
FeK	04.63	01.80
Matrix	Correction	ZAF

Figure 4.27 EDX spectra and quantitative data of (a) B-A and (b) B-L

XRD Analysis

The SEM/EDS analyses revealed some of the key elements in the material. X-ray powered diffraction (XRD) was utilised to investigate the mineralogical and crystalline nature of the prepared samples of bentonite and bentonite hydrated with leachate. Notable diffraction lines were used to examine the mineral constitution of each material. The XRD analysis showed an ettringite hydrates appearance in the crystallised phase, indicating the existence of reacted calcium atom compounds. Ettringite [$3CaO\text{-}Al_2O_3\text{-}3CaSO_4\text{-}32H_2O$] is formed due to the availability of calcium. The XRD data for clay also demonstrated the existence of clay minerals consisting of quartz (SiO_2), illite $(K,H_3O)(Al,Mg,Fe)_2(Si,Al)_4O_{10}[(OH)_2,(H_2O)]$), feldspar ($(K,Na)Si_3O_8$), kaolinite [$Al_2Si_2O_5(OH)_4$], and mica [$AlSi_2O_6(OH)_2$].

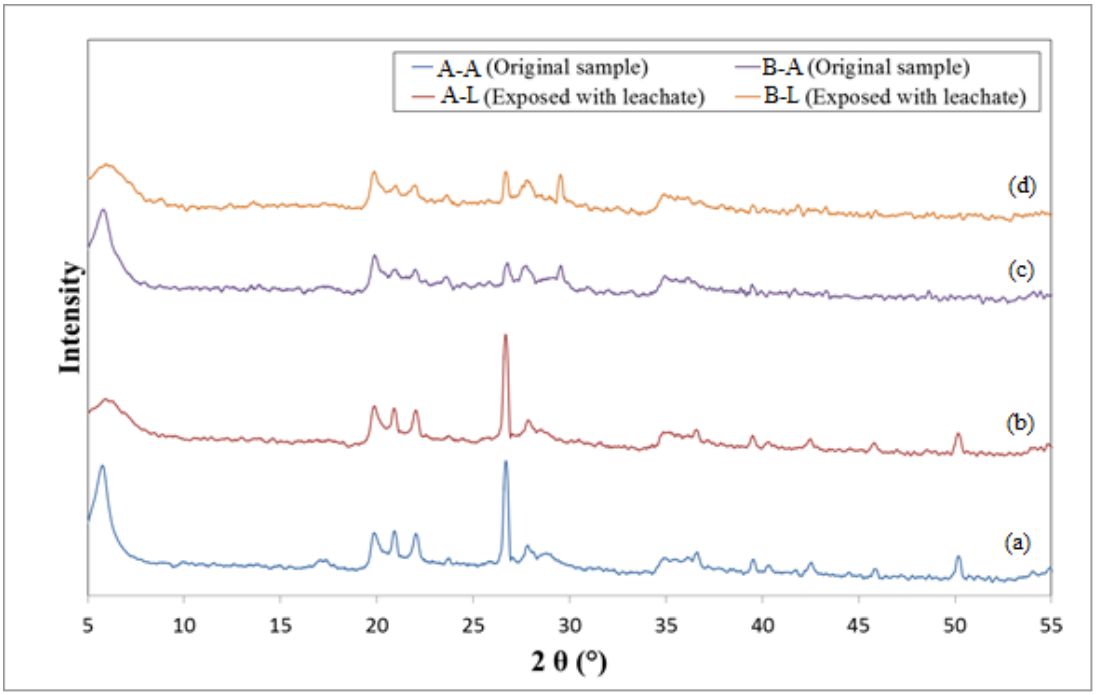

Figure 4.28 X-ray diffraction spectrum of (a) A-A, (b) A-L, (c) B-A, and (d) B-L specimens

The variation in crystallinity of the bentonite hydrated with leachate was analysed by comparing the two main peaks in both bentonite and bentonite leachate mixtures. The presence of bentonite clay was identified by two prominent diffraction peaks at 2θ angles: around 21.67° and 22.43° for the first peak. The second peak was identified around 26.57° and 26.83°. For the XRD results of the bentonite hydrated with leachate, there had been a minor variation. The first peak switched to lower 2θ angles of 21.45° and 22.18° while the second peak changed to 26.37° and 26.73°.

FTIR

The Fourier transform infrared spectroscopic analysis or FTIR technique was used to generate the absorption bands that are recognised by shape, intensity, and position (cm^{1}) in the spectrum. The FTIR spectra of the bentonite after being hydrated with distilled water and leachate are shown in Figure 4.29. FTIR data is generally used for collection of high spectral resolution used to assess the elemental composition of test specimens through the absorption of monochromatic light beams. It can then be used to identify the elements based upon the absorption wavelength peaks. After the inspection of data peaks, it was possible to observe that the FTIR results confirmed the data obtained from the XRD analyses.

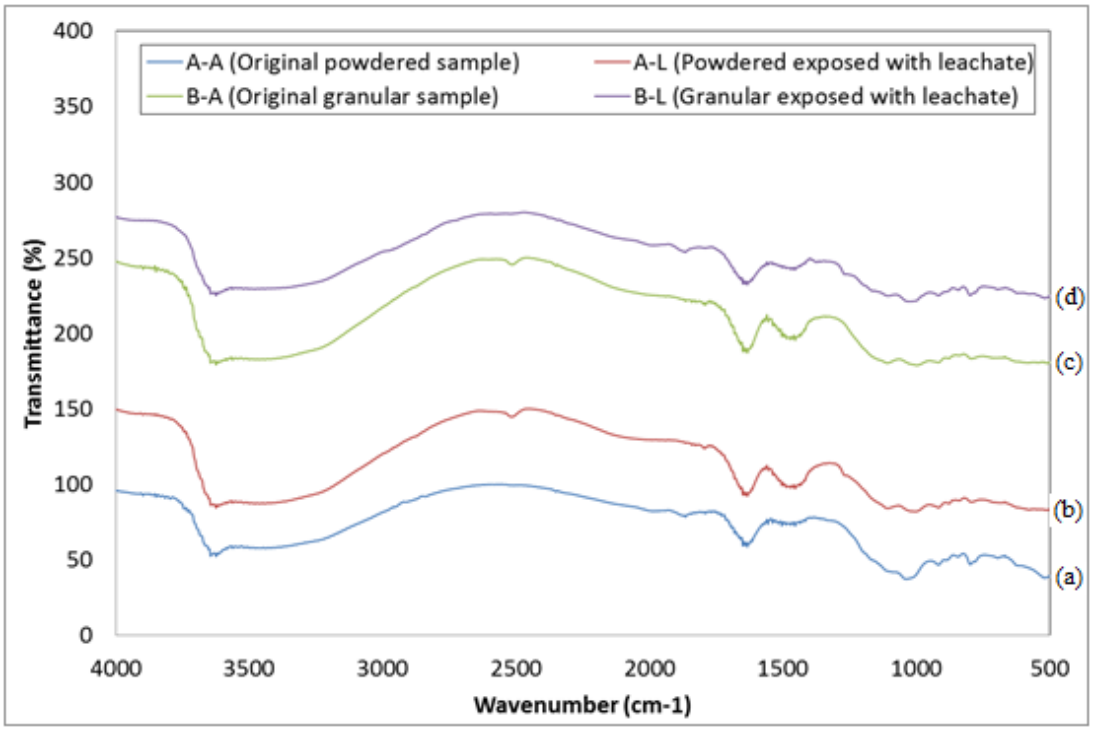

Figure 4.29 FTIR spectrum of (a) A-A, (b) A-L, (c) B-A, and (d) B-L specimens

The IR spectra of bentonite clay were found to be 3626, 1975, 1884, 1634, 1198, 1008, 915, 845, and 796 cm^{-1}. The most dominant vibration bands in both samples A-A and A-L exhibited the presence of silica group vibrations stretching in the region of 1975, 1884, 1198, and 1008 cm^{-1}. A diverse range of compounds from the hydroxyl group, associated with the peak at 3500–3650 cm^{-1} for O-H carboxylic acid monomers that have the assigned vibration in this range, and at 3590–3650 cm^{-1} O-H alcohol monomer or phenol, were found in both GCL A samples containing distilled water and leachate.

This group indicates the possibility of the presence of compounds from the kaolinite and smectite families and alkali feldspars with the possible occurrence of illite and calcite compounds. Furthermore, the vibrations associated with alkenes were also found in both A-A and A-L samples as a peak at 1610–1680 cm^{-1} indicating the presence of C=C alkene structures that fall within this wavenumber range, and a peak at 675–995 cm^{-1} showing the presence of C-H alkenes which normally appear at the wavenumber range of 675–995 cm^{-1} and 3010–3095 cm^{-1}. The vibrations associated with alkanes were also identified in both samples (A-A and A-L) at 1340–1470 cm^{-1} peak ranges indicating the possibility of C-H alkane which can be found at

wavenumber ranges of 2850– 970 and 1340–1470 cm^{-1}. Moreover, aromatic rings of C=C at a peak of 1500–1600 cm^{-1} and C-H with a peak at 690–900 cm^{-1} were also observed in A-A and A-L that respectively appear at the wavenumber ranges of 1500–1600 cm^{-1} for C=C and 690–900 cm^{-1} and 3010–3100 cm^{-1} for C-H.

In addition, vibrations assigned to the carboxylic acids/ester/ether/alcohol were also found with a peak at 1050–1300 cm^{-1} indicating C-O structures that appear in this wavenumber range for both samples A-A and A-L. Finally, both samples exhibited the vibrations assigned to nitro compounds NO_2 with peat at 1500–1570 cm^{-1}. The effect of leachate could be identified through the presence of most of the organic group compounds such as cellulose groups (2-SL), aliphatic methylene and amides with a peak at 3200–3600 cm^{-1} indicating the O-H alcohol bonding hydrogen/phenol structure. Also, vibrations assigned to carboxylic acids with hydrogen bonding with a peak at 2500–2700 cm^{-1} that appear in this wavenumber range were also found in the sample permeated with leachate.

In the GCL B sample permeated with distilled water (B-A), vibrations were observed in the peak region of 3200–3600 cm^{-1} and mostly focused on 3348.42 cm^{-1} with an intensity of 24.605, which indicates the presence of hydroxyl (O-H) alcohol hydrogen/phenol bonding which normally appears in this wavenumber range. Also, a peak was found at 2500–2700 cm^{-1} indicating O-H carboxylic acids with hydrogen bonding. Finally, the IR spectra results for the GCL B sample permeated with leachate (B-L) displayed the effect of leachate as C-N amines/amides were observed with a peak at 1180–1360 cm^{-1}.

In essence, the FTIR spectra results for bentonite correspond to the results obtained in the XRD and SEM/EDS analyses and confirm the presence of mineral materials. Generally, it was observed that the material groups did not contribute to changing the behaviour of hydrated bentonite, however, a comparative analysis of pure and leachate-hydrated bentonite samples exhibited the occurrence of further chemical bands in the mineral materials region.

Alteration of Leachate Concentration

As well as performing the leachate hydration experiment, concentration of some parameters in the leachate were monitored to examine whether there were any changes

in concentration before and after passing both GCL samples. In this experiment, the leachate from Redhill Landfill was chosen since it had a higher concentration of contaminant except for TOC, compared to the leachate from Tamala Park Landfill (L2).

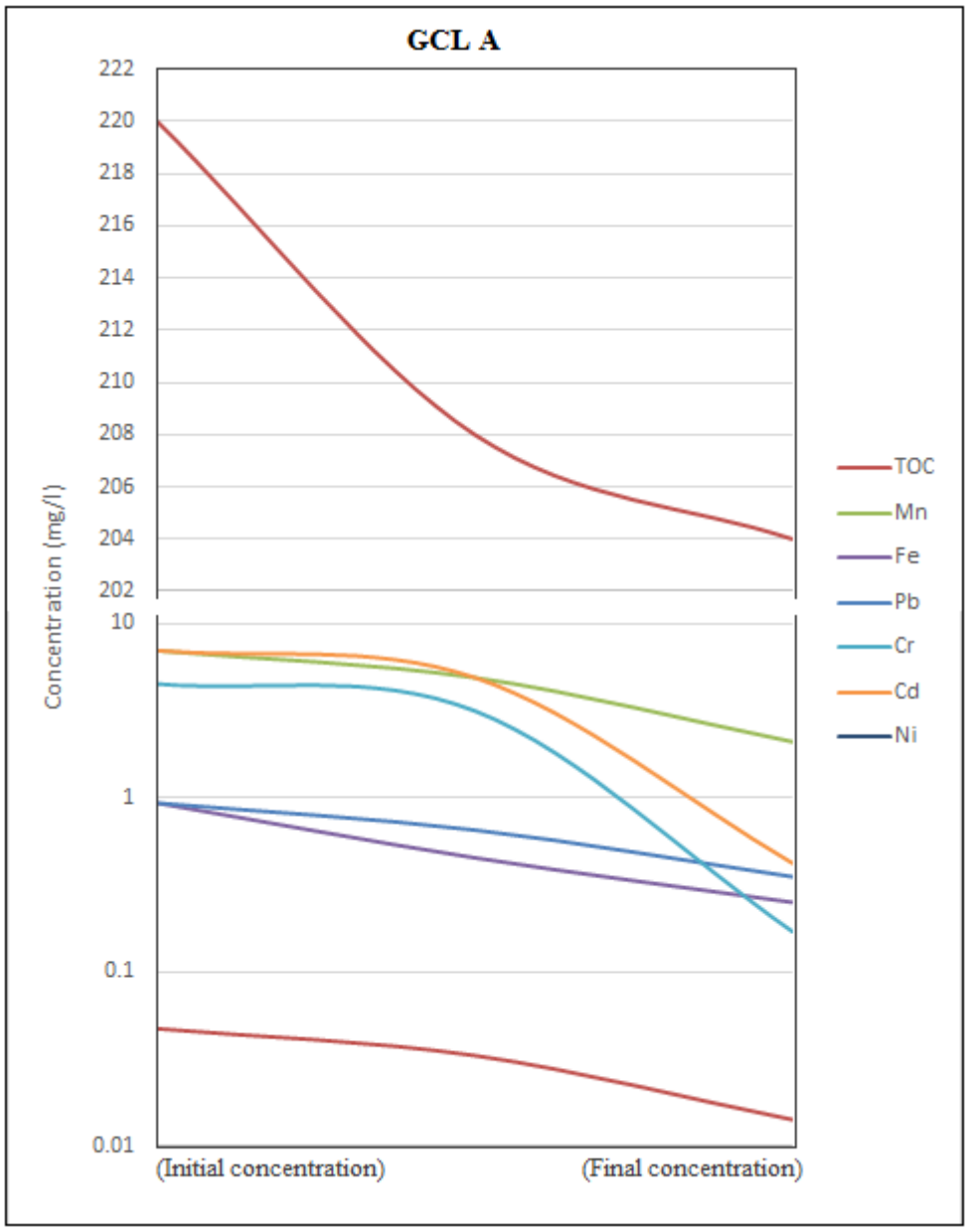

Figure 4.30 Leachate concentration after passing GCL A

Even though GCL acts as a leachate barrier in landfill, some contaminants will still be able to seep through the bentonite layer of the GCL (National Research Council 2007). However, the concentration of the contaminants tends to drop significantly after passing the GCL. Figure 4.30 illustrates the change in concentration of some

substances after passing GCL A, while Figure 4.31 depicts the alteration in leachate concentration after permeating GCL B.

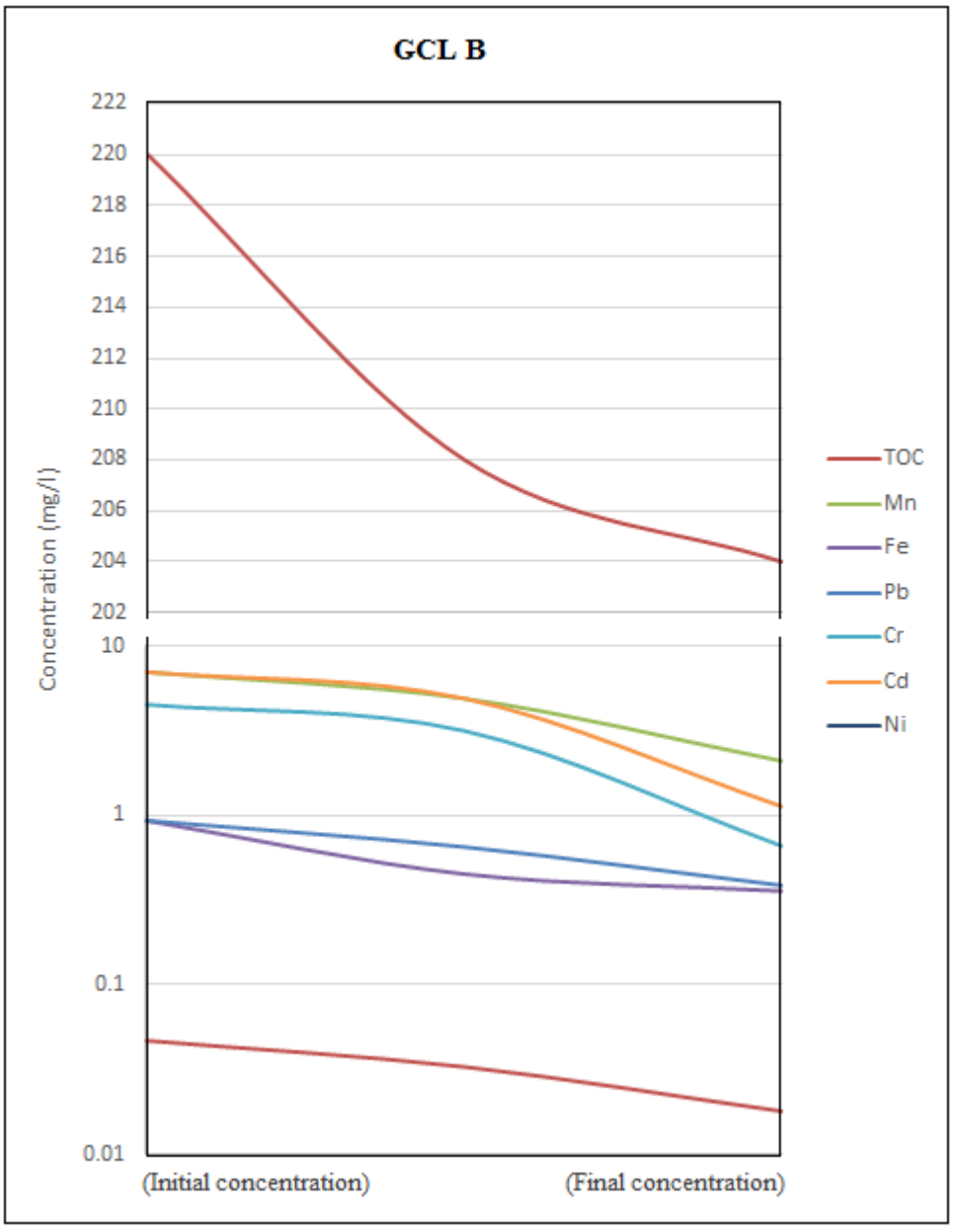

Figure 4.31 Leachate concentration after passing GCL B

Table 4.7 The percentage of concentration reduction

Parameter	Initial concentration	Reduction (%)	
	mg/l	GCL A	GCL B
TOC	220	7.2	7.47
Mn	0.047	71.6	61.65
Fe	6.981	69.2	70
Pb	0.93	73.12	61.56
Cr	0.93	62.23	58.48
Cd	4.5	96.22	85.34
Ni	6.99	93.99	83.84

The reduction in contaminant concentration varies for each substance. The concentration of TOC does not seems to alter much since the TOC concentration after passing the both GCL (GCL A and B) is only about 7% lower than the initial TOC concentration. However, the concentration of some heavy metals drops by 69.2% to 94% after passing the GCL A (Table 4.7). By contrast, the final concentration of heavy metals after permeating GCL B ranges from 61.6% to 84%.

Chapter 5
Stabilisation of Landfill Subgrade

5.1 Introduction

The stability of the liner system in a municipal solid waste landfill is critical in avoiding any kind of failure that may diminish the functioning of the liner. The role of the landfill liner is to prevent leachate contamination entering the surrounding environment, and the failure of the liner system could allow leachate to infiltrate the surrounding soil and contaminate the groundwater. Repairing a collapsed liner system will be very costly, involving leakage identification to locate the position of the failure, removal of the buried solid waste and replacement of the landfill liner. Moreover, the soil and groundwater contamination are the most cost-critical factors.

According to Qian, Koerner, and Gray (2001) and Reddy and Basha (2014), the stability of the landfill is affected by factors such as the shear strength of the material. Shear strength is a major engineering parameter that defines the soil's ability to resist failure. The stability of landfill liner is mostly affected by the shear strength of the liner subgrade. Generally, the impermeable liner rests on the compacted sand. However in cases where geosynthetic clay liner (GCL) is used as a leachate barrier, a layer of compacted clay (bentonite) is also placed in some areas of the subgrade such as under the overlapping intersections of the GCL layers.

According to Kramer (1996), sand is considered to be finer grained and has the limitation of generating high pore pressures and may undergo soil liquefaction. When the landfill is located in an area with a high groundwater level, the sand subgrade will be under-saturated or partially saturated and will lose stiffness and strength in response to applied stress. Earthquake shaking or dynamic loading creates rapid changes in stress conditions, causing the soil to behave like a liquid (Xia and Hu 1991). This situation is likely to occur in landfill areas since waste compaction is performed continuously.

Therefore, the focus of this chapter is to examine the stability of the two subgrade materials, which are compacted bentonite and sand. The shear strength of the bentonite will be discussed along with bentonite stabilisation using sludge, a by-product of waste water treatment plants. The stability of sand as a subgrade will also be discussed along with the use of slag and wood to stabilise sand. In addition, the liquefaction resistance of stabilised sand with added slag will be examined. The outline of this chapter is presented in Figure 5.1.

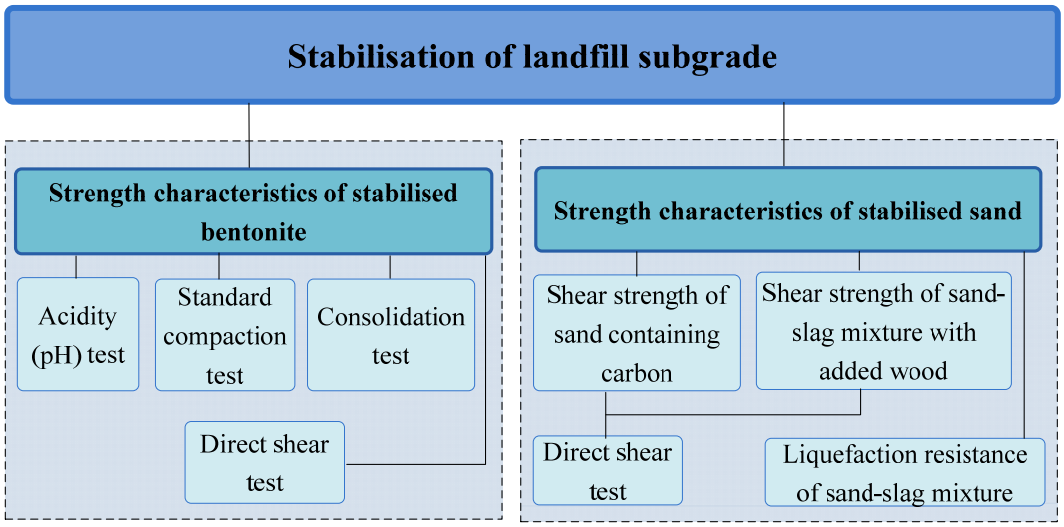

Figure 5.1 Outline of stabilisation of landfill subgrade

5.2 Strength Characteristics of Stabilised Bentonite

Shear strength is a critical factor in the stability of landfills containing geosynthetic liner systems. Supriyadi, Kriwoken, and Birley (2000) have stated that for composite materials or GCL, inadequate internal shear strength of the landfill subgrade is among the major causes of failure in the landfill system, resulting in shear failure along the surfaces of rupture. Therefore, the subgrade should remain sufficiently stable, pre- and post-construction, to prevent the effect of movement and to mitigate the magnitude of slope instability, heaves and settlements on the overlying liner system. Subgrade stabilisation has to be commissioned if a weaker subgrade exists in the liner system and the choice of subgrade depends upon availability, cost and durability, and the stability criteria of the landfill system.

On the other hand, the substantial increase in wastewater has become a critical environmental issue globally in waste management. The problem of wastewater production has been exacerbated by rapid developments in urbanisation and industrialisation processes and is another concern surrounding landfill management (Wang, Chen, et al. 2008; Manso et al. 2013). Sewage sludge (bio-solids) is the major component of all by-products of wastewater from treatment plants worldwide, with the annual production of bio-solids in Australia and New Zealand being approximately 300,000 dry tonnes (Shao et al. 2007; Smidt and Parravicini 2009; Australian & New Zealand Biosolids Partnership 2012).

Sustainability, environmental and economic aspects need to be considered when selecting any proper sewage sludge treatment in order to avoid potential pollution issues (Chen and Jeyaseelan 2001; Chen, Jeyaseelan and Graham 2002; Smidt and Parravicini 2009). Landfill, agricultural applications, incineration and sea dumping are the conventional sewage sludge waste management strategies. For Australia and New Zealand, landfill has become the most popular disposal technique for bio-solids (Australian & New Zealand Biosolids Partnership 2012; Wang, Brown, et al. 2008). However, there are still sustainability issues around sewage sludge landfilling, as well as the disadvantages of limited landfill space and high costs (Wang, Chen, et al. 2008; Smidt and Parravicini 2009). Both sewage sludge waste management and inadequate solid waste landfill subgrade strength can be resolved with the development of a common solution since the application of sludge in soil stabilisation is yet to be sufficiently studied.

Furthermore, research into dry sewage sludge crystallisation has revealed a vital role for silica and calcite in the reduction of the cement hydration process, and the pozzolanic characteristics of sewage sludge are crucial for improving the engineering properties of soil (Yagüe, Valls and Vazquez 2002; Lin et al. 2007; Davraz and Gunduz 2005; Chen and Lin 2009). The polymerisation process can occur where there is interaction between sewage sludge ash as pozzolan and calcium atoms in soil components (Chen and Lin 2009; Lin et al. 2007).

The polymerisation process produces cementitious compounds such as calcium-aluminium-silicate-hydrates (C-A-S-H), calcium-silicate-hydrates (C-S-H) and

calcium-aluminate-hydrates (C-A-H) (Cuisinier et al. 2008; Harichane et al. 2011; Solanki and Zaman 2012; Amiralian 2013).

Lime ionisation : $Ca(OH)_2$——$Ca^{2+} + 2(OH)^-$

Soluble clay silica : $Ca^{2+} + OH^- + SiO_2$——C-S-H gel

Soluble clay alumina : $Ca^{2+} + OH^- + Al_2O_3$——C-A-H gel

For the purpose of providing a simultaneous solution in municipal solid waste management to improve the subgrade shear strength, this section focuses on the use of sludge as a stabiliser for subgrade clay liners. Therefore, the purpose of this research is to introduce a comprehensive method for the analysis of improvements to understand the effect of sludge as a clay liner stabiliser.

5.2.1 Bentonite and Sludge Preparation

Four mixtures were prepared by combining sludge with bentonite clay based on weight percentages of 0%, 2%, 4% and 6% respectively. The prepared sludge was oven dried for two days at a temperature of 100ºC ± 1ºC. The quantity of water added and the dry weight of the specimens were determined based on the moisture content and maximum dry density obtained from the standard compaction test, while samples had been cured in plastic bags for two days. Prior to the actual tests, specimens of pre-determined quantities were properly compacted in shear boxes using a compaction hammer.

5.2.2 The Laboratory Testing

PH value, compaction, consolidation and direct shear tests were carried out on both original and treated samples to investigate their engineering performance. Automatic devices were used for the consolidation and direct shear tests to minimise any errors caused by user interference. PH value was determined using the electrometric method test as described in Standards Australia (1997). Standard compaction tests (Standards Australia 2001b) were conducted to obtain the maximum dry density (MDD) and optimum moisture content (OMC) of pure bentonite, and these values were then used for other specimens and tests. One-dimensional consolidation tests were carried out using an automatic device based on Standards Australia (1998).

The shear strength of the soil was determined by parameters including horizontal and vertical displacement, vertical-confining stress, shear stress, soil cohesion (c) and frictional angle (ϕ) (Budhu 2010b). Shear strength is dependent on the interactions between soil particles, which directly determine frictional resistance and cohesion between atoms (Budhu 2010b; Kalinski 2011). With a prescribed normal stress (σ), the maximum shear stress (τ) is the stress at the sample's failure point (the failure area is shown by the red dash line in Figure 5.2).

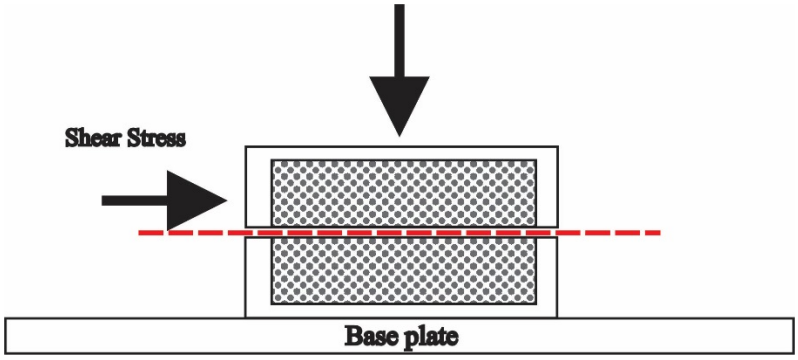

Figure 5.2 The schematic form of the direct shear test theory

There is an interrelation between the applied normal stress and the shear stress amount and utilising the results obtained, the Mohr-Coulomb failure envelope was drawn by plotting the σ versus τ over a range of prescribed normal stresses. Based on Standards Australia (2001c), the direct shear test was conducted using applied vertical loads of 50kPa, 100kPa and 200kPa respectively.

$$\sigma = \frac{N}{A} \; and \; \tau = \frac{F}{A} \tag{5.1}$$

$$\tau = \mathrm{c} + \sigma \tan \phi \tag{5.2}$$

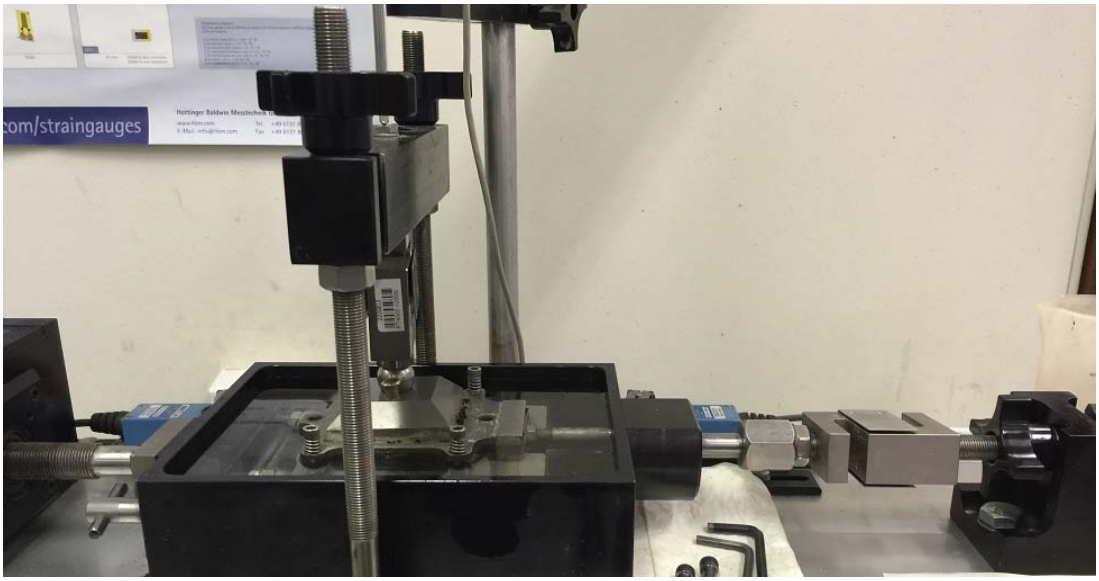

Figure 5.3 Direct shear testing

5.2.2.1 pH Values

Figure 5.4 illustrates the pH variations in different combinations of sludge and bentonite. On the pH scale, the sludge and bentonite are classified into two modes: near natural mode and free lime mode. Also indicated in Figure 5.4, the bentonite composites change from alkaline to acidic with the passing days. This is likely to be induced by the stabilisation and saturation processes of calcium, and the gradually decreasing levels of calcium in the specimens. Consequently, as demonstrated by the range of obtained results, the type of soil is Na-bentonite with a low percentage of calcium.

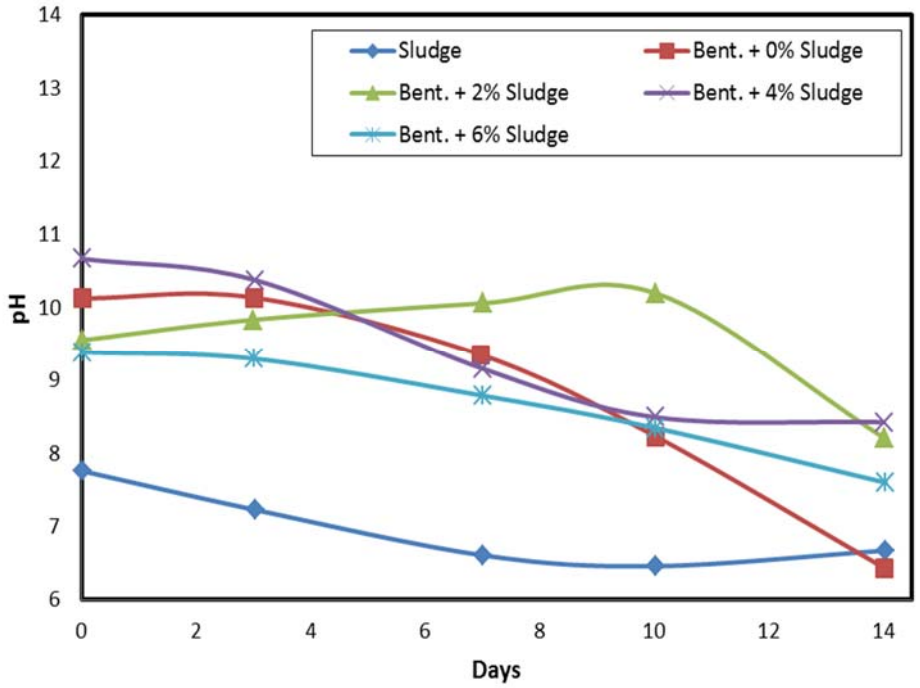

Figure 5.4 The pH results for sludge and bentonite composites

5.2.2.2 Standard Compaction Test

The repositioning of soil particles can lead to a decrease in void ratio and the exclusion of air, and this phenomenon is called soil densification (Amiralian 2013). In order to determine the maximum dry density and optimum moisture content of pure bentonite clay, the soil compaction test was utilised as an initial step. The results showed that the bentonite had optimum moisture content of 43% and maximum dry density of 1150 mg/cm^3.

5.2.2.3 One-Dimensional Consolidation Test

Another form of soil densification is consolidation, which occurs when the water and air are squeezed out from the pores in a soil body due to the application of load. By examining the changes in sample height, the void ratio and effective axial stress can be calculated. Figure 5.5 depicts the change in void ratio (e) due to either loading or unloading, as well as other parameters including the compression index (C_c) and swell index (C_s), for one pure composite and three sludge-bentonite mixture samples. Basically, for the pure compound, the consolidation-swelling behaviour is restricted by the addition of sludge.

Figure 5.5 also shows that the addition of sludge improves the consolidation behaviour of bentonite. Compared to the trend line for bentonite, sludge-bentonite mixtures saw a relatively moderate slope. The results demonstrate that, for bentonite, the void ratio changes will be reduced by adding sludge during consolidation tests. Therefore, it also indicates a decreasing compression index with an increasing amount of sludge.

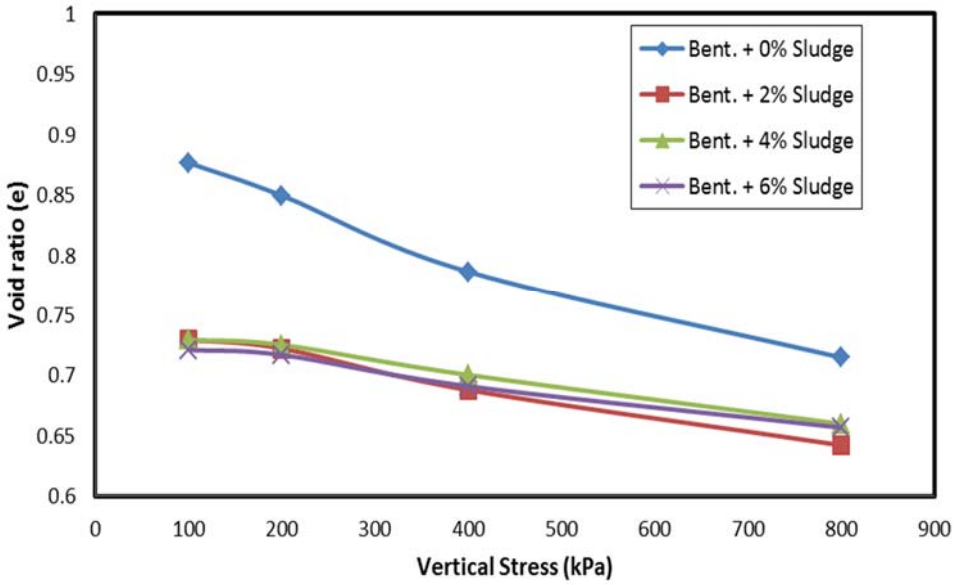

Figure 5.5 Consolidation behaviour of bentonite and sludge composites

A similar trend is identified for the swelling behaviour of the sludge mixtures (Figure 5.6). The sludge mixtures displayed a lower increment trend under the unloading step, and after a decrease in load, the sludge mixtures demonstrated a less reversible change of void ratio than bentonite. Increasing the percentage of sludge seemed to have a similar trend. A reduction in swelling index is observed in the presence of a certain percentage of sludge.

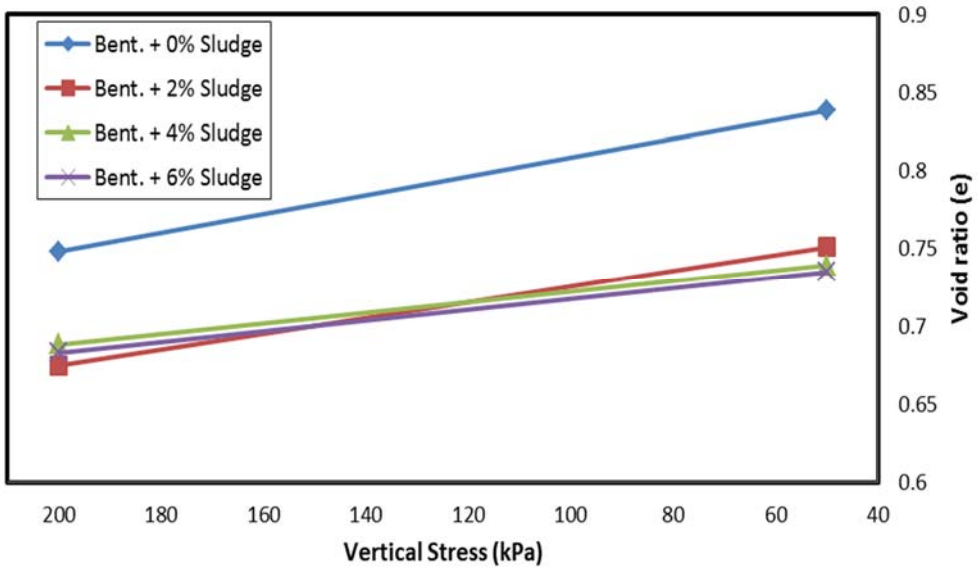

Figure 5.6 Swelling behaviour during unloading

In short, the addition of an increased percentage of sludge corresponds to a decrease in both swell index and compression index (see Figure 5.7). The lowest settlement is seen in the sample with 6% sludge, corresponding to a compression index of 9.42×10^{-5}. In comparison, untreated bentonite has a compression index of 2.31×10^{-4}.

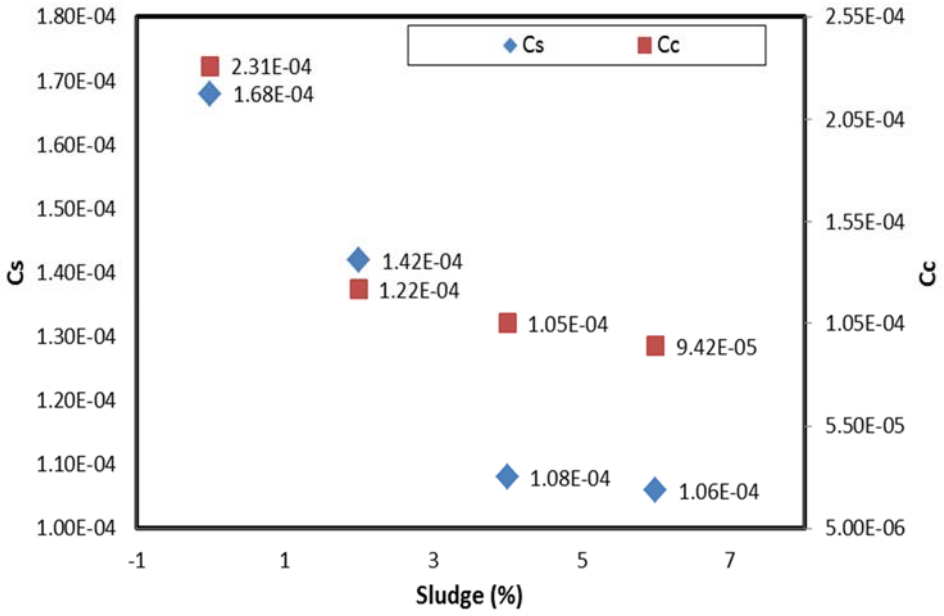

Figure 5.7 The compression index (C_c) and swell index (C_s)

Regarding the swelling behaviour of the pure combination, a similar tendency was demonstrated for the variation in compression index with the addition of sludge. In

Figure 5.7, another decreasing trend was observed for the swelling index with the increasing amount of sludge. A further addition of sludge caused the swelling index to drop from 1.68×10^{-4} to an even lower value, until a minimum C_s value of $1.06 \times 10e^{-4}$ was reached (with a sludge percentage of 6%). Figure 5.8 clearly illustrates the effect of the addition of sludge on the reduction of swelling behaviour.

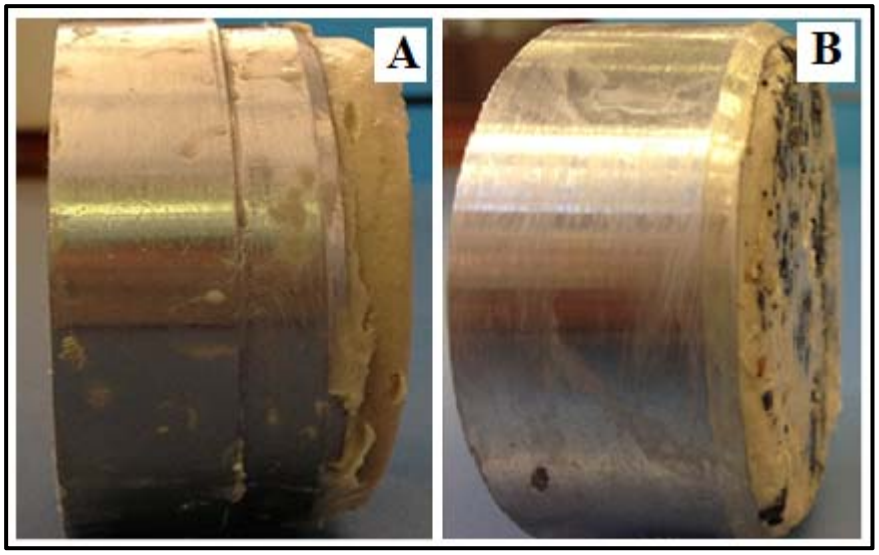

Figure 5.8 The swelling behaviour of (A) pure bentonite and (B) bentonite with sludge

However, it seems that the influence of sludge composition was stronger in reducing the C_c compared to reducing the C_s for bentonite.

5.2.3 Direct Shear Test

Generally, maximum shear strength is a crucial factor in various geotechnical analytical and design activities including slope stability, etc. The effects of sludge addition on composite strength are analysed by comparing experimental data from samples with various dosages of additives (Amiralian 2013).

Soil specimens with different percentages of sludge mixture were loaded under normal stresses of 50kPa, 100kPa and 200kPa. Figure 5.9 to Figure 5.11 illustrate shear stress development of bentonite composites with horizontal displacement. Regardless of the percentage of additives, the initial stiffness is almost the same at the same normal

stress. The results demonstrate that the shear properties of bentonite are affected by sludge mixture under all magnitudes of vertical loads.

Figure 5.9 indicates that a higher horizontal load is reached with the addition of sludge. The maximum magnitude was identified as 98.59 kPa with an added sludge percentage of 2%, and this value dropped when the addition of sludge ceased. However, the reduction in strength due to ceasing the addition of mixture was a gradual process, and the reduced strength was still greater than for the pure bentonite (82.7kPa).

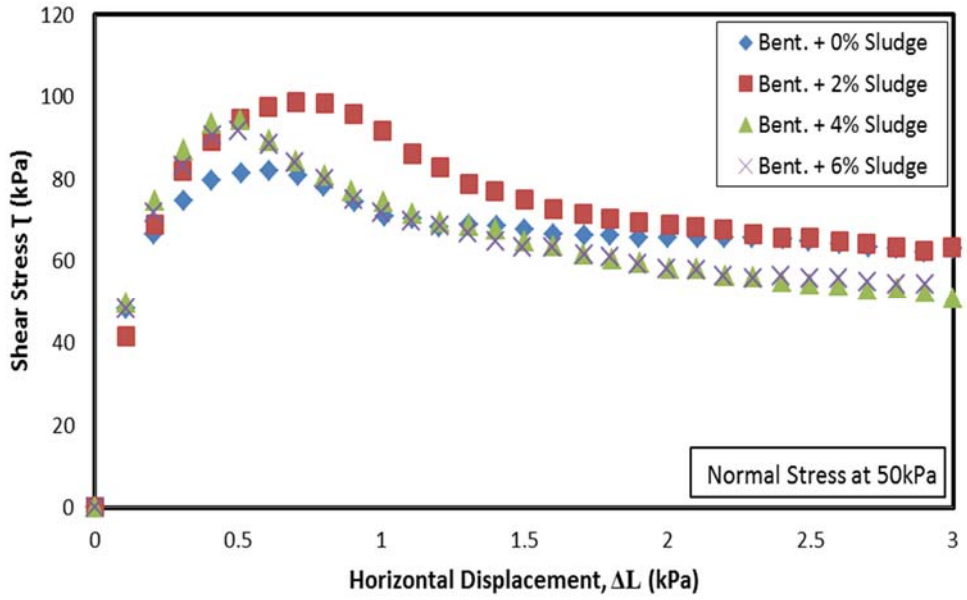

Figure 5.9 Shear stress-horizontal displacement tests for the bentonite mixtures with different proportions of sludge added under vertical load at 50 kPa

Moreover, at the maximum shear stress for untreated soil, the displacement is about 0.601 mm. The addition of 2% sludge resulted in failure at 0.7 mm. Nevertheless, same shear stress behaviour was observed when the additive dosage was increased.

In contrast, an increase in vertical load can reverse this tendency. Figure 5.10 illustrates a relationship between the improvement of strength properties and the quantity of additive. Shear strength increased from 90.08 kPa to 128.7 kPa, followed by a minor increase to 136.8 kPa with 6% added sludge. However, the greatest shear strength increment was seen with the addition of 2% sludge. The displacement mobilised in horizontal failure increased from 0.4007 mm to 0.8002 mm.

The results obtained for shear stress versus horizontal displacement for bentonite mixtures at 200 kPa normal load are shown in Figure 5.11. The results indicate that an increase in the sludge dosage improved both the shear failure point and shear strain properties of bentonite. The maximum shear failure that occurred in the sample is 193.2 kPa with a 0.9003 mm displacement for the sample with 6% added sludge. The maximum strain was normally reached in the bentonite composite containing the maximum percentage of additives.

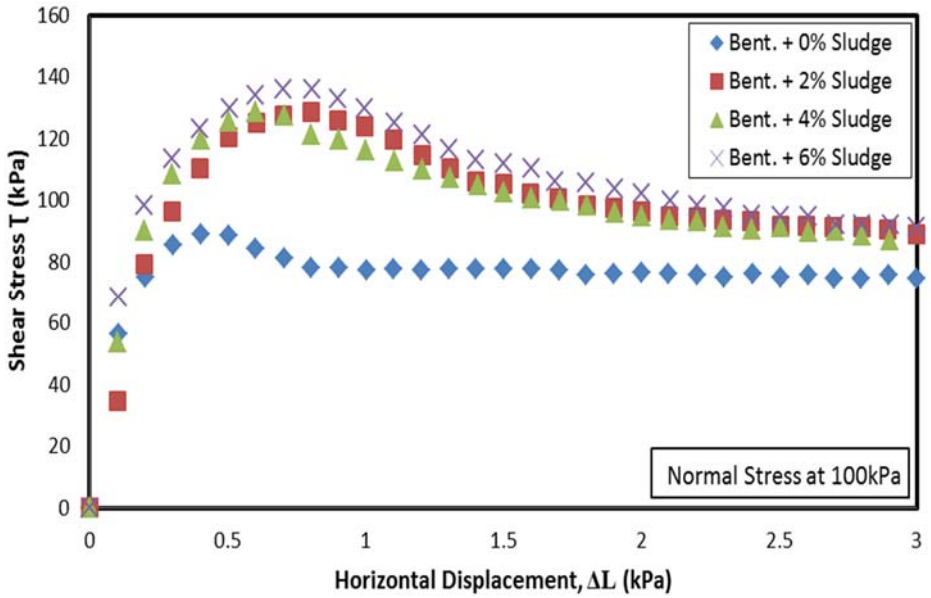

Figure 5.10 Shear stress-horizontal displacement tests for the bentonite mixtures with different proportions of sludge added under vertical load at 100 kPa

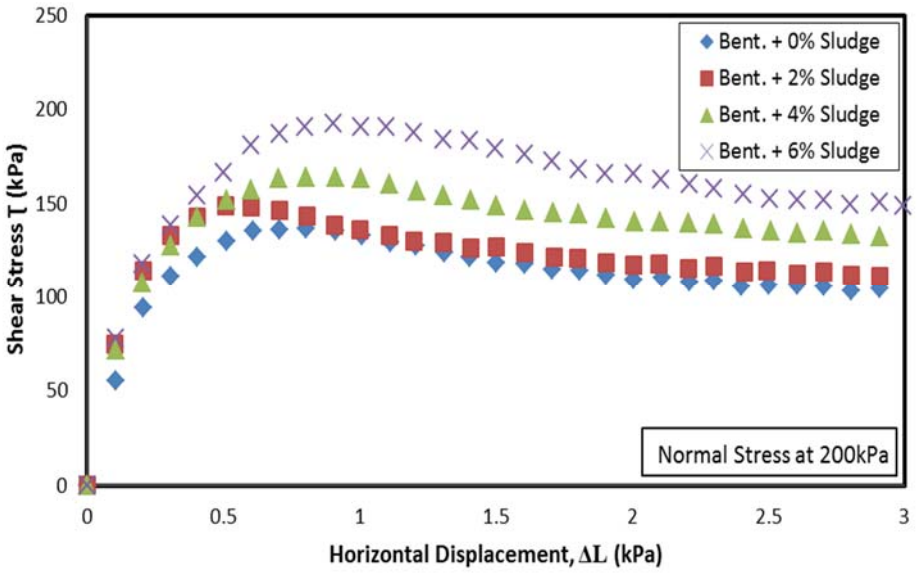

Figure 5.11 Shear stress-horizontal displacement tests for the bentonite mixtures with different proportions of sludge added under vertical load at 200 kPa (small direct shear)

There is also a minor effect on the friction angle of bentonite composites caused by the addition of sludge (Figure 5.12). The friction angles obtained from the direct shear data decreased, with 2% sludge demonstrating the largest reduction, followed by an increase with a higher percentage of additive. A similar trend was identified for the cohesion of bentonite composite, with 2% sludge demonstrating the highest increment.

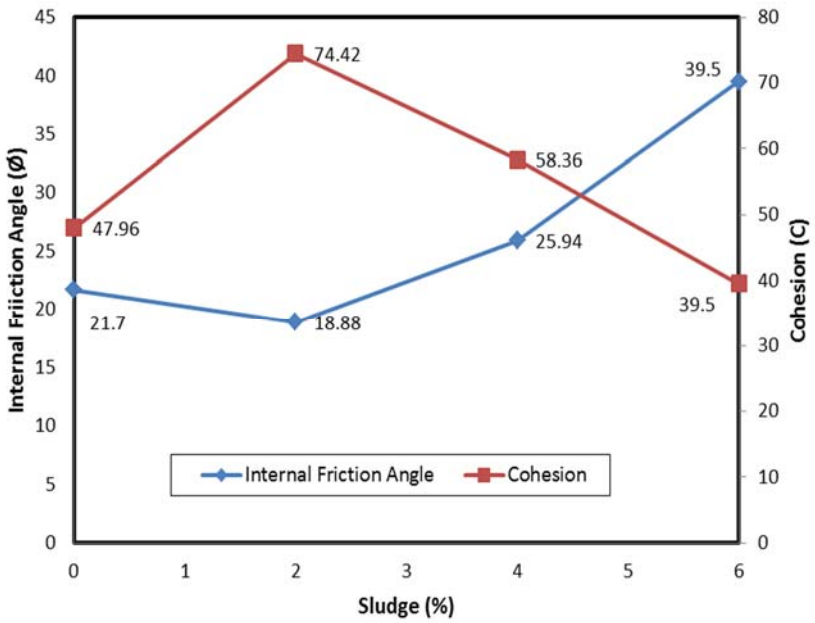

Figure 5.12 The cohesion and internal friction angle of bentonite mixture

5.3 Strength Characteristics of Stabilised Sand

The preceding case studies a technique for improving the engineering properties of bentonite. The stabilisation of the sand layer in the landfill system is discussed in this section. Several factors contribute to stability issues in landfills, and therefore, to the need for stabilisation techniques. As landfills are conventionally located in regions with persistent slope stability issues, such as quarries, reclaimed regions and open pit mines, the stability of the compacted or naturally-occurring landfill subgrade becomes a major concern.

There are many mechanisms that can trigger a structure on soil to collapse. Excessive settlement is one of them, which can be caused by the extraction of water (Budihardjo, Chegenizadeh and Nikraz 2014), and any strength reducing effects can also be detrimental. Shear strength is a parameter of soil required to analyse various geotechnical matters including soil bearing capacity, slope stability and retaining walls (Budhu 2010a), and can represent the capability of the soil to support any overlying structure such as the case for the landfill liner system.

The internal shear of the landfill subgrade is also important for maintaining the stability of the landfill system. In classical soil mechanics, the shear strength of soil is interpreted by cohesion (C) and internal friction angle (θ) (Budhu 2010b). The shear strength of soil is an important parameter in the design and analysis of various geotechnical engineering subjects. Therefore, accurate analysis and consideration of soil shear strength are required to prevent structural failure brought about by the collapse of underlying soil that will destroy the basic foundation of overlying structures (Budhu 2010a).

However, the purity and particle uniformity of sand can influence its shear strength performance (Budhu 2010b; Prabakar and Sridhar 2002). Landfill liner system soil subgrade material has inherent complexities as well as geographical variation. When there are other components present in sand, such as carbon, the purity of the sand is changed. As the percentage of carbon in the sand varies in different locations, the shear strength performance will vary as well (Yang et al. 2013).

Therefore, the study on the effects of the stabilisers on the shear strength of the landfill subgrade sand has been divided into two cases as follows:

1. Strength characteristics of sand containing carbon
2. Strength characteristics of wood-stabilised sand-slag

The first case examines the effect of carbon content on the shear strength performance of sand, and seeks to discover the potential of carbon as an additive for soil stabilisation. Meanwhile, the second case investigates the prospect of improved shear strength properties of stabilised sand. The target sand has already been stabilised by the addition of chemical stabiliser and will be further tested with the addition of timber to achieve the desired reinforcement.

There has been increasing utilisation of chemical additives such as cement, fly ash, lime and slag in land development projects due to the convenience of application (Azadegan, Yaghoubi and Pourebrahim 2011; Allan and Kukacka 1995; Tastan et al. 2011). Portland composite cement (PCC) is particularly popular due to its market availability and relatively easy application in the field. However, although soil stabilisation using cement may lead to a very high shear strength, cement also tends to make the mixture highly brittle and low in tensile strength (Yi, Liska and Al-Tabbaa 2013).

As a result, the cemented soil is an even less satisfactory construction material when the soil underlying landfill needs to be both strong and ductile. The high ductility of the liner system reduces the bending risks caused by differential settlement of waste (Mukunoki et al. 2014). The tensile behaviour of sand has rarely been studied, and in light of the susceptibility of the sand subgrade to tensile stresses, the addition of wood has gained particular interest due to the ability of the wood to improve both the tensile strength and ductility of the soil (Prabakar and Sridhar 2002).

In relation to this, timber waste from the construction industry forms a large portion of the demolition waste dumped to landfills around the world. In Australia the demand for the reuse of recovered timber is comparatively limited while timber waste generation ranges from the demolition of building structures to timber pallets (Hyder Consulting 2011). Therefore, the experiment on the strength characteristics of wood-stabilised sand-slag aims to test the effect of timber elements on the shear performance

of sand containing various percentages of slag. The objective of the investigation is to identify a means of reusing timber waste for landfill subgrade stabilisation instead of dumping it in the landfill as solid waste, which limits the solid waste management capacity of the landfill system. The significance of this study is to examine the viability of adding wood to slag-stabilised sand as an alternative means of improving the shear strength of soil. Moreover, the application of wood has the potential to lead to more sustainable solutions for soil stabilisation.

5.3.1 Materials

The sand and additive mixtures that were studied in this section included the following components.

5.3.1.1 Sand

Since this research is intended to benefit projects in Western Australia, the sand used for all the tests in this research is the one that is widely used in Western Australian construction and structural projects. Yellow sand (Baldivis sand) was selected for this experiment due to its availability in Perth, Western Australia. As its name states, Baldivis sand is a quartz sand coming from the Baldivis area (50 km south of Perth). Baldivis sand can be classified as poorly-graded sand with a specific gravity of 2.65.

A compaction test as outlined in Standards Australia (2001b) was conducted to obtain maximum dry density (MDD) and the optimum moisture content (OMC) of the Baldivis sand. The OMC and MDD values were found to be 11.27% and 1.67 respectively.

5.3.1.2 Carbon

Granular activated carbon (GAC) provided by a local supplier was used in this experiment. The adsorption surface area of this carbon material is about 650 to 1000 m^2/gram. This type of carbon is obtained from a carbon source (coal, nutshells, lignite, or wood) without the presence of air. It is also generally used in water treatment processes due to its filtration function which enables the removal of contaminants from any other liquid (Laine and Calafat 1989).

5.3.1.3 Slag

Slag is widely used as an additive material in structural engineering projects. Recently, the engineering effect of adding slag to soil has been of interest to engineering researchers (Allan and Kukacka 1995; Tastan et al. 2011). Ground granulated blast furnace slag (GGBS) is the type of slag used in this experiment, and was obtained from BGC Cement, Western Australia. The chemical constitution of GGBS includes CaO, SiO_2, Al_2O_3, and MgO (Ecocem Ireland Ltd 2012). Table 5.1 and Table 5.2 demonstrate the engineering characteristics of GGSB (Ecocem Ireland Ltd 2012).

Table 5.1 Chemical content of GGSB (Ecocem Ireland Ltd 2012)

Calcium oxide (CaO)	Silica (Amorphous CaO)	Aluminium oxide (Al_2O_3)	Sulphur (S)
30–50%	35–40%	5–< 5%	15%

Table 5.2 Physical properties of GGBS (Ecocem Ireland Ltd 2012)

Colour	Bulk density: loose (tonnes/m^3)	Bulk density: vibrated (tonnes/m^3)	Relative density	Surface area
Off-white	1.0–1.1	1.2–1.3	2.85–2.95	400–600 m^2/kg

5.3.1.4 Wood

Aspen timber is the wood employed in this experiment. The wood elements in the sample were prepared in small quantities with dimensions limited by the accommodation capabilities of the small direct shear device. The specific gravity of wood is 0.36 and the initial moisture content of the wood was 12% (Table 5.3).

Table 5.3 Properties of aspen timber (Kretschmann 2010)

Moisture content	Specific gravity	Modulus of rupture (kPa)	Modulus of elasticity (*c*) (MPa)	Shear parallel to grain (kPa)
12	0.36	37,000	7,700	5,000

5.3.2 Experimental Procedure

Based on their dry densities, the samples were loaded and compacted layer by layer in a 60mm x 60mm shear box before the start of the direct shear test. Water was added

to the shear box once the sample had been made ready in the box. The sample was allowed to consolidate properly by applying a specific normal stress. For each set of tests, the sample was subjected to stresses of 50, 150 and 250 kPa respectively.

Since the automated direct shear machine was used to execute the direct shear testing, the results were logged and saved automatically by the computer with special software for the test. After completion of the tests, the results were transferred to an Excel spreadsheet for analysis and calculations. The failure stresses were treated with high importance and preference due to their relevance to the crucial friction angle and cohesion parameters. The cohesion and friction angle of samples were then calculated once failure stresses for each composite were obtained.

In order to examine the strength characteristics of sand containing carbon, a series of direct shear tests were conducted on four different types of samples consisting of sand with nil, 5%, 10% and 15% carbon content. Particle uniformity of the sand was achieved by sieving and the initial moisture content was removed by drying. To add carbon into the mixture, the required weight of carbon corresponding to each percentage level was calculated according to the dry weight of the sand. The procedure for the direct shear test was based on AS 1289.6.1.1-1998 (Standards Australia 1998).

In order to investigate the strength characteristics of wood-stabilised sand-slag, direct shear test was conducted to examine the shear strength of the mixture, with the initial test being on the pure sand specimen, followed by sand containing various proportions of slag, and finally, the sand-slag mixture with wood additives. Of the sand specimens, the introduced sand specimens contained slag percentages of 1%, 2% and 3%. AS 1289.6.1.1-1998 (Standards Australia 1998) specifications were adopted as guidelines for the direct shear test.

5.3.3 Shear Strength of Sand Containing Carbon

The first set of direct shear tests was conducted on the sample of pure sand (without any carbon content). Three different normal stresses were applied to the sample (i.e. 50, 150, and 250 kPa). The first load applied was 50 kPa and the largest sustained shear stress was 35.87 kPa. The second normal stress applied was 150 kPa which produced a maximum shear stress of 98.86 kPa. Finally, a failure shear stress of 172.36

kPa was resulted from 250 kPa normal stress applied to the sample. These results derived an internal friction angle of 34.3° and a cohesion value of 0 (Figure 5.13).

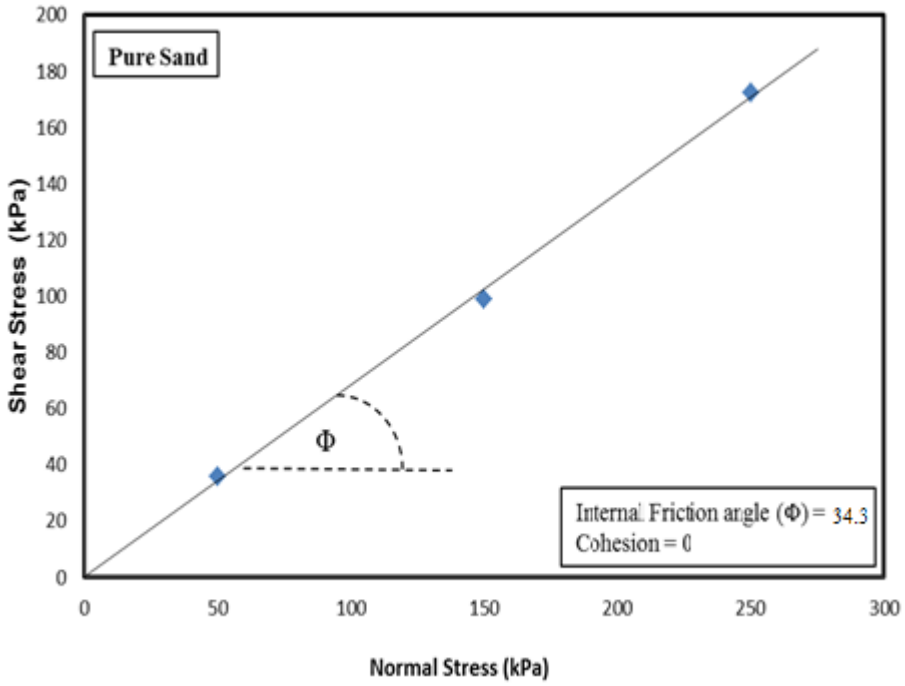

Figure 5.13 Shear stress with various normal stresses of pure sand

Once test on the pure sand has been done, the next experiment was aimed at investigating whether the presence of carbon in the soil sample contribute to any change occurred in the shear strength. Firstly, the sand containing 5% carbon additive was tested at 50, 150 and 250 kPa of normal stress. The results showed that when 50 kPa of normal stress was applied, the shear stress recorded at failure was 35.1 kPa. When normal stress increased to 150 kPa, the maximum shear stress recorded was 84.1 kPa, and a maximum shear failure of 145.9 kPa was recorded after the application of 250 kPa normal stress. As demonstrated in Figure 5.14, the internal friction angle of 29° was found for the sand sample containing 5% carbon.

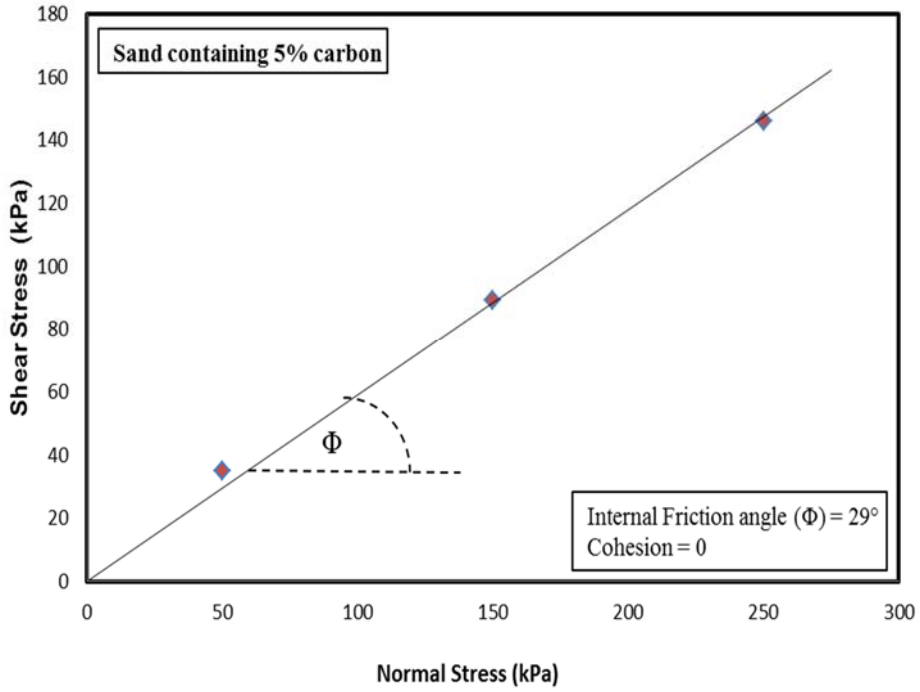

Figure 5.14 Shear stress with various normal stresses of sand with 5% carbon

Figure 5.15 depicts the results on sand samples with 10% carbon, with the same levels of normal stress (50, 150 and 250 kPa). The application of 50 kPa normal stress led to a failure shear stress of 31.1 kPa, while the application of 150 kPa and 250 kPa of normal stress obtained a failure shear stress of 84.1 kPa and 140.2 kPa respectively. For the sand sample containing 10% carbon, the plotted results derived an internal friction angle of 28.6°.

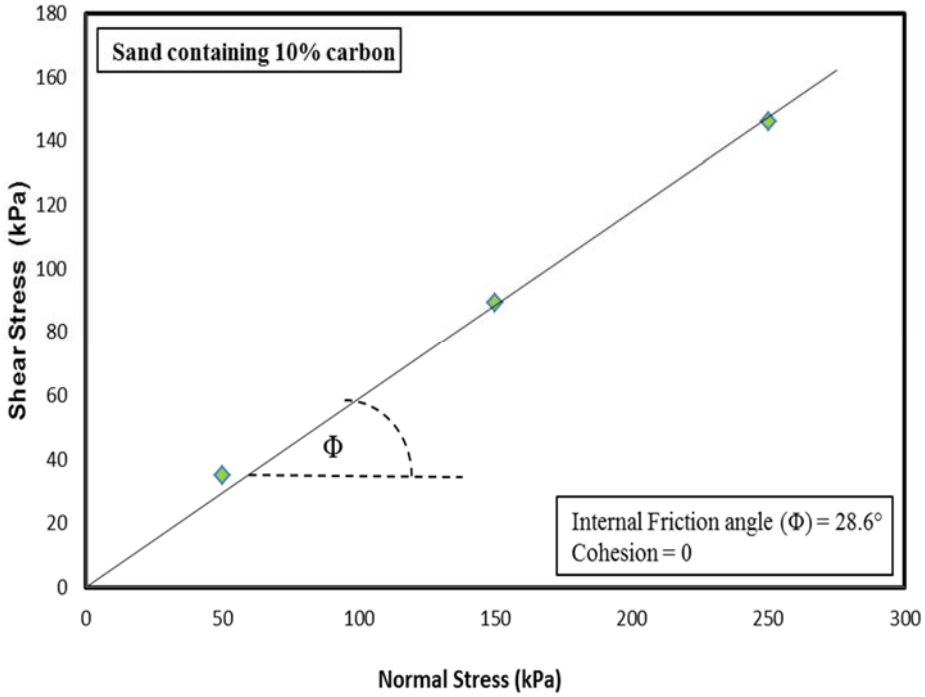

Figure 5.15 Shear stress with various normal stresses of sand with 10% carbon

Figure 5.16 illustrates the the shear strength of the sand containing 15% carbon. The application of 50 kPa of a normal stress produced a maximum shear stress value of 28.8 kPa, a normal stress of 150 kPa obtained an 80.4 kPa shear stress and 133.6 kPa shear stress was the result for 250kPa normal stress. Plotting all the results, the obtained internal friction angle was 27.6°, which was the lowest compared to other sand-carbon mixtures with different carbon content.

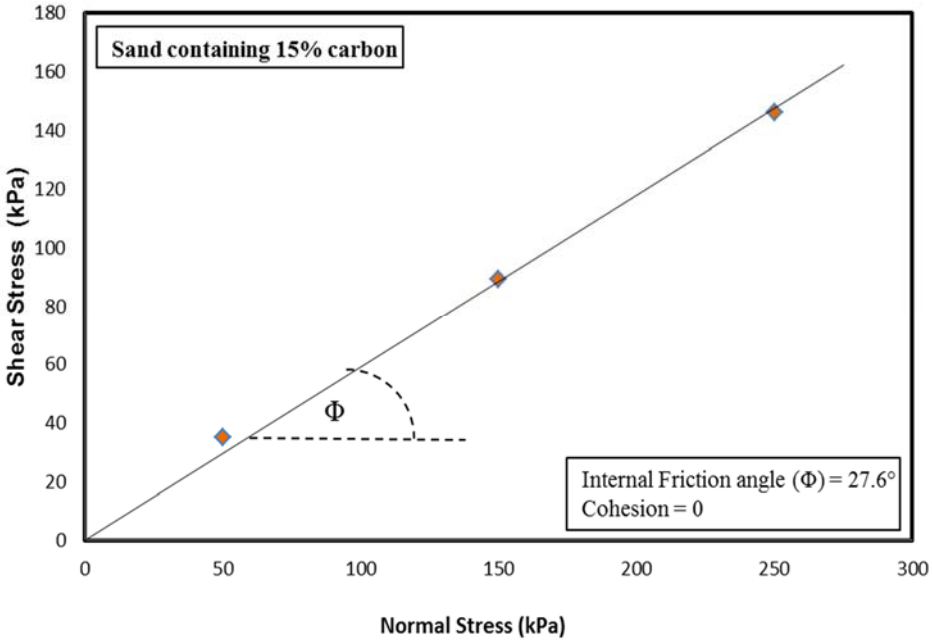

Figure 5.16 Shear stress with various normal stresses of sand containing 15% carbon

Under various normal stress, the shear strength of the sand-carbon mixture tended to decrease with an increasing amount of added carbon. Under 50 kPa of normal stress, a sand-carbon mixture with 5% carbon showed a reduction of 2.1% in the shear strength of sand, while 10% and 15% carbon respectively produce a shear strength reduction of 13.3% and 19.6%. In the case of 150 kPa normal stress, the presence of 5% carbon tended to decrease the sand-carbon mixture's shear strength by 9.7%, while the 10% and 15% carbon content lead to a respective 14.9% and 18.7% shear strength reduction. Under 250 kPa of normal stress, 5% carbon content in the sand-carbon mixture resulted in a reduction in shear strength by 15.3%, while 10% and 15% carbon content decreased the shear strength by 18.6% and 22.5% respectively, compared to the shear strength obtained from the tests on pure sand (Figure 5.17).

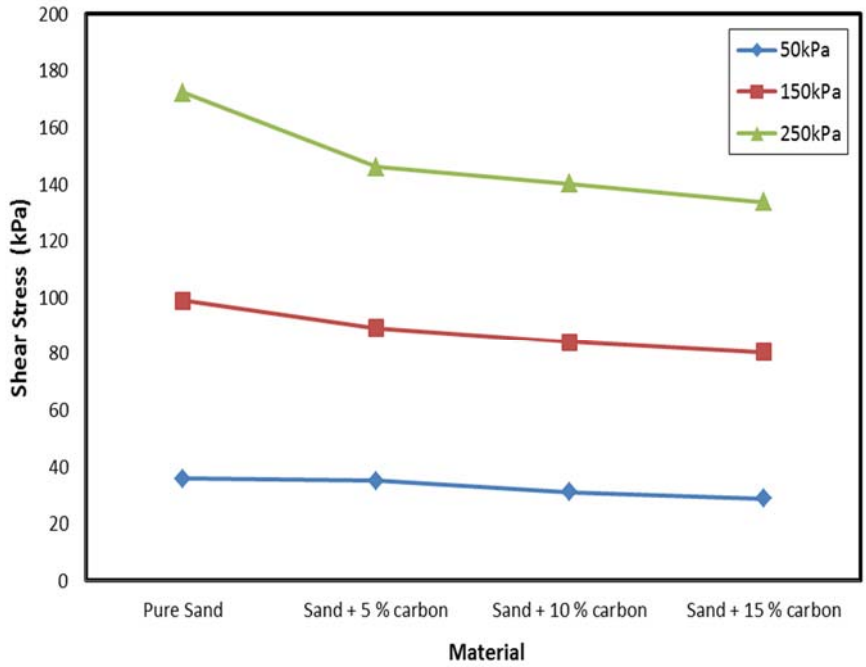

Figure 5.17 The comparison of the shear stress of sand containing 0%, 5%, 10% and 15% carbon under a range of normal stresses

5.3.4 The Effect of the Wood Addition on the Shear Strength of Sand-slag Mixture

The direct shear test results on pure sand are illustrated in Figure 5.18. The normal pressures applied were 50, 150, and 250 kPa respectively for each set of tests, and the maximum shear stresses (failure shear stresses) for each normal stress were 35.87, 98.86 and 172.36 kPa respectively. The friction angle (θ) of sand was calculated as 34.3°. This work was followed by experiments to determine the optimal amount of wood as an additive and the most effective wood element placement directions (i.e. horizontal, vertical to shear direction etc.). Preliminary tests indicated that placing the wood vertical to the shear direction exerted greater improvement in the samples' shear strength.

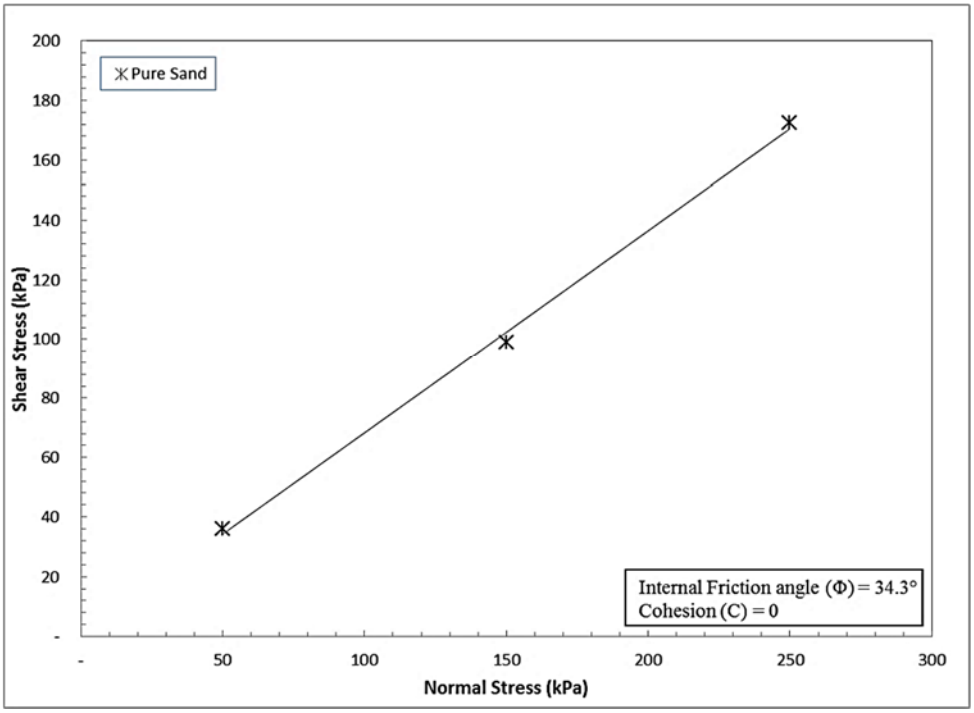

Figure 5.18 Shear stress with various normal stresses of pure sand

Slag was then added into the sand materials to form a sand-slag mixture and the same shear test was repeated with the same range of normal stresses (50, 150 and 250 kPa) applied to the sand-slag mixture to investigate the effect of adding slag to the sand to the shear strength. Figure 5.19 indicates the failure of shear stress which occurred for the sample with 1% slag, achieving a maximum shear stress of 36.4 kPa, 98.6 kPa and 174.192 kPa under 50 kPa, 150 kPa and 250 kPa of normal stresses respectively.

Similarly, the maximum shear stresses resulting from the application of all three normal stresses were also obtained for the sand sample containing 3% slag. The sand with 1% slag produced a friction angle (θ) of 34.5° (Figure 5.19), while the sand containing 2% and 3% slag produced 34.9° (Figure 5.20) and 35.1° (Figure 5.21) friction angles, respectively. The slag in the mixture acted as a chemical additive, bonding the sand particles and, when fully hydrated and cured, increasing the shear strength. However, in the present experiment, the shear performance of the sand-slag was examined without the curing time. The slag seems not to react fully as a chemical additive and only acted as a source of finer particles added to the sand.

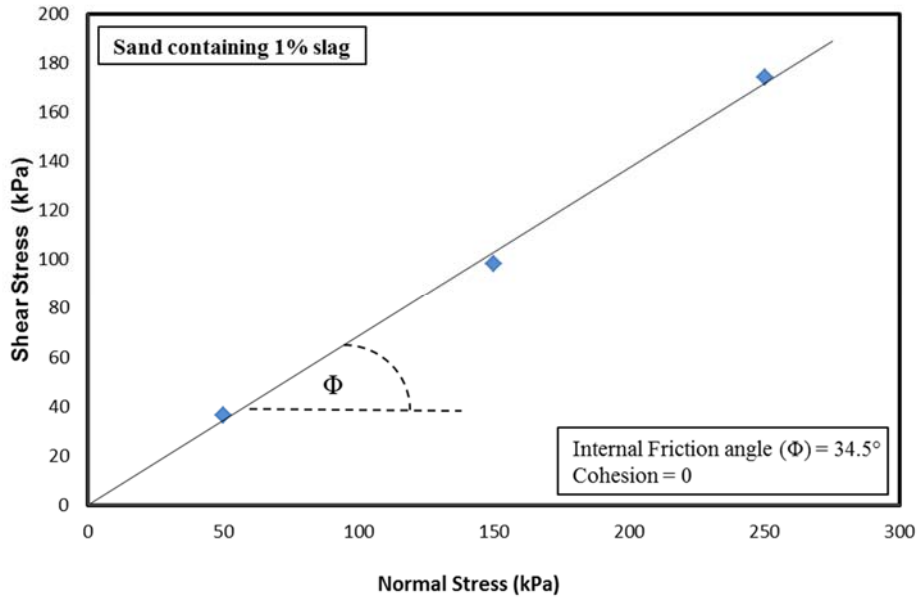

Figure 5.19. Shear stress with various normal stresses of sand containing 1% slag

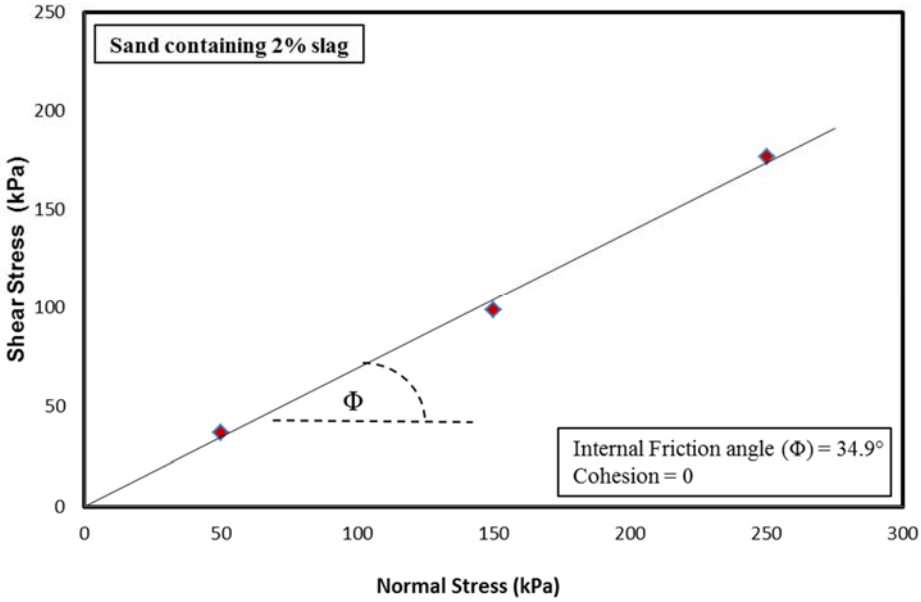

Figure 5.20 Shear stress with various normal stresses of sand containing 2% slag

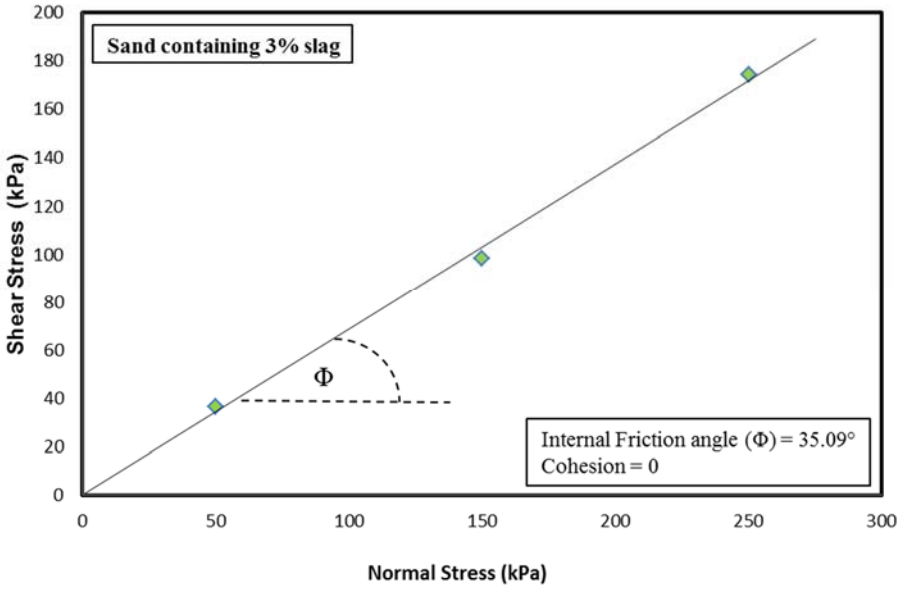

Figure 5.21 Shear stress with various normal stresses of sand containing 3% slag

Figure 5.22 to Figure 5.24 show the results obtained from applying 50 kPa of normal stress to three samples with a slag content of 1%, 2% and 3% by weight, with wood additives. The highest failure shear stress occurred when the sample had a slag content of 3% (Figure 5.24). For other slag content, the normal versus shear stress curve went into a slightly inclined phase towards the end of the test. The trend then continued with an increased rate of shear stress until reaching a maximum shear stress of 62.2 kPa. The sample with 3% slag content also showed the highest initial gradient compared to samples with lower slag contents (1% and 2%). Under a normal stress of 50 kPa, the maximum shear stresses for sand containing 1% and 2% slag were 54.8 and 56.03 kPa, respectively.

According to Figure 5.24, the sand-slag mixture sample with the highest percentage of slag (3%) achieved the greatest maximum shear stress when wood was added into the sample. The sand-slag mixture with 3% of slag produced a maximum shear stress of 62.3, 134.57 and 221.9 kPa under normal stresses 50, 150 and 250 kPa respectively. There was also an increase in the corresponding friction angles for each sand-slag mixture with wood additives. The friction angles of sand containing 1%, 2% and 3% of slag with wood additives were 35.06° (Figure 5.22), 37.71° (Figure 5.23) and 38.59° (Figure 5.24) respectively.

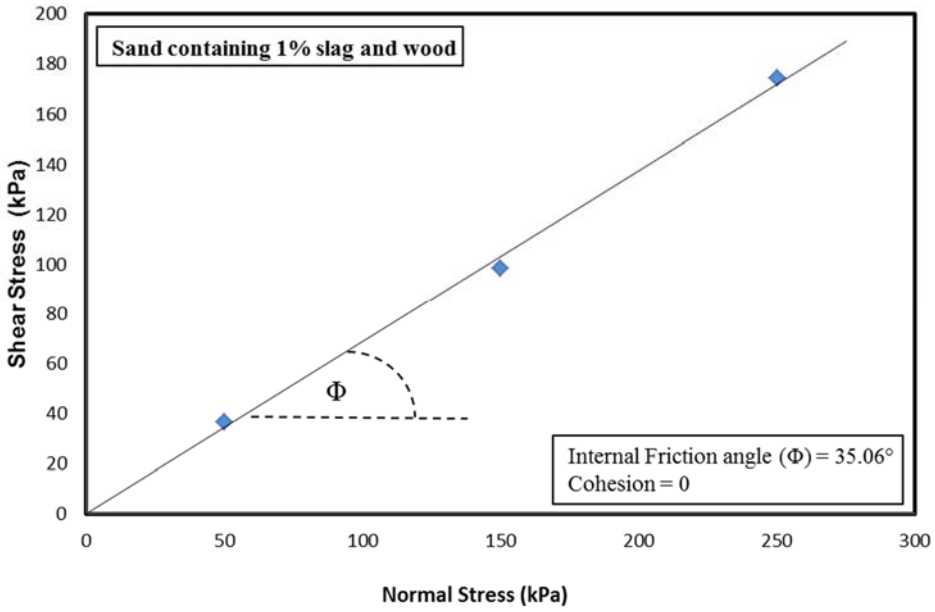

Figure 5.22 Shear stress with various normal stresses of sand containing 1% slag and wood

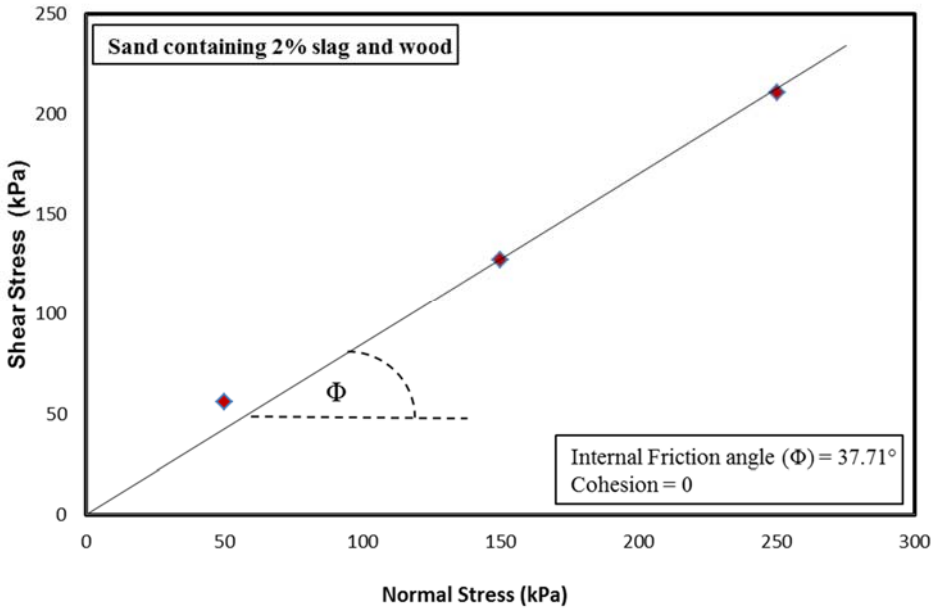

Figure 5.23 Shear stress with various normal stresses of sand containing 2% slag and wood

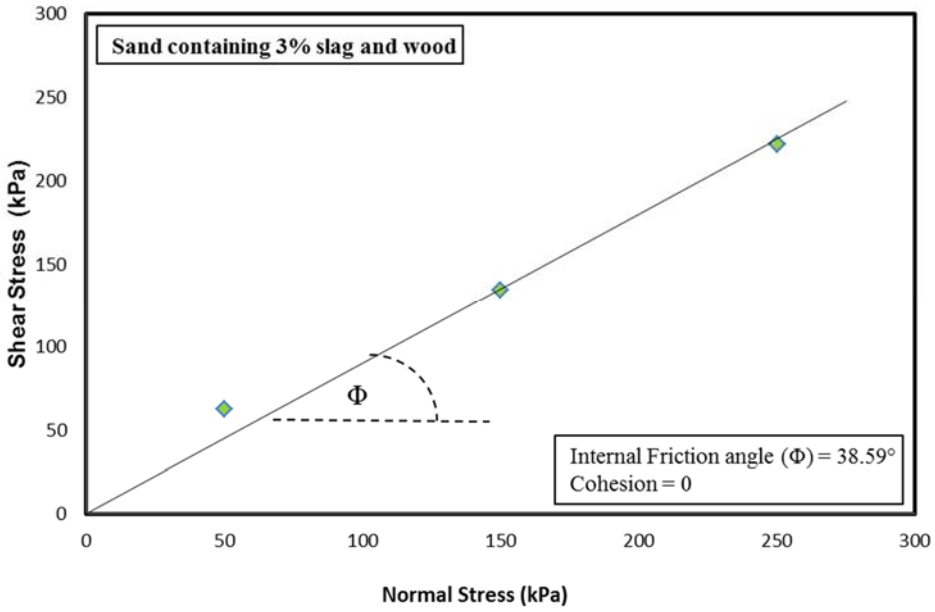

Figure 5.24 Shear stress with various normal stresses of sand containing 3% slag and wood

Figure 5.25 illustrates that after adding wood, the sample with 3% slag content encountered the highest maximum shear stress of all tested samples. With the application of a normal stress of 50 kPa, adding wood to the sand-slag mixture brought up the shear strength by 52.7%, 56.2% and 73.6% for sand containing 1%, 2% and 3% slag respectively. In the case of 150 kPa of normal stress, introducing wood to the sand-slag mixture increased the shear strength by a percentage ranging from 10.4% to 36.1% approximately. For 250 kPa normal stress, the shear strength increment changed to 13%–28% approximately for each sample referring to the experimental results. In general, it was concluded that adding wood into a sand-slag mixture contributes in improving the shear strength of the mixture for various slag contents and normal stress levels.

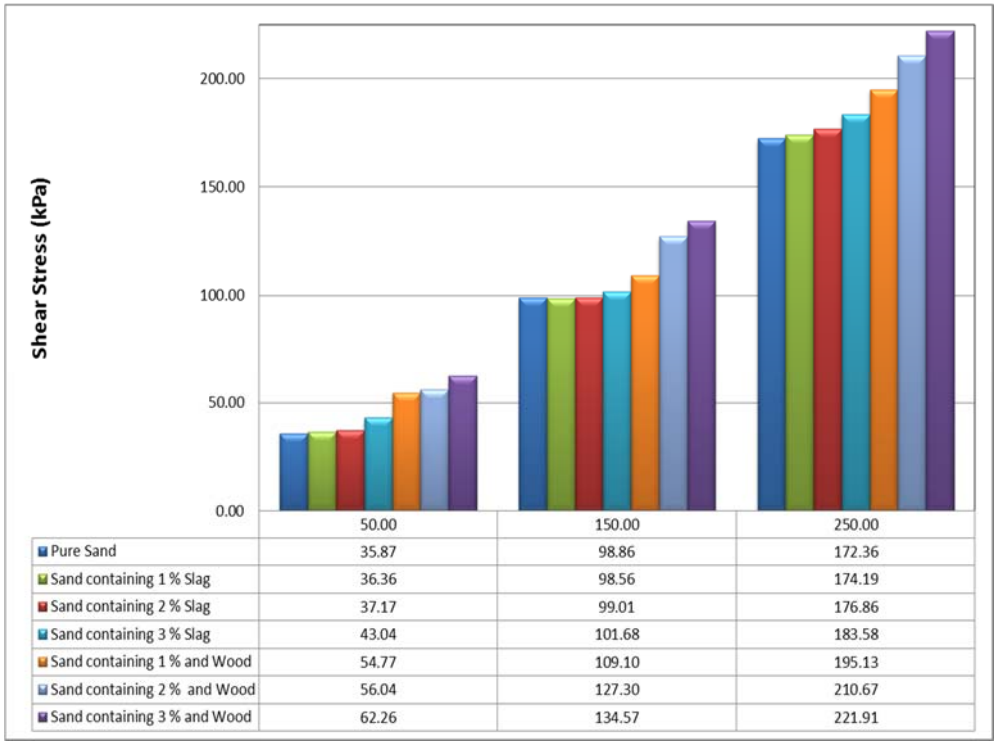

	50.00	150.00	250.00
Pure Sand	35.87	98.86	172.36
Sand containing 1 % Slag	36.36	98.56	174.19
Sand containing 2 % Slag	37.17	99.01	176.86
Sand containing 3 % Slag	43.04	101.68	183.58
Sand containing 1 % and Wood	54.77	109.10	195.13
Sand containing 2 % and Wood	56.04	127.30	210.67
Sand containing 3 % and Wood	62.26	134.57	221.91

Figure 5.25 The comparison of shear stress for sand-slag mixtures with and without wood under different normal stresses

5.3.5 Liquefaction Resistance of Stabilised Sand

In some regions where suitable locations are limited, landfills are located in areas with high groundwater levels. This means the landfill subgrade is immersed in groundwater and there would be an excess pore water pressure generation. Throughout landfill operations, the subgrade will be exposed by dynamic load as a result of waste compaction activities. Since most landfill subgrade consists of sand, there will be a reduction in the effective stress of the sand as a result of the presence of dynamic load (waste compaction and heavy vehicle activities) and the excess pore water pressure. This occurrence is widely identified as liquefaction (Ishihara 1985). As a result, the sand subgrade will lose its bearing capacity, trigger ground subsidence and cause slope displacement (Towhata 2008).

The resistance of sand to liquefaction depends on factors such the degree of density. Some soil improvement techniques have been developed to strengthen sand against liquefaction. One of them is increasing the relative density of the sand through compaction and adding materials that improve the strength of the sand. One potential additive material is slag. Therefore, this section will focus on characterisation of

liquefaction resistance of sand at a range of density levels and various types of sand-slag mixtures using cyclic triaxial tests.

5.3.5.1 Experimental Procedure

All samples were conditioned and prepared according to triaxial test standards. The sample had dimensions of 63 mm diameter and 130 mm height. The pure sand sample was tested at three different relative densities, being 85%, 90% and 95%. Sand-slag mixtures with a slag content of 3% and 8% were also tested. The samples were prepared in seven layers and compacted according to the design's relative density. The same procedure was repeated for all of the specimens, and all of the samples were tested under 50 kPa of confining pressure.

Prior to the cyclic triaxial test, the samples were saturated until reaching a Skempton's B-value of 0.95. To achieve proper saturation, de-aired water and CO_2 gas were thoroughly distributed to the specimen. Once the desired Skempton's B-value had been achieved, 50 kPa of effective confining pressure was applied followed by cyclic loading. All of the samples were tested under various cyclic stress ratios (CSR) while the axial strain rate was maintained at about 1 %/min and the frequency was set up at 0.1 Hz.

Relative Density and Liquefaction Resistance

The result of the shear stress and axial strain during the cyclic loading of pure sand are shown in Figure 5.26. This represents a typical result for the cyclic triaxial test conducted on pure sand with various relative densities (Dr) and 50 kPa of effective confining pressure. The axial strain prior to liquefaction is quite constant before increasing at the end.

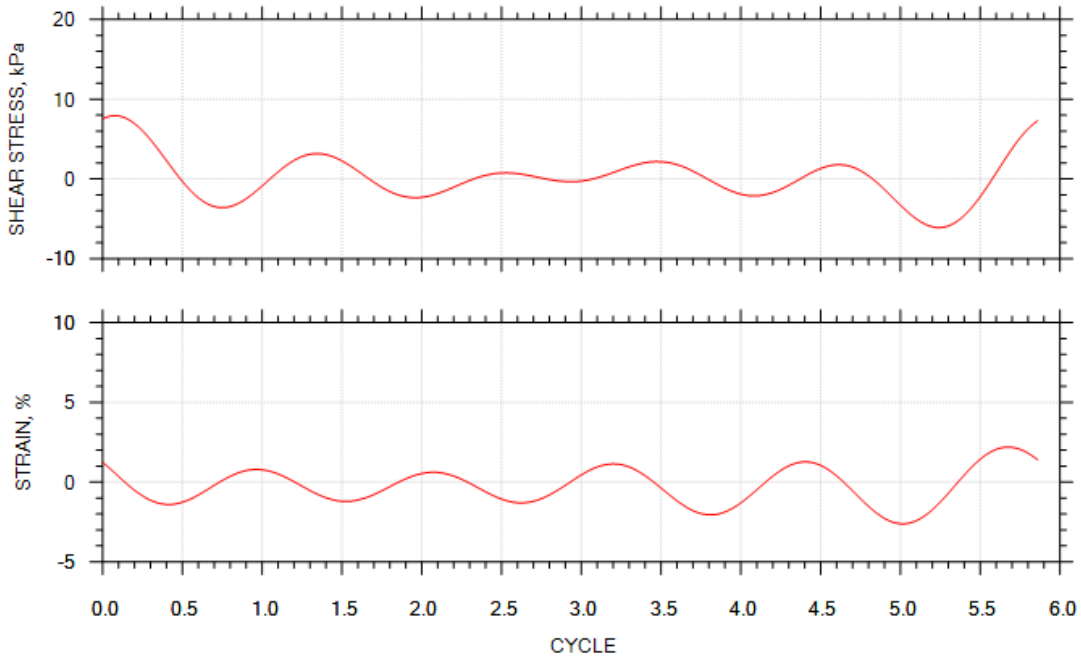

Figure 5.26 Shear stress and axial strain VS number of cycle

In general, the cyclic stress ratio is defined as follows:

$$CSR = \frac{1}{2}\left(\frac{\sigma'1 - \sigma'3}{\sigma'3}\right) \quad 5.3$$

Where σ'_1 represents the maximum effective stress and σ'_3 is the minimum effective stress. The liquefaction resistance of various relative densities of pure sand (Baldivis sand) to different cyclic stress ratios (CSR) is presented in Figure 5.27. This clearly shows that samples with higher relative density are more resistant to liquefaction. Under a CSR value of 0.4, the sand with a relative density of 85% fails after four cycles while sand with relative densities of 90% and 95% collapse after eight and eleven cycles respectively.

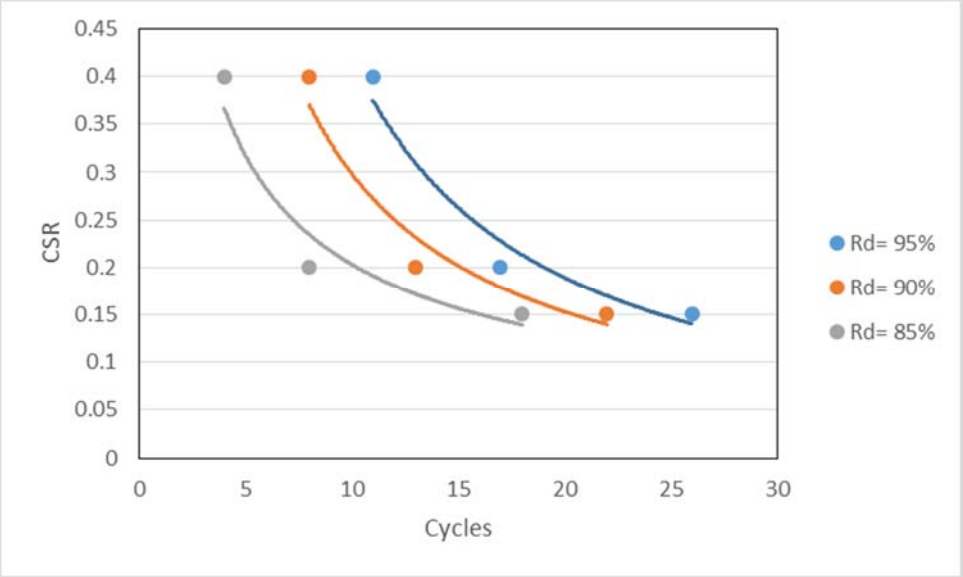

Figure 5.27 Liquefaction occurrence of pure sand with various relative densities

Reducing the CSR value will also increase the liquefaction resistance for each density. For example, in the sand sample with a CSR value of 0.2 and 85% relative density collapse after eight cycles, reducing the CSR to 0.15 will decrease liquefaction susceptibility. The same patterns occur for sand with a higher relative density.

Slag Content and Liquefaction Resistance

The liquefaction of sand-slag mixture was examined by adding three different percentages of slag which were 2%, 5% and 8%. The sample was prepared with 85% relative density and tested under a CSR of 0.4. These relative density and CSR values were chosen since they resulted in the lowest liquefaction resistance among other conditions.

The effect of adding slag to the sand is illustrated in Figure 5.28. The addition of 2% of slag increased the number of cycles causing liquefaction from four to six cycles. This means that sand containing 2% slag has more liquefaction resistance of pure sand. The sand-slag mixture containing 5% and 8% of slag failed after about 9 and 11 cycles respectively. It can be suggested that the interlocking properties of sand particles improves with the addition of slag.

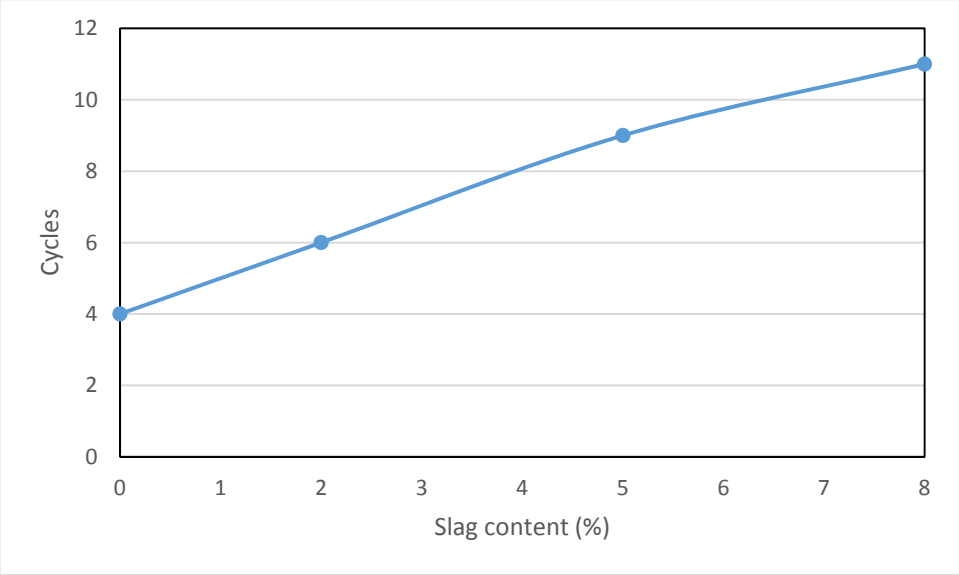

Figure 5.28 Number of cycles causing liquefaction at various percentages of slag

Chapter 6
Prediction of Contaminant Migration

6.1 Introduction

Landfills still operate as the conventional remedy and final treatment for managing solid wastes (Ludwig, Hellweg and Stucki 2002; Zhen-Shan et al. 2009). As landfill is basically a waste dumpsite, it is the cheapest and simplest solid waste treatment method wherever suitable landfilling areas are available (Tchobanoglous and Kreith 2002). Usually, landfill leachate from unsorted solid waste contains various types of hazardous chemicals including heavy metals. These hazardous components can contaminate soil and groundwater in areas surrounding the landfill. To minimise the effect of leachate contamination, it is necessary to have impervious liner acting as a barrier beneath the landfill (Tchobanoglous, Theisen and Vigil 1993). However, it is still possible for leachate to permeate through the barrier and migrate into the soil and water surrounding the landfill. Therefore, it is useful for landfill management authorities to be able to predict the potential for leachate migration to the surrounding environment both during and after the landfill operations.

The purpose of this chapter is to simulate the movement of heavy metal contaminants from a landfill by investigating the initial heavy metal concentrations below the bottom of the landfill. This research also investigated the concentration of the selected heavy metals in soil at various depths below the landfill for a period of more than 12 years. There are two cases that will be presented in this chapter. The first case focuses on the migration of lead (Pb) and chromium (Cr) through landfill liner, and the second case simulates the migratory pattern for cadmium (Cd) and Nickel (Ni) through single and double liners. Figure 6.1 shows the structure of this chapter.

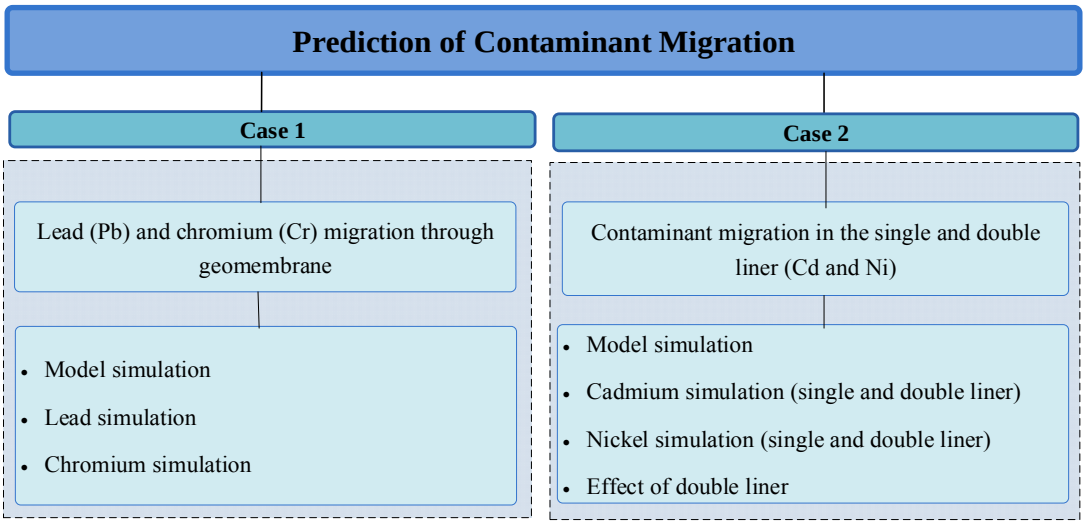

Figure 6.1 Outline of contaminant migration section

Pollute v.7 was the modelling software used for this simulation. The model was built on the basis of a blank model in which the variation and types of layers could be determined according to the proposed settings. When certain input cannot be obtained, the software can provide default values. It can run directly after entering primary and secondary data.

Table 6.1 lists the stages involved for building and running Pollute v.7.

Table 6.1 Stages of execution

Stage	Option/Input/Output
Create the model	Blank model
General data input	Number of layers, maximum depth total layer depth and Darcy velocity
Layer data input	Number of sublayers, thickness, dry density, porosity, coefficient of hydrodynamic dispersion and distribution coefficient
Set up boundary conditions	Top boundary and bottom boundary
Run parameters	Concentration vs depth, concentration vs time, depth vs time

Another important step of the simulation is to perform a sensitivity analysis. The sensitivity analysis is aimed at determining the effects based on the preferred solution of changing the input data or existing parameters. This analysis is closely related to decision-making due to its high flexibility, which enables it to adapt to varying situations and different conditions (Malczewski 1999). In the present study, conducting the sensitivity analysis, trial and error was used to amend the following

values: porosity, permeability and dry density. While other parameters were kept constant, the selected values must follow the previous theories.

6.2 Case 1: Lead (Pb) and Chromium (Cr) Migration through Geomembrane

Landfill which acts as the final treatment of solid waste is preferred due to its benefits in terms of operation cost, construction and investment (Hui et al. 2006; Zhen-Shan et al. 2009). As illustrated in Figure 6.2, landfill can be regarded as a dumpsite designed for solid waste disposal. When there is a suitable area ready for landfill, it is considered to be the cheapest and the simplest approach for the final treatment of solid wastes (Supriyadi, Kriwoken and Birley 2000). In developing countries, landfill is generally applied in two common ways: sanitary landfill and open controlled landfill. Compared to controlled landfill, sanitary landfill is usually preferred for large cities (Tchobanoglous, Theisen and Vigil 1993).

In Taiwan, Chow and Chai (2007) conducted research to examine the influence of acid precipitation on landfill management. The study highlighted the importance of landfill management and the need for an appropriate landfill modelling system. Other studies have focused on energy generation from landfill systems. For instance, an investigation into using biogas as a possible method of producing electrical energy was conducted by Barros, Tiago Filho, and da Silva (2014).

The leachate generated by landfill may be a threat to the environment. For example, metal compounds may be present in the produced leachate (Salami et al. 2013), and while certain metal compounds can be beneficial to the soil as nitrates, others may result in environmental contamination and degradation. Mor et al. (2006) has suggested that leachates carrying heavy metals may pollute the areas surrounding landfill.

In general, leachate contains toxic substances like heavy metals and various organic pollutants that can contaminate the soil and groundwater (Aziz et al. 2010). Past research has suggested that the existence of toxic heavy metals in landfill leachate is a cause for concern (Varank et al. 2011). Heavy metals normally present in leachate

include iron (Fe), mercury (Hg), copper (Cu), cadmium (Cd), nickel (Ni), lead (Pb) zinc (Zn), arsenic (As) and chromium (Cr) (Renou et al. 2008).

Usually, landfills have a liner system consisting of gravel, leachate barrier (geomembrane, CCL or GCL), geotextile and compacted soil. The function of the liner system is to restrict the migration of leachate into the soil and groundwater system near the landfill (Figure 6.2). However, even for a liner with an extremely low permeability like geomembrane, it is impossible to completely stop the leachate leaking through the liner. As suggested by Shukla (2012), pressure in leachate with heavy metals can accumulate over a long period of time, and may induce certain defects in the geomembrane. Consequently, leachate migration may increase and cause contamination of the surrounding environment.

It is preferable to prevent leachate contamination rather than to have to take remedial measures afterwards. The occurrence of leachate migration can be observed by installing monitoring equipment in the area surrounding the landfill (McBean, Rovers and Farquahar 1995). Alternatively, simulation software can be used to predict leachate migration by calculating the leachate concentration at various soil depths. The calculation is based on concentration levels at the top of the impervious layer or from the leachate collection system (Schroeder et al. 1994). According to the simulation results, measures can be taken to minimise further contamination.

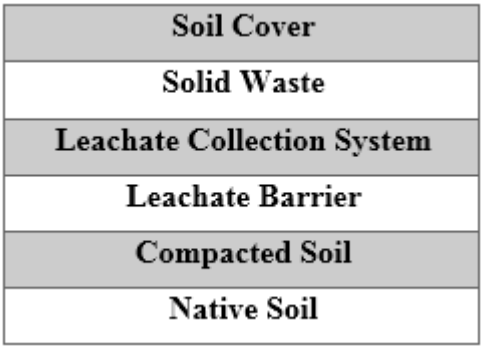

Figure 6.2 Typical landfill configuration

In the light of previous research, the present study concentrates on the migration of lead (Pb) and chromium (Cr), which are frequently encountered in leachate from landfills containing unsorted solid waste in some developing countries. Pollute v.7, a finite layer contaminant migration analysis program will be employed to run the simulation (Rowe and Booker 2005), using a contaminant transport model that

produces a 1.5 dimension simulation of contaminant transportation. The software can also predict the changes in the concentration of Pb and Cr over a period of 12 years.

6.2.1 Model and Simulation

The composition layers of the landfill liner are illustrated in Figure 6.3. The initial lead (Pb) and chromium (Cr) concentrations were assumed to be representative of the concentrations at the lowest part of the landfill. The concentrations of Pb and Cr in the gravel, geotextile, geomembrane, compacted soil and the subsoil were all assessed in the simulation. The developed model was used to predict the concentrations of Pb and Cr for each layer over a period of 12 years.

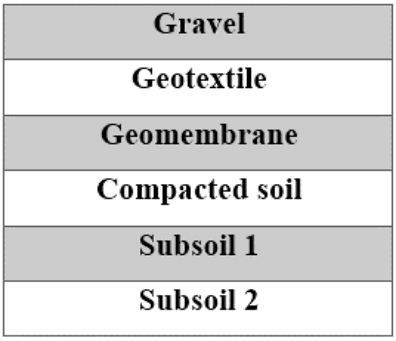

Figure 6.3 Landfill liner composition

For single liner landfill, the gravel layer is used to prevent solid waste from entering the leachate collection pipe and possibly blocking the system. The geotextile layer is a protective layer preventing the geomembrane from disruption, and can also work as a leachate filter. Meanwhile, the geomembrane, with its very low permeability, can function as the main barrier material for leachate.

In this simulation, a single landfill liner system is simulated with a gravel protection layer, leachate collection, geotextile, geomembrane and compacted soil. This liner system is representative of a common liner system applied in solid waste landfill in certain developing countries. There are also two native subsoil layers underlying the composite landfill liner in this simulation.

Table 6.2 lists the properties of the landfill liner components used in the simulation. The thickness of the gravel was set at 0.7 m, the compacted soil at 0.9 m and the two

different layers of subsoil as 2 m and 4 m respectively. The thickness of the manufactured materials such as the geotextile and geomembrane were chosen according to the recommendations of the International Geosynthetics Society (2006).

Table 6.2 Properties of landfill liner

Material	Dry density (gr/cm3)	Permeability (m/s)	Porosity	Thickness (m)
Gravel	2.47	$1 \times 10^{-2} - 1$	0.35	0.7
Geotextile	0.5	0.65×10^{-1}	0.55–0.93	0.004
Geomembrane	0.94	$5 \times 10^{-13} - 5 \times 10^{-16}$	1	0.0015
Compacted soil	1.1352	1.764×10^{-8}	0.57	0.9
Subsoil 1 (native)	1.15	5.943×10^{-6}	0.51	2
Subsoil 2 (native)	1.22	1.519×10^{-6}	0.56	4

In order to run the leachate migration simulation, the initial contaminant concentration must be determined. The initial concentrations of the contaminants were assumed to be the same as at the lowest part of the landfill, such as the concentration at the leachate pipe. The concentrations of both lead and chromium were selected as 0.93 mg/l (Table 6.3). The initial value of the concentration was chosen according to the ranges of concentration for Pb and Cr stipulated by the European Commission (2000), which suggests the concentration ranges 0.001–5 mg/l (Pb) and 0.02–1.5 mg/l (Cr). These values were far greater than the upper limit required for the standards of water quality.

Table 6.3 Initial heavy metal concentration

Parameter	Initial concentration (mg/l)	Limit Class I (Water quality standards) (mg/l)
Lead	0.93	0.1
Chromium	0.93	0.1

6.2.2 Lead (Pb) Simulation

Figure 6.4 illustrates the changing concentration of lead (Pb) over a time of 12 years, indicating a significant decline after adding the geomembrane layer. In general, according to the simulation, Pb concentration tended to increase in each layer every year. However, the greatest increase in Pb concentration was seen within the first five years, and in the first year in particular. On top of the geomembrane layer, the initial

Pb concentration was 0.93 mg/l for the first year. In the compacted soil below the geomembrane, the concentration of lead (Pb) fell to 0.25 mg/l and then kept going down to 0.15 mg/l at the bottom of the subsoil (around 7 m below the impermeable layer).

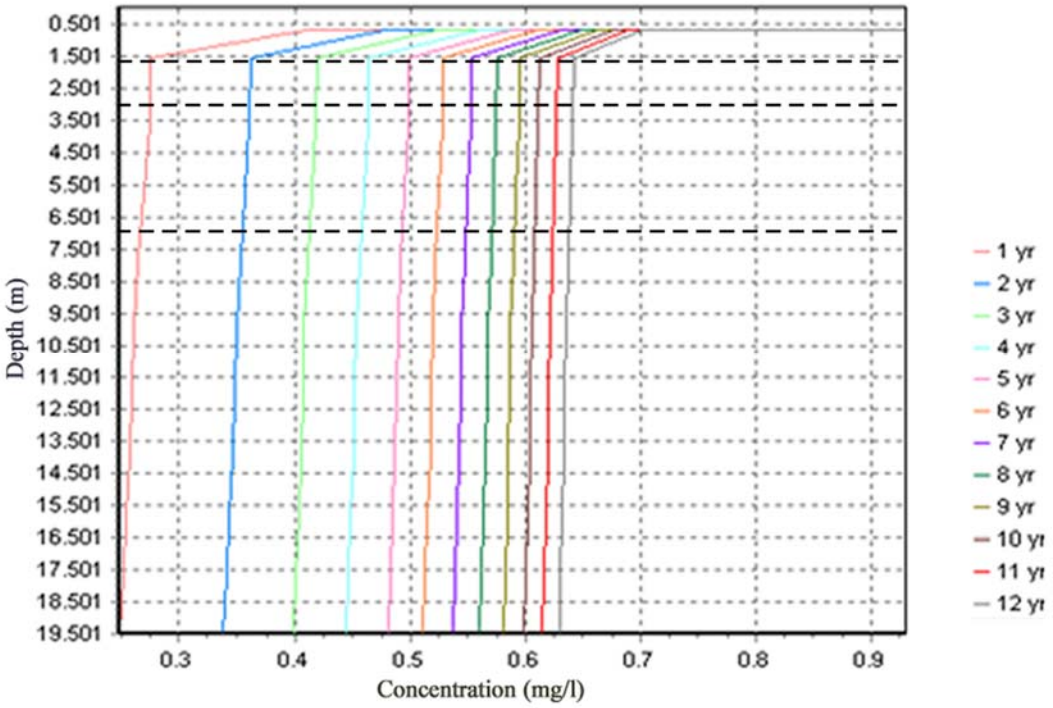

Figure 6.4 Lead (Pb) simulation

The variation in Pb concentration at different depths every year is illustrated in Figure 6.5, for a total period of 12 years. The lowest area of the landfill showed a constant Pb concentration, while the highest Pb concentration was found in a layer at 0.7055 m depth. The value was 0.42 mg/l for the first year, and rose to approximately 0.67 mg/l after a period of 12 years.

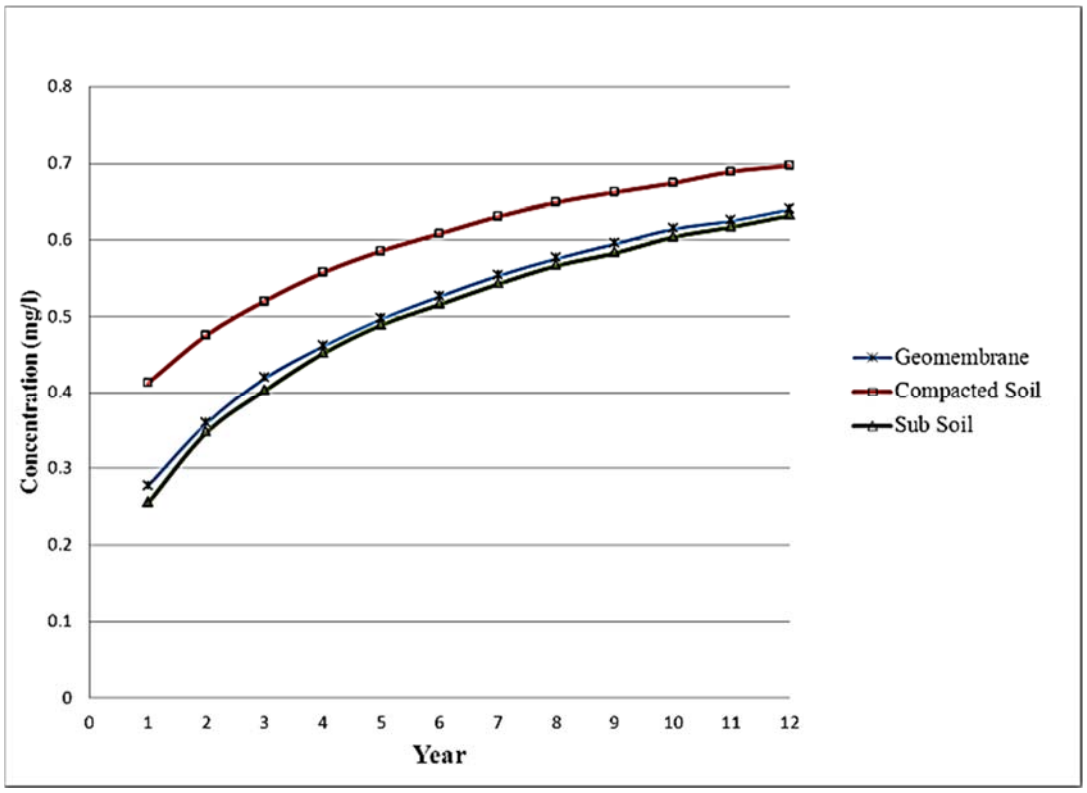

Figure 6.5 Concentration of lead (Pb) at various depths

6.2.3 Chromium (Cr) Simulation

Figure 6.6 shows the changes in chromium (Cr) concentration over a 12 year period. The Cr concentrations followed a similar pattern to those of Pb, falling by around 70% after penetrating through the geomembrane. Over the whole 12 year period of the simulation, the Cr concentration in the layer beneath the geomembrane rised to a maximum value of 0.54 mg/l in the final year. Similarly to the Pb concentration illustrated in Figure 6.5, the first five years showed the largest increase in Cr concentration, rising from 0.2 mg/l to 0.55 mg/l at 1.501 m depth.

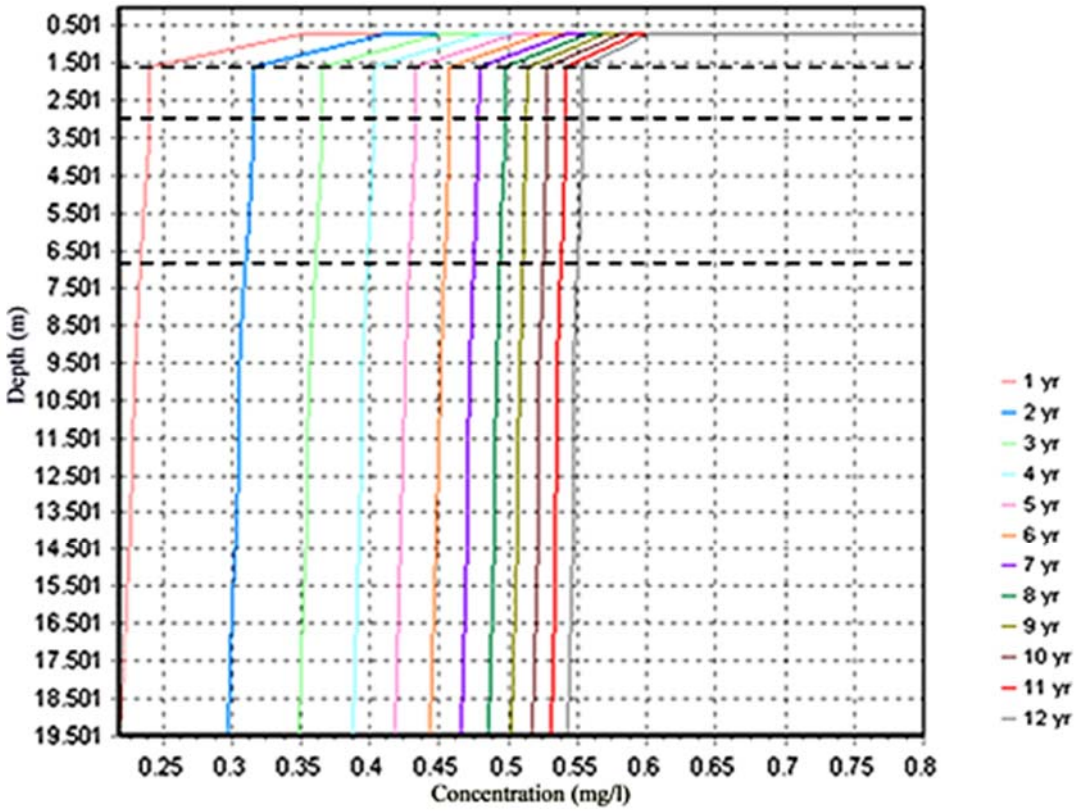

Figure 6.6 Chromium (Cr) simulation

Figure 6.7 demonstrates the variation in Cr concentration at various depths over 12 years. Similarly to the outcome for Pb concentration, the maximum Cr concentration was found at a depth of 0.7055 m, starting from 0.36 mg/l in year 1, with a slight increase every year for the whole 12 year period, finally reaching the highest concentration of 0.57 mg/l in the final year (year 12).

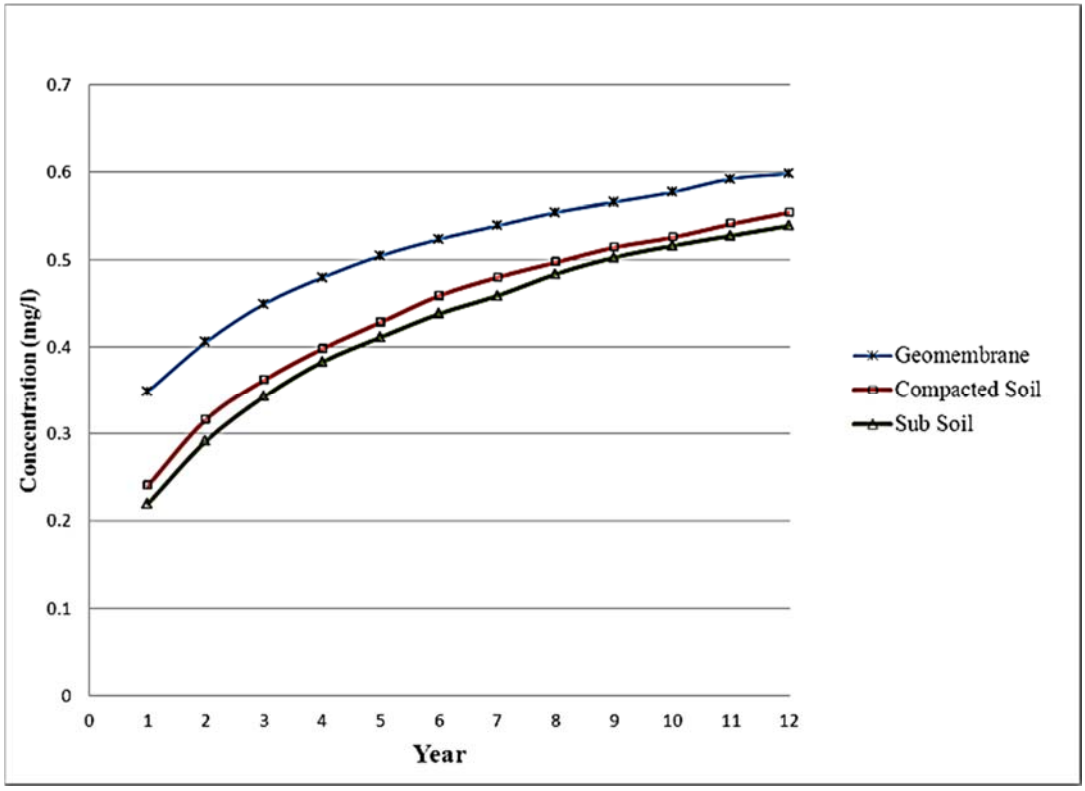

Figure 6.7 Chromium (Cr) concentration at various depths over 12 years

At a depth of 0.704 m, Pb and Cr in the leachate moved into the geotextile layer. After filtering through the geotextile, the concentrations of Pb and Cr declined as the leachate moved towards the subsoil. This decrease was caused by the presence of geotextile functioning as a filter preventing soil particles and heavy metal contaminants from being carried away with the leachate (International Geosynthetics Society 2006). In landfill, geotextile is used in a non-woven and water permeable form, so that the leachate liquid can penetrate while certain soil particles and Pb and Cr contaminants are retained.

The Pb and Cr components remaining in the leachate after the geotextile then pass into the geomembrane layer at 0.7055 m deep. The geomembrane can be regarded as an impermeable layer that prevents any leakage of leachate from solid waste (International Geosynthetics Society 2006). However, considering there were some potential defects on the geomembrane, leachate would still be able to permeate through the geomembrane. In this simulation, the geomembrane was designed to have porosity of 90% and permeability of 0.5×10^{-11}. This resulted a much reduced concentration of Pb and Cr in the leachate that had permeated both layers of geotextile and geomembrane (Table 6.4).

Table 6.4 Concentration of Pb and Cr in geomembrane (mg/l)

Year	Initial concentration	Simulation Pb	Simulation Cr
1	0.930	0.4105	0.3513
2		0.4795	0.4114
3		0.5256	0.4513
4		0.5604	0.4813
5		0.5884	0.5053
6		0.6117	0.5253
7		0.6316	0.5423
8		0.649	0.5572
9		0.6643	0.5702
10		0.678	0.5819
11		0.6904	0.5924
12		0.7015	0.6019

Over a depth of 1.605 m, the Pb and Cr in the leachate passed through the geomembrane layer and moved into the compacted soil, which had a low hydraulic conductivity. Thus, it was difficult for the leachate to further pass through. This led to a slight decline in Pb and Cr concentration for the leachate, when it flowed from the geomembrane to the compacted soil layer.

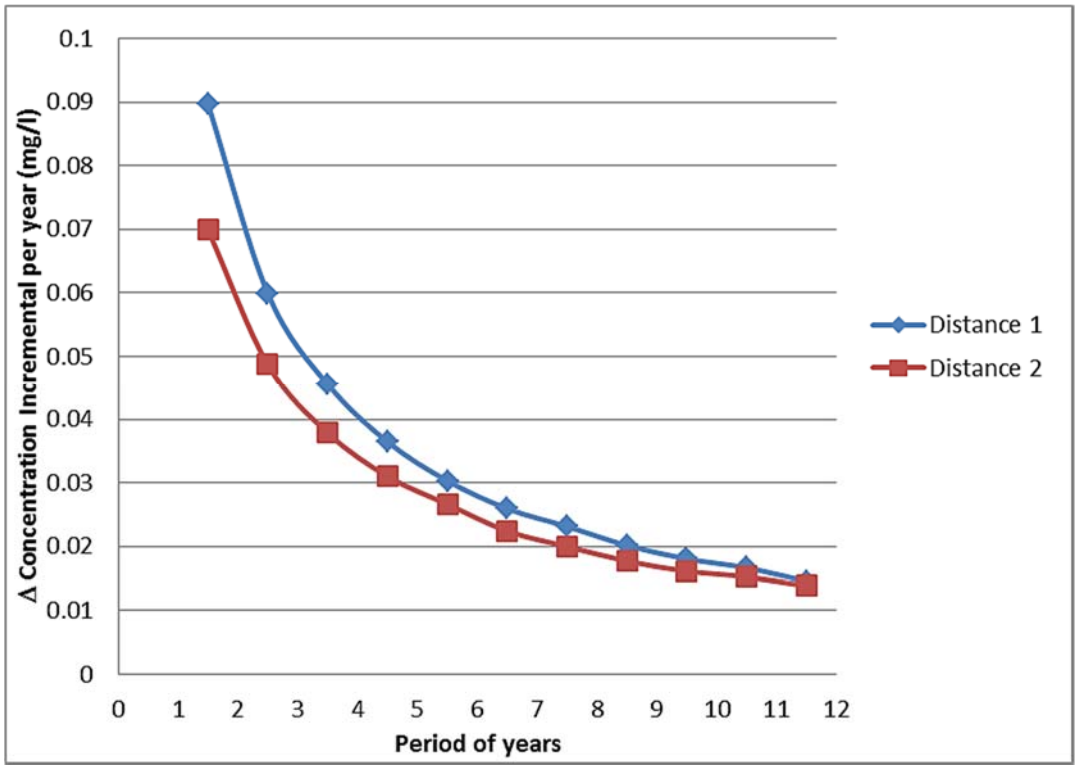

Figure 6.8 The declining rate of increase in Pb concentration over 12 years

There was an obvious increase in Pb concentration from the first to the twelfth year. However, the rate of increment declined over the years as illustrated in Figure 6.8. In Figure 6.8, Pb concentrations are indicated at two locations at different distances (100 m and 200 m) and depths (20 m and 30 m) from the landfill. Although the values varied slightly, both points demonstrate the same trend.

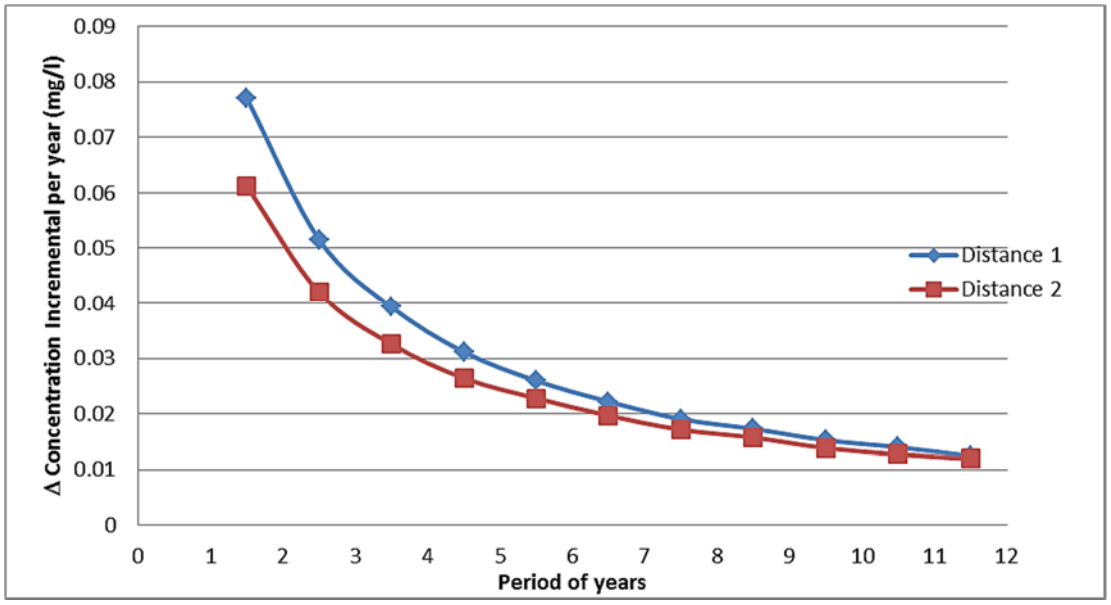

Figure 6.9 The declining rate of increase in Cr concentration over 12 years

The rate of decrease in Cr concentration at locations 1 and 2 is demonstrated in Figure 6.9. Another simulation, similar to the one for Pb concentration, was conducted to investigate the change in Cr concentration at two different locations near the landfill. A similar phenomenon was found, with a decreasing Cr concentration in both locations over a period of 12 years. It can be predicted that there will be a yearly increase in the Pb and Cr concentrations in the subsoil until a saturation point is reached. After the point of saturation, the movement of Pb and Cr will cease and runoff may occur. Salami et al. (2013) have also reported a similar downwards trend. An increasing trend for Pb and Cr concentration values is identified based on the simulation results for a total period of 12 years.

Normally, there is a comparatively higher concentration of Pb concentration than Cr in the leachate. As stated by Stegmann, Heyer, and Cossu (2005), the Pb concentration in leachate landfill ranges from 0.001 to 5 mg/l, while the Cr concentration falls to 0.02–1.5 mg/l. In landfill metal waste, the Cr content is lower than the Pb content

(European Commission 2000). In addition, it is more likely for the Cr in the leachate to be absorbed by plants. The larger the amount of leachate reaching the subsoil, the more likely it is for the groundwater to be contaminated. Moreover, there is also a possibility for surrounding shallow wells to be contaminated. Leachate contamination may cause serious problems in developing countries, since most residents consume well water as drinking water.

6.3 Case 2: Contaminant Migration in the Single and Double Liners

The liner system installed in landfills can be a single or double liner system. In the case of a small landfill, a single liner system may be sufficient. The single liner system is commonly composed of a prepared sub-base, a semi impermeable layer and a leachate drainage layer. A double or thicker clay liner system may be installed for decayable landfills in sensitive locations, also enabling the landfill to accommodate more contaminated wastes (Pichtel 2010).

The presence of metallic compounds in landfill-generated leachate renders it an environmental risk (Kjeldsen et al. 2002). Although some compounds like nitrates can be beneficial for soil, the organic contaminants and other toxic heavy metals in leachate have the tendency to cause environmental pollution, garnering global concern (Mor et al. 2006; Aziz et al. 2010; Touze-Foltz 2012; Varank et al. 2011). These heavy metal pollutants can come from several sources. For example, discarded household batteries and electroplating are the primary source of cadmium, manganese, nickel and chromium pollution in the environment (Karnchanawong and Limpiteeprakan 2009).

Even though it is desirable to completely eradicate leachate seepage through the outfitting of a liner system, leakage cannot be thwarted even by a liner with low permeability. Shukla (2012) has proposed that defects may be observed in the impermeable layer due to the pressure of heavy metals accumulating in the leachate over time, which may trigger leachate migration through the liner system.

Normally, monitoring wells are installed in the area surrounding the landfill to monitor the leachate migration (Christensen 2012). Simulation software, which is able to calculate the concentration of leachate at different soil depths from the concentration

on the top of the impermeable layer or based on the leachate collection system, may also be used for landfill leachate migratory pattern predictions (Verge and Rowe 2013) and the results can, therefore, be used to recommend suitable contamination prevention measures.

In many developing countries, leachate from landfills containing unsorted solid wastes often contains high percentages of nickel (Ni) and cadmium (Cd). The migratory pattern of Cd and Ni was the focus of this study. The effect of double and single liner systems on the migratory pattern of the contaminants was also addressed. Pollute v.7 was used to simulate 1.5 dimensional contaminant transportation and predict the variations in Cd and Ni concentrations over a 15 year period. The initial concentrations of Cd and Ni are based on the previous chapter and are to be used as reference in the model.

6.3.1 Model and Simulation

The liner system commonly used for solid waste landfills was represented by a single landfill liner system containing geosynthetic clay liner (GCL) and gravel and geotextile as the drainage layer. During simulation, the native soil layer and subgrade were overlaid by a composite landfill liner.

Figure 6.10 illustrates the single liner system used in the simulation. The thicknesses of gravel, subgrade and total native subsoil were fixed at 0.8 m, 1 m and 8 m respectively.

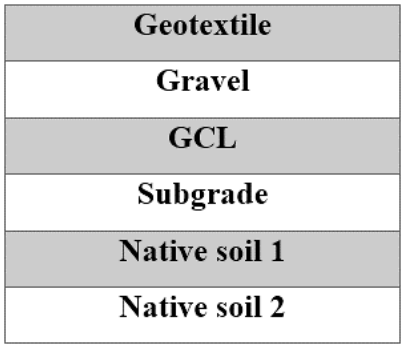

Figure 6.10 Components of single liner

During the simulation, the native soil layer and subbase were overlaid by the double landfill liner system comprised of a geotextile layer, geosynthetic clay liner (GCL),

gravel as drainage layer, compacted clay and the leak detection layer. Figure 6.11 shows the double liner system configuration that was employed for the simulation. The gravel, geotextile, native soil and subgrade layer thicknesses were kept the same as for the single liner system and the depths of the additional constituents like the compacted clay and leak detection layer were set at 1 m.

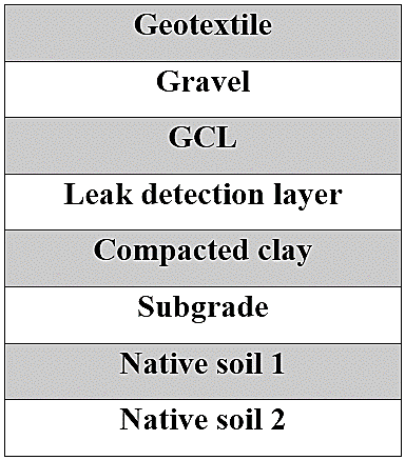

Figure 6.11 Component of double liner

To run the leachate migration simulation, the initial contaminant concentrations had to be ascertained and were taken to be the concentrations at the lowest area of the landfill, i.e., the leachate pipe. The initial concentrations were set as 6.99 mg/l for Ni and 4.5 mg/l for Cd. These values were considerably higher than the maximum treated leachate discharge limit (0.1 mg/l for Cd and 1 mg/l for Ni) (Ludwig, Hellweg and Stucki 2002).

6.3.2 Cadmium and Nickel Simulation

The initial concentrations of Cd and Ni were those at the lowest area of the landfill. A simulation was used to calculate the Cd and Ni concentrations in the subsoil, compacted soil, GCL, gravel and geotextile. Furthermore, the Cd and Ni concentrations in every layer for a 15 year period were predicted through the model.

A geotextile layer is installed in the landfill liner system to filter the dirt from the drainage system, whereas the gravel layer acts as the drainage for leachate. Moreover, GCL is employed as the primary leachate barrier for both liner systems due to its lower

permeability, while for the double liner system, the compacted clay liner acts as the secondary leachate barrier.

6.3.2.1 Cadmium (Cd) Simulation in Single Liner System

Cadmium concentration decreased significantly over the 15 years after the introduction of the GCL layer, as shown in Figure 6.12. In general, the accumulation of contaminant after each simulation year caused the Cd concentration to rise for every layer. Conversely, the highest decline in the concentration of Cd was observed in the first three years and especially in year 1. The initial Cd concentrations showed a decline in the first year as 4.5 mg/l above the GCL layer, 0.17 mg/l in the subgrade below the GCL and 0.14 mg/l at the bottom of subsoil 2 (about 9 m below the impermeable layer).

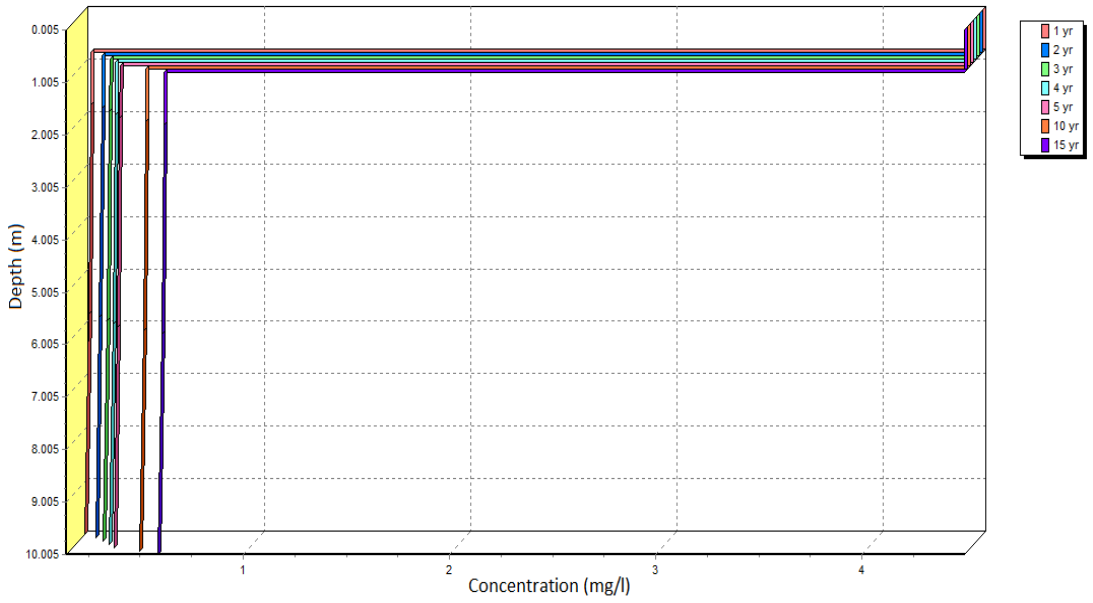

Figure 6.12 Cadmium (Cd) simulation

Figure 6.13 illustrates the variations in the concentration of Cd over the 15 year period at different depths. The maximum concentration of Cd after passing through the impermeable liner was noted at at depth of 0.81 m in the subgrade, provided that no variation is observed in the Cd concentration at the lowest landfill area (leachate collection system). The Cd concentration at that point increased from 0.17 mg/l (year 1) to 0.6136 mg/l (year 15).

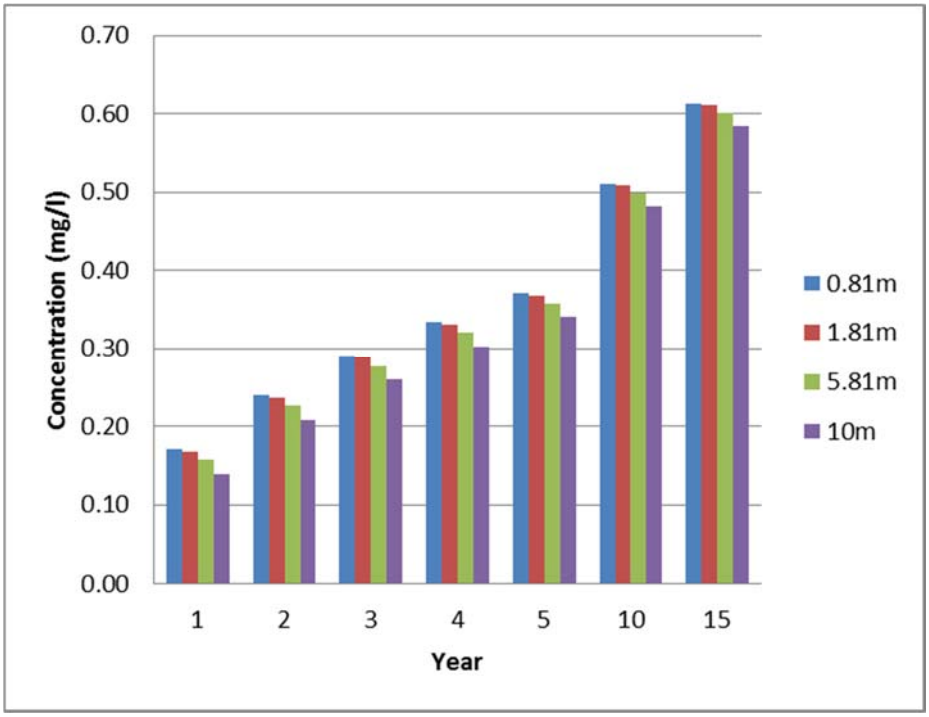

Figure 6.13 Cadmium (Cd) concentration at various depths over 15 years

6.3.2.2 Nickel (Ni) Simulation in Single Liner System

Ni concentration over the simulation period of 15 years showed a similar tendency to that of Cd, showing an approximate 92% reduction after permeating through GCL in the first year, as depicted in Figure 6.14. The highest Ni concentration was 1.73 mg/l. The first five years showed the most significant increase in Ni concentration, increasing from 0.42 mg/l to 1.0 mg/l for 10 m depth.

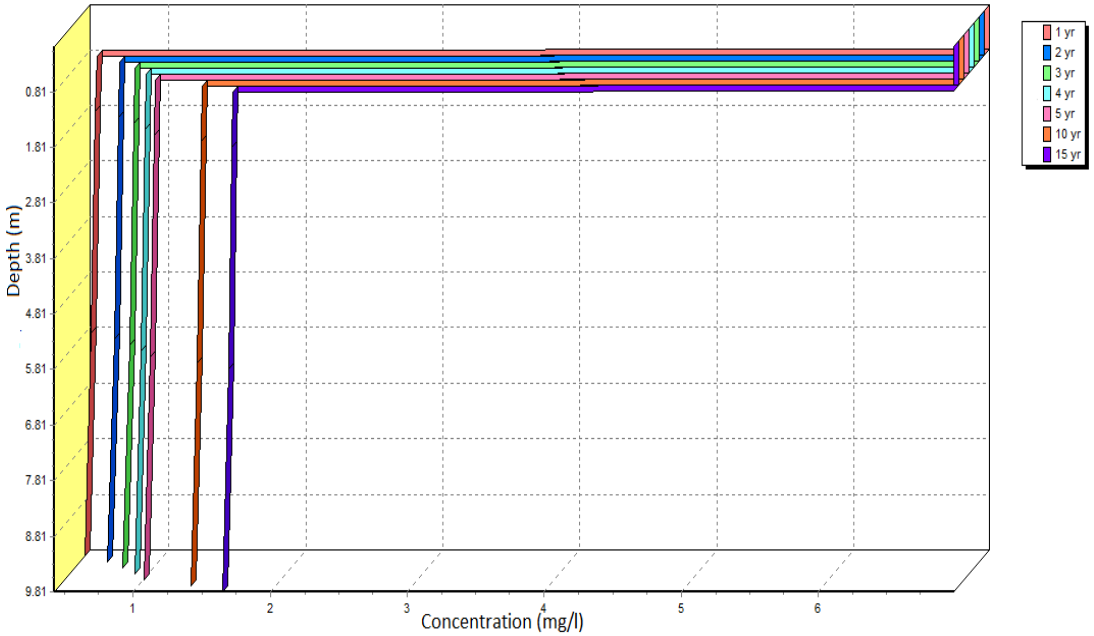

Figure 6.14 Nickel (Ni) simulation

Figure 6.15 shows the changes in the concentration of Ni over the 15 year period at different depths. A comparable trend was perceived for the Ni concentration to that of Cd concentration. The Ni concentration increased slightly each year and the maximum value was observed at 10 m depth for the 15 years as 1.65 mg/l, rising from the first year value of 0.42 mg/l.

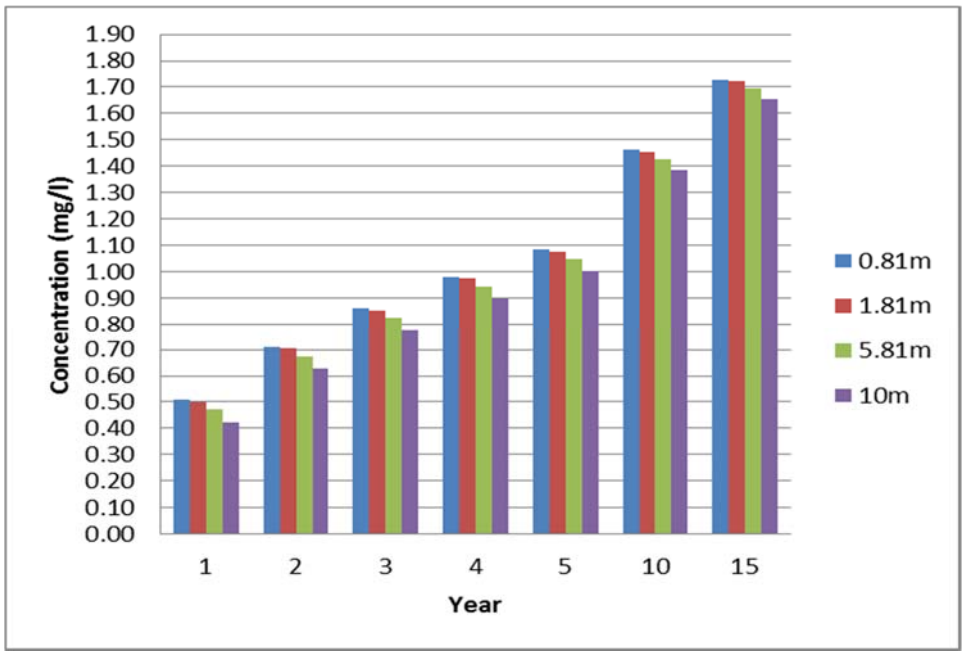

Figure 6.15 Nickel (Ni) concentration at various depths over 15 years

6.3.2.3 *Cadmium (Cd) Simulation in Double Liner System*

A significant decline in Cd concentration was observed as the leachate passed through the secondary leachate barrier of compacted clay in the double liner system (Figure 6.16). Cd concentration after year 1 at the top of the secondary layer was observed to be 2.41 mg/l and decreased to 0.06 mg/l after permeating the secondary leachate barrier. The concentration of Cd for year 1 and year 15 was 53% to 63% lower after permeating the secondary barrier, compared to the concentrations above, i.e. at the leak detection layer.

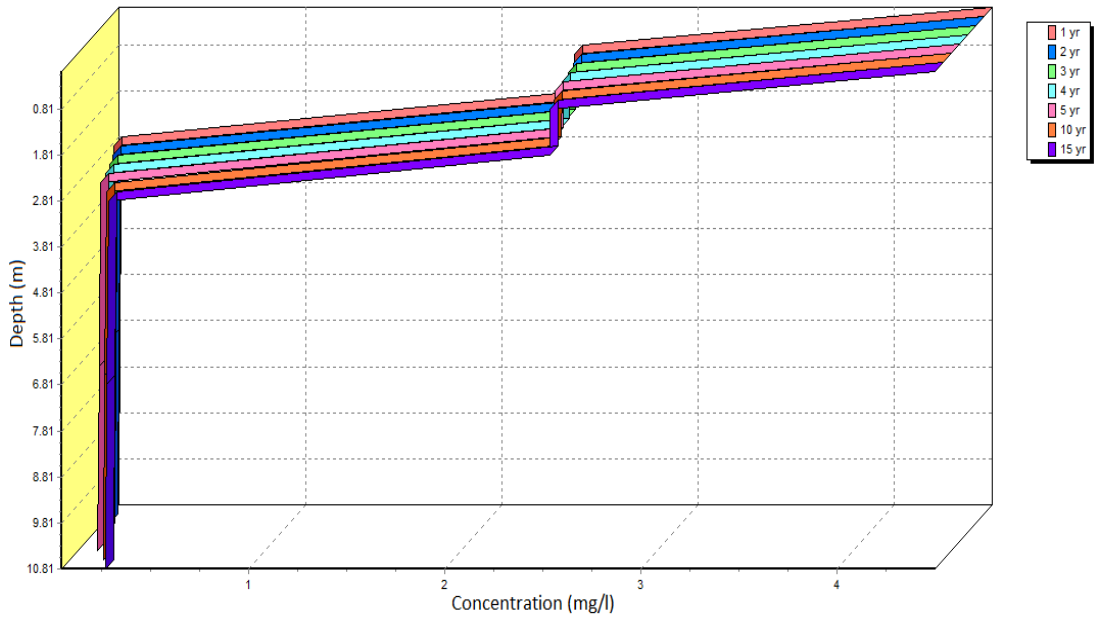

Figure 6.16 Cadmium migration in double liner system

6.3.2.4 *Nickel (Ni) Simulation in Double Liner System*

Similar migratory patterns were observed for the simulation of Ni concentration from the first to the fifteenth year, as illustrated in Figure 6.17. In the first year, Ni concentration above the secondary layer was 0.5 mg/l which then declined to 0.13 mg/l. Generally, a decline of 66% to 74% in the Ni concentration was observed after migrating through the compacted clay layer secondary leachate barrier.

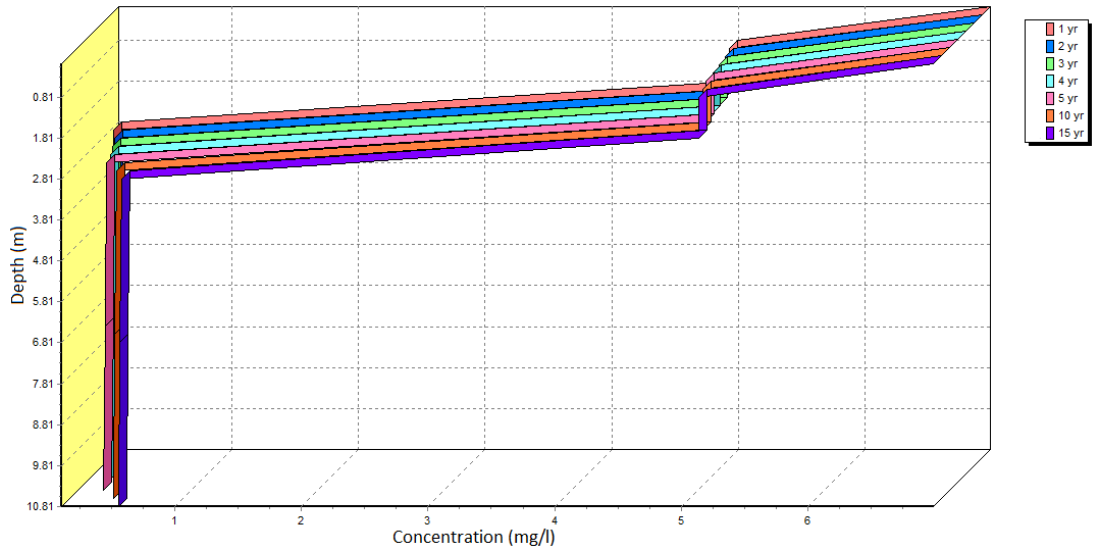

Figure 6.17 Nickel migration in double liner system

6.3.3 Effect of the Double Liner System

Cd and Ni migrated to the compacted clay in the double liner system after permeating the leak detection layer and the GCL, which are the primary leachate barriers. The migratory pattern is hindered in the secondary barrier layer because of the layer's low value of permeability (k).

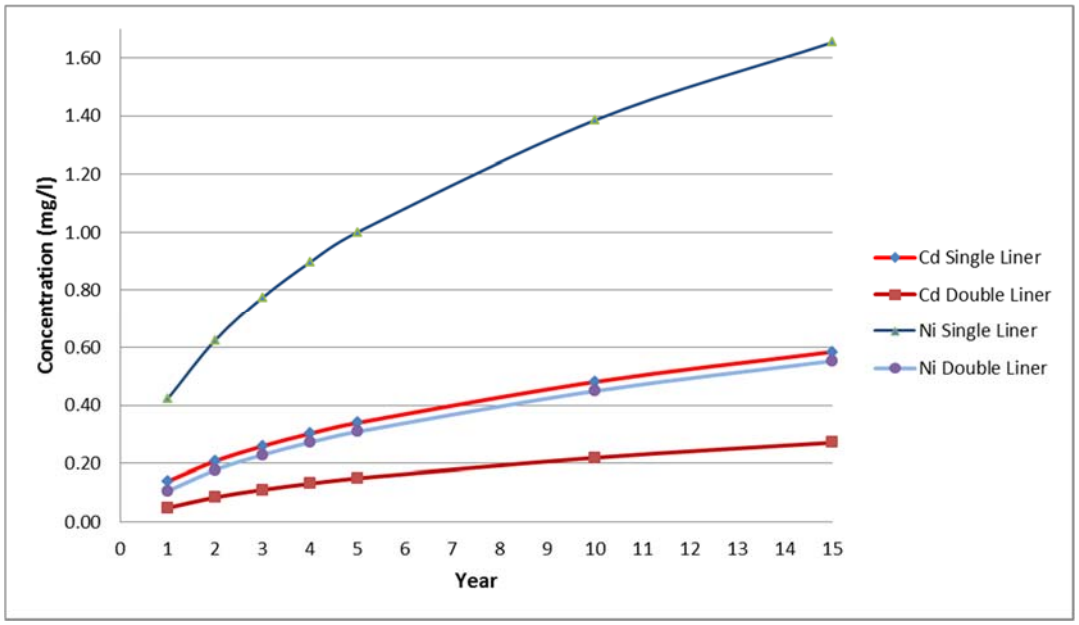

Figure 6.18 Concentration of Cd and Ni at 10 m depth in single and double liner system

The incline in Cd and Ni concentrations needs to be observed every year in the natural soil unless the subsoil saturation point has been achieved. The saturation would then be succeeded by the ceasing of Ni and Cd transportation followed by runoff. This downward trend has also been documented by Salami et al. (2013). Ni and Cd concentrations were observed to increase in the simulation as the heavy metals were transported through the liner system during the 15 year simulation period. However, due to the presence of the secondary leachate barrier of compacted clay, Cd and Ni leaching concentrations at the base of the natural soil decreased by 66% and 53% respectively over the 15 years (Figure 6.18).

Chapter 7
Simulation of Soil Deformation

7.1 Introduction

One of the major risks associated with landfill leachate is the presence of potentially hazardous heavy metals, as discussed in the preceding chapter. These pollutants have the potential to cause environmental pollution and form one of the major contemporary groundwater pollution problems (European Commission 2000; Renou et al. 2008). Seismic activity and geological catastrophes may result in the destruction of liner systems in landfills and the toxic contaminants may pollute the underlying aquifers. Furthermore, groundwater extraction activities from aquifers near landfills may also affect the stability of the landfill liner system due to soil settlement in locations surrounding landfills (Zhu et al. 2012). Therefore, it is important to understand soil deformation in landfill locations in order to mitigate the adverse effects of landfill failure.

Generally, there are different types of soils present in aquifers, and variations in groundwater level also affects aquifer response. Various aquifer constituents, such as fine and granular soils like clays and sands, behave differently in response to groundwater level changes arising from groundwater extraction activities, due to differences in soil characteristics such as hydraulic conductivity (Budhu 2010b). Over time, extended pumping activities may cause the soil in the aquifer to collapse and settle. Land subsidence in the landfill around the aquifers may cause disturbances to the liner system such as variations in elevation and damage to the fabric of the leachate barrier layers, causing excessive seepage of leachate contaminants into the groundwater (Zhu et al. 2012). Many studies have discussed subsidence problems (Budhu, 2011; Budhu and Adiyaman, 2013; Budihardjo et al., 2014). There have also been a number of incidences of troublesome land subsidence around the world such

as Suzhou, China (Shi et al. 2012), Aguascalientes Valley, México (Pacheco-Martínez et al. 2013) and Hangzhou-Jiaxing-Huzhou, China (Cao, Han, and Moser 2013).

Therefore, this research is designed to investigate the occurrence of land subsidence from groundwater extraction activities by using the finite element method (FEM). Three cases were devised in this study to gain an understanding of the occurrence of land subsidence in landfills caused by groundwater extraction activities present in the area surrounding landfills. The structure of this chapter is depicted in Figure 7.1.

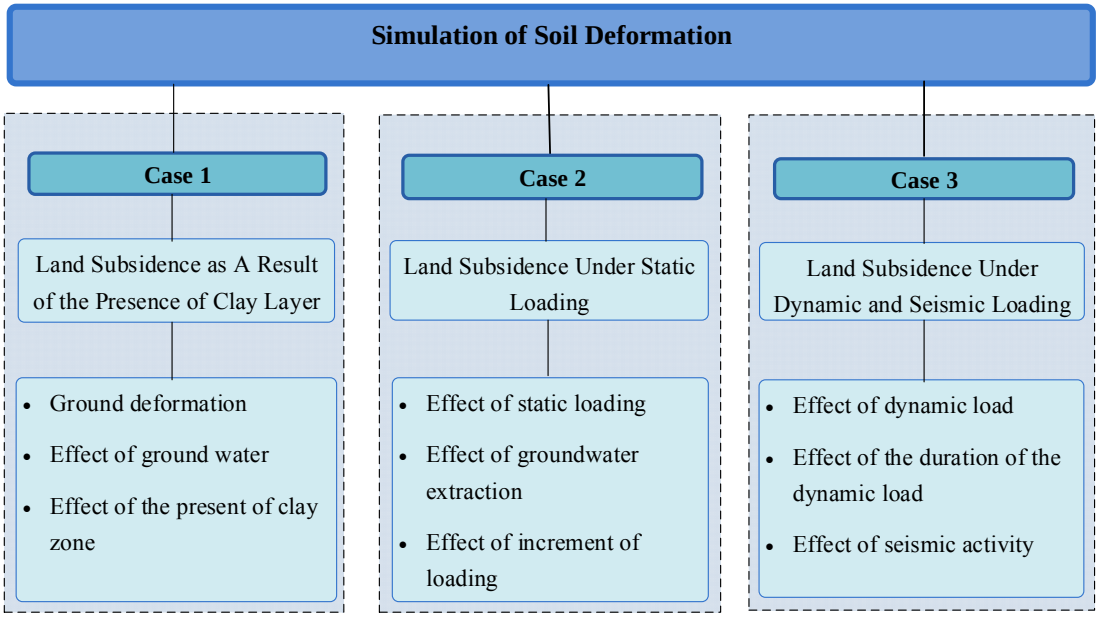

Figure 7.1 Outline of soil deformation simulation

The first research study (Case 1) evaluated diverse clay zone types, i.e. continuous and discontinuous, and thicknesses. Wells were also inserted in different locations in the clay zone, a discharge rate applied at a rate of 20m^3/day and land subsidence measured. The finite element modelling technique was employed in this research to investigate variations in the surface layer deformation response of some sand aquifers containing clay. PLAXIS 2D 2012 finite element software was used to analyse diverse scenarios with varying aquifer parameters such as deviations in groundwater levels, number and location of wells, number of clay zones and the clay layer sizes. A pumping time of five years and a 20 m^3/day groundwater discharge time were set for the simulation.

As discussed, groundwater extraction activities taking place over time around a landfill area may cause damage to the landfill, leading to subsidence of the liner system and the overlying compacted solid waste. The durability and long-term structural

stability of landfills depend upon the distortions imposed on the landfill system. Several factors may have an impact on the landfill, producing subsidence or settlement of the waste mass, and the liner system, such as spatial variability in the aquifer well distribution and the condition of the wells, as well as the characteristics of the native soil.

For that reason, the second research study (Case 2), employed PLAXIS simulation techniques to examine the contribution of well conditions on the subsidence of surface subjected to a combined distributed load from the overlying solid waste. The influence of the surface profile was also incorporated into the study. In order to investigate the likelihood of deformation of the landfill solid waste induced by groundwater level variation due to excessive well-pumping, different soil models involving one and two wells were developed. The groundwater extraction rate was set up at 20 m^3/day for each well.

The availability of suitable land is a major factor influencing landfill management operations globally. Since the cost of developing new landfills can be quite high due to the operational costs, a lack of available land and feasibility issues with available sites; it is desirable to accommodate as much waste as possible in already existing landfills. In order to achieve this, the compaction of solid waste on landfills is often practiced, with compactor trucks being employed to spread and compact the waste. The operation of compactors often induces impact loading or dynamic loading in the soil layers. Dynamic loading is related to changes in pore pressure, reduction in shear strength and variations in shear or Young's moduli etc. Therefore, it is possible that subsidence of soil layers may be affected by dynamic load. This is further complicated by the decline in the groundwater table due to pumping from wells in sand aquifers surrounding landfills.

Thus, in Case 3, PLAXIS was used to construct a sand aquifer model with two pumping wells, and a foundation was used to represent the foundation layers of the landfill. Dynamic loading was applied at the foundation and the foundation subsidence in the sand aquifer subjected to dual well pumping was investigated under zero damping dynamic excitation. The parameters such as the amplitude, frequency and duration of the dynamic loading were changed in order to investigate the influence of these upon the subsidence or deformation of the foundation. Along with the dynamic

load encountered in landfills, the influence of seismic activity was also investigated. When landfills are affected by earthquake forces, the propagation of seismic waves complicates the influence of groundwater extraction activity on landfill sites. For this reason, the study also simulated the effect of well pumping from sand aquifers in the vicinity of landfills subjected to seismic forces. Acceleration time series from an actual earthquake case of smaller magnitude and higher occurrence degree were utilised to obtain results that closely resembled field conditions.

7.2 Case 1: Land Subsidence as a Result of the Presence of a Clay Layer in Aquifer and Groundwater Extraction

Landfills are composed of multiple components such as native soil, compacted clay and geosynthetic layers, in addition to the solid waste dumped on the landfills. The different clay layers interact with each other in the form of differential slip surfaces susceptible to shear failures and therefore, land subsidence. Shear failure has been found to be among the principle causes of landfill failure (Reddy and Basha 2014). The comparatively high landfill failure rates have garnered concerns globally and led researchers to recommend that probability analyses of landfill failures, stability and feasibility analyses, and risk assessment must be performed on proposed landfill sites (Mitchell and Mitchell 1993; Qian, Koerner and Gray 2001; Blight 2008). In conjunction with stability analyses, the impact of waste loading and establishment of reliable factors for safety, shear strength and parameters leading to land subsidence due to shear failure need to be studied (Blight 2008).

Over the years, many researchers have investigated the issue of land subsidence and the factors producing land subsidence and slippage in landfills such as climatic variation, slippage of liner layers, induced loads from managed solid wastes and the settlement of soil layers due to excessive pumping from wells in the aquifers surrounding landfill areas (Leake 1990; Nguyen and Helm 1995; Budhu and Adiyaman 2010).

Budhu (2010a) and Budhu and Adiyaman (2010) have investigated the impact of water pumping through a well system on the declining groundwater table and resulting land subsidence. Based upon these studies, the general causes of soil deformation and

subsidence in adjacent landfill areas can be outlined as the compaction of surrounding aquifers in clays, sediment compaction and the accumulation of loads from soil and solid wastes over the years, causing compression and compaction in the underlying liner system layers.

In a recent study on land subsidence, Budhu and Adiyaman (2010) compared a field study and simulation of the clay zone to investigate land subsidence. Under practical field conditions the clay zone may possess diverse physical characteristics, and consequently the present research study has been primarily focused on the different clay zone properties (i.e. size, patterns) and their effect on land subsidence. The effect of the number of wells was investigated in this research by inserting a number of wells at diverse locations. The effect of the clay zone can therefore be evaluated.

The impact of pumping upon soil behaviour is quite significant from the perspective of successful landfill operations over the design life of a landfill. The clay zone patterns and the location of wells are some of the factors investigated with regard to their effect on the occurrence of land subsidence. Advancements in computational tools and the finite element method (FEM) have made it easier to conduct an investigation of this effect.

7.2.1 Model and Simulation

Clay and sand were the two distinct materials in the aquifer simulated in the models developed for this study. The recoverable soil was represented by clay while the non-recoverable soil was represented by sand. Table 7.1 shows the characteristics of the modelled materials. The soil consolidation and stress-strain behaviour were also linked by the entire model.

Table 7.1 The properties of sand and clay

Soil type	Permeability k (m/sec)	$\gamma_{sat.}$ (kN/m^3)	$\gamma_{unsat.}$ (kN/m^3)	Cohesion c_{ref} (kPa)	Poisson's ratio ν	Initial void ratio e_0
Sand	$5x10^{-4}$	20	17	0	0.25	0.5
Clay	$4.75x10^{-9}$	18	15	30	0.3	1.1

The research project conducted by Budhu and Adiyaman (2010) was used to develop the scenarios proposed in the current study. The effects of the number and sizes of clay

zones was considered in the study as some of the factors influencing variations in ground surface formation. The scenarios simulated in this study have been elaborated in Table 7.2 and Figure 7.2.

The effects of the extraction of groundwater in pure sand aquifers were investigated in the first phase. A sand aquifer with an underlying clay area was modelled in the second simulation under two different stages. The water level was set at 10 m below the surface in the first stage and further lowered to 10 m under the clay area in the second stage. The effect of the size of the clay zone was examined in the next scenario by considering two distinct clay zone sizes, i.e., thicker and thinner. Three clay zones were introduced in the sand aquifer to investigate the second parameter of the effect of the number of clay zones, followed by groundwater extraction with one and two wells.

Table 7.2 Simulations of aquifers and proposed conditions

Scenario	Phase	Well
Sand aquifer	Initial stage + transient from pumping	One, in the middle of aquifer
Sand aquifer, one clay zone	Initial stage + transient from pumping	One, in the middle of aquifer
	Initial stage + transient from pumping + GWL below the clay	One, in the middle of aquifer
	Initial stage + transient from pumping	Two, one in the middle of aquifer and another within 200 m
Sand aquifer, one thinner clay zone	Initial stage + transient from pumping	One, in the middle of aquifer
Sand aquifer, one thicker clay zone	Initial stage + transient from pumping	One, in the middle of aquifer
Sand aquifer, three clay zones	Initial stage + transient from pumping	One, in the middle of aquifer
Sand aquifer, three clay zones	Initial stage + transient from pumping	Two, in the middle of clay zone 1 and 2

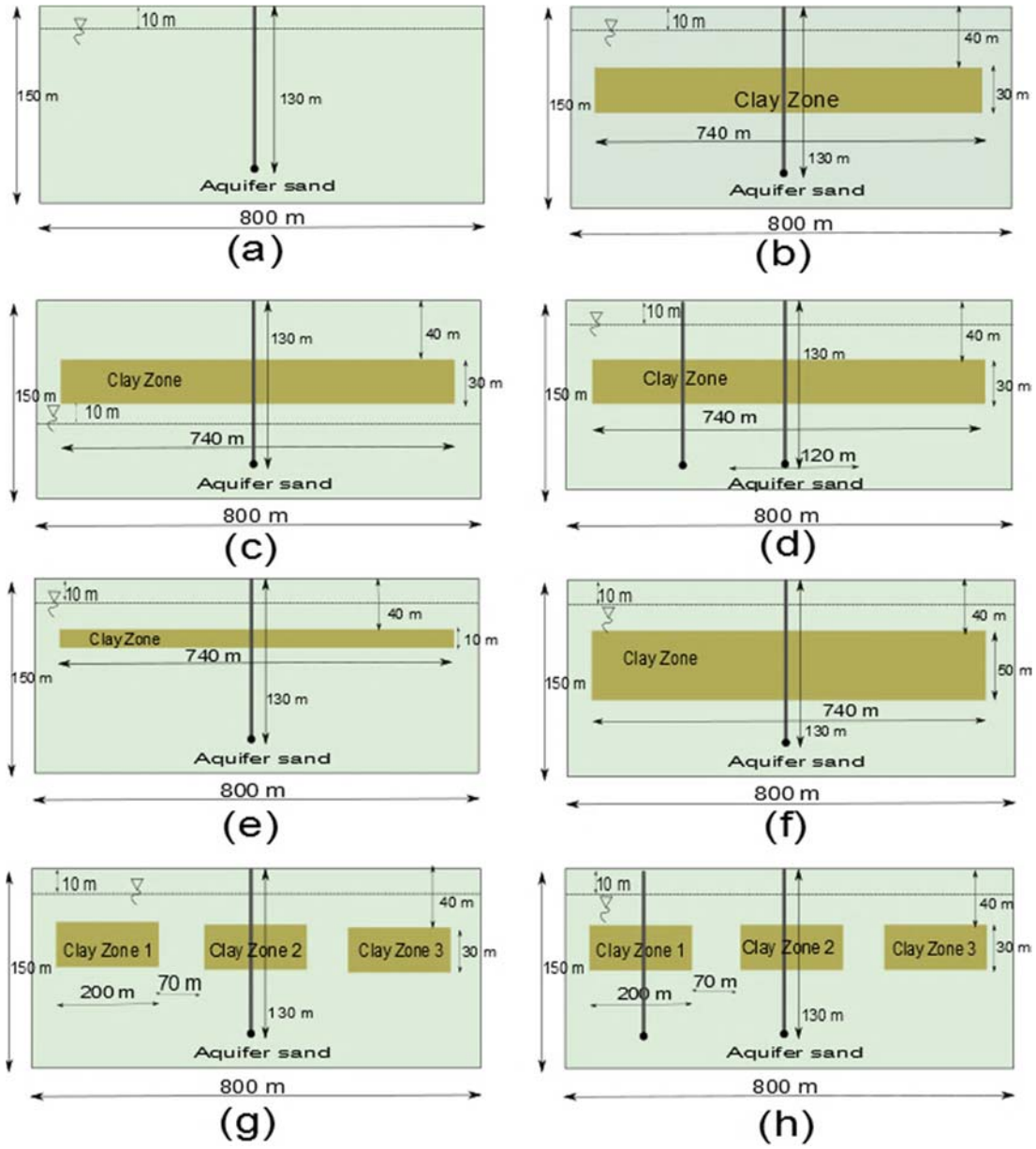

Figure 7.2 Aquifer scenarios: (a) sand without clay, (b) sand with one continuous clay zone, (c) sand with clay and low groundwater level, (d) sand with clay and two wells, (e) sand with thinner clay zone, (f) sand with thicker clay, (g) sand with three thicker clay zones, (h) sand with three clay zones and two wells

The scenarios modelled in the simulation are illustrated in Figure 7.2. A sand aquifer 800 m in length and 150 m in depth was proposed as the main aquifer in this simulation. A pumping well with a 20 m^3/day capacity was installed at 140 m depth to extract the groundwater. The groundwater extraction capacity was further increased to 40 m^3/day after the installation of the second well in the model. The flow of groundwater was set to be transient in order to simulate variation in the level of groundwater. As stated earlier, the initial groundwater level was set up at 10 m below

the surface and the clay zone was set at 40 m underneath the surface to examine the influence of soil with lower permeability in the sand aquifer upon the deformation of ground surface. The effect of groundwater level on land settlement was also examined by lowering the groundwater level to 10 m below the clay zone and an extra well was introduced at a different location to examine the effect of pumping rate and well location on surface deformation.

7.2.2 Ground Surface Deformation

Figure 7.3(a) depicts the initial shape of the homogenous sand aquifer. The surface of the sand aquifer was assumed to be flat along its area and a 140 m deep well was placed at the aquifer's centre. The groundwater level was initially set at 10 m below the surface and 20 m^3/day of groundwater was extracted for five years. The deformation of the ground surface was observed as the level of the groundwater began plummeting, triggering shrinkage of the sand aquifer in the direction of the well location. Figure 7.3(b) further illustrates the noticeable change in the level of the ground surface after five years of pumping activity. The area near the well face demonstrated the greatest ground surface deformation of 1.135 m in the sand aquifer, whereas the area further away from the well showed the least settlement.

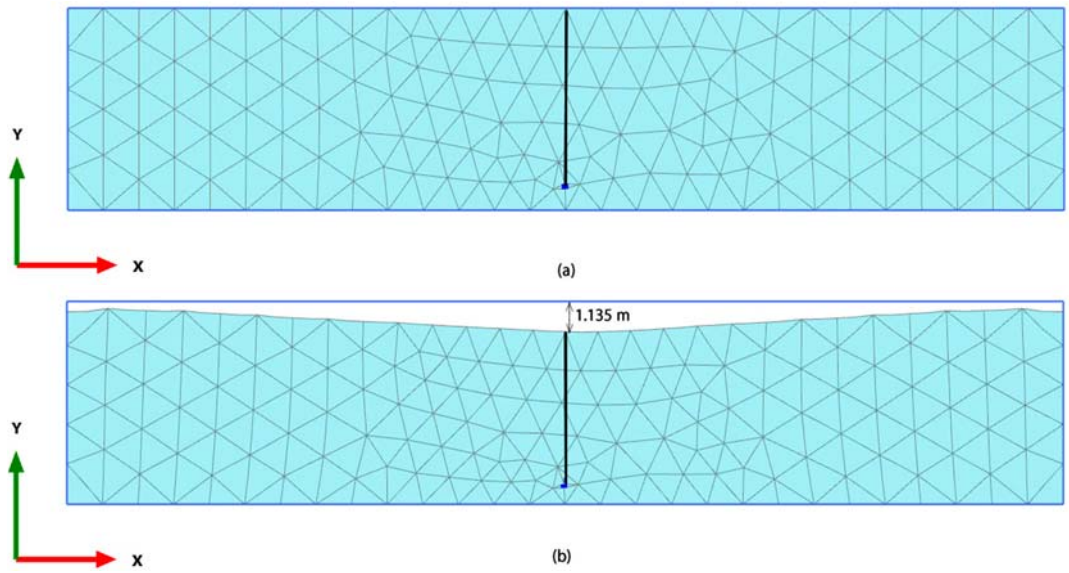

Figure 7.3 Changes in the ground surface of a sand aquifer (a) before pumping and (b) after pumping

Figure 7.4 illustrates the effect of a clay zone upon land subsidence and shows that the clay zone was drawn downwards by developments in the sand underneath the clay layer, followed by the downward vertical movement of the surface area. Land surface deformation, with 1.51 m of estimated maximum displacement, appeared to occur alongside the surface area in the sand aquifer with one large clay zone, and the maximum subsidence was also documented close to the well face. The clay zone triggered more settlement in the ground surface area compared to the pure sand aquifer.

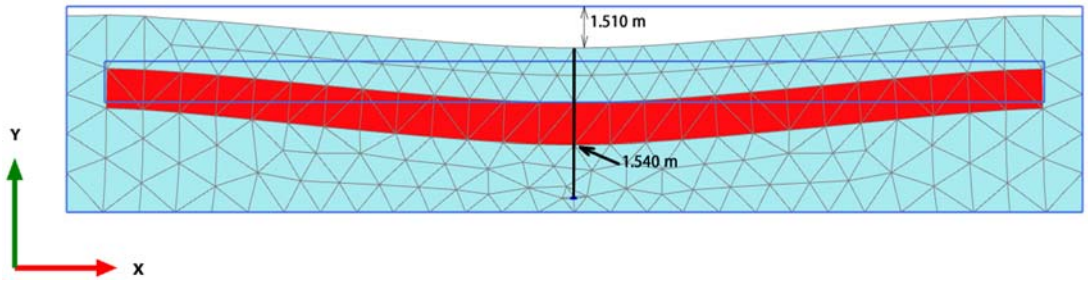

Figure 7.4 Land subsidence in a sand aquifer containing one large clay zone

7.2.3 Effect of Groundwater Level Alteration and Additional Pumping Well

The groundwater level was lowered to beneath the clay layer to examine the effect of groundwater, and the variation in groundwater level was expected to influence the ground deformation pattern. Furthermore, the sand saturation level was projected to be lower than that for the previous simulation. The groundwater extraction rate was maintained at 20 m^3/day and the ground displayed a tendency to settle evenly along its surface as the sand-clay aquifer deformation with initial groundwater level below the clay layer exhibited a considerably different pattern after five years of groundwater pumping (Figure 7.5). The ground surface displacement was observed to be in the range of 2.807–2.944 m. The area farthest from the well location unpredictably displayed the maximum deformation and the same displacement pattern was observed for the clay layer as the ground surface. It can be noted after the examination of the mesh deformation that the area under the clay layer also displayed an increase in pore stresses.

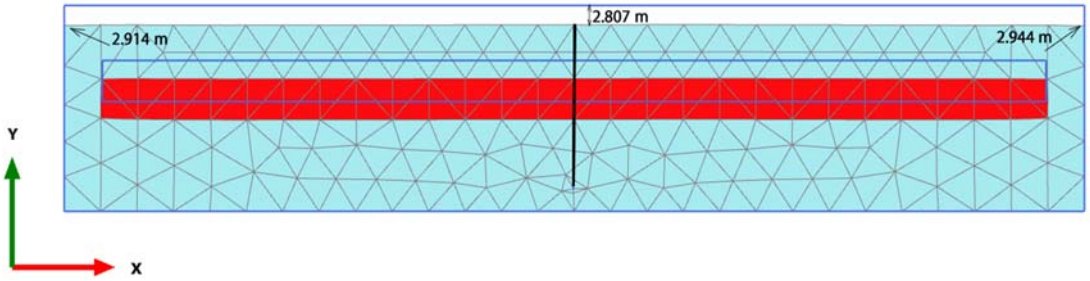

Figure 7.5 Effect of lowering the groundwater level upon the deformation of the ground surface

An additional well was placed about 200 metres from the existing well in the middle of the sand-clay aquifer and the simulation results are shown in Figure 7.6. The effects of excessive groundwater pumping and the location of the well on the deformation of the ground surface were examined in this simulation. A fully saturated clay zone was achieved by maintaining the groundwater level at 10 m below the surface and a pumping rate of 20 m^3/day for five years was set for both wells. The area between well faces 1 and 2 showed the maximum ground surface settlement of 3.453 m in the simulation results, with less deformation occurring near the edge of the area, producing a wavy surface shape. Although both edges of the area depicted similar deformations, the right edge area displayed comparatively less settlement than the left edge area. This could be because well number 1 was installed at the left side of the aquifer. Possibly, a similar deformation pattern occurred in the clay layer, with the deformation of the clay zone becoming significant after excessive extraction of groundwater.

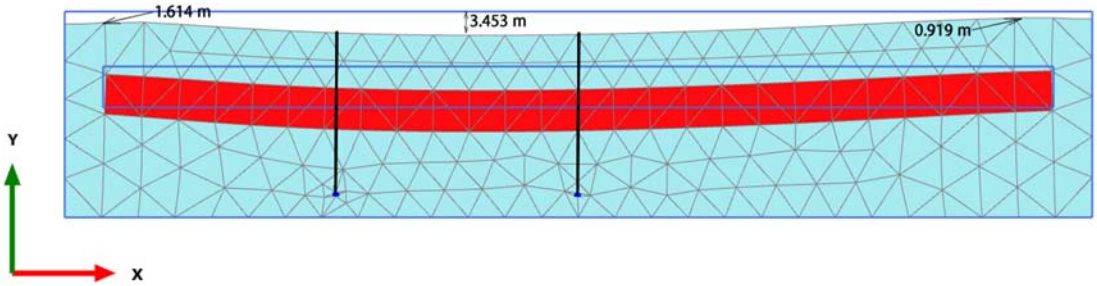

Figure 7.6 Effect of additional well upon ground surface deformation

7.2.4 Effect of Clay Zone Dimensions upon Surface Deformation

Clay zone thickness was modified in order to examine the influence of clay zone dimensions on ground surface deformation. Clay zone thickness was decreased from 30 m to 10 m in the first simulation (Figure 7.7); the thickness was then increased to 50 m (Figure 7.8) for the subsequent setup. A pumping rate was set of 20 m^3/day over five years and the groundwater level was set at 10 m underneath the surface. The centre of the clay zone around the well face displayed the maximum displacement of 2.63 m for the thinner clay zone simulation and a similar deformation was observed in the clay zone after simulation of groundwater extraction. Figure 7.7 depicts the variations in the ground surface at the top of the clay layer. The deformation was affected by the change in clay thickness from 30 m to 10 m. The simulation with thinner clay layer triggered more surface deformation than the previous simulation employing a pure sand aquifer and a sand-clay aquifer with 30 m thickness.

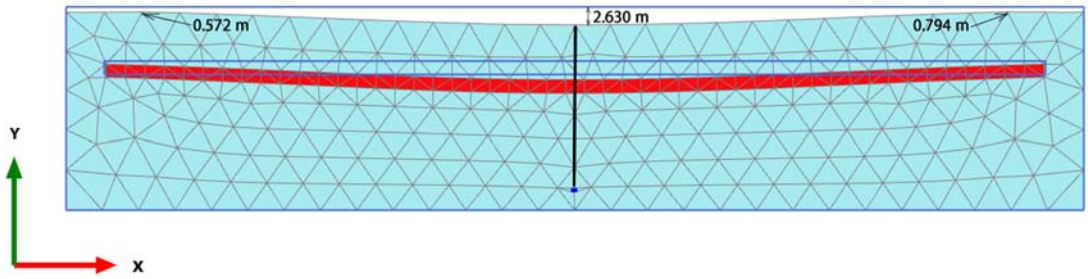

Figure 7.7 The ground surface deformation in an aquifer with a thinner clay zone

Following this, the effect of a comparatively thicker clay zone on land settlement was net evaluated in the following simulation (Figure 7.8) by increasing the thickness of the clay zone to 50 m. The pump was placed at the aquifer's centre and a similar pumping rate and groundwater level were used, i.e., 20 m^3/day for five years and 10 m, respectively. Although a similar surface deformation pattern was observed to that in the previous model with clay zone thicknesses of 10 m and 30 m, a greater deformation was noted with 2.84 m being the maximum.

Figure 7.9 shows the next modelled scenario with three clay zones in the sand aquifer. Initially the level of groundwater was 10 m below the surface and the groundwater extraction rate was kept at 20 m^3/day from a well located underneath clay zone 2. This scenario displayed a similar deformation pattern to the ground surface with the same

maximum ground surface deformation of 2.840 m as in the previous simulation (Figure 7.8).

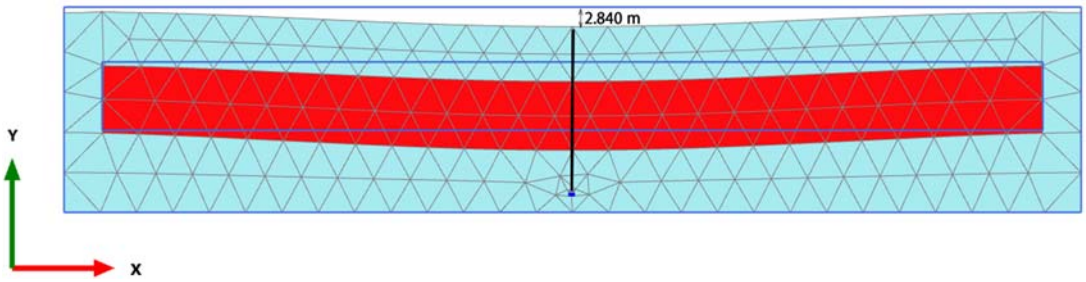

Figure 7.8 The ground surface deformation in an aquifer with a thicker clay zone

A sand aquifer with three clay zones was outfitted with an extra well in the final scenario. The subsidence of the three clay zones affected the level of the surface as presented in Figure 7.10. A maximum displacement of 1.627 m was observed between the first and second clay zones in this scenario, whereas ground surface above the clay zone on the left side displayed other marked surface movement.

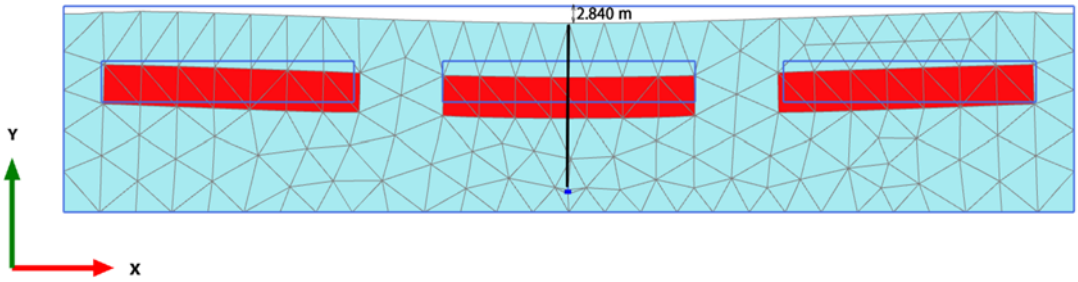

Figure 7.9 Land subsidence in an aquifer containing three clay zones and one well

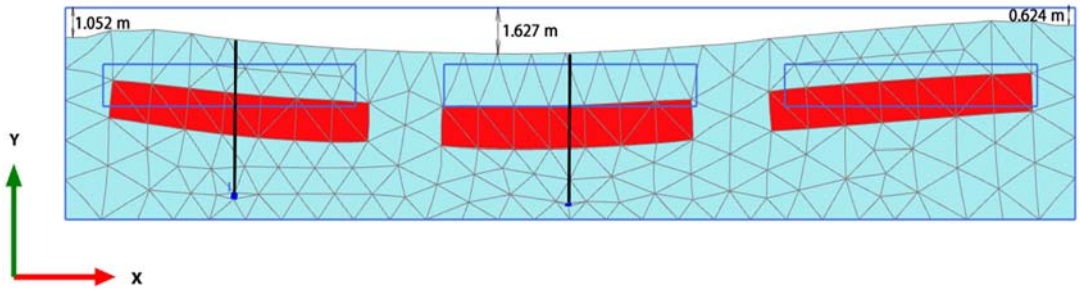

Figure 7.10 Land subsidence in an aquifer containing three clay zones and two wells

Table 7.3 Comparison between scenarios

Aquifer	Clay thickness (m)	GWL	Number of clay zones	Number of wells	Max. surface deformation (m)	Surface shape
Sand	N/A	Above clay zone	1	1	1.135	Lowest sagging area is close to the well
Sand-Clay	30	Above clay zone	1	1	1.51	Lowest sagging area is close to the well
Sand-Clay	30	Below clay zone	1	1	2.807	Nearly flat
Sand-Clay	30	Above clay zone	1	2	3.453	Lowest sagging area is close to the well
Sand-Clay	10	Above clay zone	1	1	2.63	Lowest sagging area is close to the well
Sand-Clay	50	Above clay zone	1	1	2.84	Lowest sagging area is close to the well
Sand-Clay	30	Above clay zone	3	1	2.84	Wavy, lowest area is close to the well
Sand-Clay	30	Above clay zone	3	2	1.627	Wavy, sagging in between wells

A comparative evaluation of each developed model is briefly presented in Table 7.3. The sand aquifer comprising a 30 m thick clay layer and two wells displayed the highest surface deformation. This model had a total groundwater extraction of 40 m^3/day. A maximum surface deformation of only 1.627 m was observed unexpectedly in the aquifer model having three clay zones of 30 m thickness each and two pumping

wells with 40 m^3/day as the cumulative extraction rate. Once the rate of groundwater extraction is kept constant, non-continuous clay zones may produce less aquifer surface deformation than a continuous and elongated clay zone. Furthermore, a sand-clay aquifer causes comparatively more surface deformation than a sand aquifer without any clay layer underneath, which displays more stability.

7.3 Case 2: Land Subsidence under Static Loading

Excessive groundwater withdrawal has been previously identified as a trigger for the deformation of the ground surface, a finding that is also supported by researchers (Chai et al. 2004; Budhu 2010a; Chaussard et al. 2013). As discussed earlier, the consequences of ground surface deformation in landfills can be varied and may be direct or indirect and temporary or permanent. These may include damage to the natural soil, subgrade of sand or compacted clay barrier and fabric of the leachate liner layers, and may even result in settlement of the overlying solid waste loading (Zhu et al. 2012). Therefore, the durability and stability of the landfill may be threatened by the deformation of the ground and in order to maintain successful landfill operations, it is essential that they are taken into consideration during the urban planning process.

Land subsidence prediction models are much employed in urban planning to directly assess the land subsidence characteristics and to ascertain the rate and magnitude of land subsidence in landfills. Over the years, excessive subsidence of landfill systems has incurred widespread concern due to its influence on the stability and serviceability of landfills and the solid waste managed in the landfills. Several factors influence the occurrence and severity of land subsidence such as the imposition of extra loading, lowering of water levels, transported deposits, etc. (Zhu et al. 2012).

The subsidence of landfill layers causes excessive damage to the overlying solid waste which acts as an overburden loading. In order to maintain successful landfill operations, it is imperative that the landfill soil layers provide adequate support to the waste. Therefore, the soil layers perform a function in landfill which is similar to that of a foundation subjected to subsidence stresses (Zhu et al. 2012). In a study on the probable damage caused by land subsidence to foundations, laboratory testing supported by numerical verification was employed by Shahriar et al. (2013) to conduct a quantitative investigation of the influence of water table fluctuation on the settlement

of various types of foundations, along with other parameters like foundation shape, stress level and soil density.

Therefore, it is important to perform a numerical evaluation of the characteristics and magnitude of influence of subsidence and its relevant parameters upon landfills with consideration to the loads imposed by solid waste on the landfill foundation layers. Moreover, different modes of load like vertical pressure and bending may produce different impacts on the underlying soil and therefore generate different responses upon the occurrence of soil subsidence. These aspects have been incorporated in this part of the study on landfill land subsidence covered in this section.

7.3.1 Model and Simulation

In this study, the model constituted sand was employed to perform the simulation. The model had also considered soil consolidation and stress-strain behaviour. The influence of the location and number of wells on the subsidence of landfill foundation layers, assumed as a foundation under overlying loads, was investigated in this study. The model area was 50×200 m and the loading profile was as follows:

- 100 kN/m of point load at the left side of foundation.
- Bending moment of 100 kN/m.
- Two different distributed loads of 150 and 300 kN/m.

All models maintained a transient flow model with the initial groundwater level set at 10 m below the surface at the start of all stages. The depth of the well was 40 m below the surface in the two cases and the discharge rate was maintained at 20 m^3/day for each well.

7.3.2 Single Well Model

A well was installed at the right side of the modelled soil area for the development of a single well model and the face of the well was placed 70 m from the point of load application and 30 m from the right end of the loaded foundation layer. The pumping rate of the well was maintained at 20 m^3/day and the settlement (vertical displacement) of the ground surface area was recorded at three nodes, as tabulated in Table 7.4.

Table 7.4 Data of the points on the surface profile of Figure 7.11

Node	y deformation (10^{-3} m)
691	127.641
475	152.262
311	115.498

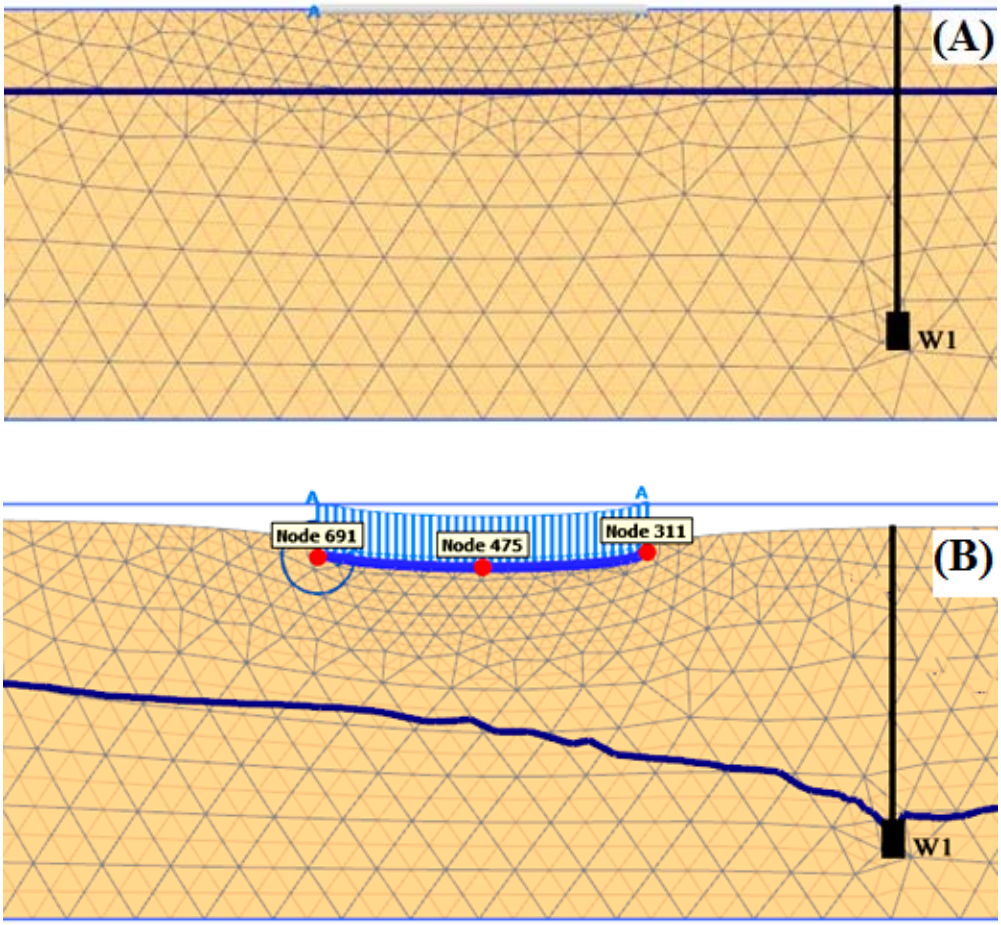

Figure 7.11 Initial mesh (A) and final deformed mesh (B) of single well model with distributed load of 150 kN/m

The maximum deformation of 152.262 x 10^{-3} m was observed at the centre of the foundation at node 475, as illustrated in Figure 7.11. Furthermore, the application of bending moment and point loading at the left-hand side of the foundation resulted in comparatively more deformation at the left edge (node 691) than the right edge. However in the soil model, the left-hand side showed less displacement than the right-hand side, which was assumed to be caused by the water-head imbalance as the right side water level of the soil model was lower than the left side due to the location of

the pumping well. A comparatively lesser displacement was observed in the foundation than the neighbouring soil profile.

7.3.3 Two Wells Model

The left-hand side of the soil area was provided with a new well, located 30 m from the left edge of foundation, to create the two wells model. The well depth was 40 m beneath the ground surface with a pumping rate of 20 m^3/day and a per day groundwater extraction volume of 40 m^3.

Table 7.5 Data of the points on the surface profile of Figure 7.12

Node	y deformation (10^{-3} m)
729	149.066
404	163.788
307	127.770

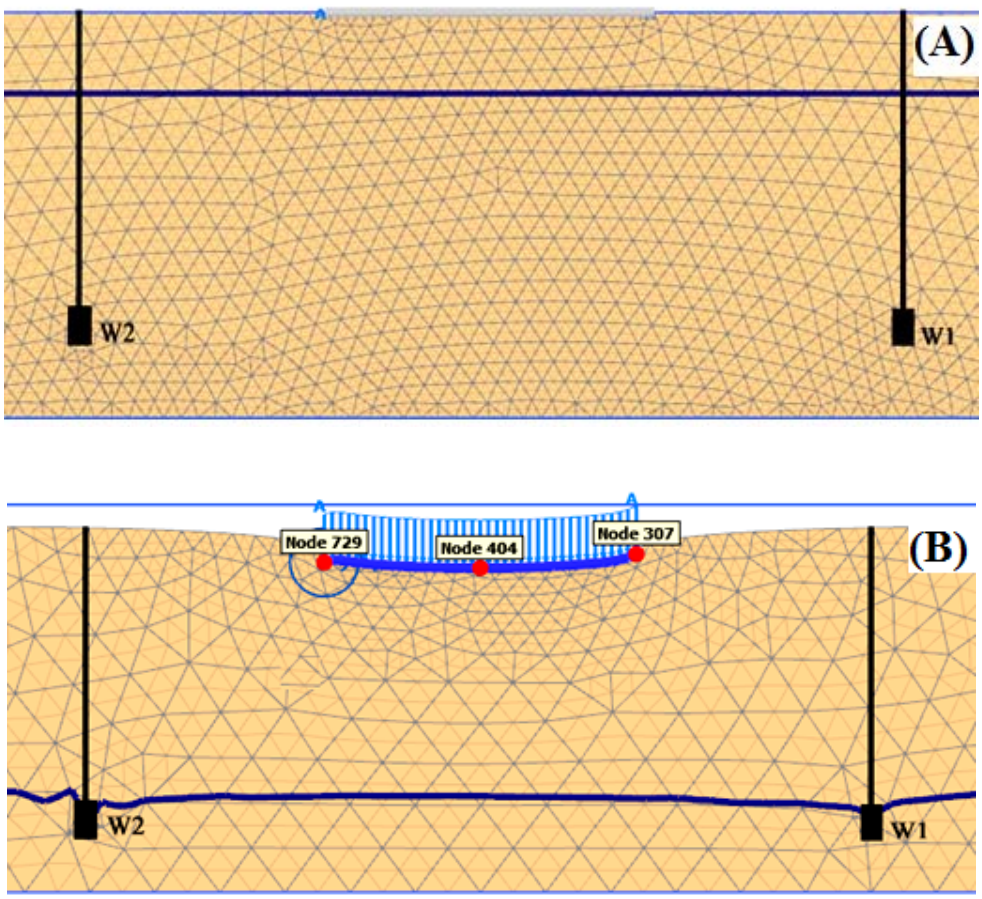

Figure 7.12 Initial mesh (A) and final deformed mesh (B) of two wells model with distributed load of 150 kN/m

The maximum displacement was again observed in the centre of the foundation node 404 (Figure 7.12), if the installation of the two wells was done symmetrically with respect to the centre of the loaded foundation. However, a slightly higher maximum displacement of 163.78 x 10^{-3} m (Table 7.5) was obtained from the PLAXIS results, compared with the results of the earlier discussed model. In addition, the occurrence of greater subsidence, compared to Figure 7.11 and Table 7.4, caused the water table to be comparatively lower and more level after the groundwater extraction than for the single well system. Theoretically, grain repositioning and higher effective stress could have caused this behaviour, but the maximum displacement was not observed at the lowest point of the water table. The displacement increased when the point was nearer to the foundation's centre, and at the area where the foundation was placed, general sagging in the soil profile was observed.

7.3.4 Effect of Increment of Distributed Load

Landfills are generally intended to operate over longer periods of time, and the magnitude of the load induced by the solid waste therefore increases with time and the accumulation of waste. In other words, the magnitude of the distributed load supported by landfill foundation layers is not constant over time. The situation is further complicated by the extraction of groundwater from wells situated in sand aquifers surrounding the landfill area. Over time, the groundwater level will decline and the soil layers will tend to consolidate while the load from the overlying wastes will increase. This means that the deformation or subsidence of the foundation layers may be affected by the coupling of the processes. The effect of the magnitude of distributed load on the subsidence of foundation placed over sand aquifers with pumping wells was investigated in this section of the study. The magnitude of distributed load on the foundation for both single and dual well systems was doubled to 300 kN/m. Figure 7.13 and Figure 7.14 show the deformation results while Table 7.6 and Table 7.7 list the magnitude of deformation for significant points.

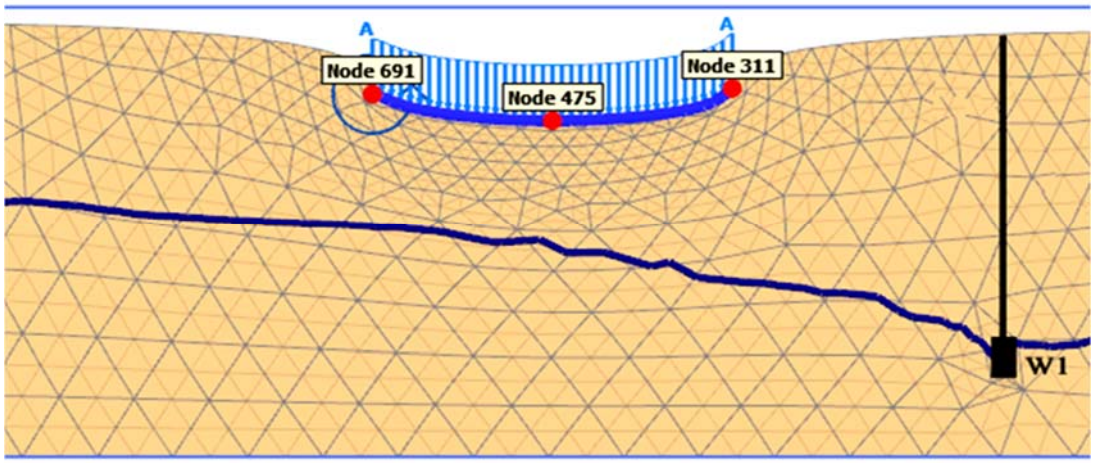

Figure 7.13 Deformed mesh of one well model with 300 kN/m of distributed load

The symmetry or location of the maximum subsidence for both types of well systems remained unchanged with the increase in load from 150 kN/m to 300 kN/m. This means that models with same well conditions had the maximum subsidence occurring at the same location with similar subsidence symmetry irrespective of the difference in the applied distributed load. For example, in the single well systems of Figure 7.11 and Figure 7.13, maximum foundation subsidence at the centre and sagging surface profiles in the foundation area were observed. Figure 7.12 and Figure 7.14 display similarly equal results in subsidence location and symmetry.

Table 7.6 Data of the points on the surface profile of Figure 7.13

Node	y deformation (10^{-3} m)
691	193.184
475	252.245
311	180.621

However, the increasing load increased the magnitude of subsidence. For instance, the maximum displacement at the centre of the foundation (node 475) in Figure 7.13 and Table 7.6 was 252.245 x 10^{-3} m, which was higher than that seen in Figure 7.11 and Table 7.4 (node 475). The difference in the deformation between those two points is about 99.983 x 10^{-3} m.

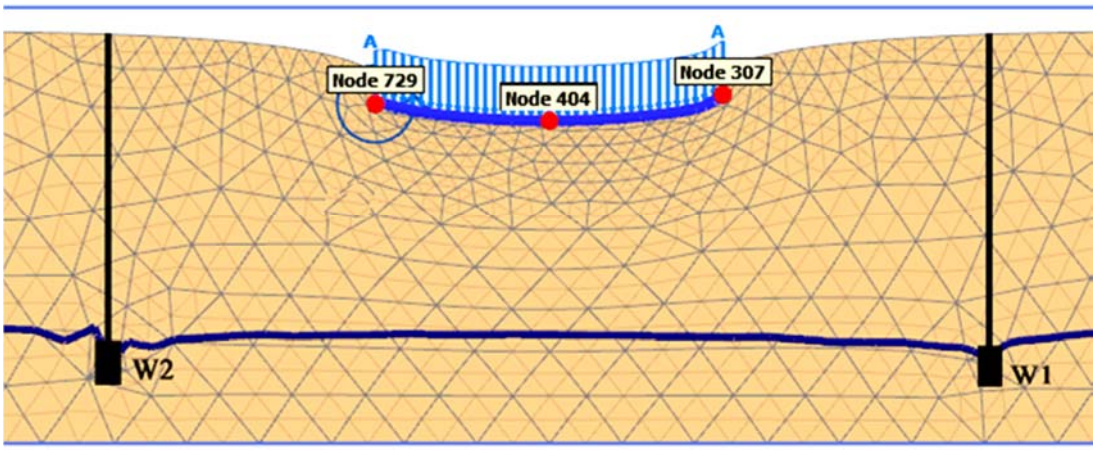

Figure 7.14 Deformed mesh of two well model with distributed load of 300 kN/m

The corresponding points between points in Table 7.5 and Table 7.7 also showed similar results. Nonetheless, slight variations in some values were observed, specifically in the left edge region of the soil models, but these dissimilarities are negligible for the purpose of drawing conclusions and are disregarded as a result of inevitable computational variations.

Therefore, the applied load on the foundation can be considered as the main factor influencing the subsidence of the foundation. Interestingly, the subsidence was observed at the centre of the foundation even though the applied load was distributed along the foundation. Meanwhile, the effective stress and vertical deformation along the ground surface area continued to increase due to the lowering of the water level caused by groundwater extraction activities.

Table 7.7 Data of the points on the surface profile of Figure 7.14

Node	y deformation (10^{-3} m)
729	149.066
404	163.788
307	127.770

7.4 Case 3: The Basic Influence of Dynamic Amplitude, Duration and Frequency on Land Subsidence of Sand Aquifer with Pumping Wells

The previous sections have discussed the occurrence of soil displacement in landfills due to the changes in the groundwater table caused by well pumping from sand aquifers surrounding landfills. The foundation layers of a landfill are prone to subsidence, thereby making the landfill susceptible to deformation and failure over time. The extent of the foundation deformation depends upon several factors such as decline in water table, dry soil submergence, and accumulation of solid waste over time (Zhu et al. 2012).

Shahriar et al. (2013) have investigated damage caused to foundations due to subsidence, evaluating the settlement of different foundations against fluctuations in water level by numerical and laboratory work. They also studied other factors such as the shape of foundation, density of soil and level of stress. Furthermore, the type of load, such as vertical load or bending moment, influenced the subsidence responses like varied location/magnitude of maximum subsidence and the overall shape of the deformation.

Even though the influence of underlying factors like groundwater extraction on land subsidence has been researched, landfills also encounter surcharge loading induced by the overlying solid wastes. Over the years, as more groundwater is pumped out of the soil layers surrounding the landfill, the surcharge load increases due to the accumulation of solid waste. It is a common practice in landfill operations to compact solid wastes after dumping them.

Landfill compactors are heavy trucks/machines that have two basic functions: spreading and compacting solid waste. In order to achieve this, impact or dynamic loading is applied again and again to compress the waste to much higher densities so that more waste can be accommodated. These dynamic forces induce variations in the pore water pressure and may even influence the subsidence of the foundation layers of the landfill. This study investigates the influence of various dynamic loading parameters such as amplitude, duration and frequency upon the subsidence of landfill

foundation layers, modelled as a loaded foundation, in the vicinity of sand aquifers subjected to groundwater extraction from well pumping.

In addition to the dynamic load induced during landfill operation by the compaction of solid waste, landfills may be subjected to seismic forces depending upon the location of the landfill. Many researchers have investigated several aspects of land subsidence, as discussed earlier, however there is a lack of study into the effect of earthquakes on the land subsidence process. The complexity of seismic activity is related to the propagation process of seismic waves and their effect on the sites and other specific phenomena. Consequently, the influence of seismic activity upon the subsidence or deformation of landfill soil layers should also be investigated.

Therefore, the effect of groundwater extraction through well pumping in sand aquifers surrounding the landfill subjected to seismic forces was also studied in this research. In order to obtain results that closely represent real world situations, acceleration time series from a real earthquake case representing smaller quakes that have a high degree of occurrence were employed.

7.4.1 Model and Simulation

The developed models used the non-recoverable soil (sand) as the base material and the properties of the sand used are listed in Table 7.8. The model considered both consolidation and stress-strain behaviour of the soil and damping ratio was ignored as no damping effect was taken into account.

Table 7.8 The properties of sand

Soil type	γsat (kN/m^3)	γunsat (kN/m^3)	Cohesion c_{ref} (kPa)	Poisson ratio ν	Initial void ratio e_0
Sand	20	17	0	0.2	0.5

The effect of zero damping dynamic load including distributed and point loads of different frequencies and magnitudes upon the subsidence of foundations were investigated in this section. In all scenarios, 100 kN/m distributed static load was applied to the foundation to represent the overlying load and a 50×200 m model area was used. Two wells with 40 m well depth below the ground surface and a 20 m^3/day

extraction rate were symmetrically added on both sides of the foundation. Initially, groundwater extraction for three days from two symmetrical wells under transient flow conditions was used to cause subsidence. This was followed by the investigation of the influence of a dynamic distributed load of different amplitude (10 kPa and 20 kPa), frequencies (10 Hz and 20 Hz) and durations (20 s and 40 s) imposed on the foundation on the subsidence of the foundation (see Figure 7.15).

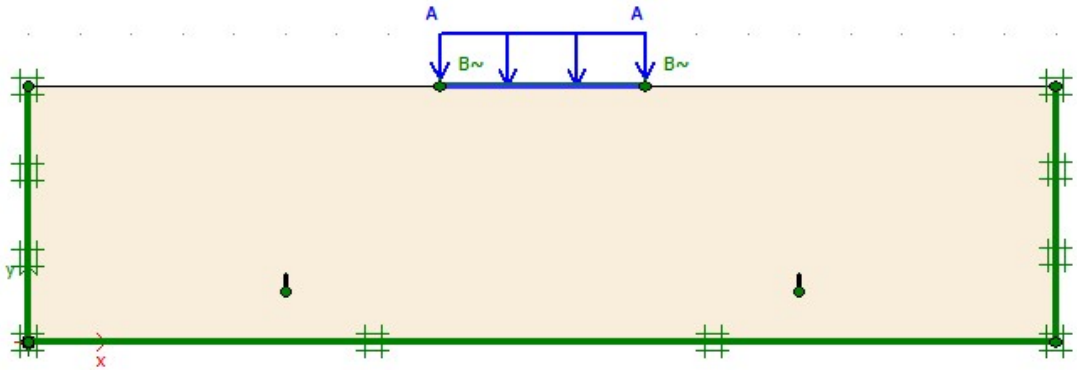

Figure 7.15 PLAXIS model with dynamic distributed load on the surface of foundation ('A' represents self-weight and 'B' is dynamic load)

In order to examine the effect of seismic activity on land subsidence in landfills surrounding sand aquifers subjected to well pumping activities, the model was modified to incorporate seismic loading. As earlier, the landfill foundation soil was represented by a foundation 40 m in width. The soil model geometry was developed as 100 m × 400 m. The properties of the sand were kept as listed in Table 7.8 and 20 m^3/day was maintained as the groundwater extraction rate. The model geometry is presented in Figure 7.16.

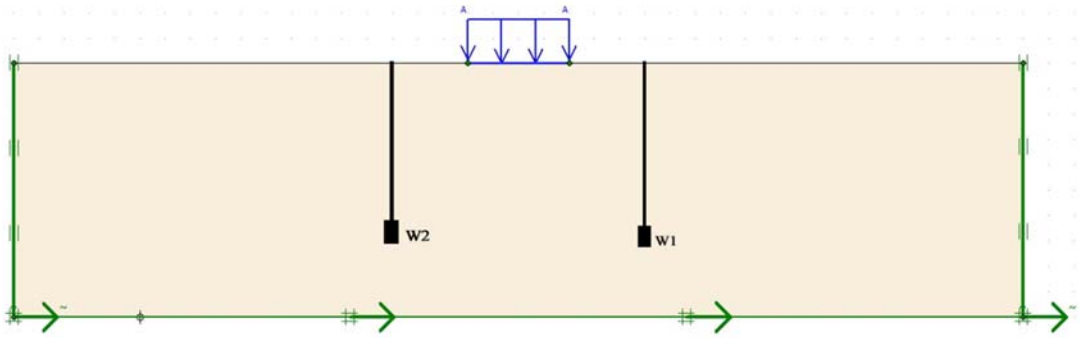

Figure 7.16 PLAXIS model of foundation on sand aquifer with two pumping wells subjected to seismic activity

The record of the earthquake was obtained from the actual magnitude 4.4 earthquake at Encino, California as recorded by the U.S. Geological Survey (2014). Earthquakes of this magnitude are more frequently encountered in actual conditions (see Figure 7.17).

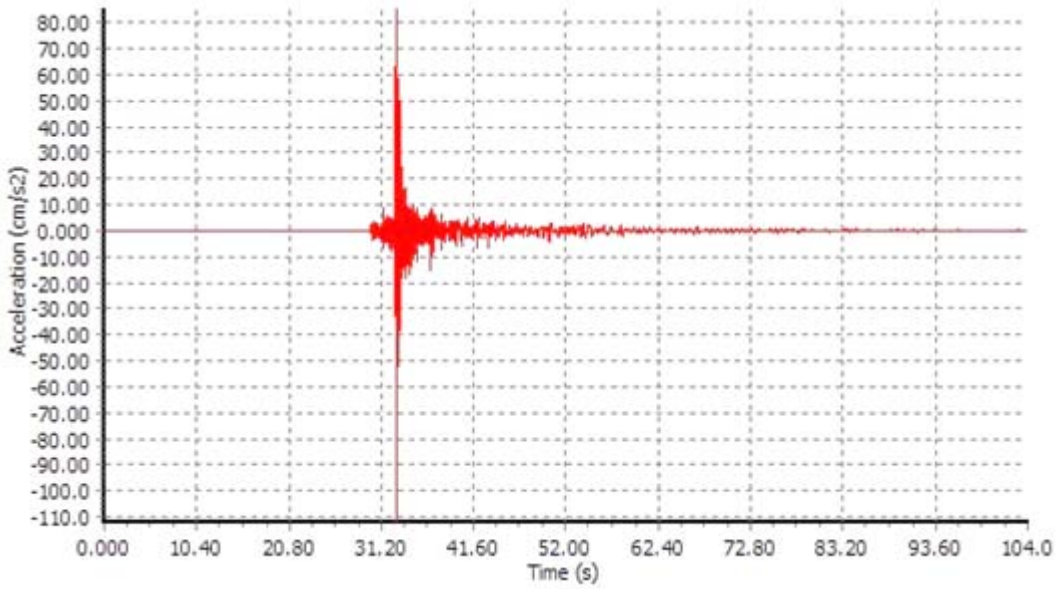

Figure 7.17 Acceleration versus dynamic time diagram for Encino, California earthquake (U.S. Geological Survey, 2014)

7.4.2 Foundation Subsidence without Dynamic Load

The deformation effect of groundwater extraction and self-weight of the foundation were simulated so that comparisons could be drawn to investigate the influence of the dynamic parameters at a later stage. Figure 7.18 shows the subsidence mesh and Table 7.9 lists the foundation subsidence values corresponding to the nodes 712, 417 and 325. The studies presented in the preceding sections discussed the influence of groundwater extraction and lowering water table as main contributors of foundation subsidence. The largest vertical deformation of 130.031 mm was observed at the centre of the foundation as displayed in Figure 7.18 and Table 7.9 while the two edges encountered similar vertical deformation generally commensurate with the symmetrical nature of this model, as has been observed in earlier sections.

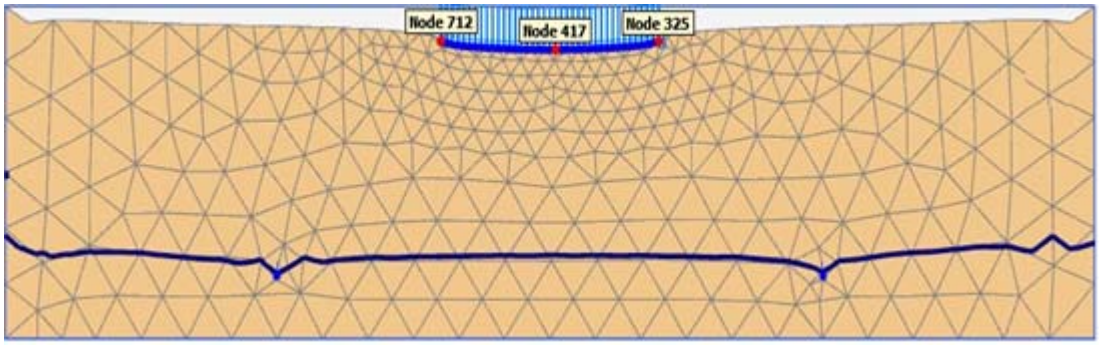

Figure 7.18 Pre-dynamic schematic view of deformation after pumping for 30 days

Table 7.9 Data corresponding to points on the foundation of Figure 7.18

Node point	Vertical deformation (mm)
712	-104.453
417	-130.031
325	-105.244

7.4.3 Effect of Dynamic Load Activity

The dynamic load was applied after the groundwater extraction was continued for 30 days and subsidence with static distributed load was observed. Table 7.10 lists the different dynamic parameters investigated in each run of the model calculations.

Table 7.10 Dynamic configurations for each model

No. of dynamic model	Amplitude (kPa)	Frequency (Hz)	Duration (s)
1	10	10	20
2	10	20	20
3	20	20	20
4	10	10	40
5	20	10	40

7.4.3.1 Effect of Dynamic Loads of 20 s Duration

Dynamic Model 1

The application of the dynamic load slightly increased the degree of foundation subsidence to 145.446 mm while the location of the maximum deformation remained unchanged as the centre of the foundation. This maximum subsidence value was

approximately 15 mm higher than the subsidence after groundwater extraction of 30 days. The 20 s duration of dynamic loading is crucial to the increase in the maximum subsidence compared with the 30 day extraction period as it implies that the increased subsidence was due to the effect of the dynamic load and not due to further pumping of the groundwater.

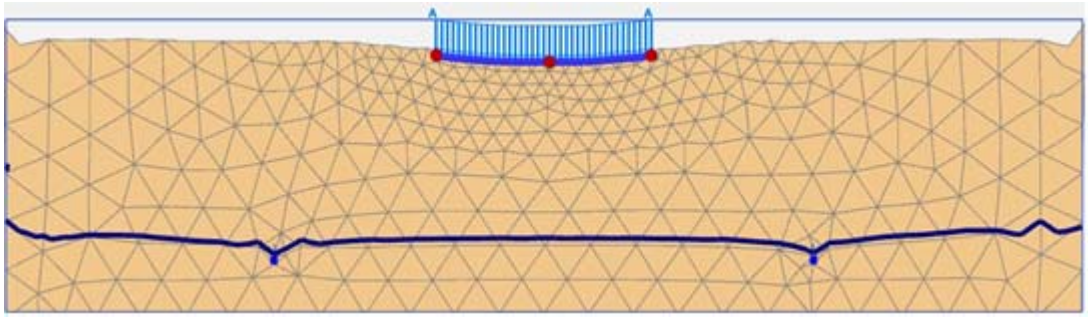

Figure 7.19 Deformation under dynamic load of frequency 10 Hz, amplitude of 10 kPa, duration of 20 s

Table 7.11 Data corresponding to points on the foundation in Figure 7.19

Node point	y deformation (mm)
712	-122.277
417	-145.446
325	-122.878

Dynamic Model 2

The load frequency was doubled from 10 Hz to 20 Hz in the second dynamic model, whereas other factors were kept similar to the first dynamic model. Figure 7.20 and Table 7.12 display the results from the PLAXIS calculations. It can be seen that only negligible fluctuations in foundation subsidence were observed after the increase in frequency and overall, the foundation subsidence remained relatively the same at all three nodes. Therefore, it may be deduced that the frequency of dynamic load has a negligible influence upon the subsidence of the foundation. However, these results have only incorporated a dynamic load of 10 kPa amplitude and 20 s duration and further investigation may be needed to study the effect of dynamic load frequency on foundation subsidence.

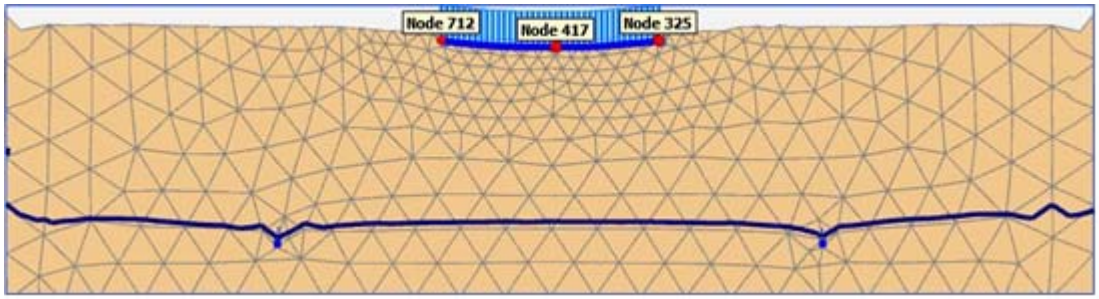

Figure 7.20 Deformation subjects to dynamic load of frequency 20 Hz, amplitude of 10 kPa, duration of 20 s

Table 7.12 Data corresponding to points on the foundation of Figure 7.20

Node point	y deformation (mm)
712	121.649
417	147.954
325	123.174

Dynamic Model 3

The amplitude was doubled to 20 kPa in model 3, while the frequency was maintained at 20 Hz. Greater foundation subsidence, with a maximum subsidence of 152.955 mm, was observed at the centre of the foundation (node 417) due to the increased amplitude of the dynamic load **(**Table 7.13 and Figure 7.21). The observed subsidence displayed divergence from the symmetric nature of the model as the left edge showed greater subsidence than the right edge. This observation may be attributed to the calculation method of the software and is beyond the scope of this study, but it confirms the practical observations of asymmetrical foundation subsidence cases that are encountered in field conditions.

Furthermore, both of the foundation edges were subjected to upheavals as illustrated in Figure 7.21, and models 1 and 2 did not display this discontinuously deformed foundation shape. The upheaval may have influenced the subsidence on both edges of the foundation. It can be said that the groundwater extraction and dynamic load might have caused the displacement of soil particles towards the centre of the foundation, producing upheavals. Nonetheless, this simulation has showed the tendency of dynamic load to produce a discontinuously deformed shape when the magnitude of the dynamic load is increased. Moreover, relevant strength analysis must be performed

due to the shear forces and bending moments produced in such foundations because of the upheavals at both edges.

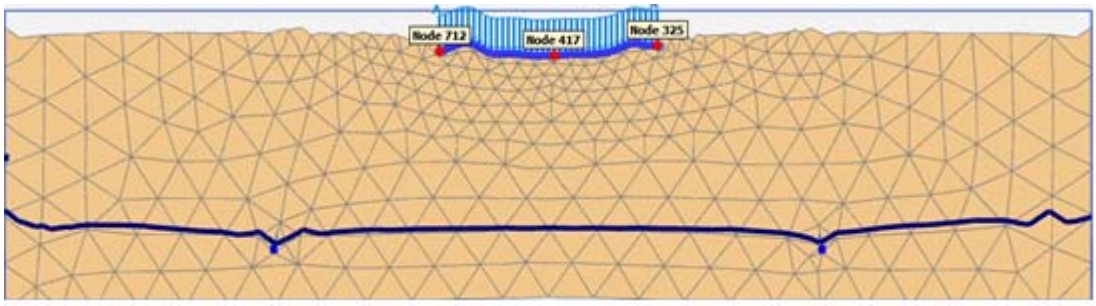

Figure 7.21 Deformation subjects to dynamic load of frequency 20 Hz, amplitude of 20 kPa, duration of 20 s

Table 7.13 Data corresponding to points on the foundation of Figure 7.21

Node point	y deformation (mm)
712	139.299
417	152.955
325	119.395

7.4.3.2 Effect of Longer Duration of Dynamic Loads

Two dynamic models, model 4 and model 5, were constructed in this section with a prolonged dynamic load duration of 40 s.

Dynamic Model 4

Model 4 had a dynamic load with 10 kPa amplitude, 10 Hz frequency and 40 s duration. The deformations incurred in the foundation due to the application of this load configuration are displayed in Figure 7.22 and Table 7.14. The foundation deformation was slightly discontinuous with marginal upheavals at both edges, but the extent of discontinuity was less than that encountered in Figure 7.21. This shows that although the duration of the dynamic load affects the formation of a discontinuous foundation deformation shape, it is only a marginal effect.

However, these three points displayed higher foundation subsidence values than observed earlier for the third dynamic model in Figure 7.21. This shows that even though model 3 had higher frequency and amplitude, the duration of the dynamic load had a greater influence on the subsidence of the foundation. The relationship between the duration of the dynamic loading and the vertical displacement for model 4 is

depicted in Figure 7.24. It shows that the extent of foundation subsidence increased with time during the 40 s period investigated, indicating that dynamic time and foundation subsidence are generally linearly related with a slope of approximately 0.74 mm per second.

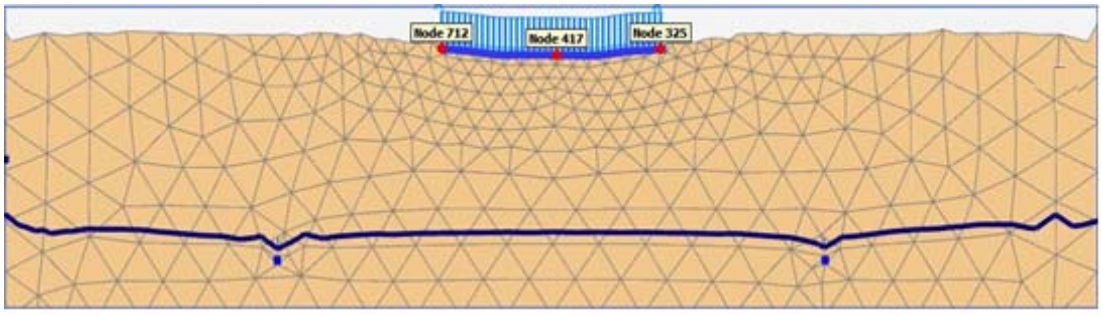

Figure 7.22 Deformation mesh of dynamic load of frequency 10 Hz, amplitude of 10 kPa and duration of 40 s

Table 7.14 Deformation values corresponding to points on the foundation of Figure 7.22

Node point	y deformation (mm)
712	-137.009
417	-160.584
325	-140.216

Dynamic Model 5

The magnitude of the dynamic load was doubled in model 5 from model 4. However, a smaller maximum foundation subsidence at the centre of the foundation, 145.856 mm, than Table 7.15 value of 160.584 mm, was observed. This observation is in contrast to the findings from earlier sections of this study.

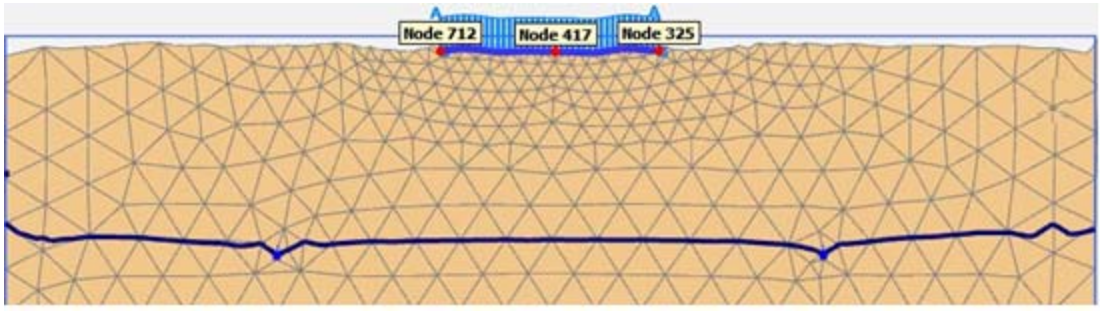

Figure 7.23 Deformation mesh of dynamic load of frequency 10 Hz, amplitude of 20 kPa and duration of 40 s

Table 7.15 Deformation values corresponding to points on the foundation of Figure 7.23

Node point	y deformation (mm)
712	-141.229
417	-145.856
325	-136.337

The relationship between the dynamic load duration and foundation subsidence is displayed in Figure 7.24. This shows that vertical displacement reversed when the duration reached approximately 26 s, from which point the foundation started to 'bounce back'. Compared to model 4, the larger amplitude of model 5 initially produced greater subsidence but the reverse point was also reached earlier for model 5 (Figure 7.24). The reverse point of model 4 is not displayed in Figure 7.24 because of the time limitation, as it occurred after the 40 s mark.

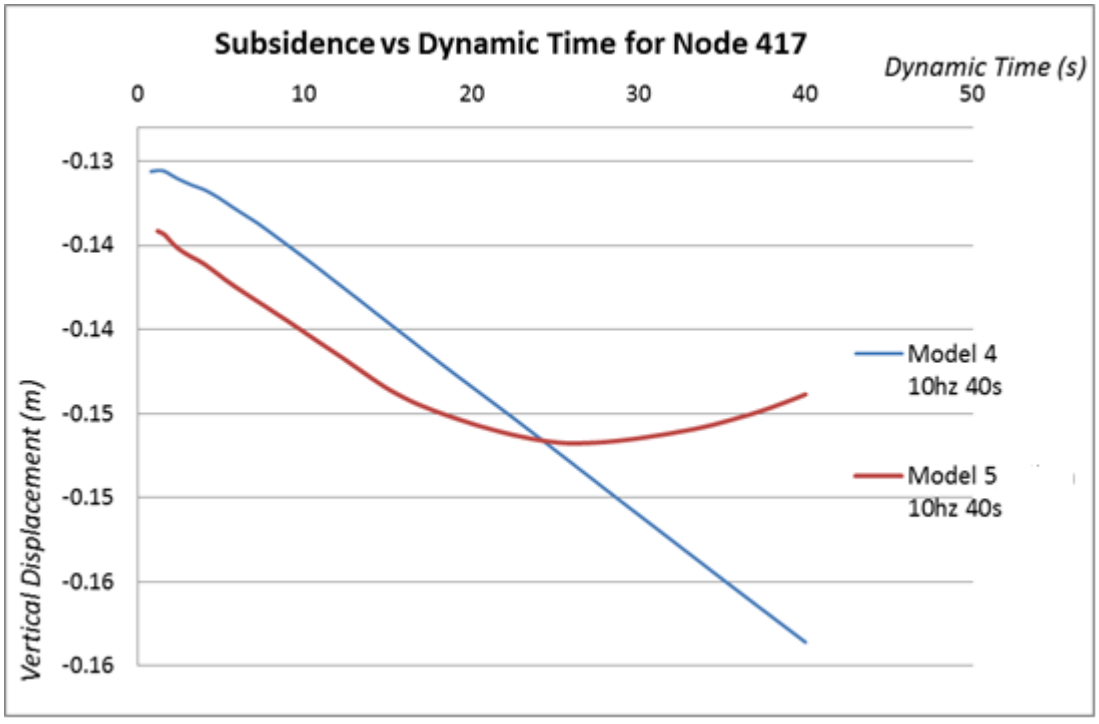

Figure 7.24 Dynamic time versus vertical displacement for model 4 and model 5

Furthermore, both edges of the foundation displayed upheavals in Figure 7.24, whereas a slight indication of upheaval is also displayed in Figure 7.22. This reconfirms the observation that discontinuous foundation deformation is encountered for dynamic loads with greater amplitudes. Figure 7.23 shows that the extent of

discontinuous foundation deformation increases with increased duration, as can be compared with the model 1 duration of 20 s (Figure 7.19).

7.4.4 Effect of Seismic Activity on Foundation Subsidence

Two dynamic models were constructed for seismic effect investigation, namely: model 6 for subsidence of the foundation due to groundwater extraction of 30 days without any seismic activity; and model 7 for foundation subsidence under the Encino earthquake.

7.4.4.1 Dynamic Model 6

Dynamic model 6 simulated the subsidence of the foundation under groundwater extraction. Figure 7.25 illustrates the mesh resulting from the subsidence of the foundation after 30 days of well pumping. Once again, the maximum subsidence (0.2655 m) along the entire surface profile was observed at the centre of the footing represented by node number 1852.

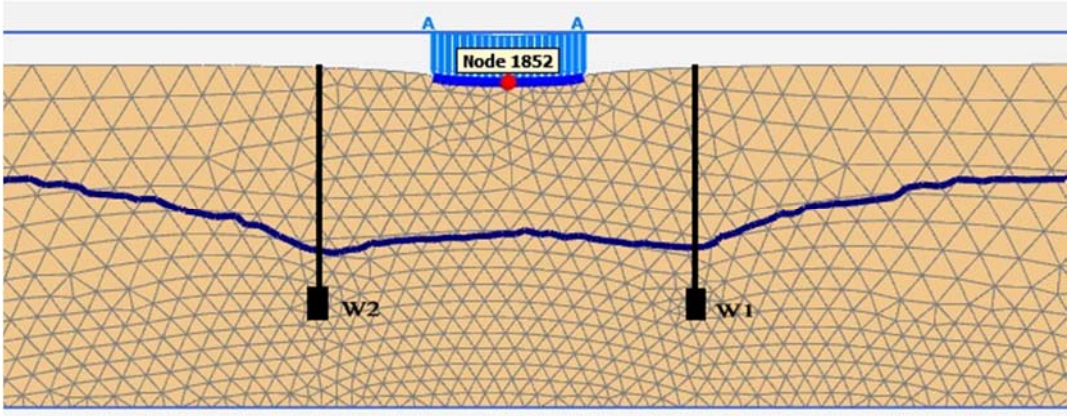

Figure 7.25 Deformation mesh after 30 days of water extraction from two wells

7.4.4.2 Dynamic Model 7

Once the subsidence has been encountered after 30 days of pumping under static distributed load, an earthquake load was applied by inputting an acceleration time series generated by SMC file to develop dynamic model 7. The significant ground acceleration began at approximately 32 s which was then followed by a dynamic duration of 60 s (Figure 7.17). The deformation from the results of dynamic model 6 was followed by further deformation due to seismic activity as illustrated in Figure

7.26, which shows the subsequent deformation mesh after 60 seconds of the Encino earthquake (scaled up 500 times).

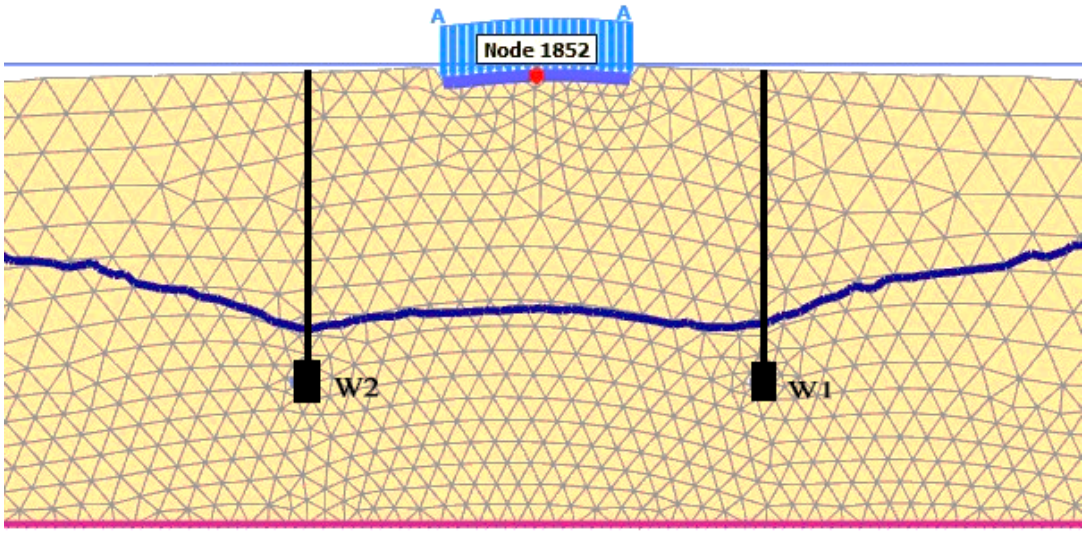

Figure 7.26 Deformation mesh after 60 dynamic seconds of the Encino earthquake (500 times scaled up)

A deformation value of 5.041 x10^{-3} m was observed at the centre of the foundation at node 1852. This rise in the value of the vertical displacement is significantly smaller compared with the initial value of 0.2655 m, which occurred due to groundwater extraction. These results show that the foundation subsidence was only marginally affected by an earthquake of small amplitude and short acceleration period. Figure 7.27 shows the relationship between the duration or dynamic time and the vertical displacement. For the initial 32 s, almost no subsidence was observed as the small values that can be seen on the graph may attributed to the 'computation noise' generated by PLAXIS during dynamic simulation calculations. This follows the trend of Figure 7.17, with an initial 'silent' period. However, a rapid increase was observed in the subsidence as a dramatic mounting up of earthquake acceleration occured (see Figure 7.17). Therefore, it can be deduced that the additional subsidence of the foundation was induced by the significant ground acceleration.

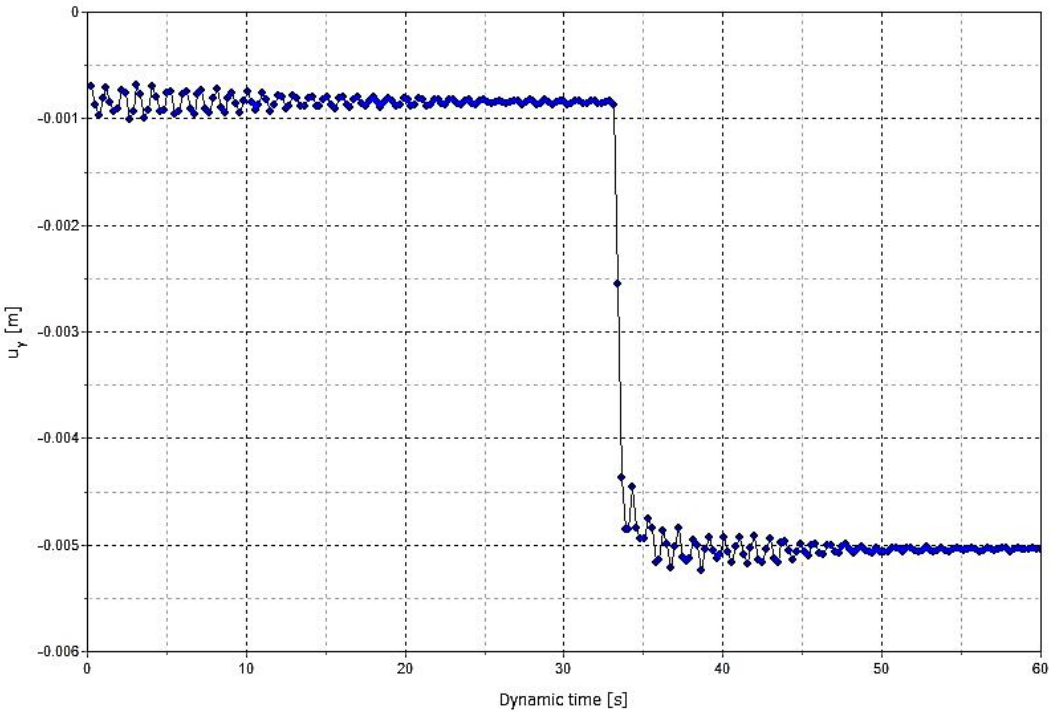

Figure 7.27 Vertical displacement with dynamic time curves of node 1852 for the Encino, California earthquake

Chapter 8
Summary, Conclusions and Recommendations

8.1 Summary

The principle purpose of this study was to investigate the performance of landfill liners. After performing the literature review, as presented in Chapter Two of this thesis, the research goals identified were to examine the hydraulic performance of the GCL against varying confining pressures, static loading and permeant liquids; analyse subgrade stability, predict heavy metal contaminant migratory patterns through the landfill and perform soil deformation simulations.

In order to accomplish these goals, a series of laboratory experiments and simulations were completed. To study the hydraulic performance and ability of GCL to function as an effective leachate barrier, the deformation of GCL under applied pressures and permeating liquids was studied. Both microscopic and SEM-EDS techniques were utilised to provide visual insight regarding the surface morphology and behaviour of GCL bentonite particles.

The hydraulic performances and alterations in the surface profiles of the GCL samples were also investigated. As two types of GCL specimens have been investigated in this study, powdered and granular, both were separately studied. The samples were subjected to plastic limit and cone penetration tests to determine the Atterberg's limits. These tests were then followed by free swell tests to calculate the swelling characteristics of bentonite.

In the second stage of the swelling and hydraulic behaviour testings, the swelling of the GCL containing the cover and carrier geosynthetic layers was investigated under vertical loading and different confining pressures. Initially, the GCL was allowed to swell completely and was then subjected to permeability tests under confining pressures. Unconfined swell tests were conducted only under the weights of axial load and perforated disk, while both samples were subjected to 50kPa and 150kPa loads

during confined tests. The swelling behaviour was recorded whereas permeability tests were performed after the sample had fully swollen, marked by the height becoming constant. It was then followed by the examination of surface deformations of the two GCLs and LDPE geomembrane under static load, in the next stage of investigation.

The response of GCL, both before and after hydration with distilled water and sodium chloride (100 mM) as permeant solutions, was also studied to identify liner swelling and changes in permeability after being hydrated with both liquids. Two types of GCLs consisting of powder and granular bentonite were used for the investigation to obtain comparative observations.

The subgrade functions as an integral part of the landfill system and the stability of the subgrade system must be considered during landfill design, with regard to confirm the durability and reliability of the landfill for the design life. To achieve this function, the subgrade must be able to sustain the shear and tensile stresses imparted by landfill operation. This study was proposed to examine the use of recycled additives for the stabilisation of the landfill subgrade. Three additives, sewage sludge, slag and aspen timber, were investigated with regard to reusing materials that might alternatively be dumped on already depleted landfill sites. In addition, the effect of carbon impurities in the sand subgrade on the shear strength and the possibility of using carbon as a sand stabiliser were investigated.

As a bentonite layer is sometimes provided between sand layers in the case of GCLs, and each element in the landfill system has to have sufficient internal shear strength for the landfill to maintain its operations, bentonite stabilisation with sewage sludge was tested. Standard compaction tests were conducted to examine the effect of adding sludge on optimum moisture content and maximum dry density. Consolidation tests were done to observe the consolidation and shrink-swell behaviour of sludge-stabilised bentonite. Sludge addition can also improve the shear strength properties of soil and direct shear tests were performed in the laboratory to compare shear strength parameters; i.e.; τ, c, ϕ. The experimental results led to findings regarding the effect of sewage sludge on the engineering properties of soft soil.

Furthermore, since the permeable liner rests on compacted sand, the stabilisation of sand with carbon and sand-slag with timber to mitigate the tensile strains was

researched through direct shear tests. The soil used in these direct shear tests was Baldivis sand, which is abundant in Western Australia. An automated direct shear machine was used to conduct a series of direct shear tests to examine the effect of carbon content in sandy soil. To further the prospect of reusing waste material for stabilisation, timber waste from construction and demolition activities and blast furnace slag from the iron industry were used. A series of direct shear tests was also performed on sand-slag mixtures with wood additives. The added slag percentages were 1%, 2% and 3% respectively. According to the preliminary tests, the amount of wood in the sample was represented as a percentage of its top surface area on the surface areas of the sample. The wood element was positioned vertical to the shear direction, since this seemed to bring about the greatest improvement in sample strength.

The literature review in Chapter 2 showed that the leachate generated in landfills often contains heavy metals as pollutants that can contaminate the landfill subgrade soil and thereby the underlying aquifers and groundwater. In this study, heavy metal contamination in landfill systems was modelled using PLAXIS 2D 2012 and Pollute v.7 simulation software for specific periods. Four heavy metals were studied in two different cases. In case 1, a single landfill liner system was simulated with a gravel protection layer, leachate collection, geotextile, geomembrane and compacted soil. There were also two native subsoil layers underlying the composite landfill liner in this simulation over a simulation period of more than 12 years of lead (Pb) and chromium (Cr) migration. The second case dealt with the modelling of the nickel (Ni) and cadmium (Cd) contaminants migratory patterns over the 1–15 year period in landfills serviced with single and double liner systems. Moreover, deformation and settlement of the liner system, or in other words, land subsidence, has been identified by researchers as one of the major causes of landfill failures.

Land subsidence is influenced by the location and composition of fine aquifer layers, groundwater level, rate of groundwater extraction, location of wells and landfill loading conditions. Three cases were devised in this study to examine the occurrence of land subsidence in landfills caused by groundwater extraction activities from aquifers present in the area surrounding landfills, using PLAXIS 2D 2012 finite element modelling software. Case 1 evaluated diverse clay zone types, i.e. continuous

and discontinuous, and thicknesses. Wells were also inserted in different locations in the clay zone, a discharge rate applied at rate of 20m^3/day, and the land subsidence measured. In case 2, two PLAXIS models with single and dual well systems were developed to investigate the influence of groundwater extraction on the subsidence of landfill subjected to overlying load from accumulated solid waste, represented by a loaded foundation in the models.

The compaction of solid waste in landfills often imposes dynamic loading on the foundation layers of the landfill system; therefore, case 3 studied the influence of dynamic loading on land subsidence. Five PLAXIS models with different dynamic parameters of amplitude, duration and frequency were developed to investigate the effect on foundation subsidence in a soil profile with sand aquifer subjected to groundwater extraction, without considering any damping dynamic excitation. The influence of dynamic impact loading on the subsidence of landfill foundation layers, represented by a foundation subjected to dynamic load in the simulation models, was then investigated. Another observation made from the literature review was that landfills are often built in areas that may be prone to seismic activity. In order to ascertain the influence of seismic activity upon the subsidence of foundations, actual seismic data from the Encino earthquake was used. A model was constructed and land subsidence due to static distributed load and groundwater extraction over a 30 day period was simulated in a sand aquifer containing two pumping wells, followed by earthquake excitation to calculate the influence of seismic activity on the subsequent modification of the model.

8.2 Conclusions

The experimental and numerical study of landfill liner performances, the results of which have been presented in this thesis, suggest the following:

- The GCL containing powder bentonite produced higher swell, higher compressive swell ratio and lower hydraulic conductivity compared to GCL containing granular bentonite. A plastic limit of 55% and liquid limit of 530% was observed for the powdered GCL A sample, whereas the granular GCL B sample displayed lower plastic and liquid limits at 50% and 433%, respectively. Moreover, both powdered and granular samples exhibited a

respective swelling index of 44 and 31. The permeability of the two GCLs was also examined and was respectively observed as 1.24 x 10^{-11} m/sec and 6.91 x 10^{-11} m/sec.

- Confining pressure applied equally to all GCL surfaces would increase the compressive swell ratio and lower the hydraulic conductivity. GCL A exhibited a swelling of approximately 9.2mm without loads and displayed swelling of 6.3mm and 2.8mm under respective loads of 50kPa and 150kPa, compared to the initial 6.4mm thickness. A reduction in permeability was observed upon increment of the confining pressure as it reduced to 1.06 x 10^{-11} m/sec and 7.79 x 10^{-12} m/sec from the initial unconfined value of 1.24 x 10^{-11} m/sec as the applied load exceeded to 50kPa and 150kPa, respectively.
- Static load applied through the gravel layer reduced the GCL thickness and created a wavy surface profile for the GCL, however, the installation of geomembrane on the top of the GCL would lessen the reduction in the GCL thickness. Generally, the deformation followed the crests and depressions of the gravel layer for both powdered GCL A and granular GCL B. The maximum and minimum heights for powdered GCL A were 15.6mm and 9.0mm, accordingly, while granular GCL B exhibited respective heights at 11.04mm and 7.4mm. The variation in the heights of deformations in the surface profile were reduced after the installation of the LDPE geomembrane on the top, for both GCLs. GCL A showed maximum and minimum heights of 11.4mm and 10.1mm, while GCL B exhibited respective values of 11.04mm and 8.1mm.
- According to optical microscopic examination, distilled water hydration produced no changes to the GCL after drying. On the other hand, crystal deposits were found at both the bentonite surface and geosynthetic cover when sodium chloride with 100 mM concentration was used as the hydration solution.
- Hydration of GCL with both distilled water and sodium chloride brought about alterations in the surface morphology of the bentonite particles. A trend was observed for the bentonite particles to approach/attach to each other when distilled water hydration was carried out. However, sodium chloride hydration (with 100 mM concentration) seemed to bring about less swelling.

- Utilising X-ray detector (EDS) and the resulting images, silicon, aluminium and iron were found to be the main elements in both granular and powder forms of bentonite. Sodium was present in the bentonite in the form of sodium oxide (Na_2O).
- Distilled water hydration had no influence on GCL elemental distribution. However, the bentonite surface area was found to contain chlorine after GCL hydration using unevenly dispersed NaCl solution. The hydraulic conductivity of GCL also appeared to change under the influence of NaCL hydration. To sum up, both granular and powdered bentonite GCL samples exhibited the tendency for hydraulic conductivity to increase after hydration with NaCl solution.
- The hydraulic conductivity of GCL was also found to change under the influence of NaCl hydration. To sum up, when GCL samples containing either granular or powder bentonite were hydrated using NaCl solution, the hydraulic conductivity tended to increase.
- The addition of sewage sludge can lead to a minor improvement in the engineering properties of soft soil. By increasing the sludge content, the maximum dry density of bentonite composite was increased while the optimum moisture content dropped.
- The results of consolidation tests indicated that adding sludge could improve the consolidation behaviour of cohesive soil. Both compression and swelling indices of pure bentonite were decreased by increasing the amount of additives.
- Examination of the shear strength parameters under various normal stresses demonstrated that 2% sludge can produce optimal improvement in bentonite's engineering properties. Results indicate that sewage sludge is an effective means of improving the geotechnical properties of the bentonite layer in landfill subgrade.
- The results of shear tests on compacted Baldivis sand obtained an internal friction angle of 35° and a cohesion value of 0. The presence of carbon seemed to change the shear strength and thus the friction angle of the sand. Sand containing 5%, 10% and 15% of carbon changed the internal friction angles to 30°, 29° and 18° respectively.

- Also for the shear tests on carbon-stabilised Baldivis sand, the cohesion value remained unchanged by the presence of carbon. The sample under different normal stresses was subjected to maximum shear stress reductions of 10% to 19% for sand containing 5% to 15% carbon respectively. To sum up, these results demonstrated the shear strength reduction effect of carbon content, indicating therefore that carbon material may be unsuitable for soil stabilisation techniques and the presence of carbon impurities in the sand subgrade may cause the sand to have inadequate shear strength and may result in shear failure of the landfill.
- Based on the experimental results, adding wood into sand-slag mixtures can drastically rise the shear strength of the mixtures. The level of shear strength improvement varied from 10.4% to 73.6% approximately when the samples were subjected to normal stresses of 50 kPa, 150 kPa and 250 kPa. A 50 kPa normal stress incurred the greatest shear strength improvement. Under all normal stress levels applied in this experiment, the highest slag content of 3% exerted the greatest maximum shear stresses compared to the samples with lower slag contents of 1% and 2%. However, in this case, the durability aspect of wood was not studied due to time constrain.
- The simulation of Pb and Cr transportation in the landfill leachate indicated an increasing concentration of Pb and Cr from year 1 to year 12. For the first subsoil, the Pb concentration was assessed to be in between 0.2484–0.6298 mg/l, while the Pb concentration in subsoil 2 was 0.1886 to 0.5078 mg/l. The Cr concentration in subsoil 1 was 0.2191–0.5432 mg/l while in subsoil 2, it varied from 0.1644 to 0.4392 mg/l.
- After permeating the geomembrane, the concentration of both Pb and Cr declined by more than 70%. However, it can be predicted that the heavy metal concentration in the subsoil would mount up after a period of 12 years due to the accumulation of leachate seepage. Taking the initial concentrations into account, it is foreseeable that both contaminants will possibly contaminate the groundwater surrounding the landfill.
- Simulation results on Ni and Cd migration pattern over a 1–15 year period showed that the concentrations of both heavy metals increased as the contaminants accumulated over each succeeding year, and the contaminant

concentration variations for every succeeding layer were also predicted. At 0.81 m depth in the subgrade, the highest Cd contaminant value was observed for the single liner within the 0.17 mg/l–0.6136 mg/l range for the respective simulation period range of 1–15 years.

- Ni concentrations showed a similar trend with highest concentration value at 10 m depth, and the range of 0.42 mg/l–1.65 mg/l from 1–15 years. The lower permeability of the secondary leachate barrier installed in the double liner system (compacted clay), reduced the concentration of the seeping heavy metals as they migrated from GCL primary leachate barrier towards the secondary barrier. This shows that groundwater contamination can be mitigated to a significant degree by the provision of a double liner system, but absolute leachate prevention cannot be established. Nonetheless, the increase in temperature due to climatic variation over the years may increase the Ni and Cd concentrations, as in addition to other factors it may catalyse liner system degradation and generation of the leachate.
- A simulation study on land subsidence for ground surface displayed consistent results in all simulation scenarios after the extraction of groundwater, except for the low initial groundwater level. In aquifers subjected to well pumping, surface deformation appeared in the form of a wavy ground surface and the surface deformation process tended to increase with the increasing rate of groundwater extraction. Ground surface subsidence will continue to take place even when the low permeability materials are far away from the well location. A saggy ground surface could be one indication of the presence of low permeability material in the aquifer.
- Results for PLAXIS models with single and dual well-pumping systems on landfill subjected to overlying load showed maximum subsidence at the middle of the foundation with a generally symmetrical and even surface profile. Increasing the number of wells from one to two wells, increased the degree of foundation subsidence. The location of the maximum subsidence at the foundation centre remained unchanged with the changes in the distributed load on the foundation, but at the scale investigated in the study, the increasing load had a great effect on foundation subsidence. The dominant factors influencing

the subsidence behaviour of the entire sand aquifer subjected to well pumping are the conditions of the well.

- Results showed that dynamic impact loading influences the subsidence of landfill foundation layers. Furthermore, the shape, degree and direction of the foundation deformation were affected by the dynamic load. A dynamic load with higher amplitude increased the extent of deformation, producing an uneven foundation subsidence, while reducing the time required for the reversal of the deformation to occur. A longer duration of dynamic load increased the duration before the foundation subsidence was reversed and the deformation tended to be more uneven with increasing time. It is proposed that the disposition of soil particles under the foundation due to the application of dynamic load lifts the foundation, producing discontinuous or uneven foundation subsidence.
- The subsidence profile due to seismic excitation displayed an increase in subsidence with increasing distance from the well and a dramatic increase in the foundation area. This may indicate that seismic excitation might have reversed the trend that was only induced by the pumping of groundwater from the wells. Moreover, it was observed from the PLAXIS simulation results that an earthquake with a smaller magnitude (like Encino with 4.4) nominally affected the subsidence of the foundation. This implies that in a foundation deformed by 30 days of well pumping, the extent of any further subsidence depends upon the magnitude of maximum ground acceleration. In other words, the ground acceleration must reach a certain threshold level before any significant subsidence can be observed.

8.3 Recommendations for Further Work

The research work conducted for this thesis outlined several topics that might be beneficial for enhancing the performance of landfill liners and therefore, improve overall landfill operation. Although many neglected areas of liner performance research were studied in this project, some areas highlighted in Chapter 2 still require further study. The changing of bentonite swelling behaviour as a result of fluctuation in inorganic salt or leachate concentration in field applications needs to be examined in more depth, along with the hydraulic performance effect of the GCL subjected to

concentration changes in those permeants. The recovery performance of GCL from surface deformation also needs to be investigated further.

Even though the stabilisation of bentonite and subgrade sand using recycled industrial and municipal wastes was investigated in this study, more research can be proposed. Based upon the implications of this research for the reclaiming of sludge, timber and slag for commercial purposes in the stabilisation of landfill subgrade, an economic, safe and durable solution can be devised. Since the landfill subgrade seems always to be in a moist condition, the long term performance of wood application needs to be examined in relation to its durability. In the application of slag, the moist conditions are also suspected to have an effect on the stabilisation performance, thus further study into this is required. Since the experiment on stabilisation using slag did not consider the curing period, research is needed into the contribution of curing period on subgrade stabilisation using slag.

In some cases, landfills are located in the area that are subject to groundwater extraction or well-pumping activities. This may also affect the stability of the landfill liner system due to soil settlement, and the intention was to establish an understanding of liner defects and soil deformation in the landfill liner system, in regard to mitigate the adverse effects of calamities. Furthermore, different types of soils are present and tend to behave differently due to variations in characteristics such as hydraulic conductivity as changes in the groundwater level occur triggered by well-pumping. This may well change the aquifer responses, as investigated in this study. However, it should be noted that although this simulation employed absorbent boundary conditions, the horizontal and vertical movements at the boundaries are restricted. This is in violation of the principle of either continuous soil ground or further complex geological distrubution, and in actual conditions the damping effect must be acknowledged. Also, liquefaction may occur due to seismic activity in real world situations and ground profiles may be greatly disturbed, causing simultaneous heaving and subsidence of some ground areas. Nonetheless, the simulation is still sufficient for the purpose of providing a general picture of the extent of landfill foundation subsidence under horizontal earthquake shaking.

The threshold level can be further investigated in future research for different ground conditions and types of soils, as earthquakes exceeding the threshold limits are alone

responsible for the occurrence of seismic influence on land subsidence. Furthermore, an empirical relationship can be derived between the footing subsidence and acceleration after investigating further records of actual seismic activities.

References

Abramson, Lee W. 2002. *Slope Stability and Stabilization Methods*. New York: John Wiley & Sons.

Abu-Rukah, Y., and Osama Al-Kofahi. 2001. "The Assessment of the Effect of Landfill Leachate on Ground-Water Quality—a Case Study. El-Akader Landfill Site—North Jordan." *Journal of Arid Environments* 49 (3): 615-630.

Al-Yaqout, AF, and MF Hamoda. 2003. "Evaluation of Landfill Leachate in Arid Climate—a Case Study." *Environment International* 29 (5): 593-600.

Allan, M. L., and L. E. Kukacka. 1995. "Blast-Furnace Slag-Modified Grouts for In-Situ Stabilization of Chromium-Contaminated Soil." *Waste Management* 15 (3): 193-202.

Allen, A. 2001. "Containment Landfills: The Myth of Sustainability." *Engineering Geology* 60 (1): 3-19.

Amiralian, Saeid. 2013. "Study on Soil Stabilisation Technique Using Lime & Fly Ash." Master's thesis, Civil Engineering, Curtin University.

Andreottola, Gianni, Piero Cannas, T. H. Christensen, R. Cossu, and R. Stegmann. 1992. "Chemical and Biological Characteristics of Landfill Leachate." In *Landfilling of Waste: Leachate*, edited by Thomas H. Christenson, R. Cossu, and R. Stegmann, 65-88. New York: Elsevier Applied Science.

Artieres, O., and P. Delmas. 1995. "Puncture Resistance of Geotextile-Geomembrane Lining Systems" *Fifth International Landfill Symposium*, *Sardinia,* Cagliari: CISA Publisher.

Ashmawy, Alaa K., Darwish El-Hajji, Nestor Sotelo, and Naim Muhammad. 2002. "Hydraulic Performance of Untreated and Polymer-Treated Bentonite in Inorganic Landfill Leachates." *Clays and Clay Minerals* 50 (5): 546-552.

ASTM D5084-10. 2010. *Standard Test Methods for Measurement of Hydraulic Conductivity of Saturated Porous Materials Using a Flexible Wall Permeameter*. ASTM International www.astm.org.

ASTM D5311/D5311M-13. 2013. *Standard Test Method for Load Controlled Cyclic Triaxial Strength of Soil*. ASTM International www.astm.org.

ASTM D5887-09. 2009. *Standard Test Method for Measurement of Index Flux Through Saturated Geosynthetic Clay Liner Specimens Using a Flexible Wall Permeameter*. ASTM International www.astm.org.

ASTM D5890-11. 2011 *Standard Test Method for Swell Index of Clay Mineral Component of Geosynthetic Clay Liners*. ASTM International www.astm.org.

Australian & New Zealand Biosolids Partnership. 2012. "Biosolids, Carbon and Climate Change." NSW: Australian Water Association.

Azad, Farzad M., Abbas El-Zein, R. K. Rowe, and David W. Airey. 2012. "Modelling of Thermally Induced Desiccation of Geosynthetic Clay Liners in Double Composite Liner Systems." *Geotextiles and Geomembranes* 34: 28-38. doi: 10.1016/j.geotexmem.2012.02.012.

Azadegan, Omid, Mohammad Javad Yaghoubi, and Gh. R. Pourebrahim. 2011. "A Laboratory Study of the Behavior of the Lime/Cement Slurry and Compacted

Un-Reinforced Piles." *Electronic Journal of Geotechnical Engineering* 16: 375-386.

Aziz, Shuokr Qarani, Hamidi Abdul Aziz, Mohd Suffian Yusoff, Mohammed J. K. Bashir, and Muhammad Umar. 2010. "Leachate Characterization in Semi-Aerobic and Anaerobic Sanitary Landfills: A Comparative Study." *Journal of Environmental Management* 91 (12): 2608-2614.

Barlaz, Morton A., and Robert K. Ham. 1993. "Leachate and Gas Generation." In *Geotechnical Practice for Waste Disposal*, edited by Daniel, D. E, 113-136. London, United Kingdom: Chapman & Hall.

Barros, Regina Mambeli, Geraldo Lúcio Tiago Filho, and Tiago Rodrigo da Silva. 2014. "The Electric Energy Potential of Landfill Biogas in Brazil." *Energy Policy* 65: 150-164.

Bear, Jacob, Shaul Sorek, and Viacheslav Borisov. 1997. "On the Eulerian–Lagrangian Formulation of Balance Equations in Porous Media." *Numerical Methods for Partial Differential Equations* 13 (5): 505-530.

Blight, Geoffrey. 2008. "Slope Failures in Municipal Solid Waste Dumps and Landfills: A Review." *Waste Management & Research* 26 (5): 448-463.

Bostwick, L., R. K. Rowe, W. A. Take, and R. W. I. Brachman. 2010. "Anisotropy and Directional Shrinkage of Geosynthetic Clay Liners." *Geosynthetics International* 17 (3): 157-170.

Bouazza, A. 2002. "Geosynthetic Clay Liners." *Geotextiles and Geomembranes* 20 (1): 3-17.

Bouazza, Abdelmalek, and John J. Bowders. 2010. *Geosynthetic Clay Liners for Waste Containment Facilities*. Leiden, Netherlands: CRC Press.

Bovea, M. D., Valeria Ibáñez-Forés, A. Gallardo, and Francisco José Colomer-Mendoza. 2010. "Environmental Assessment of Alternative Municipal Solid Waste Management Strategies. A Spanish Case Study." *Waste Management* 30 (11): 2383-2395.

Bowders Jr, John J., and David E. Daniel. 1987. "Hydraulic Conductivity of Compacted Clay to Dilute Organic Chemicals." *Journal of Geotechnical Engineering* 113 (12): 1432-1448.

Brachman, R. W. I., and S. Gudina. 2008. "Geomembrane Strains from Coarse Gravel and Wrinkles in a Gm/Gcl Composite Liner." *Geotextiles and Geomembranes* 26 (6): 488-497.

Brinkgreve, R. B. J. 2002. PLAXIS (Version 8) User's Manual. Netherlands: Delft University of Technology and PLAXIS B.V.

Brinkgreve, R. B. J., E. Engin, and W. M. Swolfs. 2013. "PLAXIS 2D 2012 Material Models Manual." Delft: PLAXIS B.V.

Brown, G., and G. W. Brindley. 1980. "Crystal Structures of Clay Minerals and Their X-Ray Identification." London: Mineralogical Society.

Buckley, John, Will P. Gates, and Daniel T. Gibbs. 2012. "Forensic Examination of Field Gcl Performance in Landfill Capping and Mining Containment Applications." *Geotextiles and Geomembranes* 33: 7-14.

Budhu, Muniram. 2010a. "Earth Fissure Formation from the Mechanics of Groundwater Pumping." *International Journal of Geomechanics* 11 (1): 1-11.

———. 2010b. *Soil Mechanics and Foundation*. 3rd ed. New York : John Wiley & Sons Inc.

Budhu, Muniram, and Ibrahim Bahadir Adiyaman. 2010. "Mechanics of Land Subsidence Due to Groundwater Pumping." *International Journal for Numerical and Analytical Methods in Geomechanics* 34 (14): 1459-1478.

Budihardjo, Mochamad Arief, Amin Chegenizadeh, and Hamid Nikraz. 2014. "Land Subsidence: The Presence of Well and Clay Layer in Aquifer." *Australian Journal of Basic & Applied Sciences* 8 (6): 217-224.

Burmister, Donald Martin. 1949. "Burmister Concepts in Soil Mechanics." Department of Civil Engineering, Columbia University,

Burnley, Stephen J. 2007. "A Review of Municipal Solid Waste Composition in the United Kingdom." *Waste Management* 27 (10): 1274-1285.

Cao, Guoliang, Dongmei Han, and Jessa Moser. 2013. "Groundwater Exploitation Management under Land Subsidence Constraint: Empirical Evidence from the Hangzhou–Jiaxing–Huzhou Plain, China." *Environmental Management* 51 (6): 1109-1125.

Carlsson, Kjell. 2007. "Light Microscopy." Compendium compiled for course SK2500, Physics of Biomedical Microscopy Stockholm: Applied Physics Dept., KTH.

Castro-Fresno, Daniel, Diana Movilla-Quesada, Ángel Vega-Zamanillo, and Miguel A. Calzada-Pérez. 2011. "Lime Stabilization of Bentonite Sludge from Tunnel Boring." *Applied Clay Science* 51 (3): 250-257.

Chai, J. C., S. L. Shen, H. H. Zhu, and X. L. Zhang. 2004. "Land Subsidence Due to Groundwater Drawdown in Shanghai." *Geotechnique* 54 (2): 143-147.

Chaussard, Estelle, Falk Amelung, Hasanudin Abidin, and Sang-Hoon Hong. 2013. "Sinking Cities in Indonesia: Alos Palsar Detects Rapid Subsidence Due to Groundwater and Gas Extraction." *Remote Sensing of Environment* 128: 150-161.

Chen, Li, and Deng-Fong Lin. 2009. "Stabilization Treatment of Soft Subgrade Soil by Sewage Sludge Ash and Cement." *Journal of Hazardous Materials* 162 (1): 321-327.

Chen, Xiaoge, and S. Jeyaseelan. 2001. "Study of Sewage Sludge Pyrolysis Mechanism and Mathematical Modeling." *Journal of Environmental Engineering* 127 (7): 585-593.

Chen, Xiaoge, S. Jeyaseelan, and N. Graham. 2002. "Physical and Chemical Properties Study of the Activated Carbon Made from Sewage Sludge." *Waste Management* 22 (7): 755-760.

Chofqi, Amina, Abedelkader Younsi, El Kbir Lhadi, Jacky Mania, Jacques Mudry, and Alain Veron. 2004. "Environmental Impact of an Urban Landfill on a Coastal Aquifer (El Jadida, Morocco)." *Journal of African Earth Sciences* 39 (3): 509-516.

Chow, Jing-Dong, and Wan-Lan Chai. 2007. "The Influences on Leachate from Landfill of Incineration Residuals by Acid Precipitation." *Journal of Hazardous Materials* 142 (1): 483-492.

Christensen, T.H., R. Cossu, and R. Stegmann. 2012. "Sanitary Landfilling: Process, Technology and Environmental Impact." London: Academic Press.

Chu, L. M., K. C. Cheung, and M. H. Wong. 1994. "Variations in the Chemical Properties of Landfill Leachate." *Environmental Management* 18 (1): 105-117.

Contreras, Francisco, Keisuke Hanaki, Toshiya Aramaki, and Stephen Connors. 2008. "Application of Analytical Hierarchy Process to Analyze Stakeholders Preferences for Municipal Solid Waste Management Plans, Boston, USA." *Resources, Conservation and Recycling* 52 (7): 979-991.

Cuisinier, Olivier, Farimah Masrouri, Manuel Pelletier, Fréderic Villieras, and Régine Mosser-Ruck. 2008. "Microstructure of a Compacted Soil Submitted to an

Alkaline Plume." *Applied Clay Science* 40 (1–4): 159-170. doi: 10.1016/j.clay.2007.07.005.

Czurda, K. 2006. ".3 Clay Liners and Waste Disposal." *Developments in Clay Science* 1: 693-701.

Dananaj, Ivan, Jana Frankovská, and Ivan Janotka. 2005. "The Influence of Smectite Content on Microstructure and Geotechnical Properties of Calcium and Sodium Bentonites." *Applied Clay Science* 28 (1): 223-232.

Daniel, David E. 1993. "Clay Liners." In *Geotechnical Practice for Waste Disposal,* edited by Daniel, D. E, 137-163. London, United Kingdom: Chapman & Hall.

Daniel, David E., and Heather B. Scranton. 1997. "Report of 1995 Workshop on Geosynthetic Clay Liners." US Environmental Protection Agency, Washington, DC.

Daniel, D. E., H. Y. Shan, and J. D. Anderson. 1993. "Effects of Partial Wetting on the Performance of the Bentonite Component of a Geosynthetic Clay Liner." *Proceedings of Geosynthetics* '93, Vancouver, B.C., Canada, St. Paul, MN: IFAI.

Davraz, M., and L. Gunduz. 2005. "Engineering Properties of Amorphous Silica as a New Natural Pozzolan for Use in Concrete." *Cement and Concrete Research* 35 (7): 1251-1261.

Degirmenci, Nurhayat, Arzu Okucu, and Ayse Turabi. 2007. "Application of Phosphogypsum in Soil Stabilization." *Building and Environment* 42 (9): 3393.

Dickinson, S., and R. W. I. Brachman. 2010. "Permeability and Internal Erosion of a Gcl beneath Coarse Gravel." *Geosynthetics International* 17 (3): 112-123. doi: 10.1680/gein.2010.17.3.112.

Dixon, Neil, and D. Russell V. Jones. 2005. "Engineering Properties of Municipal Solid Waste." *Geotextiles and Geomembranes* 23 (3): 205-233.

Domenico, Patrick A., and Franklin W. Schwartz. 1998. *Physical and Chemical Hydrogeology*. Vol. 44. New York: Wiley.

Du, Y.-J., S.-L. Shen, S.-Y. Liu, and S. Hayashi. 2009. "Contaminant Mitigating Performance of Chinese Standard Municipal Solid Waste Landfill Liner Systems." *Geotextiles and Geomembranes* 27 (3): 232-239.

Ecocem Ireland Ltd. 2012. History of the Use of Ggbs. Ecocem Ireland Ltd. Accessed September 9, 2013, http://www.ecocem.ie.

Egloffstein, Thomas A. 2001. "Natural Bentonites—Influence of the Ion Exchange and Partial Desiccation on Permeability and Self-Healing Capacity of Bentonites Used in Gcls." *Geotextiles and Geomembranes* 19 (7): 427-444.

Ehrig, H-J. 1983. "Quality and Quantity of Sanitary Landfill Leachate." *Waste Management & Research* 1 (1): 53-68.

Eid, Hisham T., Timothy D. Stark, W. Douglas Evans, and Paul E. Sherry. 2000. "Municipal Solid Waste Slope Failure. I: Waste and Foundation Soil Properties." *Journal of Geotechnical and Geoenvironmental Engineering* 126 (5): 397-407.

El-Fadel, Mutasem, Angelos N. Findikakis, and James O. Leckie. 1997. "Environmental Impacts of Solid Waste Landfilling." *Journal of Environmental Management* 50 (1): 1-25.

European Commission. 2000. "European Commission, Dg Environment, Waste Management Unit. Working Document on Sludge." 3rd Draft. Env.E3/Lm, Brussels, 2000.

Fernandez, Federico, and Robert M. Quigley. 1985. "Hydraulic Conductivity of Natural Clays Permeated with Simple Liquid Hydrocarbons." *Canadian Geotechnical Journal* 22 (2): 205-214.

Filz, George M., Jacob J. B. Esterhuizen, and J. Michael Duncan. 2001. "Progressive Failure of Lined Waste Impoundments." *Journal of Geotechnical and Geoenvironmental Engineering* 127 (10): 841-848.

Flyhammar, P. 1997. "Estimation of Heavy Metal Transformations in Municipal Solid Waste." *Science of the Total Environment* 198 (2): 123-133.

Gaffney, Jeffrey S., Nancy A. Marley, and Darin E. Jones. 2012. "Fourier Transform Infrared (Ftir) Spectroscopy." *Characterization of Materials*, Little Rock, Arizona, USA: University of Arkansas at Little Rock.

Garratt-Reed, A. J., and D. C. Bell. 2003. *Energy Dispersive X-Ray Analysis in the Electron Microscope in the Electron Microscope*. Oxford: BIOS Scientific Publisher Limited.

Giusti, L. 2009. "A Review of Waste Management Practices and Their Impact on Human Health." *Waste Management* 29 (8): 2227-2239.

Global Synthetics. 2010. *Proliner: Lldpe Smooth Geomembrane*. Australia.

Goodge, John. 2011. Geochemical Instrumentation and Analysis. Geological Sciences, University of Minnesota-Duluth. Accessed January 21, 2013, http://serc.carleton.edu/research_education/geochemsheets/eds.html.

Hammouri, Nezar Atalla, Abdallah I. Husein Malkawi, and Mohammad M. A. Yamin. 2008. "Stability Analysis of Slopes Using the Finite Element Method and Limiting Equilibrium Approach." *Bulletin of Engineering Geology and the Environment* 67 (4): 471-478.

Harichane, Khelifa, Mohamed Ghrici, Said Kenai, and Khaled Grine. 2011. "Use of Natural Pozzolana and Lime for Stabilization of Cohesive Soils." *Geotechnical and Geological Engineering* 29 (5): 759.

Harichane, Khelifa, Mohamed Ghrici, and Hanifi Missoum. 2011. "Influence of Natural Pozzolana and Lime Additives on the Temporal Variation of Soil Compaction and Shear Strength." *Frontiers of Earth Science* 5 (2): 162-169. doi: 10.1007/s11707-011-0166-1.

Hoornweg, Daniel, and Perinaz Bhada-Tata. 2012. "What a Waste: A Global Review of Solid Waste Management." Washington DC, USA: World Bank,

Hui, Yuan, Wang Li'ao, Su Fenwei, and Hu Gang. 2006. "Urban Solid Waste Management in Chongqing: Challenges and Opportunities." *Waste management* 26 (9): 1052-1062.

Hullings, D., and R.M. Koerner. 1991. "Puncture Resistance of Geomembranes Using a Truncated Cone Test." In Proceeding of Geosynthetics '91, Atlanta, 1991. 273–285, . Roseville, Minnesota, USA: IFAI.

Hyder Consulting. 2011. *Management of Construction and Demolition Waste in Australia.Construction and Demolition Waste Status Report;2001.* Queensland, Australia.

Indian Standards. 1977. *Methods of Test for Soils - Part Xl: Determination of Free Swell Index of Soils, Is 2720-40*. New Dehli: Bureau of Indian Standards.

Secretariat, I.G.S. 2006. "Guide to the Specification of Geosynthetics." South Carolina, USA: IGS Secretariat.

Ishihara, K. 1985. "Stability of Natural Deposits During Earthquakes." In *Proceedings of the 11th International Conference on Soil Mechanics and Foundation Engineering*, *San Francisco*, 12-16 August 1985, 321-76.

James, Anthony Noel, David Fullerton, and Ramon Drake. 1997. "Field Performance of Gcl under Ion Exchange Conditions." *Journal of Geotechnical and Geoenvironmental Engineering* 123 (10): 897-901.

Jha, Arvind K., S. K. Singh, G. P. Singh, and Prabhat K. Gupta. 2011. "Sustainable Municipal Solid Waste Management in Low Income Group of Cities: A Review." *Tropical Ecology* 52 (1): 123-131.

Jo, Ho Young, Craig H. Benson, Charles D. Shackelford, Jae-Myung Lee, and Tuncer B. Edil. 2005. "Long-Term Hydraulic Conductivity of a Geosynthetic Clay Liner Permeated with Inorganic Salt Solutions." *Journal of Geotechnical and Geoenvironmental Engineering* 131 (4): 405-417.

Jo, Ho Young, Takeshi Katsumi, Craig H. Benson, and Tuncer B. Edil. 2001. "Hydraulic Conductivity and Swelling of Nonprehydrated Gcls Permeated with Single-Species Salt Solutions." *Journal of Geotechnical and Geoenvironmental Engineering* 127 (7): 557-567.

Kalinski, Michael E. 2011. *Soil Mechanics Lab. Manual*. 2nd ed. Hoboken, New Jersey: Wiley.

Karnchanawong, Somjai, and Pawena Limpiteeprakan. 2009. "Evaluation of Heavy Metal Leaching from Spent Household Batteries Disposed in Municipal Solid Waste." *Waste Management* 29 (2): 550-558.

Katsumi, T. 2010. "Hydraulic Conductivity of Geosynthetic Clay Liners." In *Geosynthetic Clay Liners for Waste Containment Facilities*, edited by A. Bouazza and J. Bowders, 55-83. London: CRC Press/Balkema.

Katsumi, T., C. H. Benson, G. J. Foose, and M. Kamon. 2001. "Performance-Based Design of Landfill Liners." *Engineering Geology* 60 (1): 139-148.

Katsumi, Takeshi, Hiroyuki Ishimori, Masanobu Onikata, and Ryoichi Fukagawa. 2008. "Long-Term Barrier Performance of Modified Bentonite Materials against Sodium and Calcium Permeant Solutions." *Geotextiles and Geomembranes* 26 (1): 14-30.

Katsumi, Takeshi, Atsushi Ogawa, Shugo Numata, Craig H. Benson, D. C. Kolstad, H. Jo, Tuncer B. Edil, and Ryoichi Fukagawa. 2002. "Geosynthetic Clay Liners against Inorganic Chemical Solutions" *Proceedings of the Second Japan-Korea Joint Seminar on Geoenvironmental Engineering, May 18, 2002.* Kyoto University, Kyoto, Japan.

Kavak, Aydın, and Adnan Akyarl. 2007. "A Field Application for Lime Stabilization." *Environmental Geology* 51 (6): 987.

Kavak, Aydin, Gamze Bilgen, and Omer Faruk Capar. 2011. "Using Ground Granulated Blast Furnace Slag with Seawater as Soil Additives in Lime-Clay Stabilization." *Journal of ASTM International* 8 (7): 1-12. doi: 10.1520/jai103648.

Kim, Bumjoo, and Monica Prezzi. 2008. "Evaluation of the Mechanical Properties of Class-F Fly Ash." *Waste Management* 28 (3): 649.

Kjeldsen, Peter, Morton A. Barlaz, Alix P. Rooker, Anders Baun, Anna Ledin, and Thomas H. Christensen. 2002. "Present and Long-Term Composition of Msw Landfill Leachate: A Review." *Critical Reviews in Environmental Science and Technology* 32 (4): 297-336. doi: 10.1080/10643380290813462.

Koerner, Robert M., and G. R. Koerner. 2005. "In-Situ Separation of Gcl Panels beneath Exposed Geomembranes." *Geotechnical Fabrics Report* 23 (5): 34.

Kolias, S., V. Kasselouri-Rigopoulou, and A. Karahalios. 2005. "Stabilisation of Clayey Soils with High Calcium Fly Ash and Cement." *Cement & Concrete Composites* 27 (2): 301.

Kolstad, D. C., C. H. Benson, T. B. Edil, and H. Y. Jo. 2004. "Hydraulic Conductivity of a Dense Prehydrated Gcl Permeated with Aggressive Inorganic Solutions." *Geosynthetics International* 11 (3): 233-241.

Kramer, S. L. 1996. *Geotechnical Earthquake Engineering*. Upper Saddle River, NJ: Prentice Hall.

Kretschmann, David E. 2010. "Wood Handbook, Chapter 05: Mechanical Properties of Wood." *Series: General Technical Reports FPL-GTR-190*, 5-1-5-46, Madison, WI: U.S. Department of Agriculture, Forest Service, Forest Products Laboratory

Kulikowska, Dorota, and Ewa Klimiuk. 2008. "The Effect of Landfill Age on Municipal Leachate Composition." *Bioresource Technology* 99 (13): 5981-5985.

Kunze, G. W. and B. Dixon. 1986. "Pretreatment for mineralogical analysis." In *Methods of Soil Analysis. Part 1. 2nd ed. Agronomy Monograph 9*, edited by Klute A., 91-100. Madison, WI: American Society of Agronomy and Soil Science Society of America

Kylefors, Katarina. 2002. "Predictions of Leaching from Municipal Solid Waste (Msw) and Measures to Improve Leachate Management at Landfills." PhD diss., Luleå University of Technology.

Laine, J., and A. Calafat. 1989. "Preparation and Characterization of Activated Carbons from Coconut Shell Impregnated with Phosphoric Acid." *Carbon* 27 (2): 191-195.

Lake, Craig B., and R. Kerry Rowe. 2000. "Swelling Characteristics of Needlepunched, Thermally Treated Geosynthetic Clay Liners." *Geotextiles and Geomembranes* 18 (2–4): 77-101.

Leake, S. A. 1990. "Interbed Storage Changes and Compaction in Models of Regional Groundwater Flow." *Water Resources Research* 26 (9): 1939-1950.

Lee, Aik Heng, Hamid Nikraz, and Yung Tse Hung. 2010. "Influence of Waste Age on Landfill Leachate Quality." *International Journal of Environmental Science and Development* 1 (4): 347-350.

Lee, Jae-Myung, Charles D. Shackelford, Craig H. Benson, Ho-Young Jo, and Tuncer B. Edil. 2005. "Correlating Index Properties and Hydraulic Conductivity of Geosynthetic Clay Liners." *Journal of Geotechnical and Geoenvironmental Engineering* 131 (11): 1319-1329.

Lee, Jae-Myung, and Charles D. Shackelford. 2005. "Impact of Bentonite Quality on Hydraulic Conductivity of Geosynthetic Clay Liners." *Journal of Geotechnical and Geoenvironmental Engineering* 131 (1): 64-77.

Lema, J. M., R. Mendez, and R. Blazquez. 1988. "Characteristics of Landfill Leachates and Alternatives for Their Treatment: A Review." *Water, Air, and Soil Pollution* 40 (3-4): 223-250.

Li, X., Y. M. Shu, and X. R. Wu. 2009. "Characteristics of Self-Healing of Gcl." In *Geosynthetics in Civil and Environmental Engineering*, edited by Guangxin Li, Yunmin Chen and Xiaowu Tang, 87-90. Berlin: Springer.

Lin, Deng-Fong, Kae-Long Lin, Min-Jui Hung, and Huan-Lin Luo. 2007. "Sludge Ash/Hydrated Lime on the Geotechnical Properties of Soft Soil." *Journal of Hazardous Materials* 145 (1-2): 58.

Lin, Ling-Chu, and Craig H. Benson. 2000. "Effect of Wet-Dry Cycling on Swelling and Hydraulic Conductivity of Gcls." *Journal of Geotechnical and Geoenvironmental Engineering* 126 (1): 40-49.

Lu, Ning, and William J. Likos. 2006. "Suction Stress Characteristic Curve for Unsaturated Soil." *Journal of Geotechnical and Geoenvironmental Engineering* 132 (2): 131-142.

Ludwig, Chr, Stefanie Hellweg, and Samuel Stucki. 2002. *Municipal Solid Waste Management*. Berlin and Heidelberg: Springer-Verlag.

Lysmer, J., and R. L. Kuhlemeyer. 1969. "Finite Dynamic Model for Infinite Media." *Journal of Engineering Mechanics Division,* ASCE, 95: 859–877

Malczewski, Jacek. 1999. *Gis and Multicriteria Decision Analysis*. New York: John Wiley & Sons.

Manso, Juan M., Vanesa Ortega-López, Juan A. Polanco, and Jesús Setién. 2013. "The Use of Ladle Furnace Slag in Soil Stabilization." *Construction and Building Materials* 40: 126-134.

McBean, Edward A., Frank A. Rovers, and Grahame J. Farquahar. 1995. *Solid Waste Landfill; Engineering and Design*. Englewood Cliffs, NJ: Prentice Hall.

McCarthy, M. J., L. J. Csetenyi, A. Sachdeva, and R. K. Dhir. 2012. "Identifying the Role of Fly Ash Properties for Minimizing Sulfate-Heave in Lime-Stabilized Soils." *Fuel* 92 (1): 27-36.

Melchior, Stefan. 1997. "In-Situ Studies on the Performance of Landfill Caps (Compacted Soil Liners, Geomembranes, Geosynthetic Clay Liners, Capillary Barriers)." *Land Contamination and Reclamation* 5 (3): 209-216.

Mesri, Gholamreza, and Roy E. Olson. 1971. "Mechanisms Controlling the Permeability of Clays." *Clay and Clay Minerals* 19: 151-158.

Meyer-Jacob, Carsten. 2010. "Fourier Transform Infrared Spectroscopy (Ftirs): Model Development for Inferring Biogeochemical Properties in the 3.6 Ma Sediment Record of Lake Elgygytgyn, Ne Siberia." Diploma Thesis, Institute of Geologi and Mineralogy, University of Cologne.

Mitchell, James K., Raymond B. Seed, and H. Bolton Seed. 1990. "Kettleman Hills Waste Landfill Slope Failure. I: Liner-System Properties." *Journal of Geotechnical Engineering* 116 (4): 647-668.

Mitchell, Richard A., and James K. Mitchell. 1993. "Stability Evaluation of Waste Landfills" *The ASCE Specialty Conference on Stability and performance of Slopes and Embankments - II*, *June 29-July 1, 1992*, Berkeley, CA: ASCE.

Moore, Duane Milton, and Robert C. Reynolds. 1989. *X-Ray Diffraction and the Identification and Analysis of Clay Minerals*. Vol. 378. Oxford: Oxford University Press.

Mor, Suman, Khaiwal Ravindra, R. Dahiya, and A. Chandra. 2006. "Leachate Characterization and Assessment of Groundwater Pollution near Municipal Solid Waste Landfill Site." *Environmental Monitoring and Assessment* 118 (1): 435-456.

Mukunoki, T., T. Nakano, J. Otani, and J. P. Gourc. 2014. "Study of Cracking Process of Clay Cap Barrier in Landfill Using X-Ray Ct." *Applied Clay Science* 101: 558-566.

Murphy, Douglas B., and Michael W. Davidson. 2012. *Fundamentals of Light Microscopy and Electronic Imaging*. New York: John Wiley & Sons.

National Research Council. 2007. "Assessment of the Performance of Engineered Waste Containment Barriers." In *Report of the Committee to Assess the Performance of Engineered Barriers to National Research Council of the US National Academies, ISBN-13*, Washington, DC: The National Academies Press.

Nguyen, Tung Q., and Donald C. Helm. 1995. "Land Subsidence Due to Groundwater Withdrawal in Hanoi, Vietnam." *IAHS Publications-Series of Proceedings and Reports-Intern Assoc Hydrological Sciences* 234: 55-60.

Pacheco-Martínez, Jesús, Martín Hernandez-Marín, Thomas J. Burbey, Norma González-Cervantes, José Ángel Ortíz-Lozano, Mario Eduardo Zermeño-De-Leon, and Alfredo Solís-Pinto. 2013. "Land Subsidence and Ground Failure Associated to Groundwater Exploitation in the Aguascalientes Valley, México." *Engineering Geology* 164: 172-186.

Patel, M. A., and H. S. Patel. 2012. "A Review on Effects of Stabilizing Agents for Stabilization of Weak Soil." *Civil and Environmental Research* 2 (6): 1-7.

Petrov, Robert J., and R. Kerry Rowe. 1997. "Geosynthetic Clay Liner (Gcl)-Chemical Compatibility by Hydraulic Conductivity Testing and Factors Impacting Its Performance." *Canadian Geotechnical Journal* 34 (6): 863-885.

Petrov, Robert J., R. Kerry Rowe, and Robert M. Quigley. 1997. "Selected Factors Influencing Gcl Hydraulic Conductivity." *Journal of Geotechnical and Geoenvironmental Engineering* 123 (8): 683-695.

Petry, T. M., and D. N. Little. 2002. "Review of Stabilization of Clays and Expansive Soils in Pavements and Lightly Loaded Structures-History, Practice and Future." *Journal of Materials in Civil Engineering* 14 (6): 447-460.

Pichtel, John. 2010. *Waste Management Practices: Municipal, Hazardous, and Industrial*. Boca Raton: CRC Press.

PLAXIS, 1998, PLAXIS Bulletin No 5, Accessed December 21, 2013, http://www.PLAXIS.nl/files/files/05%20PLAXIS%20Bulletin%20(S).pdf

Pohland, Frederick G, and Stephen R Harper. 1985. *Critical Review and Summary of Leachate and Gas Production from Landfills*. Cincinnati, OH, USA: Solid and Hazardous Waste Research Division, Office of Research and Development, US Environmental Protection Agency.

Prabakar, J., and R. S. Sridhar. 2002. "Effect of Random Inclusion of Sisal Fibre on Strength Behaviour of Soil." *Construction and Building Materials* 16 (2): 123-131.

Qian, Xuede, Robert M. Koerner, and Donald H. Gray. 2001. *Geotechnical Aspects of Landfill Construction and Design*. Englewood Cliffs, NJ: Prentice Hall.

Ramadas, T. L., N. Darga Kumar, and G. Yesuratnam. 2011. "Geotechnical Characteristics of Three Expansive Soils Treated with Lime and Flyash." *International Journal of Earth Sciences and Engineering.* 4: 46-49.

Reddy, K. R., and B. M. Basha. 2014. "Slope Stability of Waste Dumps and Landfills: State-of-the-Art and Future Challenges" *Proceedings of Indian Geotechnical Conference IGC*, *Kakinada, India,* December 18-20, 2014.

Reddy, K. R., and R. E. Saichek. 1998. "Performance of Protective Cover Systems for Landfill Geomembrane Liners under Long-Term Msw Loading." *Geosynthetics International* 5 (3): 287-307.

Reilly, Thomas E., O. Lehn Franke, Herbert T. Buxton, and Gordon D. Bennett. 1987. *A Conceptual Framework for Ground-Water Solute-Transport Studies with Emphasis on Physical Mechanisms of Solute Movement*. Reston, Virginia: Department of the Interior, US Geological Survey.

Reinhart, Debra R., and A. Basel Al-Yousfi. 1996. "The Impact of Leachate Recirculation on Municipal Solid Waste Landfill Operating Characteristics." *Waste Management & Research* 14 (4): 337-346.

Renou, S., J. G. Givaudan, S. Poulain, F. Dirassouyan, and P. Moulin. 2008. "Landfill Leachate Treatment: Review and Opportunity." *Journal of Hazardous Materials* 150 (3): 468-493.

Rowe, R. K., and University of Western Ontario. Geotechnical Research Centre. 1995. *Leachate Characteristics for Msw Landfills*: University of Western Ontario, Department of Civil Engineering, Faculty of Engineering Science.

Rowe, R. K., L. E. Bostwick, and W. A. Take. 2011. "Effect of Gcl Properties on Shrinkage When Subjected to Wet-Dry Cycles." *Journal of Geotechnical and Geoenvironmental Engineering* 137 (11): 1019-1027.

Rowe, R. K., and C. Orsini. 2003. "Effect of Gcl and Subgrade Type on Internal Erosion in Gcls under High Gradients." *Geotextiles and Geomembranes* 21 (1): 1-24.

Rowe, R. K., R. M. Quigley, R. W. I. Brachman, and J.R. Booker. 2004. *Barrier Systems for Waste Disposal Facilities*. London: Taylor and Francis (E and FN Spon).

Rowe, R. K., and J. R. Booker. 2005. *Pollute v7 Pollutant Migration through a Nonhomogeneous Soil,© 1983-2005.* Ontario, Canada: Distributed by GAEA Environmental Engineering, Ltd 87.

Ruhl, Janice Lee. 1994. "Effects of Leachates on the Hydraulic Conductivity of Geosynthetic Clay Liners (Gcls)." Master's thesis, University of Texas, Austin.

Salami, Lukmon, Olaosebikan A. Olafadehan, Gutti Babagana, and Alfred A. Susu. 2013. "Prediction of Concentration Profiles of Contaminants in Groundwater Polluted by Leachates from a Landfill Site." *International Journal of Research and Reviews in Applied Sciences* 15 (3): 13.

Schroeder, Paul R., Tamsen S. Dozier, Paul A. Zappi, Bruce M. McEnroe, John W. Sjostrom, and R. Lee Peyton. 1994. *The Hydrologic Evaluation of Landfill Performance (Help) Model: Engineering Documentation for Version 3*, EPA/600/R-94/168b . Cincinnati, OH US: Environmental Protection Agency Risk Reduction Engineering Laboratory,

Scott, Jason, Donia Beydoun, Rose Amal, Gary Low, and Julie Cattle. 2005. "Landfill Management, Leachate Generation, and Leach Testing of Solid Wastes in Australia and Overseas." *Critical Reviews in Environmental Science and Technology* 35 (3): 239-332.

Seco, A., F. Ramirez, L. Miqueleiz, and B. Garcia. 2011. "Stabilization of Expansive Soils for Use in Construction." *Applied Clay Science* 51 (3): 348-352. doi: 10.1016/j.clay.2010.12.027.

Seed, Raymond B., James K. Mitchell, and H. Bolton Seed. 1990. "Kettleman Hills Waste Landfill Slope Failure. Ii: Stability Analyses." *Journal of Geotechnical Engineering* 116 (4): 669-690.

Seeger, S., and W. Müller. 1996. "Limits of Stress and Strain: Design Criteria for Protective Layers for Geomembranes in Landfill Liner Systems" *Geosynthetics: Applications, Design and Construction, Proceedings of the First International European Geosynthetics Conference (Eurogeo 1)* Maastricht, Netherlands, September 30 -October 2, 1996. Rotterdam: AA Balkema,

Shackelford, Charles D., Craig H. Benson, Takeshi Katsumi, Tuncer B. Edil, and L. Lin. 2000. "Evaluating the Hydraulic Conductivity of Gcls Permeated with Non-Standard Liquids." *Geotextiles and Geomembranes* 18 (2): 133-161.

Shackelford, Charles D., Gerald W. Sevick, and Gerald R. Eykholt. 2010. "Hydraulic Conductivity of Geosynthetic Clay Liners to Tailings Impoundment Solutions." *Geotextiles and Geomembranes* 28 (2): 149-162. doi: 10.1016/j.geotexmem.2009.10.005.

Shahriar, M. A., N. Sivakugan, A. Urquhart, M. Tapiolas, and B. M. Das. 2013. "A Study on the Influence of Ground Water Level on Foundation Settlement in Cohesionless Soil." *The 18th International Conference on Soil Mechanics and Geotechnical Engineering: challenges and innovations in geotechnics Paris, France,* September 2-6, 2013.

Shan, Hsin-Yu, and Ray-Ho Chen. 2003. "Effect of Gravel Subgrade on Hydraulic Performance of Geosynthetic Clay Liner." *Geotextiles and Geomembranes* 21 (6): 339-354.

Shan, H. Y., and D. E. Daniel. 1991. "Results of Laboratory Tests on a Geotextile/Bentonite Liner Material." In proceedings *of Geosynthetics' 91*, (2): 517–535, St. Paul, MN: IFAI

Daniel, D. E., H. Y. Shan, and J. D. Anderson. 1993. "Effects of Partial Wetting on the Performance of the Bentonite Component of a Geosynthetic Clay Liner." *Proceedings of Geosynthetics* '93, 3: 1482–1496, Vancouver, B.C., Canada: IFAI, St. Paul, MN, USA

Shang, J. Q., K. Y. Lo, and Robert M. Quigley. 1994. "Quantitative Determination of Potential Distribution in Stern-Gouy Double-Layer Model." *Canadian Geotechnical Journal* 31 (5): 624-636.

Shao, Jingai, Rong Yan, Hanping Chen, Baowen Wang, Dong Ho Lee, and David Tee Liang. 2007. "Pyrolysis Characteristics and Kinetics of Sewage Sludge by Thermogravimetry Fourier Transform Infrared Analysis†." *Energy & Fuels* 22 (1): 38-45.

Sharma, N. K., S. K. Swain, and U. C. Sahoo. 2012. "Stabilization of a Clayey Soil with Fly Ash and Lime: A Micro Level Investigation." *Geotechnical and Geological Engineering,* 30 (5): 1197-1205.

Shi, Xiaoqing, Rui Fang, Jichun Wu, Hongxia Xu, YuanYuan Sun, and Jun Yu. 2012. "Sustainable Development and Utilization of Groundwater Resources Considering Land Subsidence in Suzhou, China." *Engineering Geology* 124: 77-89.

Shukla, Sanjay Kumar. 2012. *Handbook of Geosynthetic Engineering*. London: ICE.

Singh, Umesh Kumar, Manish Kumar, Rita Chauhan, Pawan Kumar Jha, A. L. Ramanathan, and V. Subramanian. 2008. "Assessment of the Impact of Landfill on Groundwater Quality: A Case Study of the Pirana Site in Western India." *Environmental Monitoring and Assessment* 141 (1-3): 309-321.

Sivapullaiah, Puvvadi V., and Samudrala Savitha. 1999. "Index Properties of Illite-Bentonite Mixtures in Electrolyte Solutions." *Geotechnical Testing Journal,* 22 (3): 257–265

Slayter, Elizabeth M. 1992. *Light and Electron Microscopy*. Cambridge: Cambridge University Press.

Smidt, E., and V. Parravicini. 2009. "Effect of Sewage Sludge Treatment and Additional Aerobic Post-Stabilization Revealed by Infrared Spectroscopy and Multivariate Data Analysis." *Bioresource Technology* 100 (5): 1775-1780.

Smith, Stephen R. 2009. "A Critical Review of the Bioavailability and Impacts of Heavy Metals in Municipal Solid Waste Composts Compared to Sewage Sludge." *Environment International* 35 (1): 142-156.

Solanki, Pranshoo, and Musharraf Zaman. 2012. "Microstructural and Mineralogical Characterization of Clay Stabilized Using Calcium-Based Stabilizers." *Scanning electron microscopy,* Kazmiruk, V. (ed), Intech, Rijeka, 771–798.

Standards Australia. 1997. *Methods of Testing Soils for Engineering Purposes - Soil Chemical Tests - Determination of the Ph Value of a Soil - Electrometric Method, as 1289.4.3.1-1997*. New South Wales: SAIGlobal.

———. 1998a. *Methods of Testing Soils for Engineering Purposes - Soil Strength and Consolidation Tests - Determination of the One-Dimensional Consolidation Properties of a Soil - Standard Method, as 1289.6.6.1-1998*. New South Wales: SAIGlobal.

———. 1998b. *Methods of Testing Soils for Engineering Purposes – Soil Strength and Consolidation Tests - Determination of the Shear Strength of a Soil – Direct Shear Test Using a Shear Box, as 1289.6.1.1-1998*. New South Wales: SAIGlobal

———. 2001a. *Methods of Testing Soils for Engineering Purposes - Method 6.7.2: Soil Strength and Consolidation Tests - Determination of Permeability of a Soil - Falling Head Method for a Remoulded Specimen, as 1289.6.7.2-2001*. New South Wales: SAIGlobal.

———. 2001b. *Methods of Testing Soils for Engineering Purposes - Soil Compaction and Density Tests: Determination of the Dry Density/Moisture Content Relation of a Soil Using Standard Compactive Effort, As1289.5.1.1-2001*. New South Wales: SAIGlobal.

———. 2001c. *Methods of Testing Soils for Engineering Purposes - Soil Strength and Consolidation Tests - Determination of the Shear Strength of a Soil-Direct Shear Test Using a Shear Box, as 1289.6.2.2-2001*. New South Wales: SAIGlobal.

———. 2002. *Methods of Testing Soils for Engineering Purposes - Method 3.1.2: Soil Classification Tests - Determination of the Cone Liquid Limit of a Soil, as 1289.3.9.1-2002*. New South Wales: SAIGlobal.

———. 2003a. *Methods of Testing Soils for Engineering Purposes - Method 5.1.1: Soil Compaction and Density Tests - Determination of the Dry Density/Moisture Content Relation of a Soil Using Standard Compactive Effort, as 1289.5.1.1-2003*. New South Wales: SAIGlobal.

———. 2003b. *Methods of Testing Soils for Engineering Purposes - Method 7.1.1: Soil Reactivity Tests - Determination of the Shrinkage Index of a Soil - Shrink-Swell Index, as 1289.7.1.1-2002*. New South Wales: SAIGlobal.

———. 2009a. *Methods of Testing Soils for Engineering Purposes - Method 3.2.1: Soil Classification Tests - Determination of the Plastic Limit of a Soil - Standard Method, as 1289.3.2.1-2009*. New South Wales: SAIGlobal.

———. 2009b. *Methods of Testing Soils for Engineering Purposes - Method 3.3.1: Soil Classification Tests - Calculation of the Plasticity Index of a Soil, as 1289.3.3.1-2009*. New South Wales: SAIGlobal.

Stegmann, R., K. U. Heyer, and R. Cossu. 2005. "Leachate Treatment." *Tenth International Waste Management and Landfill Symposium,* S. Margherita di Pula, Cagliari, Italy, October 3-7, 2005

Stern, Roslyn T., and Charles D. Shackelford. 1998. "Permeation of Sand-Processed Clay Mixtures with Calcium Chloride Solutions." *Journal of Geotechnical and Geoenvironmental Engineering* 124 (3): 231-241.

Supriyadi, Slamet, Lorne K. Kriwoken, and Imogen Birley. 2000. "Solid Waste Management Solutions for Semarang, Indonesia." *Waste Management and Research* 18 (6): 557-566.

Tarrant, Richard. 2011. *Experiment 31 – the Scanning Electron Microscope*. Australia: School of Physics, University of Sydney.

Tastan, E. O., T. B. Edil, C. H. Benson, and A. H. Aydilek. 2011. "Stabilization of Organic Soils with Fly Ash." *Journal of Geotechnical and Geoenvironmental Engineering* 137 (9): 819-833.

Tchobanoglous, George, and Frank Kreith. 2002. *Handbook of Solid Waste Management*. New York: McGraw-Hill.

Tchobanoglous, George, Hilary Theisen, and Samuel Vigil. 1993. *Integrated Solid Waste Management: Engineering Principles and Management Issues*. New York: McGraw-Hill, Inc.

Terzaghi, Karl. 1996. *Soil Mechanics in Engineering Practice*. Canada: John Wiley & Sons.

Thiel, R., J. P. Giroud, R. Erickson, K. Criley, and J. Bryk. 2006. "Laboratory Measurements of Gcl Shrinkage under Cyclic Changes in Temperature and Hydration Conditions."Proceeding in *8th International Conference on Geosynthetics*, Yokoham, Japan, International Geosynthetic Society, 1: 21-44, September 18-22, 2006

Tonjes, David J., and Krista L. Greene. 2012. "A Review of National Municipal Solid Waste Generation Assessments in the USA." *Waste Management & Research* 30 (8): 758-771.

Touze-Foltz, N. 2012. "Discussion on Paper Entitled 'Migration Behaviour, of Landfill Leachate Contaminants through Alternative Composite Liners' by G. Varank, A. Demir, E. Sekman, A. Akkaya, K. Yetilezsoy, M.S. Bilgili." *Science of the Total Environment,* 450: 372-373

Towhata, I. 2008. *Geotechnical Earthquake Engineering.* Berlin Heidelberg: Springer-Verlag.

Tu, Wei. 2009. "Constant Rate of Strain Consolidation of Resedimented Class F Fly Ash." *Fuel* 88 (7): 1154-1159.

U.S. EPA. 2013. "Municipal Solid Waste in the United States: 2011 Facts and Figures." Edited by Office of Solid Waste. As EPA530-R-13-001 Washington, DC

U.S. Geological Survey, 2014. National strong-motion project earthquake data set. 20140317 13:252 UTC Mw 4.4 Encino, California Earthquake. Accessed March 17, 2014, http://nsmp.wr.usgs.gov/data_sets/20140317_1325.html.

Vangpaisal, Thaveesak, and Abdelmalek Bouazza. 2004. "Gas Permeability of Partially Hydrated Geosynthetic Clay Liners." *Journal of Geotechnical and Geoenvironmental Engineering* 130 (1): 93-102.

Varank, Gamze, Ahmet Demir, Selin Top, Elif Sekman, Ebru Akkaya, Kaan Yetilmezsoy, and M Sinan Bilgili. 2011. "Migration Behavior of Landfill Leachate Contaminants through Alternative Composite Liners." *Science of the Total Environment* 409 (17): 3183-3196.

Verge, Ashley, and R. Kerry Rowe. 2013. "A Framework for a Decision Support System for Municipal Solid Waste Landfill Design." *Waste Management & Research,* 0 (0): 1-11.

Wang, Hailong, Sally L. Brown, Guna N. Magesan, Alison H. Slade, Michael Quintern, Peter W. Clinton, and Tim W. Payn. 2008. "Technological Options

for the Management of Biosolids." *Environmental Science and Pollution Research-International* 15 (4): 308-317.

Wang, Xin, Tao Chen, Yinghua Ge, and Yongfeng Jia. 2008. "Studies on Land Application of Sewage Sludge and Its Limiting Factors." *Journal of Hazardous Materials* 160 (2): 554-558.

Whittig, L. D., and W. R. Allardice. 1986. "12 X-Ray Diffraction Techniques." *Methods of Soil Analysis: Physical and Mineralogical Methods* 9: 331.

Xia, H., and T. Hu. 1991. "Effects of Saturation and Back Pressure on Sand Liquefaction." *Journal of Geotechnical Engineering* 117 (9): 1347-1362.

Yagüe, A., S. Valls, and E. Vazquez. 2002. "Use of Cement Portland Mortar of Stabilised Dry Sewage Sludge in Construction Applications." *Waste Management and the Environment*, 527–536.

Yang, Wei, Zhaoxia Li, Chongfa Cai, Zhonglu Guo, Jiazhou Chen, and Junguang Wang. 2013. "Mechanical Properties and Soil Stability Affected by Fertilizer Treatments for an Ultisol in Subtropical China." *Plant and Soil* 363 (1-2): 157-174.

Yesiller, N., and C. D. Shackelford. 2010. "Chapter 13: Geoenvironmental Engineering." In *Geotechnical Engineering Handbook*, Edited by: B. M. Das, Fort Lauderdale, United States: J.Ross Publishing.

Yi, Yaolin, Martin Liska, and Abir Al-Tabbaa. 2013. "Properties of Two Model Soils Stabilized with Different Blends and Contents of Ggbs, Mgo, Lime, and Pc." *Journal of Materials in Civil Engineering* 26 (2): 267-274.

Yılmaz, Gonca, Temel Yetimoglu, and Seracettin Arasan. 2008. "Hydraulic Conductivity of Compacted Clay Liners Permeated with Inorganic Salt Solutions." *Waste Management & Research* 26 (5): 464-473.

Zhang, Dong Qing, Soon Keat Tan, and Richard M. Gersberg. 2010. "Municipal Solid Waste Management in China: Status, Problems and Challenges." *Journal of Environmental Management* 91 (8): 1623-1633.

Zhen-Shan, Li, Yang Lei, Qu Xiao-Yan, and Sui Yu-Mei. 2009. "Municipal Solid Waste Management in Beijing City." *Waste Management* 29 (9): 2596-2599.

Zheng, Chunmiao, and Gordon D. Bennett. 2002. *Applied Contaminant Transport Modeling*. Vol. 2. New York: Wiley-Interscience.

Zhu, Bin, Deng Gao, Jun-chao Li, and Yun-min Chen. 2012. "Model Tests on Interaction between Soil and Geosynthetics Subjected to Localized Subsidence in Landfills." *Journal of Zhejiang University-Science A* 13 (6): 433-444.

Zhu, Chun-Ming, Wei-Min Ye, Yong-Gui Chen, Bao Chen, and Yu-Jun Cui. 2013. "Influence of Salt Solutions on the Swelling Pressure and Hydraulic Conductivity of Compacted Gmz01 Bentonite." *Engineering Geology* 166: 74-80.